Numerical Study on the Structural Performance of Buckling-Restrained Braces and End Connections.

A thesis submitted in fulfilment of the
requirements for the degree of
Doctor of Philosophy (PhD)
at the
University of Canterbury

Dan Court-Patience
Project supervisor: Associate Professor Mark Garnich

May 2021

College of Engineering
Department of Mechanical Engineering
University of Canterbury
Christchurch
New Zealand

"He who knows his destination
and heads directly for it
will get there quickly.

He who knows his destination
but takes the odd wrong turn along the way
will still get there
and be wiser for the experience."

Peter Karsten

ABSTRACT

A buckling-restrained braced frame (BRBF) is a structural bracing system that provides lateral strength and stiffness to buildings and bridges. They were first developed in Japan in the 1970s (Watanabe et al. 1973, Kimura et al. 1976) and gained rapid acceptance in the United States after the Northridge earthquake in 1994 (Bruneau et al. 2011). However, it was not until the Canterbury earthquakes of 2010/2011, that the New Zealand construction market saw a significant uptake in the use of buckling-restrained braces (BRBs) in commercial buildings (MacRae et al. 2015). In New Zealand there is not yet any documented guidance or specific instructions in regulatory standards for the design of BRBFs. This makes it difficult for engineers to anticipate all the possible stability and strength issues within a BRBF system and actively mitigate them in each design. To help ensure BRBF designs perform as intended, a peer review with physical testing are needed to gain building compliance in New Zealand. Physical testing should check the manufacturing and design of each BRB (prequalification testing), and the global strength and stability of each BRB its frame (subassemblage testing). However, the financial pressures inherent in commercial projects has led to prequalification testing (BRB only testing) being favoured without adequate design specific subassemblage testing. This means peer reviewers have to rely on BRB suppliers for assurances. This low regulation environment allows for a variety of BRBF designs to be constructed without being tested or well understood. The concern is that there may be designs that pose risk and that issues are being overlooked in design and review.

To improve the safety and design of BRBFs in New Zealand, this dissertation studies the behaviour of BRBs and how they interact with other frame components. Presented is the experimental test process and results of five commercially available BRB designs (Chapter 2). It discusses the manufacturing process, testing conditions and limitations of observable information. It also emphasises that even though subassemblage testing is impractical, uniaxial testing of the BRB only is not enough, as this does not check global strength or stability. As an alternative to physical testing, this research uses computer simulation to model BRB behaviour. To overcome the traditional challenges of detailed BRB modelling, a strategy to simulate the performance of generic BRB designs was developed (Chapter 3). The development of nonlinear material and contact models are important aspects of this strategy. The Chaboche method is employed using a minimum of six backstress curves to characterize the combined isotropic and kinematic hardening exhibited by the steel core. A simplified approach, adequate for modelling the contact interaction between the restrainer and the core was found. Models also capture important frictional dissipation as well as lateral motion and bending associated with high order constrained buckling of the core. The experimental data from Chapter 2 was used to validate this strategy.

As BRBs resist high compressive loading, global stability of the BRB and gusseted connection zone need to be considered. A separate study was conducted that investigated the yielding and buckling strength of gusset plates (Chapter 4). The stress distribution through a gusset plate is complex and difficult to predict because the cross-sectional area of gusset plate is not uniform, and each gusset plate design is unique in shape and size.

This has motivated design methods that approximate yielding of gusset plates. Finite element modelling was used to study the development of yielding, buckling and plastic collapse behaviour of a brace end bolted to a series of corner gusset plates. In total 184 variations of gusset plate geometries were modelled in Abaqus®. The FEA modelling applied monotonic uniaxial load with an imperfection. Upon comparing results to current gusset plate design methods, it was found that the Whitmore width method for calculating the yield load of a gusset is generally un-conservative. To improve accuracy and safety in the design of gusset plates, modifications to current design methods for calculating the yield area and compressive strength for gusset plates is proposed.

Bolted connections are a popular and common connection type used in BRBF design. Global out-of-plane stability tends to govern the design for this connection type with numerous studies highlighting the risk of instability initiated by inelasticity in the gussets, neck of the BRB end and/or restrainer ends. Subassemblage testing is the traditional method for evaluating global stability. However, physical testing of every BRBF variation is cost prohibitive. As such, Japan has developed an analytical approach to evaluate out-of-plane stability of BRBFs and incorporated this in their design codes. This analytical approach evaluates the different BRB components under possible collapse mechanisms by focusing on moment transfer between the restrainer and end of the BRB. The approach have led to strict criteria for BRBF design in Japan. Structural building design codes in New Zealand, Europe and the United States do not yet provide analytical methods to assess BRB and connection stability, with prototype/subassemblage testing still required as the primary means of accreditation. Therefore it is of interest to investigate the capability of this method to evaluate stability of BRBs designs and gusset plate designs used in New Zealand (including unstiffened gusset connection zones).

Chapter 5 demonstrates the capability of FEA to study to the performance of a subassemblage test under cyclic loading – resembling that of a diagonal ground storey BRBF with bolted connections. A series of detailed models were developed using the strategy presented in Chapter 3. The geometric features of BRB 6.5a (Chapter 2) were used as a basis for the BRBs modelled. To capture the different failure mechanisms identified in Takeuchi et al. (2017), models varied the length that the cruciform (non-yielding) section inserts into the restrainer. Results indicate that gusset plates designed according to New Zealand's Steel Structures Standard (NZS 3404) limit BRBF performance. Increasing the thickness of the gusset plates according to modifications discussed in Chapter 4, improved the overall performance for all variants (except when $L_{in}/ B_{cruc} = 0.5$). The effect of bi-directional loading was not found to notably affect out-of-plane stability. Results were compared against predictions made by the analytical method used in Japan (Takeuchi method). This method was found to be generally conservative is predicting out-of-plane stability of each BRBF model. Recommendations to improve the accuracy of Takeuchi's method are also provided. The outcomes from this thesis should be helpful for BRB manufacturers, researchers, and in the development of further design guidance of BRBFs.

ACKNOWLEDGEMENTS

To my Professor, Mark Garnich –You have been committed every step of the way. Your superior experience, high standard of work and coaching ensured the success of this project and more importantly, you were dedicated to helping me develop the aptitude required for this level of research. Even during times when you were extremely active in teaching and research, you have always been available, providing me with firm technical guidance and detailed feedback. Thank you.

The opportunity to undertake this research has been made possible by financial support from the Building Research Association of New Zealand (BRANZ), the Mechanical Engineering Department at the University of Canterbury (UC), Callaghan Innovation and UC Quake Centre. In addition, Grayson Engineering, Holmes Solutions and the National Center of Research in Earthquake Engineering (NCREE) provided mentoring, work experience, commercial test data and manufacturing details. All these groups helped ensure the outcomes of this research are useful for the wider engineering community.

Thanks to Mechanical Engineering department, my supervisory teams, and administrative staff for their support and responsiveness. Whenever I had an issue, a query or request for resources it was never a problem. This made all the difference, especially in difficult times. Special thanks to the technical IT staff, particularly Paul Southward, Olive Dalton and Francois Bissey who provided me with the resources and help I needed. This was especially challenging during the set-up of the new computer cluster and during the Covid lockdown period.

To my many friends who have encouraged me along the way. Doctoral research is all-consuming at times and is filled with long stretches of getting it wrong. Thank you for helping restore my confidence and reminding me about all the life outside of my cubicle.

To my immediate family, I am so very fortunate to have you. The past five years has been a long and winding road but your love and support has helped me endure and continue to strive for my goals. I dedicate this to you.

Dan Court-Patience

31th May 2021

CO-AUTHORSHIP

Deputy Vice-Chancellor's Office
Postgraduate Research Office

UNIVERSITY OF CANTERBURY
Te Whare Wānanga o Waitaha
CHRISTCHURCH NEW ZEALAND

Co-Authorship Form

This form is to accompany the submission of any thesis that contains research reported in co-authored work that has been published, accepted for publication, or submitted for publication. A copy of this form should be included for each co-authored work that is included in the thesis. Completed forms should be included at the front (after the thesis abstract) of each copy of the thesis submitted for examination and library deposit.

Please indicate the chapter/section/pages of this thesis that are extracted from co-authored work and provide details of the publication or submission from the extract comes:

Chapter 1: D. Court-Patience, M. Garnich and A. Lovisa, "Design Review of Diagonal Buckling-Restrained Braces in New Zealand", Published and presented, 12th Pacific Structural Steel Conference Tokyo, Japan, November 9 -11, 2019

Chapter 2: D. Court-Patience and M. Garnich, "Experimental Testing Results of Commercially Available Buckling-Restrained Braces", presented, SESOC conference, Auckland Aug 19.

D. Court-Patience and M. Garnich, "Evidence Collected for Peer Review of Buckling-Restrained Braced Frames in New Zealand", Published, NZSEE Bulletin September 2021, https://doi.org/10.5459/bnzsee.54.3.197-210.

Chapter 3: D. Court-Patience and M. Garnich, "FEA Strategy for Realistic Simulation of Buckling-Restrained Braces", Published, Journal of Structural Engineering ASCE, February 2021. *DOI: 10.1061/(ASCE)ST.1943-541X.0003033*

Chapter 4: D. Court-Patience and M. Garnich, "Predicting Yielding of Gusset Plates in Seismic Frames using Finite Element Modelling", Published, NZSEE conference proceedings April 2020. *https://repo.nzsee.org.nz/handle/nzsee/1719*

D. Court-Patience and M. Garnich, "Buckling Analysis of Gusset Plates with Bolted Connections using Finite Element Modeling", Published, Journal of Constructional Steel Research ELSEVIER, November 2020. *DOI: 10.1016/j.jcsr.2020.106420*

Chapter 5: D. Court-Patience and M. Garnich, "Stability of Diagonal Buckling-Restrained Braced Frames using Finite Element Modelling", submitted, Journal of Constructional Steel Research ELSEVIER, September 2021

Please detail the nature and extent (%) of contribution by the candidate:

The candidate was the primary author and did all of the work included in the publications under my supervision.

Certification by Co-authors:

If there is more than one co-author then a single co-author can sign on behalf of all.

The undersigned certifies that:

- **The above statement correctly reflects the nature and extent of the Doctoral candidate's contribution to this co-authored work**
- **In cases where the candidate was the lead author of the co-authored work he or she wrote the text**

Name: *Associate Professor Mark Garnich*

Signature: 

Date: *31 May 2021*

TABLE OF CONTENTS

LIST OF FIGURES

LIST OF TABLES

LIST OF TERMS

Steel material parameters

$\boldsymbol{\sigma}$	Axial stress
$\boldsymbol{\sigma}_y$	Yield stress
ε	Strain
ε_{pl}	Plastic strain
$\boldsymbol{n}$	Normal direction
k	Yield stress
$\boldsymbol{X}$	Tensor variable of kinematic hardening
$\boldsymbol{C}$	Initial hardening modulus
Υ	Fading memory effect of the strain path
$\boldsymbol{J}\ (\sigma\text{-}k)$	Yield surface
$\boldsymbol{J}\ (\sigma)$	Limit surface
$\boldsymbol{\alpha}$	Backstress curve for non-linear hardening modelling

Concrete material parameters

$\boldsymbol{E}$	Elastic modulus.
$\boldsymbol{\sigma}_{yc}$	Compressive yield stress
$\boldsymbol{\sigma}_{yt}$	Tensile yield stress
φ	Dilation angle - measured in the p-q plane at high confining pressure. Controls an amount of plastic volumetric strain developed during plastic shearing
ε	Eccentricity - defines the rate at which the functions approach asymptote.
$\boldsymbol{\sigma}_{b0}/\boldsymbol{\sigma}_{c0}$	Ratio of initial equibiaxial to initial uniaxial compressive yield stress.
K	Ratio of the second stress invariant on the tensile meridian to the compressive meridian.
μ_c	Viscosity parameter – Causes the consistent tangent stiffness of the softening material to become positive for sufficiently small time increments, thereby reducing convergence issue.

Surface contact interaction parameters

$\boldsymbol{Po}$	Pressure when clearance equals zero
Co	Clearance when pressure equals zero
μ	Static friction coefficient

Load parameters

$\pm\Delta_{by}$	Yield displacement amplitude
$\pm\Delta_{bm}$	Axial displacement as a function of the design storey drift
β	Strain hardening adjustment factor
ω	Compressive strength adjustment factor
$\boldsymbol{N}^*$	Axial load
$\boldsymbol{N}_y^*$	Yield load
$\boldsymbol{N}_t^*$	Axial design load in tension
$\boldsymbol{N}_c^*$	Axial design load in compression
$\boldsymbol{T}_{2\Delta_{bm}}$	Axial tension load used in the design of BRB frame elements
$\boldsymbol{C}_{2\Delta_{bm}}$	Axial compression load used in the design of BRB frame elements

Geometric parameters

A_{core}	Cross sectional area of a BRBs core plate
b_e	Effective width used to predict yielding of a gusset plate
$b_{bolt\ array}$	Width between the centers of the outer bolts in a bolted array
$L_{bolt\ array}$	Length between the centers of the outer bolts in a bolted array
$L_{1,3}$	The outer lengths as per the Thornton length method.
L_2	The mid length, using the Thornton length method.
L_{avg}	The average of all three lengths, using the Thornton length method.
L_{el}	The elastic buckling length, determined from the elastic member stiffness from axial force-displacement response from each simulation.
L_i	Initial length

L_f	Final length
h_i	Initial height
h_f	Final height
b_i	Initial width
Δ_m	Displacement relative to frame height i.e. 1%, 2% etc.

BRB stability parameters

$N^R{}_{cr}$	Elastic buckling of the cruciform section
L_0	The total diagonal length (working point to working point)
ξ'	Total length of the cruciform of BRB divided by the total diagonal length
ξ	Exposed length of the cruciform of BRB divided by the total diagonal length
EI_B	Flexural stiffness of the restrainer (grout + steel casing)
Υ_J	Flexural stiffness of cruciform divided by flexural stiffness of restrainer
$\xi\kappa_{Rg}$	Normalised rotational stiffness of the gusset
λ	Slenderness ratio of the gusset
i_g	Radius of gyration of the gusset plate
I'	Second moment of area of the gusset
A'	Effective yielding area of the gusset
a_r	Initial imperfection at the restrainer end
y_r	Additional out-of-plane displacement due to compressive loading
N_{cr}^B	Maximum elastic buckling capacity
N_{cr}^r	Inelastic compressive capacity of the BRBs end connection
M_p^r	Plastic moment capacity of the limiting failure mechanism
i_c	Radius of gyration of the connection zone
s_r	Thickness of debonding material or gap between core and restrainer at rest

$\emptyset_0$	Construction tolerance
$M^r{}_0$	Bending moment due to out-of-plane drift
δ_0	Out-of-plane displacement
L_{in}	Insert length of the cruciform section
N_{cu}	Ultimate strength of the BRB core
M_p^g	Plastic moment of the gusset plate
N_{lim1}	Stability limit path assuming the gusset plates remain elastic under collapse
N_{lim2}	Stability limit path assuming plastic hinges in the gusset plates under collapse
L_{neck}	Exposed cruciform length
L_{rest}	Length of the restrainer
B_w	Width of the cruciform

1 BACKGROUND AND MOTIVATION

In moderate to severe earthquakes, ductile building design prioritizes life safety of its occupants by anticipating and avoiding collapse mechanisms. However, for buildings to absorb energy from these moderate to severe earthquakes, they often experience extensive yielding and deformation. This was the case in Christchurch, New Zealand during 2010/2011, where even though recorded ground accelerations were up to twice the expected design level (Bradley 2012), only two buildings experienced catastrophic failure. Importantly, the CTV building had several design failings and neither the CTV or the Pyne Gould Corporation building were deemed to have met current structural design requirements (Jury 2011, Fenwick et al. 2020). This means that the vast majority of buildings in Christchurch performed as intended even though a significant rebuild of Christchurch was required. This rebuild, still not completed almost 10 years later, has prompted the engineering community to seek out alternative and innovative designs to control damage in addition to prioritizing life safety.

Buckling-restrained braces (BRBs), form a structural bracing system that provides lateral strength and stiffness for a building, as well as the ability to absorb large amounts of energy. First developed in Japan in the late 1970s they gained rapid acceptance in the US after the 1994 Northridge Earthquake (Watanabe et al. 1973, Kimura et al. 1976, Rabbat et al. 1985, Bruneau et al. 2011). The majority of BRBs used commercially are proprietary off the shelf products. To reduce damage to other building components, BRBs are designed to be the yielding element that can to be replaced following a severe earthquake. With the destructive power of earthquakes forced into the public eye following the Canterbury earthquakes of 2010/11, BRBs quickly become a popular design choice in the New Zealand construction market (MacRae et al. 2017).

BRBs behave very differently to traditional steel bracing systems. BRBs may seem simple in principal, where a slender steel core yields inside a restrainer, which suppresses global buckling in compression. However, to achieve large energy dissipation BRBs experience highly non-linear behaviour that is difficult to observe, study and predict. Other countries have a longer history of implementing BRBs. Japan and Taiwan have included in their design codes strict rules related to the design of buckling-restrained braces frames (BRBFs) and have developed their own methods to assess combined BRB and gusseted connection stability. This reduces the amount of variation among BRBF designs, often requiring stiffened connections and instructs structural engineers on how to incorporate BRBs into their buildings (Takeuchi et al. 2017) (NCREE 2014). Internationally, few design codes have this governance. From the above discussions, it can be said that there is a need to study the behaviour of deforming BRBs and how they interact with different connection types. Specifically to highlight areas of risk, where unwanted failure may occur and to suggest ways to overcome these.

This research project started out as an experimental endeavor. The aim was to test a series of full-scale BRBFs using BRBs made in New Zealand, and observe how they would behave in a maximum considered earthquake event. It then evolved into a finite-element modelling effort aimed at better understanding what was happening

on the interior of these BRBs. That, in turn, evolved into trying to understand how such models could benefit those who incorporate BRBs in their building designs and aspects specific to qualifying BRBs in New Zealand. As a consequence, much of the discussion revolves around New Zealand design practice while many of the conclusions are more generally applicable to BRB technology.

1.1 **Scope**

To improve the safety and design of BRBFs in New Zealand, this research uses high fidelity modelling to study BRB behaviour and how they interact with other frame components. Design methods of the gusseted connections are also examined. This project partnered with the Building Research Association of New Zealand (BRANZ) and was supported by Callaghan Innovation to ensure outcomes were related to industry requirements. The results and evidence in this dissertation can be used to inform committees and working groups in preparing design guidance for the marketplace and structural engineers.

Objectives of this research aimed to make progress toward addressing the needs stated above. In particular, answers were sought to the following questions, which formed the framework of this research:

When using steel-concrete BRBs in a diagonal configuration within a steel frame:

1) What are the common procedures and considerations that are followed in New Zealand for the design of BRBFs?

2) Is prequalification testing alone adequate to demonstrate appropriate performance during design level earthquakes?

3) How does the BRB core interact with the restrainer under loading, and what effects does this have on performance?

4) What is considered in gusset plate design and what is the suitability of these methods in BRBFs?

5) What criteria are required when designing connections of a BRBF to ensure appropriate performance during design level earthquakes?

1.2 **Organization of thesis**

This thesis has been written as a collection of seven chapters, each largely represent a conference or journal paper submission (thesis with publications). In order for each chapter to be read independently, there is some minor repetition between the introductory sections. A separate list of references for each chapter has also been provided. The motivation, objectives of this research and introduction are described here in **CHAPTER 1**. Chapters 2, 3, 4 and 5 aim to address each of the five research objectives.

CHAPTER 2: BRBs have shown to perform well in uniaxial testing providing stable hysteretic performance. However, structural engineers in New Zealand are not yet well versed in all the nuances of BRB design and testing and test data for BRBs manufactured in New Zealand are not publically available. As such, this chapter presents the process and results of prequalification testing for five commercially available BRB architypes. This type of testing isolates the brace, checking manufacturing and design details under ideal conditions. This chapter also discusses the manufacturing process, testing conditions and limitations of prequalification testing.

CHAPTER 3: Due to the core of BRB being concealed by its restrainer, studying the local deformation of a BRB core as it interacts with its restrainer and the implications this has on connecting frame elements is difficult to observe, study and predict in physical testing. Continuum modelling offers a way to study this local deformation and stress-strain behaviour. Chapter 3 presents a novel strategy for modelling generic BRBs that captures realistic BRB behaviour. This strategy was only requires shop drawing and material test data to calibrate. Experimental data from Chapter 2 was used for validation. This modelling strategy forms the foundation for simulating the performance of other generic BRB designs and how they interact with other frame components

CHAPTER 4: Next, the suitabilty of current design methods used to size gusset plates against local failure and instability are investigated. Specifically, finite element modelling is used to study the development of yielding, buckling and plastic collapse behaviour of a brace end bolted to a series of corner gusset plates. Of interest is how different geometric features of a gusset, such as the size of the connection area, shape of the gusset plate and angle of inclination affect yielding and buckling behaviour.

CHAPTER 5: Further to brace prequalification testing, it is important to consider both local and global stability of a BRB and its gusseted connection zone. Chapter 5 investigates combined BRB and frame behaviour using FEA. Detailed models use the strategy presented in Chapter 3 to capture the realistic behaviour of a deforming BRB with the addition of frame components. The effect of bi-directional loading is also evaluated. Results are compared against existing analytical methods for assessing the out-of-plane stability of BRBFs.

CHAPTER 6/7: Chapter 6/7 are stand-alone chapters. Chapter 6 summarises the research presented within this thesis. The novel contributions made and the significant research outcomes that are presented in the earlier chapters are restated. Chapter 7 contains suggestions for future research.

1.3 **Introduction**

Extensive earthquake damage to structural braced frames without ductile detailing has led to 'seismic specific' steel braced frames. These seismic specific braced frames provide improved lateral support, stiffness and energy dissipation to buildings vulnerable to earthquake loads (AIJ 1995, Tremblay et al. 1995, Tremblay et al. 1996). Extensive research and guidance into these systems has continued over several decades. A buckling-restrained braced frame (BRBF) is one of these braced systems and is the focus of this dissertation. However, firstly introduced are other types of seismic specific steel braced frames, that unlike BRBFs have been steadily incorporated into modern design codes worldwide.

Special concentrically braced frames (SCBFs) are an advancement on the traditional concentrically braced frame (CBF). Guidance on SCBFs were first developed in 1997. The aim is to maximize the inelastic drift capacity of a CBF, through controlling the reduction of the inelastic response. SCBFs commonly target interstorey drifts of 2.5% before brace fracture. The primary deformation mechanisms are buckling and plastic deformation of the diagonal brace. For these mechanisms to occur and remain stable at larger lateral drifts, rules are provided. These rules include how to proportion the web thickness of each frame element, how to size its gusset plates, and how to account for brace slenderness for different types of frame configurations. These rules aim is to reduce the chance of weld tearing and web damage of the beam or column, and to enable out-of-plane bending of the gusset plate to occur, instead of the brace ends (which is unfavourable).

SCBFs still exhibit different load carrying capacity between compression (buckling) and tension (yielding). This behaviour means the inelastic response of the brace degrades after each cycle (Figure 1-1b). To account for this non-ideal inelastic behaviour, many design codes increase the lateral force coefficient applied to the building (Standards New Zealand 1997). This larger lateral force coefficient means larger members are required. When sizing the beam in an SCBF, there are two possibilities: (1) The beam is strong enough to resist the unbalanced brace force, in which case you will get hinges at the column bases and beam column joints and yielding in the braces or (2) The beam is not strong enough to resist the unbalanced brace force and you will get hinges at the column bases and beam column joints as well as a hinge in the beam. However, the SCBF system is still generally considered an economical system for use in low-rise buildings within areas of high seismicity. They are also popular because designers and fabricators have experience with this system (NEHRP 2013). Figure 1-1 demonstrates the theoretical improvement in cyclic performance a SCBF has compared to a CBF.

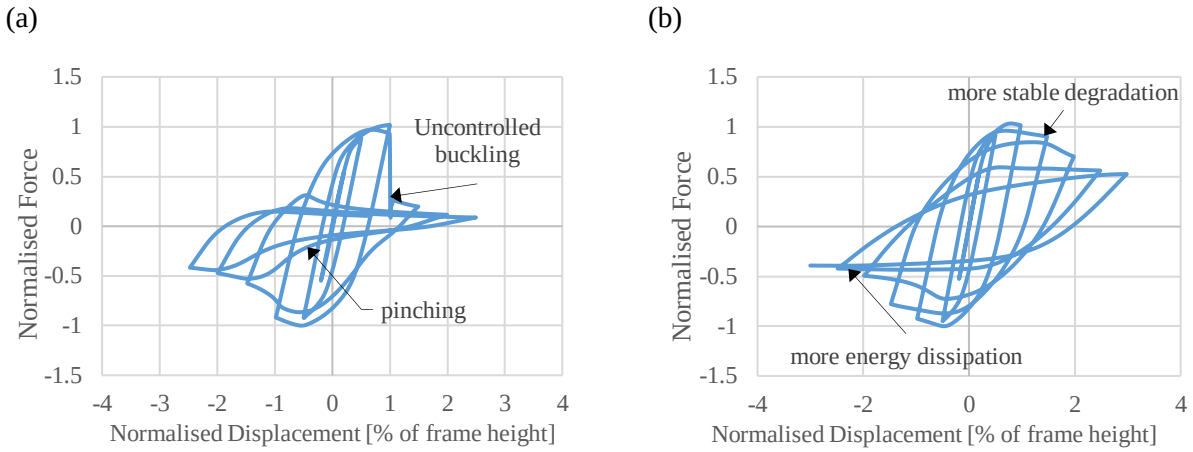

Figure 1-1. Idealised theoretical cyclic performance of braced frames (up to 3 times storey drift)
(a) CBF, (b) SCBF

Eccentrically Braced Frames (EBFs) are different to SCBFs in that a beam link (eccentric link) between the brace and connection zone is incorporated. This link is designed to rotate and yield due to bending and can be flexure dominant or shear dominant. To achieve more stable hysteresis and larger ductility, EBFs should be shear dominant whereby the length of the active link is short with flange stiffeners included at intervals within the link. When designing EBFs, structural engineers need to consider the rotation of the shear link and continuity of this action with the floor diaphragm. In addition, web sections should be large enough to reduce the chance of buckling, and welds should be sized to minimise tearing. Figure 1-2 compares the theoretical cyclic performance of an EBF with a flexure dominant link, and an EBF with a well detailed shear dominant link.

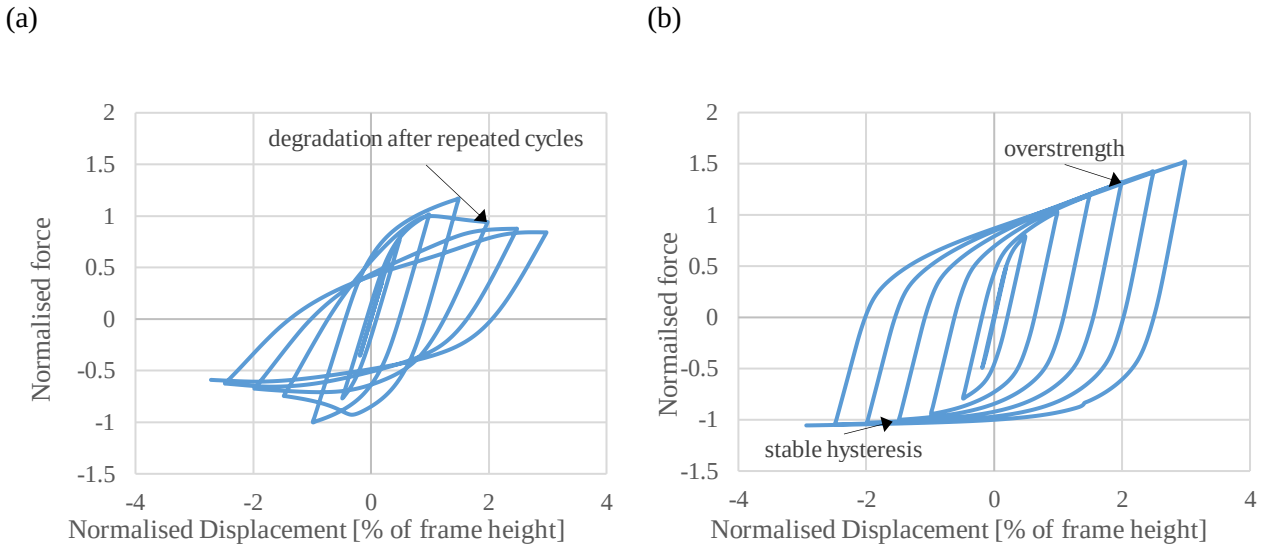

Figure 1-2. Idealised theoretical cyclic performance of braced frames (up to 3 times storey drift)
(a) EBF (flexure dominant), (b) EBF (shear dominant with flange stiffeners)

BRBFs are an addition to options of steel braced frames and were first developed in Japan in the late 1970s (Watanabe et al. 1973, Kimura et al. 1976, Rabbat et al. 1985, Bruneau et al. 2011). Figure 1-3 highlights where in Christchurch some of these systems have been implemented in the wake of the 2011 Christchurch earthquake.

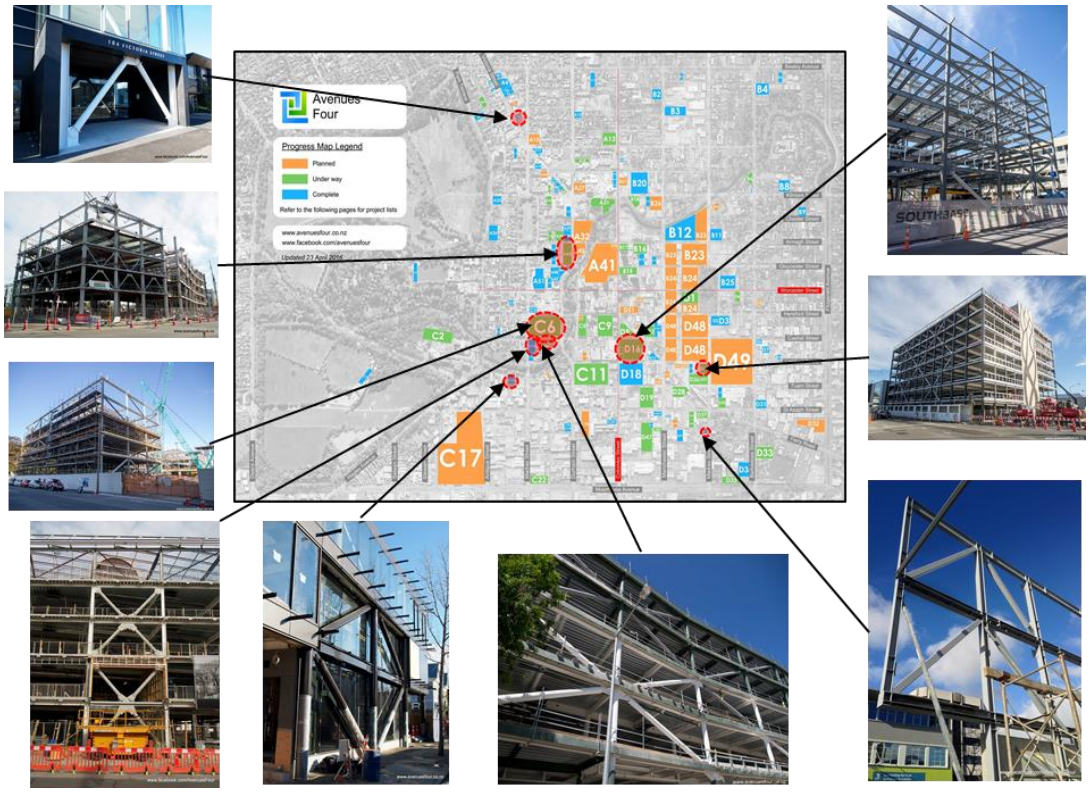

Figure 1-3. Map and images of BRBs located in Christchurch city (Avenues Four 2014)

Similar to a SCBF, a BRBF is also a horizontal load resisting structural frame where a brace is connected diagonally using gusseted connections. However, a BRB is used in place of a standard structural member (I section, angle or square section). A BRB is generally a propriety member, and is designed to yield almost evenly in both tension and compression over large displacements. A BRB has a slender steel core that carries the axial load and deforms inside a restrainer. This restrainer provides high bending stiffness to resist buckling. In tension, the core stretches, exhibiting strain hardening and a reduction in cross sectional area. In compression, the specimen is also configured for axial ideal loading. However, the slender nature of the steel tendon and de-bonded contact with the restrainer results in constrained buckling. This generally progresses through several modes of buckling as compressive uniaxial displacement of the specimen increases. These two behaviours (axial compressive and bending due to constrained buckling) are superimposed. Figure 1-4 illustrates the idealised behaviour of a BRB in tension and compression. There are different BRB variations offered across the market, with options that include different restrainer designs, multi-plate/layered cores, different connections and frame configurations.

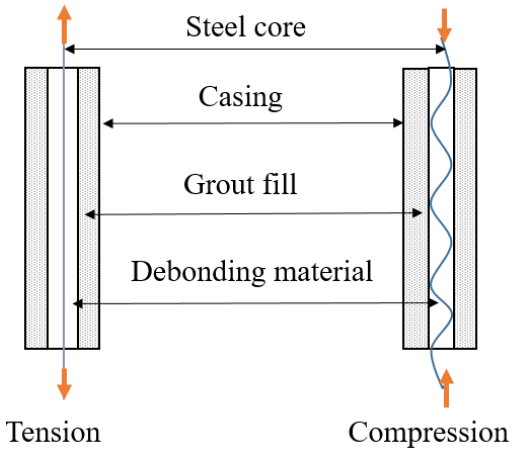

Figure 1-4. Schematic of BRB behaviour

Each type of braced frame develops plasticity and damage differently. Figure 1-5 presents a schematic of the idealised deformation of the different braced frames discussed. Each figure depicts the original and deformed shapes, and highlights the main zones of plasticity that occur under horizontal displacement. Similar to EBFs with well-detailed short links, BRBFs has been shown to achieve stable and almost even energy dissipation for cyclic loading up to 3% interstorey drift. BRBFs are also becoming a popular choice as they are marketed or perceived to be a "low damage" solution with characteristics to perform well during a large earthquake and significant aftershock events. BRBFs are also attractive, as they do not have the same detailing and proportioning requirements that EBFs and SCBFs do, which drive up project costs. BRBFs are also more flexible compared to SCBFs, this means the horizontal design action coefficient (to calculate the seismic load) is also lower. Both the non-ideal inelastic response and stiffness of SCBFs relative to BRBFs mean the size of the members required for SCBFs are larger. An advantage, BRBFs have over EBFs is that they do not need to account for the rotation of the eccentric link. This rotation can have implications with the floor diaphragm and can be difficult and expensive to replace after damage. However, unlike SCBFs and EBFs, design responsibility of a BRBF is generally shared. This requires the engineering consultants (designing the building) and BRB suppliers to work together, with testing and peer review required to gain building compliance in New Zealand. Design guides and standards around the world usually focus on system-level design, with only some including provisions for BRB design. Regardless, in almost all jurisdictions the brace itself is treated as a proprietary product that must conform to testing requirements. Cost implications of review, testing and lack of industry knowledge are a current disadvantage when designing with BRBFs.

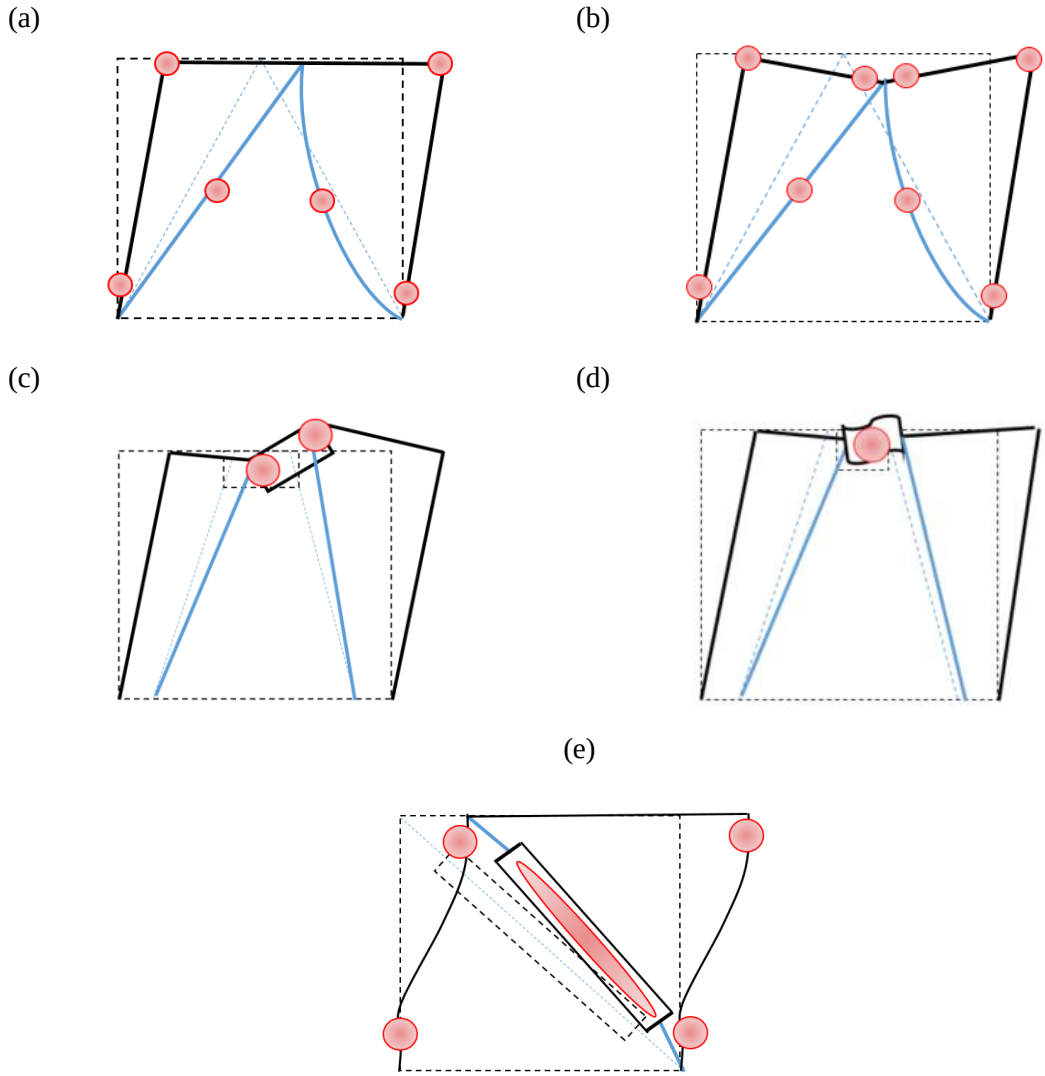

Figure 1-5. Idealised deformation and plastic hinge location of typical seismic steel frames
(a) SCBF (with strong beam), (b) SCBF (with weak beam),
(c) EBF (flexure dominant) (d) EBF shear dominant,
(e) BRBF

1.3.1 **Composition and manufacturing of a BRB**

A BRB is a fabricated assembly commonly consisting of a ductile-grade steel core plate designed as the main yielding section. A steel tube encases the core, which acts as permanent formwork for grout contained within. To restrict excessive movement of the restrainer in relation to the centre of the brace, a shear key in the centre of the core exists. To promote independent movement of the core and the restrainer, the core is intentionally de-bonded from the grout and casing. This is achieved by wrapping the core in a thin film-like material that creates a low friction gap between the core and the restrainer. The area of the BRB core is sized for the applied seismic load for that frame using the cross-sectional area of the core multiplied by the material yield strength. Other types of cross-sections, such as cruciform or multiple plates are also used. Shown in Figure 1-6 is a schematic of the key components of a BRB with pinned end connections. Not shown is the concrete that fills the space between the core and the casing. The polystyrene spacers help promote core movement independent of the restrainer.

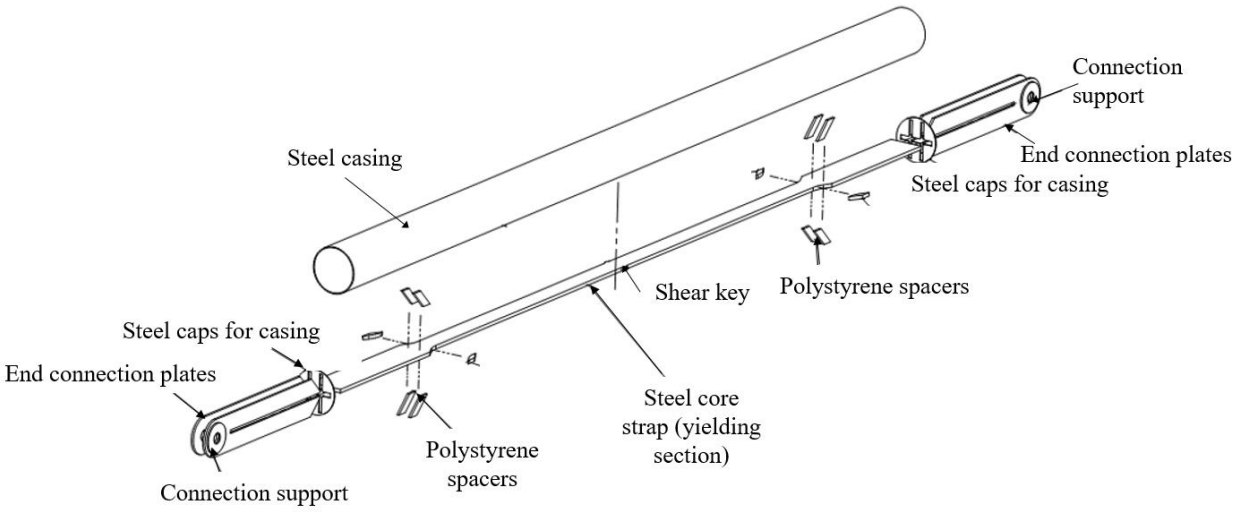

Figure 1-6. Example of components for a BRB

BRBs appear simple enough. However, BRBs experience highly non-linear behaviour inside the restrainer, particularly in compression. Performance and stability conditions are sensitive to changes in geometry, material and construction. Ideally, the manufacturing process for the range of BRBs is standardised for the different BRB architypes, with only geometric dimensions differing among design types. Figure 1-7 presents the assembly of a BRB from different views.

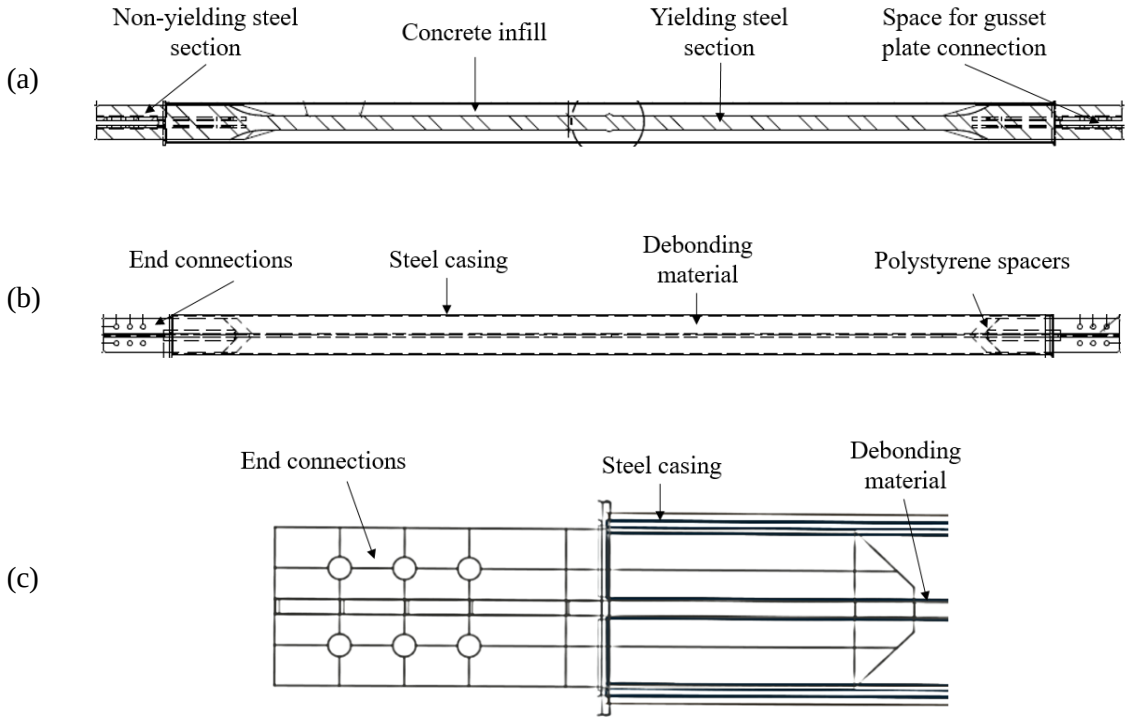

Figure 1-7. Example of components for a BRB
(a) plan view, (b) side elevation, (c) side elevation (close up with end connection)

In the manufacturing of a BRB, initially the end connections and core are cut from one piece of steel. These parts are welded together. A debonding material is applied to the external surface of this welded section. A steel casing is made by folding or bending a sheet of steel to form the desired shape. Polystyrene spacers are attached to the transition zone of the tapered zones of the welded core section. The spacers create a zone free of concrete that allows the core to deform under compressive loading without pressing directing onto the restrainer. This reduces damage to the concrete restrainer. The welded core section is placed in the centre of the casing and fixed in place with an end cap. Once in place, cement-based grout is poured in the mould made by the core and steel casing. The restrainer is then sealed by the other end cap. Once the grout has cured the BRB is complete.

In general, all BRBs work on the same mechanical principles. However, designs vary due to form, function and cost. For example, the geometric dimensions are sized for specific construction projects and connections types vary depending on the structural design strategy, cost and construction environment.

1.3.2 **Previous testing**

Product validation testing by BRB manufacturers has resulted in a large number of successful uniaxial and subassemblage tests. However, the majority of these subassemblage tests may suffer from a reporting bias with only successful tests reported due to their proprietary nature. This being said, several independent full-scale 3D frame and numerous subassemblage tests have demonstrated that well designed BRBs can perform satisfactorily in design level earthquake events (Fahnestock et al. 2007, Vargas et al. 2009, Kasai et al. 2010). Good performance was also observed in a building with BRBs following the 2011 Tohoku, Japan earthquake (Architectural Institute of Japan (AIJ) 2014)

Major designers and manufacturers of BRBs include CoreBrace in the United States, Nippon Steel in Japan and NCREE in Taiwan. Due to the confidential and proprietorial nature of BRBs, failed tests are rarely made available to the public. Good performance is indicated by stable energy dissipation. The following experimental studies show good performance. At UC Berkley, five BRB specimens were tested (Black et al. 2002). These BRBs achieved post-yield loads of between 1800 kN and 2700 kN and had core lengths of 4500mm. The test results demonstrated good performance under various load histories including large displacement and low cycle fatigue protocols. Figure 1-8 presents the specimens tested and Figure 1-9 shows the test set up used.

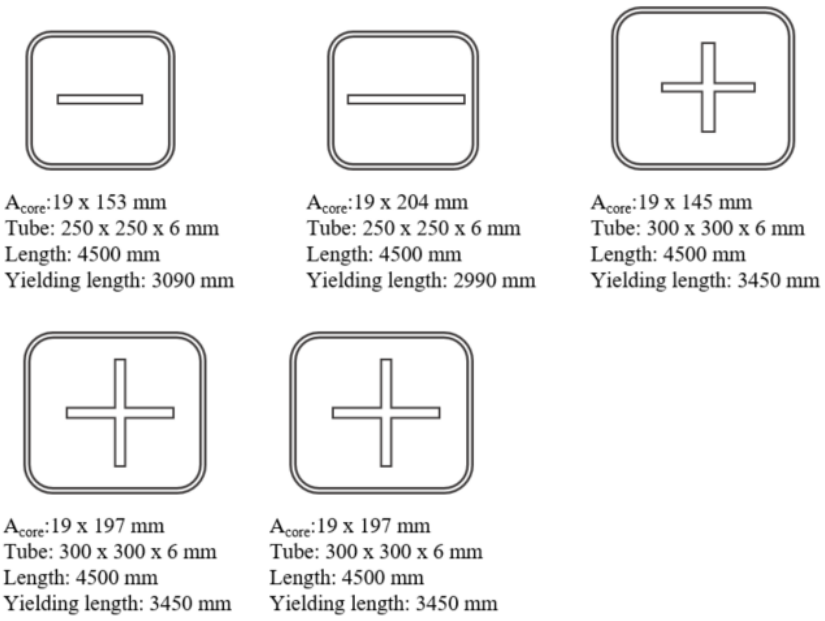

Figure 1-8. Specimens tested at UC Berkley (Black et al. 2002)

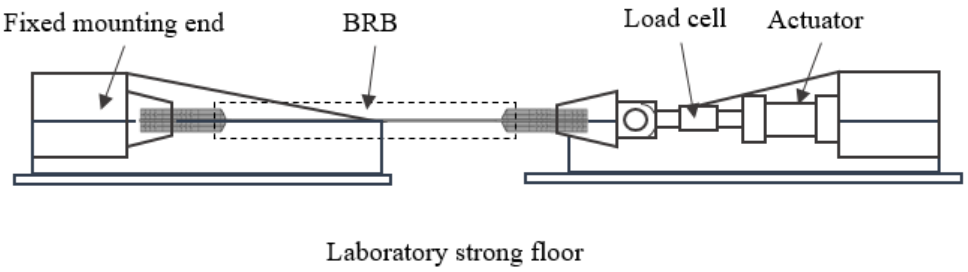

Figure 1-9. Schematic of experimental test set up for specimens tested at UC Berkley (Black et al. 2002)

In addition to these groups, Star-Seismic (now CoreBrace) tested two BRBs at the Budapest University of Technology and Economics. Testing was in accordance with the European Standard for Anti-seismic devices (EN 15129). Results showed that the two brace specimens performed well (Dunai et al. 2011). With a core area of 20x40 mm^2 and an average yield strength of 240 kN, these braces would be deemed as relatively small. Testing of each BRB occurred vertically as depicted in Figure 1-10.

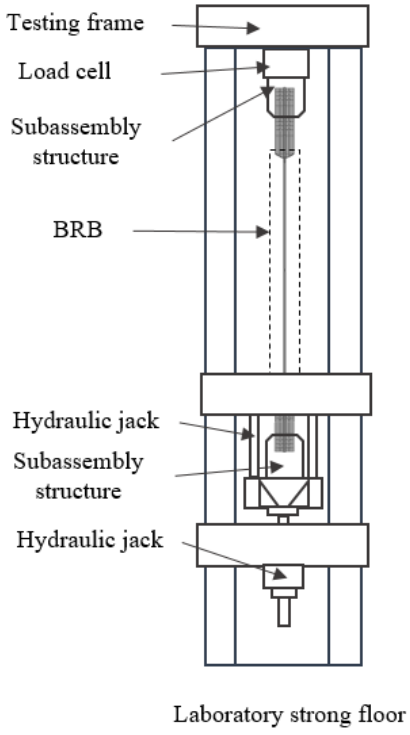

Figure 1-10. Schematic of test set up conducted for CoreBrace (Dunai et al. 2011)

Global stability is another important BRB consideration and general requires subassemblage testing. This type of testing can include eccentric loading of partial systems, full frame or complete storey specimens. Evidence following the 2011 Tōhoku Earthquake (Hikino 2016) and from several full frame tests have shown BRBFs to perform well. Japan has conducted several subassemblage test including partial or full frames. Figure 1-11 depicts the cross-sections of some of the documented BRBs tested in Japan.

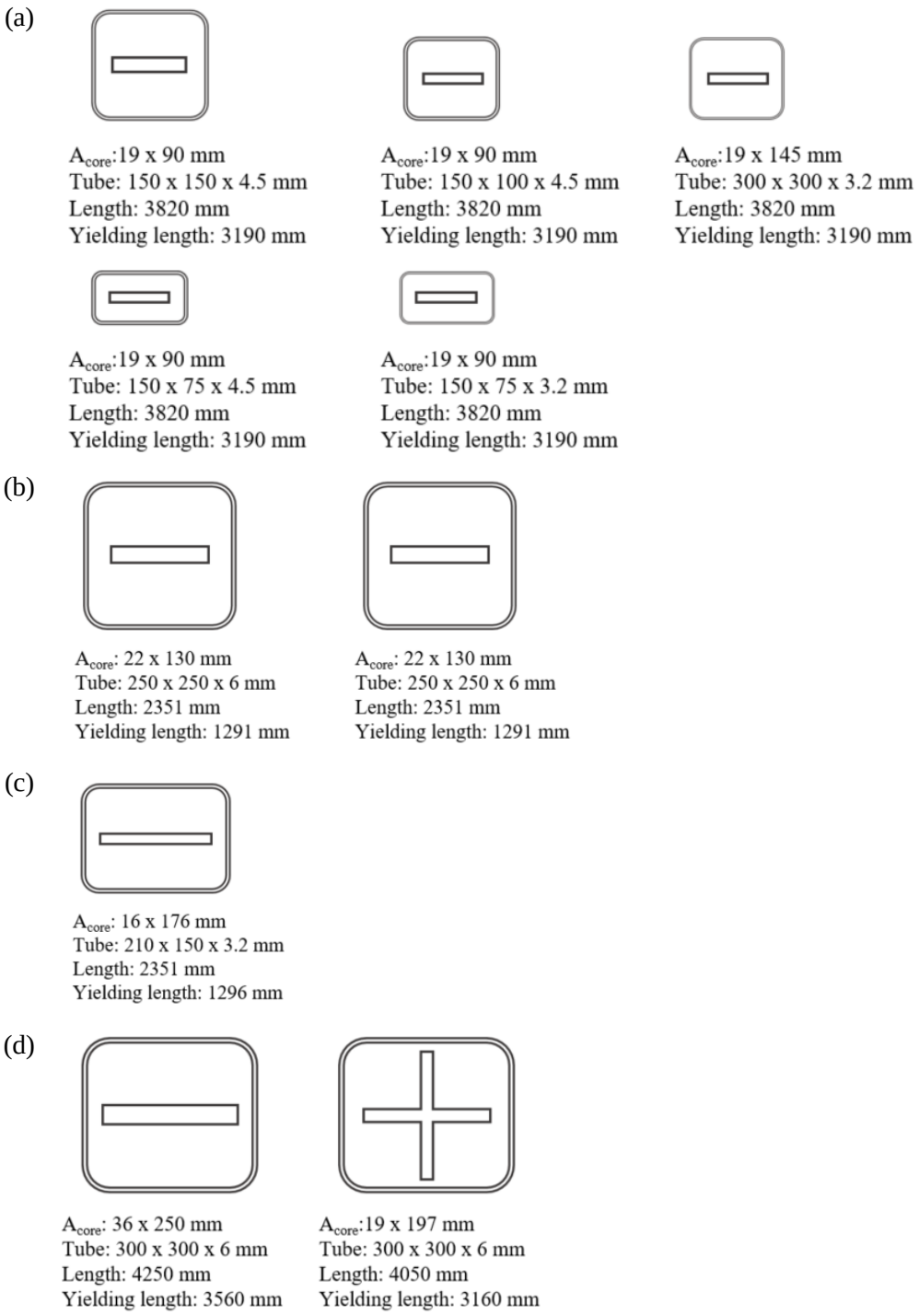

Figure 1-11. BRB specimens tested by Japanese investigators
(a) (Watanabe et al. 1988, Wada et al. 1989, Watanabe 1992), (b) (Hasegawa et al. 2000),
(c) (Konami et al. 1999), (d) (Iwata et al. 2000)

Other successful subassemblage tests include six un-bonded BRBs tested in Canada. The average design yield load of the six BRBs was 587kN. Testing followed a quasi-static cyclic protocol similar to that prescribed in the American standard of seismic provisions for structural steel buildings (ANSI/AISC 341-16) (Tremblay et al. 2006). Figure 1-12 presents the experimental set up used for these tests.

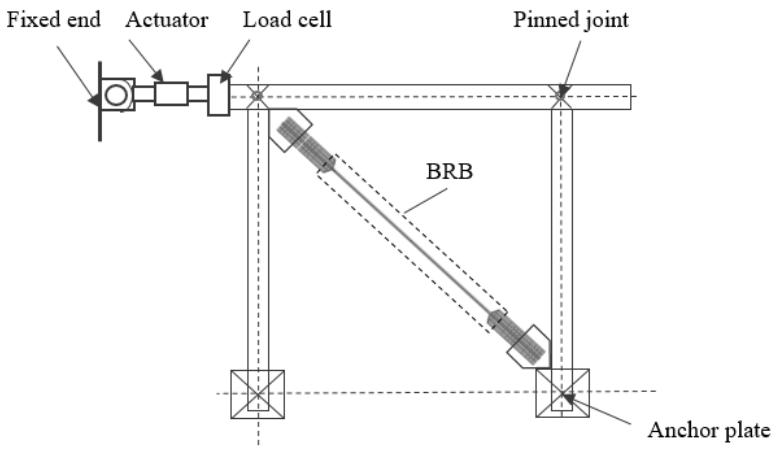

Figure 1-12. Schematic of test set up (laboratory at Ecole Polytechnique of Montreal) (Tremblay et al. 2006)

A similar test set-up was used at the University of Washington where six single storey, one-bay planar frames were tested using Star Seismic braces. All tests displayed excellent hysteretic behaviour with good energy dissipation up an average strain of 2.2% drift. The large displacements causes out-of-plane buckling to occur in the web and flange of the beam adjacent to the gusseted connection, which led to the failure of the BRBF. This suggests that flexible connection designs are more at risk during severe earthquake loads (Palmer et al. 2014).

Another experimental investigation that included both a bolted and pinned BRBF was undertaken at the University of Auckland. The BRBs were designed and manufactured in-house with yield capacities between 200-250kN. The experimental test results showed stable hysteresis loops (Wijanto et al. 2014).

A few large multi-storey tests have also been conducted. In Taiwan a series of pseudo-dynamic tests of a three storey, three bay BRBF system was tested (Figure 1-13). The testing focused on investigating the structures overall behaviour as well the suitability of certain gusseted connections (Tsai et al. 2008). Results and findings helped refine the brace-on-demand software, a BRBFs design guidance tool used in Taiwan (NCREE 2014).

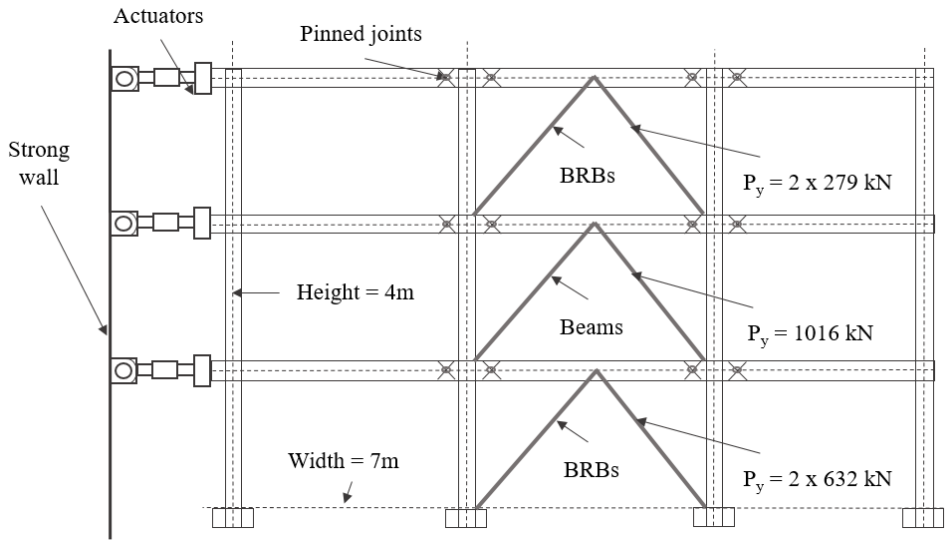

Figure 1-13. Schematic of large multi-storey testing of BRBFs (Tsai et al. 2008)

Similar other large scale BRBF tests were conducted at Lehigh University in the United States. The study investigated the performance of BRBFs with improved gusseted connection design. This testing demonstrated that improved gusset plate design can increase the performance of a BRBF to sustain severe seismic demands and maintain full-load carrying capacity.

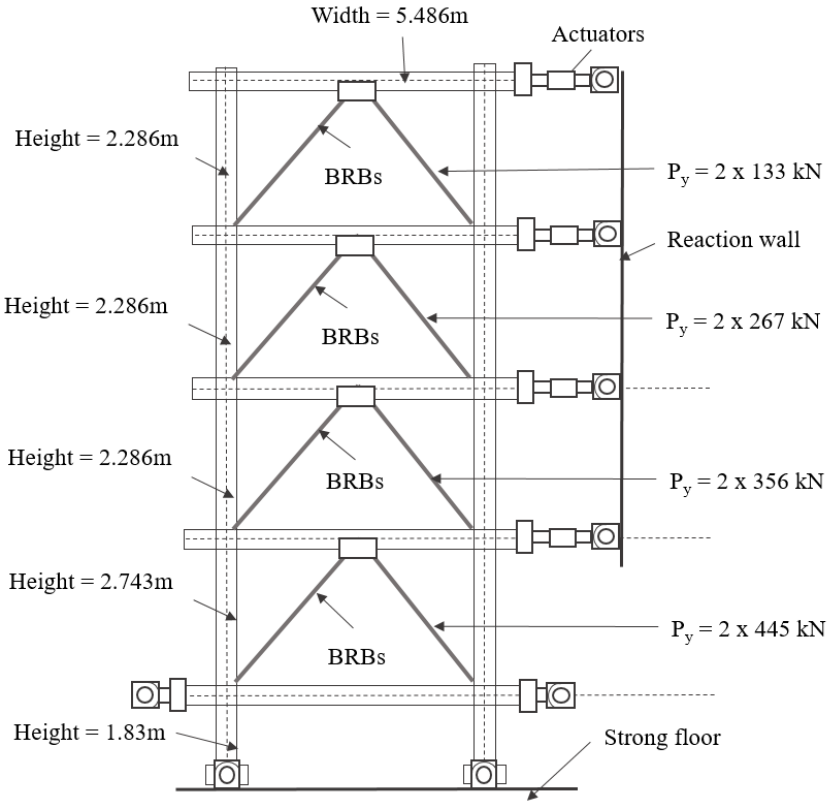

Figure 1-14. Large multi-storey testing of BRBFs (Fahnestock et al. 2007)
(a) Schematic of experimental test set-up, (b) Image during testing

1.3.3 **BRB designs considerations**

The experimental investigations presented in the previous section represent only a small number of studies conducted globally. Many research groups have contributed significant work and improved the safety and implementation of BRBFs worldwide. Figure 1-15 highlights the different BRB strength and stability considerations in orange.

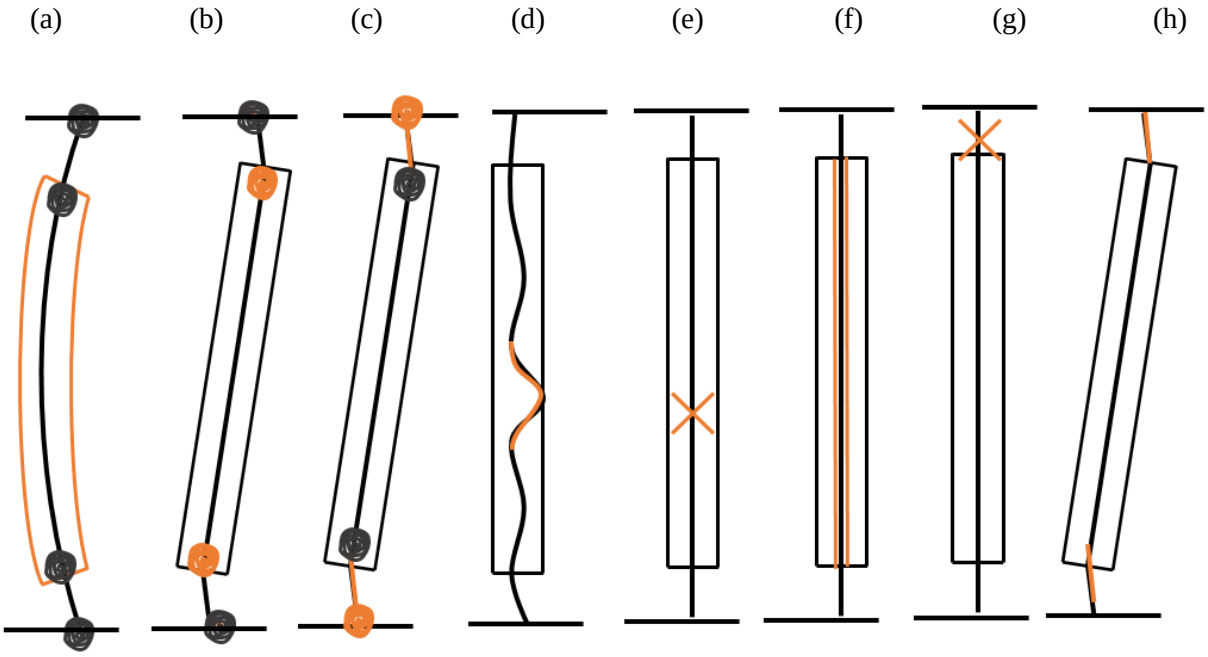

Figure 1-15. BRB strength and stability considerations (Takeuchi et al. 2017)
(a) global stability – restrainer, (b) global stability – restrainer end, (c) global stability – connections,
(d) higher mode buckling and bulging, (e) low cycle fatigue and fracture , (f) compression/tension ratio,
(g) connection strength, (h) rotation compatibility due to frame deformation

Physical testing has demonstrated BRBFs can perform well but the complexity of BRB behaviour makes it difficult to verify stability for all configurations and sizes without testing. Evidence in recent years has demonstrated particular failure mechanisms can occur at loads and displacements significantly less than anticipated by conventional design checks (Uriz et al. 2008, Kasai et al. 2010, Chou et al. 2012, Palmer et al. 2014, Lin et al. 2015, Westeneng et al. 2016). The following section discusses the failure mechanisms that need to be considered in BRBF design, and some of the challenges in predicting the strength and stability conditions illustrated in Figure 1-15.

1.3.4 **Global stability**

As BRBs resist high compressive loading, global stability and plastic collapse of the BRB and gusseted connection zone need to be considered. Generally, out-of-plane stability governs as the gusset zones are more flexible in this direction. Past research has highlighted the risk of global BRB buckling behaviour through connection failure (Tsai et al. 2008, Wigle et al. 2010, Zhao et al. 2011, Lin et al. 2012). In addition, several other tests have investigated the strength and stiffness requirements of gusseted connections in BRBFs (Chou et al. 2009, Eryasar et al. 2010, Chou et al. 2012).

When investigating the performance of a BRB and its gusseted connection zone, the research on the effect of bi-directional loading is limited. This particularly effects the ground storey where the base of the connections are fixed in both directions. This is unlike other levels that generally rotate less relative to each other when the building moves laterally. As the building moves out-of-plane, a flexural demand develops about the weak axis of the gusset plate. Figure 1-16 presents a schematic of in-plane and out-of-plane displacements.

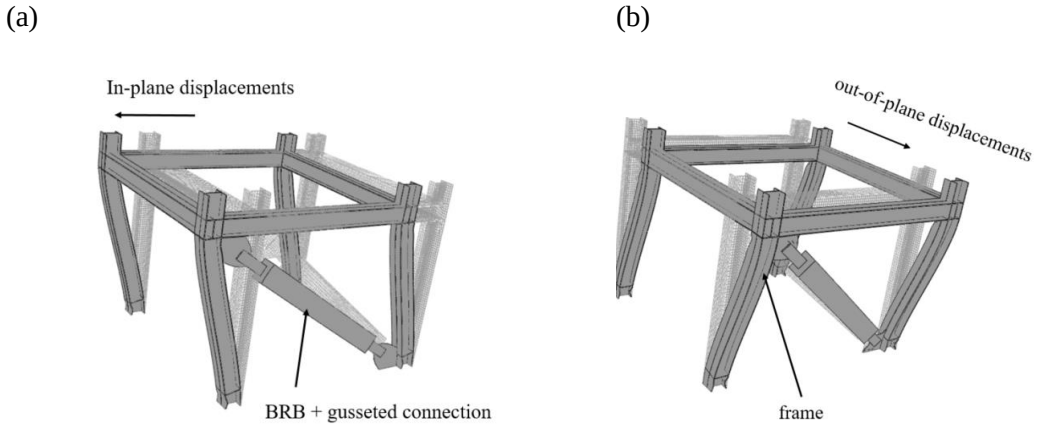

Figure 1-16. Schematic of bi-directional loads of a three dimensional structural frame (a) in-plane deformation of a BRBF, (b) out-of-plane deformation of a BRBF

Subassemblage testing is one way to assess global stability and plastic collapse. However, each subassemblage test can only investigate one specific design and load combination. As it is not practical to test every variation, results provided by manufacturers may be not represent the on-site conditions. For example, gusseted connections used in testing may be more rigid and the BRB geometries may misrepresent conditions on site.

Japan has developed an alternative approach to subassemblage testing and incorporated this approach into their design codes. The approach uses analytical methods to assess the out-of-plane stability of a BRBF system under different collapse mechanisms by focusing on moment transfer. The approach considers two stability design concepts proposed by Architectural Institute of Japan (AIJ) (2009).

1) The Cantilever Connection Concept (Figure 1-17a). This concept assumes a pin mechanism occurs at the BRB end connection/restrainer interface. This concept is only valid when the insert length of the non-yielding section of the BRB into the restrainer is low, such that a pin-like mechanism occurs under compressive loading. The method designs the end connection zone of the BRB with enough flexural stiffness to enable the core to reach its ultimate strength. Generally, for this design method to work, the BRB frame elements need to rigid, requiring substantially stiffened gusset plates and frame elements.

(2) Restrainer Continuity Concept (Figure 1-17b): This concept assumes moment transfer can occur between the restrainer and end connection. As a rule of thumb, this concept occurs when the insert length of the BRB end connection into the restrainer is equal to or greater than the width of the cruciform. This concept permits more economical designs as it permits slightly more flexible gusset plates and frame elements.

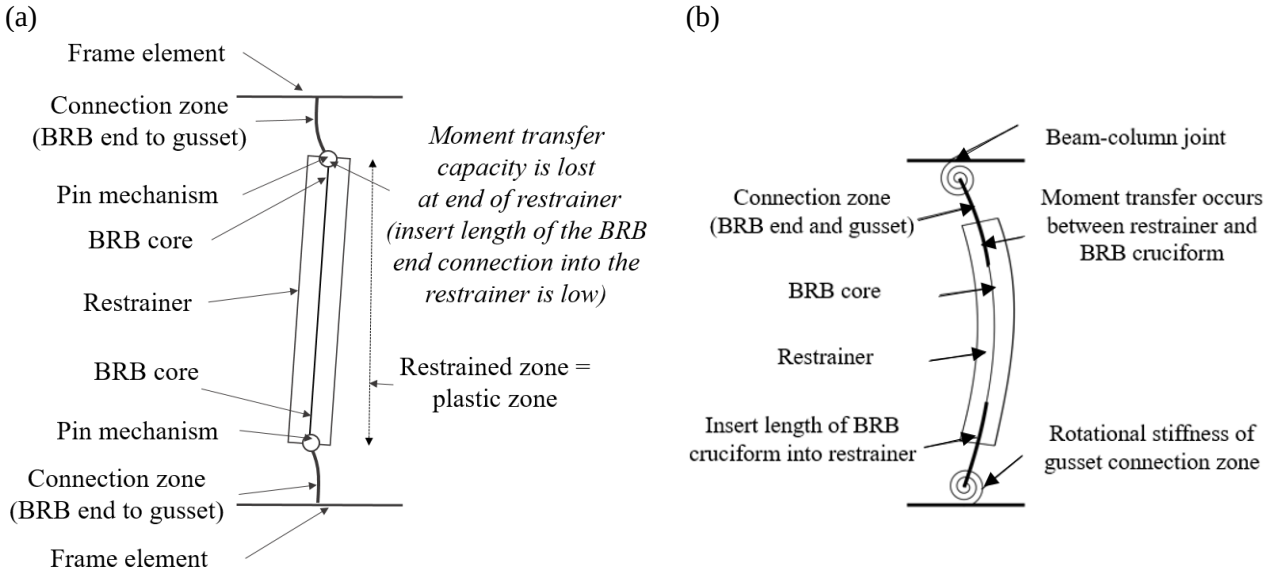

Figure 1-17. Buckling-restrained brace stability concepts (Takeuchi et al. 2013)
(a) Cantilever Connection Concept, (b) Restrainer Continuity Concept

Both concepts make assumptions about BRB behaviour and the rigidity of the gusseted connection zone. The suitability of a gusseted connection zone (specifically its rigidity) depends on the ability of the restrainer to transfer moment to the exposed end of the BRB. Both methods also require the rotational stiffness of both the adjacent frame elements and gusset plate, which is far from straight forward, requiring testing or finite element modelling. Published research only contains the stiffness properties for a select few gusset plate designs, all of which have some form of stiffeners.

A different design methodology is used in Taiwan, where BRBs with welded end connections are used. This design methodology has been developed into an online tool called Brace-on-Demand (NCREE 2014). Welded connections cost more to fabricate so are seldom used in countries with higher labor costs such as New Zealand and the United States. In both Japan and Taiwan, design instructions limit the amount of variation in designs and instruct structural practitioners on how best to incorporate BRBs. Consequently, connection zones for BRBFs are stiffened and relatively rigid.

1.3.5 **Local stability of a connection zone**

Another BRBF design consideration is local plastic collapse or buckling of the gusseted connection zone. To prevent this behaviour, design codes treat gusset plates as an equivalent column and use equations based on column buckling behaviour to size them. The compression design load for a gusset plate is based on the post-yielding strength of the BRB at displacements equivalent to two times the design storey drift ($2\Delta_{bm}$). The load transfer from the BRB is assumed to be a uniaxial load. Secondary effects such as eccentric loading and bending stresses transferred from the BRB core and restrainer are not considered. The impact of these secondary effects is difficult to quantify for every BRBF variation. Figure 1-18 shows how the secondary effects can develop inside a deforming BRB. Note: as the BRB core is rectangular, the deformation is different for each orientation.

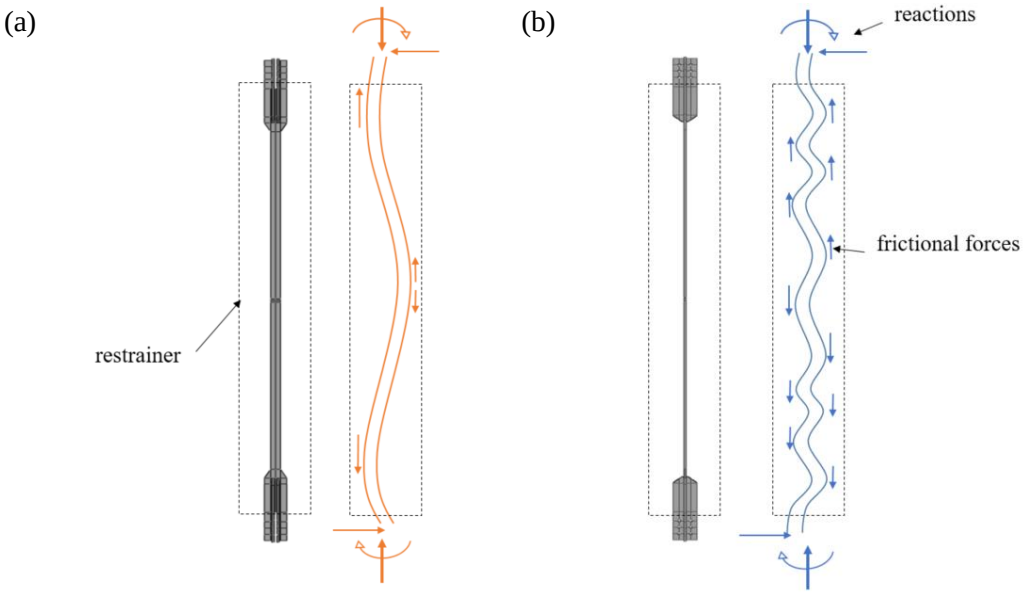

Figure 1-18. Free-body-diagram of deformation, forces and reactions of BRB core inside a restrainer (a) bending about the strong axis, (b) bending about the weak axis

Zaboli et al. (2018) proposed a new approach to design gusset plates in BRBF, called the simplified notional load yield line method. This method acknowledges the moment transfer mechanisms of the Takeuchi model used in Japan (Takeuchi et al. 2013). This approach builds on research by Dowswell (2016) by improving the definition of possible yield line patterns in gusset plates. Improvements were based on observations of different BRB collapse mechanisms. The method assumes a gusset plate will fail in one of three ways. When a BRB moves out-of-plane, without a plastic hinge at the end of the restrainer, the gusset plate is expected to buckle under the yield line (Figure 1-19a). When a BRB does form a plastic hinge at the end of the restrainer, plastic failure over a yield line will occur. This yield line will run from the corner of the gusset to the underside of the brace and back to the other corner (Figure 1-19b). If the BRB is not pulled in tight to the beam-column joint, the yield line will run in a straight line parallel to the end of the brace to the first re-entrant corner of the gusset (Figure 1-19c). A comparison between a small number of tests and predictions made the simplified notional yield line method showed the method to be suitably conservative.

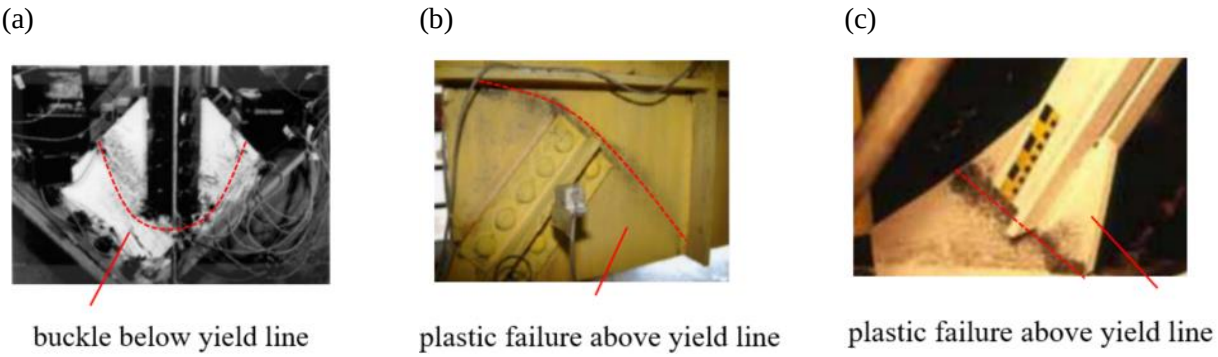

Figure 1-19. Possible gusset plate buckling failures (a) under the yield line (Yam et al. 2002), (b) plastic failure over the yield line (Tsai et al. 2008), (c) plastic failure over the yield line (uninterrupted) (Astaneh-Asl et al. 2006)

Frame action effects are another consideration in BRBF design. As the frame undergoes lateral displacement, rotation causes pinching of one corner and pulling apart of the other. This action reverses and repeats with each cycle of loading. This pinching and pulling induces additional stresses on the welds in the gussets. Figure 1-20 shows a schematic of the additional forces (in red), caused from frame action effects.

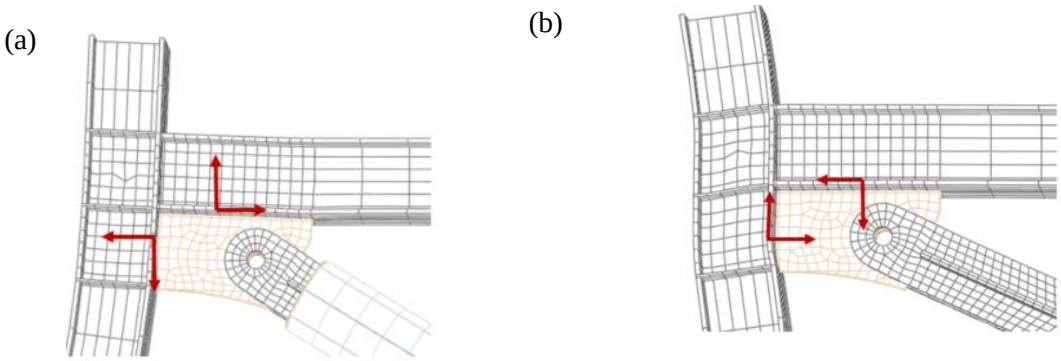

Figure 1-20. Schematic of frame action (Lin et al. 2015)
(a) brace in compression, (b) brace in tension

Lin et al. (2005) presents research on seismic design, and the performance of gusset connections in a full-scale two storey BRBF experiment. Frame action effects are discussed in detail. Described is a systematic approach for gusset plate design including verification of the generalised uniform force method and improved equivalent strut method (IESM). This method shows how to calculate accumulative normal, shear and von Mises stress account for frame action effects. Also from this set of experiments, Khoo et al. (2016) published results showing gusset plates performed well using the IESM. However, damage at large storey drift ratios forced webs within the column and beam to yield before the BRB, which is undesired.

1.3.6 **Design requirements for BRBFs in New Zealand**

All building designs in New Zealand are required to meet the Building Code contained in the regulations under the Building Act 2004 (Ministry of Business Innovation and Employment 2017). The Act governs the building sector and sets out the rules for the construction, alteration, demolition and maintenance of new and existing buildings in New Zealand. The field of structural design is primarily focused on ensuring building stability by working out the expected loads and selecting an appropriate structural system. To establish requisite loading conditions, engineers follow NZS 1170 (commonly referred to as the loadings code) (Standards New Zealand 2002). To ensure their structural system, elements, and detailing are acceptable, designers can follow a set of prescribed standards. These prescribed standards are essentially a set of instructions based on evidence and statistical data. New design ideas that are not yet within the prescribed standards are deemed as an alternative building solution. In order for alternative solutions to gain Building Code compliance, designers are required to provide evidence that the idea is safe and will perform as intended. These designs often require peer review. Instructions for how to collect and present evidence is outlined in the alternative design clause of Section B in the loadings code (Standards New Zealand 2002). Accepted evidence may include experimental testing, numerical analysis or evidence from a supplier. Currently in New Zealand, BRBs are deemed an alternative solution and structural designs with BRBs require testing and a peer review in order to gain building compliance.

BRBs are widely used throughout seismic areas in the world with some countries developing their own tools and documents to guide designers. In New Zealand, the American standard ANSI 341-16 (ANSI/AISC 2016) is the document used to guide the collection of evidence showing the BRBF building design will perform as intended. It is recognized that testing of BRBs and subassemblages can be costly and time-consuming. Consequently, it has been written with the simplest testing requirements possible. To improve the quality of BRBF design and safe guard against stability issues, alternative methods for testing and guidance specific to New Zealand construction environment should be developed.

1.3.7 **Design process for BRBFs in New Zealand**

During the concept phase of a building design, the brief dictates the layout and size of floors and bays. Then through iteration, the size and type of structural members are selected based on the expected loads. In New Zealand, seismic loading often governs. To ensure a design is adequately sized, force-based design methodology is often followed. This is an iterative process where the estimated mass of the building is multiplied by an acceleration coefficient that represents the design level earthquake event. This co-efficient is based on factors that consider the importance and location/region of the building. The mass of the building and acceleration is multiplied to determine a pseudo shear force that is applied at the base of the building. This shear force is distributed at each level of the building. With the applied loads, the load path is established and used to determine the expected demands on each BRB. With the expected demand, an off-the-shelf BRB with the appropriate capacity is selected.

Once the main structural members have been sized, detailing takes place. This is when the connections (gusset plates) are sized. To ensure a ductile design of the system the connection zones should remain elastic. This helps restrict unwanted behaviour such as weld tearing and connection zone failure. To achieve this, gusset plates are sized using the post-yielding capacity of the BRB obtained from testing.

As mentioned BRBF design fall outside of the instructions in the prescribed standards. To gain compliance the building designs with BRBs require a peer review from an experienced team. However, New Zealand engineers are not well versed in all the possible stability issues. To help structural engineers, BRB manufacturers need to engage in research and testing to provide evidence there product will perform adequately in the intended structural system. This is challenging if project specific conditions are not tested.

1.3.8 **Guidance for testing**

Section K3 in the American standard of seismic provisions for structural steel buildings (ANSI/AISC 341-16) is the adopted document used in New Zealand to guide BRB testing requirement. These provisions were motivated by the relatively small amount of test data on BRBF systems available to structural engineers. In addition, at the time of publishing ANSI/AISC 341-16 there was no data available on the response of BRBF to severe ground motion. Therefore, the seismic performance of these systems are relatively unknown compared to more conventional braced-framed structures (CBFs and EBFs).

It is recognized that testing of BRBs as well as subassemblage testing is expensive. Consequently, Section K3 was written with the simplest testing requirements possible, while still providing reasonable assurance that a prototype BRBF tested in accordance with these provisions will perform satisfactorily in an actual earthquake.

Two types of physical testing are referred to in ANSI/AISC 341-16. Brace prequalification testing ensures each BRB specimen is suitably designed and manufactured to perform effectively in design level earthquake events. This type of testing isolates the performance of a BRB by applying a cyclic uniaxial loading protocol (ANSI/AISC 2016). The displacement amplitudes of each loading cycle are a function of the design storey drift, determined by the height of the storey where the BRB is located. Figure 1-21 displays an example of loading regime prescribed in (ANSI/AISC 2016).

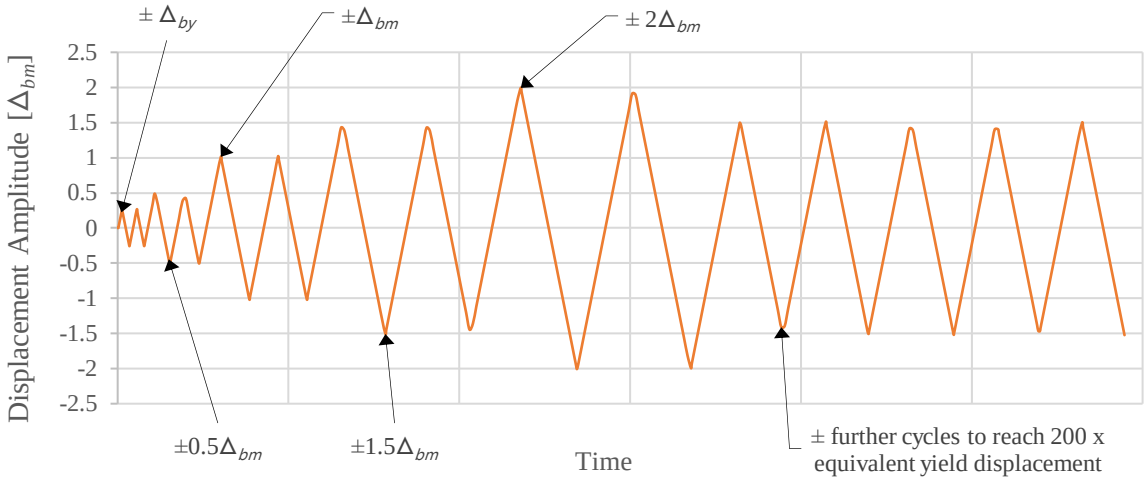

Figure 1-21. Loading regime for uniaxial cycle BRB testing as per ANSI/AISC 341-16 Manual (AISC, 2016)

The displacements targets in the loading protocol (±0.5, 1.0, 1.5, 2.0... Δ_{bm}) are based on the expected length change of the brace as result of horizontal displacement to the frame (Δ_{bm}). The amount of horizontal displacement is equal to multiples of the design storey drift. Figure 1-22 presents a schematic of a frame subjected to a horizontal displacement and the relative effect this has on the braces diagonal length. By using

Pythagoras Theorem to calculate the diagonal lengths of the original and deformed frame (based on the design storey drift), the change in length of the brace (displacement target) can be found.

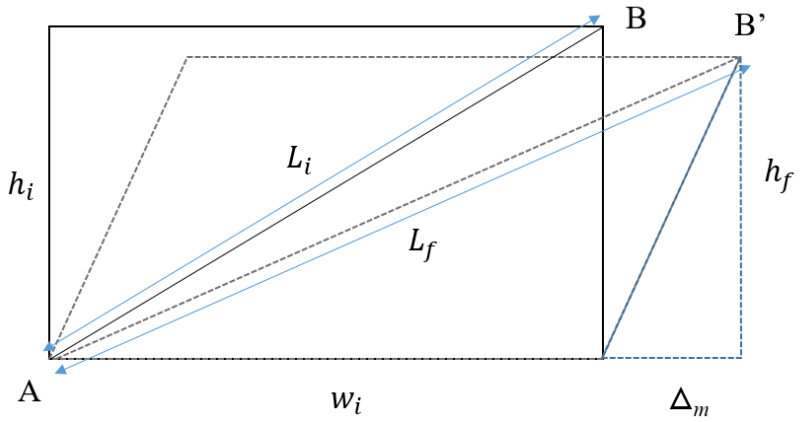

Figure 1-22. Schematic to calculate displacement increments relative to design storey drift targets

Where, L_i = initial length of the brace, h_i = the initial height of the frame, b_i = the width of the frame, Δ_m = horizontal displacement equal to the design storey drift, L_f = the final length of the brace, Δ_{bm} = the axial displacement target of the brace.

As the guidance prescribed in ANSI/AISC 341-16 (ANSI/AISC 2016) is not binding in New Zealand, it is open to interpretation to meet project limitations/requirements. Generally, in New Zealand, only uniaxial testing is conducted. This type of testing captures the axial force response to the targeted uniaxial displacements specific to the project. In prequalification testing, ANSI/AISC 341-16 deems a BRB fit for purpose if the following conditions are met:

- Display stable, repeatable load - displacement history with positive incremental stiffness.
- No rupture, brace instability or brace end connection failure during testing protocol.
- The maximum tension and compression force during each subsequent cycle after yield, shall be no less than the yield force.
- The ratio of maximum compression to tension force during each subsequent cycle after yield shall not exceed 1.3.

Figure 1-23 shows the results from a typical prequalification BRB test. The vertical axis of this figure has been normalised in terms of its yield force, and the horizontal axis has been normalised in terms the design storey drift. Important features of the cyclic response of BRBs include 1) the initial yield value, 2) the strain hardening adjustment factor (ω) (the ratio of peak load at $2.0\Delta_{bm}$ to the yield load), and 3) the compression strength adjustment (β) (ratio of peak compression to peak tension at $\pm 2.0\Delta_{bm}$)

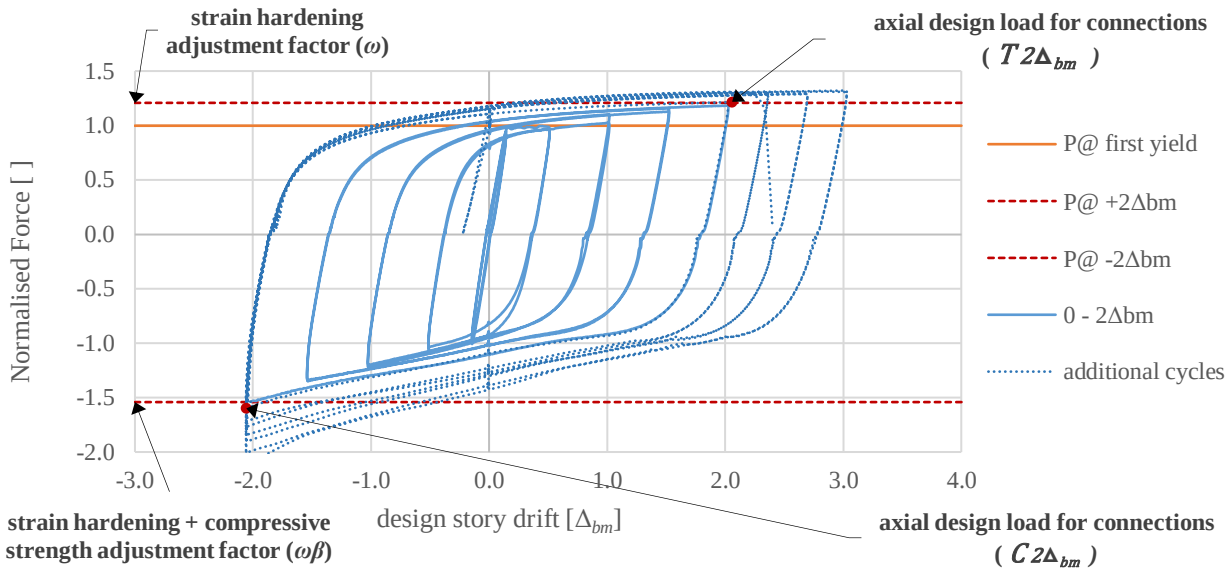

Figure 1-23. Prequalification testing of BRB and how over strength factors are determined

Subassemblage testing focuses on checking the stability of the complete BRBF system. This type of testing can include eccentric loading of partial systems, full frame or complete storey specimens. Figure 1-24 presents four possible subassemblage tests that can be performed as suggested in ANSI/AISC 341-16.

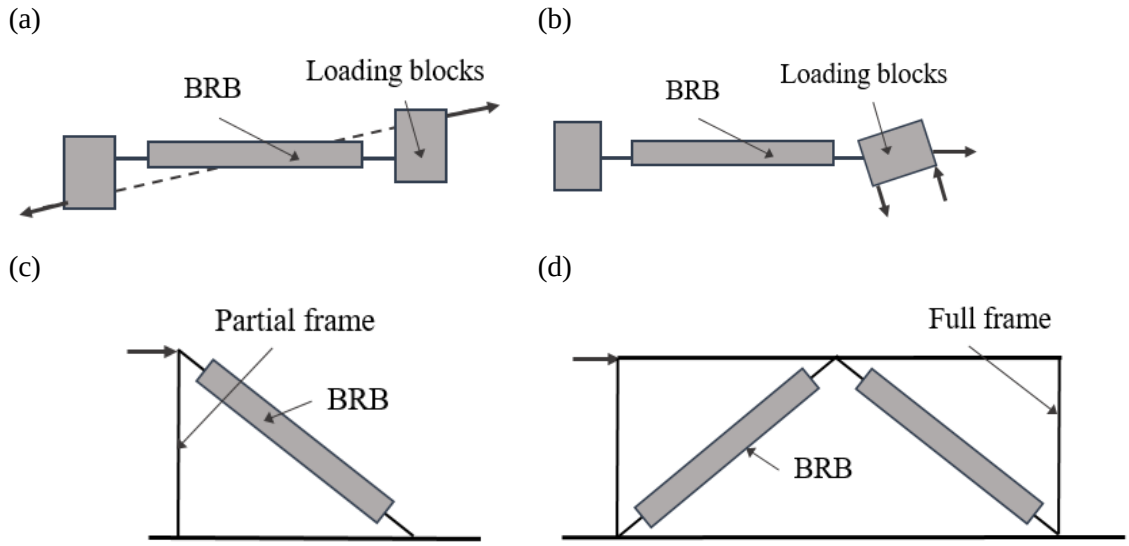

Figure 1-24. Possible test subassemblies (ANSI/AISC 2016)
(a) eccentric loading of brace, (b) loading of brace with constant imposed rotation,
(c) loading of brace and column, (d) loading of braced frame

It is recognized that subassemblage testing is more difficult and expensive than BRB prequalification testing. However, the combined rotational and axial demand in BRBs, and the relative lack of test data on the performance of these systems, mean subassemblage testing should be performed. Without subassemblage testing it is difficult to assure adequate performance of the brace and frame elements under realistic conditions. That being said, ANSI/AISC 341-16 does not intend for subassemblage testing to be required for every building project. Rather it is expected that brace manufactures will perform testing for a reasonable range of conditions and that this data be available to engineers on projects using BRBs. Alternatively, ANSI/AISC 341-16 allows for alternate testing programs as part of qualified peer review. Such programs may include nonlinear finite element analysis, partial specimen testing, and reduced-scale testing, in combination with full-scale uniaxial testing (ANSI/AISC 2016).

1.3.9 **Sizing gusseted connection zones**

To restrict unwanted weld tearing and connection zone failure, design loads for BRB frame elements are based on the post-yielding strength of BRB core caused by displacements equivalent to two times the design storey drift ($2\Delta_{bm}$). In tension, the design load is the product of the core area, yield strength and strain hardening adjustment factor. In compression, a strain hardening and a compressive adjustment factor are multiplied by the core area and yield strength. The axial design loads for connections are defined by equations (2.1)-(2.3).

$$\boldsymbol{P}_{ysc} = 0.9\,\boldsymbol{\sigma_y}\,A_{core} \tag{2.1}$$

$$\boldsymbol{T}_{2\Delta_{bm}} = \omega\,\boldsymbol{P_{ysc}} \tag{2.2}$$

$$\boldsymbol{C}_{2\Delta_{bm}} = \beta\,\omega\,\boldsymbol{P_{ysc}} \tag{2.3}$$

Where, $\boldsymbol{P}_{ysc}$ = adjusted force at yield of the BRB core; $\boldsymbol{\sigma_y}$ = yield strength of the BRB core material; A_{core} = cross sectional area of the BRB core; $\boldsymbol{T}_{2\Delta_{bm}}$ = design load on BRB frames elements in tension; ω = strain hardening adjustment factor; $\boldsymbol{C}_{2\Delta_{bm}}$ = design load on BRB frame elements in compression; β = compressive strength adjustment factor. Figure 1-25 shows how the load from a BRB is simplified and considered in the design of gusset plates as per NZS3404.

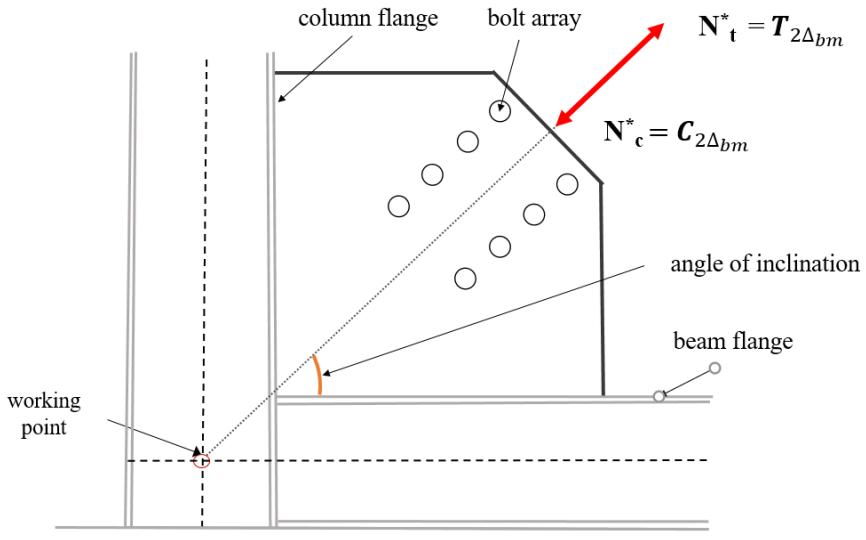

Figure 1-25. Axial design configuration for gusset plate design

To prevent tension or crushing failure of a gusset plate it is common to size the gusset plate using the Whitmore width method. This approximates the yield area of the gusset plate. This area is obtained by multiplying the thickness of the plate by an effective width. The effective width is defined in equation (2.4).

$$b_e = b_{\,bolt\ array} + 2\,L_{\,bolt\ array}\,tan\,30^0 \tag{2.4}$$

Where, $b_{bolt\ array}$ and $L_{bolt\ array}$ is the width and length of the bolt array. Figure 1-26 illustrates how the effective width is calculated with 30^0 lines from the outer fasteners of the first row to their intersection with a line perpendicular to a line passing through the bottom row (ANSI/AISC 2016).

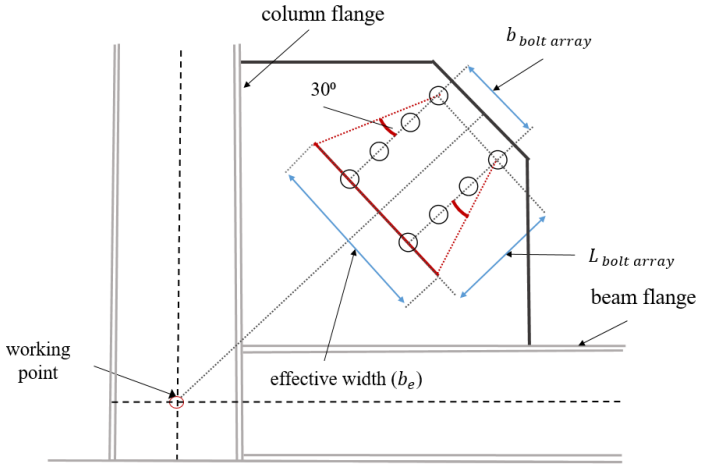

Figure 1-26. Schematic of Whitmore width (b_e) (ANSI/AISC 2016)

To prevent local instability of gusset plate, NZS 3404 treats a gusset plate as an equivalent column and uses buckling design curves to size them. These buckling curves are based on column buckling behaviour using the Whitmore width method (with a load dispersion angle of 30º) to determine its load carrying capacity. To construct the equivalent column, the buckling length is approximated by the average of the three lengths equally spaced along the Whitmore width (as shown in Figure 1-27).

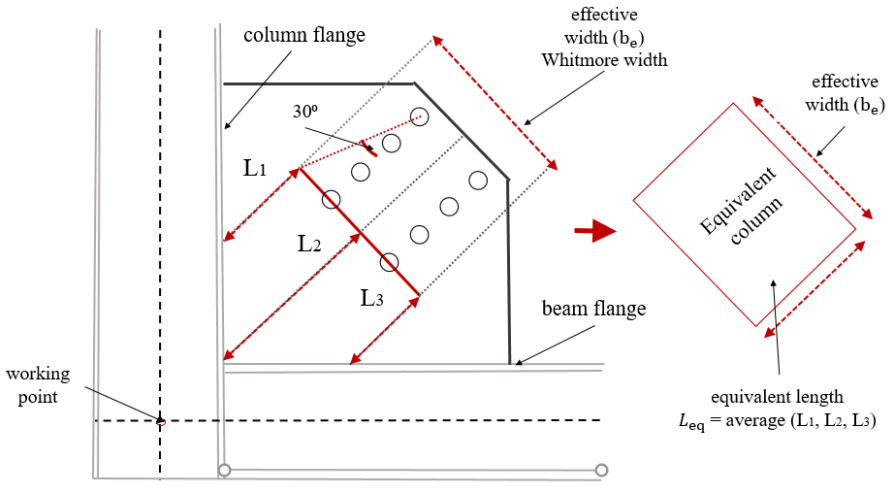

Figure 1-27. Schematic of Whitmore width (b_e) and Thornton lengths (L_1, L_2 and L_3)

To account for different sections and fabrication methods of typical columns, NZS 3404 defines five different strength curves to describe buckling. These account for different stress distributions, and magnitudes of residual stresses among sections types. These curves require a comprehensive set of equations. To reduce

manual calculations, a set of design tables are also provided. (Section 6.3.4 of NZS3404 and in Appendix B). Gussets plates are not specifically accounted for in these curves but are treated as a ‘H’ or ‘I’ section with a thickness up to 40mm.

1.3.10 **Experimental testing and the role of finite-element analysis**

Without a robust alternative to check the global and local stability of a BRBF design, physical testing is required. Earthquakes can cause complex loadings on large structures. Earthquake loading can be difficult to predict and replicate in a laboratory. As a result, it is not known exactly how a building will structurally perform in a severe earthquake until the real earthquake event happens. As engineers, we do our best through small scale and substructure testing, using idealized/estimated loadings to demonstrate component performance in an extreme event. We then extrapolate test results to more complex subsystems and full building systems through computational models. These models can be validated against available test data to give confidence in predictions for other larger complex structural systems. BRBs are relatively new and only a few designs have seen service in extreme earthquake events. To accurately predict the behaviour of building with BRBs we must first be able to study the local deformation of the core as it interacts with the restrainer and implications this has on connecting frame elements. As the core of a BRB is concealed by a restrainer this is difficult to observe, study and predict. Continuum modelling offers a way to study the local deformation and stress-strain behaviour of BRBs.

The interaction of the core and the restrainer is a complex nonlinear phenomena that has limited the development of detailed FEA models. It involves combined instability effects, nonlinear constitutive laws and frictional contact. These behaviours play a significant role in the performance of the BRB system. The restrainer is designed to confine transverse displacements of the core and prevent global buckling of the BRB core. However, transverse displacements are caused by the slender nature of the core that leads to constrained buckling at very low axial compressive loads (less than yield). Simplified approaches are traditionally used to model the features related to this behaviour. These methods are appealing as they significantly reduce computational demand. The sacrifice, however, is they lack of fidelity and therefore do not represent realistic local deformation.

1.4 **Overview**

BRBs have been shown to perform well in uniaxial testing, providing stable hysteretic performance. Test results also show BRBs can perform well in full-frame systems if gusseted connection zones are adequately designed. However, it is not practical to test and verify every BRBF variation. As such, alternative methods to check global and local stability, and plastic collapse of a BRBF (that includes out-of-plane displacements and second order effects) should be sought. Japan and Taiwan have developed methods to ensure safe BRBF design specific to their construction environments. To determine if these methods are suitable for all BRBF design types further examination of these methods are required. To evaluate BRB stability, a good understanding of the local behaviour of deforming BRBs and how they interact with different connecting elements is required. Continuum modelling along with component testing can be used to better understand these behaviours and interactions.

In the next chapter (Chapter 2), the experimental programme and results from prequalification testing is presented. These BRBs are commercially available in New Zealand that have been installed in commercial buildings. Test data like this is not publically available due to their proprietary nature. Then in Chapter 3, the development of a FEA modelling strategy that incorporates realistic BRB mechanical behaviour is presented. The experimental data from Chapter 2 is used to validate this strategy. Chapter 4 presents a separate study that investigates gusset plate design methods and the suitability of these methods when incorporated in BRBFs. Finally. Chapter 5 investigates combined BRB and frame behaviour using FEA. The detailed models use the strategy (presented in Chapter 3) to capture the realistic behaviour of a deforming BRB with the addition of frame components. Specifically investigated is the suitability of using the gusset plates design methods presented in Chapter 4. The effect of bi-directional loading is also evaluated. Results are compared against predictions made by the analytical method used in Japan (Takeuchi method).

1.5 **References**

AIJ (1995). Reconnaissance report on damage to steel buildings structures ibserved frin 1995 Hyogken-Nanbu Earthquake. M. B. Nakashima, M., Isaja: Architectural Institute if Japan

ANSI/AISC (2016). Seismic provisions for structural steel buildings - ANSI/AISC. One East Wacker Drive, Suite 700, Chicago, Illinois 60601-1802, American Institute of Steel Construction

Architectural Institute of Japan (AIJ) (2009). Recommendations for stability design of steel structures. Japan, AIJ 74-79. (in Japanese)

Architectural Institute of Japan (AIJ) (2014). Notable cases following Tohoku Earthquake (Multistory Parking Garage).Japanese

Astaneh-Asl, A., M. L. Cochran and R. Sabelli (2006). Seismic detailing of gusset plates for special concentrically braced frames. Structural Research Series. Department of Civil Engineering University of Illinois Urbana, Moraga, CA, Steel Technical Information and Product Services (Steel TIPS)

Avenues Four. (2014). "Avenues Four." from https://www.facebook.com/AvenuesFour/.

Black, C., N. Makris and I. Aiken (2002). Component testing, stability analysis and characterization of buckling-restrained unbonded braces, Pacific Earthquake Engineering Research Center

Bradley, B. A. (2012). Ground motion and seismicity aspects of the 4 Spetember 2010 Darfield and 22 February 2011 Christchurch Earthquakes, Technical Report Prepared for the Canterbury Earthquakes Royal Commission

Bruneau, M., C.-M. Uang and R. Sabelli (2011). Ductile design of buckling-restrained braced frames. Ductile Design of Steel Structures. New York, McGraw Hill**:** 651-687.

Chou, C.-C. and P.-J. Chen (2009). Compressive behavior of central gusset plate connections for a buckling-restrained braced frame. Journal of Constructional Steel Research **65**: 1138-1148

Chou, C.-C. and J.-H. Liu (2012). Frame and brace action forces on steel corner gusset plate connections in buckling-restrained braced frames. Earthquake Spectra **28**(2): 531-551

Dowswell, B. (2016). Advances in steel connection analysis. 2016 NASCC (the Steel Conference Proceedings)

Dunai, L., L. Kaltenbach, M. Kallo, M. Kachichian and A. Halasz (2011). Type testing of buckling-restrained braces according to EN 15129, Budapest University of Technology and Economics

Eryasar, M. E. and C. Topkaya (2010). An experimental study on steel-encased buckling-restrained brace hysteretic dampers. Journal of Earthquake Engineering and Structural Dynamics **39**: 561-581

Fahnestock, L. A., J. M. Ricles and R. Sause (2007). Experimental evaluation of a large-scale buckling-restrained braced frame. Journal of Structural Engineering: 1205-1214

Fenwick, R. and D. Bradley (2020). Collapse of the Canterbury Television (CTV) Building. SESOC. SESOC website

Hasegawa, H., T. Takeuchi, Y. Nakata, M. Iwata, S. Yamada and H. Akiyama (2000). Experimental study on dynamic behavior of unbonded braces. AIJ Journal of Technology and Design - in Japanese: 103-106

Hikino, T. (2016). Experimental study on remained fatigue of used BRB (Tohoku Earthquake). Summary of the Annual Meeting. Kyushu, Architectural Institute of Japan. (in Japanese)

Iwata, M. and T. W. Kato, A. (2000). Buckling-restrained braces as hysteretic dampers. Third International Conference on Behavior of Steel Structures in Seismic Areas (STESSA 2000). Montreal, Canada

Jury, R. (2011). Investigation into the collapse of the Pyne Gould Corporation Building on 22nd February 2011. B. C. H. a. F. Ltd

Kasai, K., H. Ito, Y. Ooki, T. Hikino, K. Kajiwara, S. Motoyui, H. Ozaki and M. Ishii (2010). Full-scale shake table tests of a 5-story steel building with various dampers. 7th International Conference on Urban Earthquake Engineering. Tokyo, Japan

Khoo, H.-H., K.-C. Tsai, C.-Y. Tsai, C.-Y. Tsai and K.-J. Wang (2016). Bidirectional substructure pseudo-dynamic tests and analysis of a full-scale two-story buckling-restrained braced frame. Earthquake Engineering & Structural Dynamics

Kimura, K. Y., K. and T. Takeda (1976). Tests on braces encased by mortar in-filled steel tubes. Summaries of Technical Papers of Annual Meeting, Architectural Institute of Japan. (in Japanese)

Konami, S., H. Sugihara, M. Narikawa, Y. H. Huan, Y. Maeda and A. Wada (1999). Seismic performance of moment resisting frames with hysteretic damper. Annual Meeting of the Architectural Institute of Japan (in Japanese)

Lin, M.-L., K.-C. Tsai, P.-O. Hsiao and C.-Y. Tsai (2005). Compressive behavior of buckling-restrained brace gusset connections. The First International Conference on Advances in Experimental Structural Engineering. Nagoya, Japan

Lin, P.-C., K.-C. Tsai, A.-C. Wu, M.-C. Chuang, C.-H. Li and K.-J. Wang (2015). Seismic design and experiment of single and coupled corner gusset connections in a full-scale two-story buckling-restrained braced frame. Earthquake Engineering & Structural Dynamics **44**: 2177-2198

Lin, P.-C., K.-J. Wang, Y.-J. Yu, C.-Y. Wei, A.-C. Wu, C.-Y. Tsai, C.-H. Lin, C.-H. Chen, A.-H. Schellenberg, S.-A. Mahan and C.-W. Roeder (2012). Seismic design and hybrid tests of a full-scale three story buckling-restrained braced frame using welded end connection and thin profile. Journal of Earthquake Engineering and Structural Dynamics **41**: 1001-1020

MacRae, G. and G. C. Clifton (2017). New Zealand research applications of, and developments in, low damage technology for steel structures. 16th World Conference on Earthquake Engineering. Santiago, Chile

Ministry of Business Innovation and Employment (2017). Acceptable solutions and verification methods For New Zealand building code clause B1 Structure

NCREE (2014). National Center for Research on Earthquake Engineering - User Guide for BOD: Buckling-restrained brace and connection design procedure. Taiwan, National Taiwan University

NEHRP (2013). Seismic Design of Steel Special Concentrically Braced Frame Systems: A Guide for Practicing Engineers. R. Sabelli, C. W. Roeder and J. F. Hajjar, National Institute of Standards and Technology

Palmer, K. D., A. S. Christopulos, D. E. Lehman and C. W. Roeder (2014). Experimental evaluation of cyclically loaded, large-scale, planar and 3-d buckling-restrained braced frames. Journal of Constructional Steel Research **101**: 415-425

Rabbat, B. G. and H. G. Russell (1985). Friction coefficient of steel on concrete or grout. Journal of Structural Engineering **111**: 505-515

Standards New Zealand (1997). NZS 3404:1997 Steel Structures Standard. Wellington, New Zealand

Standards New Zealand (2002). AS/NZS 1170.0:2002, Structural design actions, Part 0: General Principles Wellington, New Zealand

Takeuchi, T., H. Ozaki, R. Matsui and F. Sutcu (2013). Out-of-plane stability of buckling-restrained braces including moment transfer capacity. Earthquake Engineering & Structural Dynamics **43**: 851–869

Takeuchi, T. and A. Wada (2017). Buckling-restrained braces and applications. Tokyo, Japan, The Japan Society of Seismic Isolation.

Tremblay, R., R. Bolduc, R. Neville and R. DeVall (2006). Seismic testing and performance of buckling-restrained bracing systems. Canadian Journal of Civil Engineering **33**

Tremblay, R., A. Filiatrault, M. Bruneau, M. Nakashima, R. DeVall and G. L. P. Helmut (1996). Seismic Design of Steel Buildings: Lessons from the 1995 Hyogen-ken Nanbu Earthquake. Canadian Journal of Civil Engineering **23**(3): 757-770

Tremblay, R., P. Timler, M. Bruneau and A. Filiatrault (1995). Performance of Steel Structures dueing the January 17, 1994, Northridge Earthquake. Canadian Journal of Civil Engineering **22**(2): 338-360

Tsai, K. C. and P.-O. Hsiao (2008). Pseudo-dynamic test of a full-scale CFT/BRB frame—Part II: Seismic performance of buckling-restrained braces and connections. Earthquake Engineering & Structural Dynamics **37**: 1099-1115

Tsai, K. C., P.-O. Hsiao, K.-J. Wang, Y.-T. Weng, M.-L. Lin, K.-C. Lin, C.-H. Chen, J.-W. Lai and S.-L. Lin (2008). Pseudo-dynamic tests of a full-scale CFT/BRB frame—Part I: Specimen design, experiment and analysis. Earthquake Engineering & Structural Dynamics **37**: 1081-1098

Uriz, P. and S. Mahin (2008). Toward earthquake-resistant design of concentrically braced steel-frame structures, Pacific Earthquake Engineering Research Center

Vargas, R. and M. Bruneau (2009). Experimental response of buildings designed with metallic structural fuses. II. Journal of Structural Engineering **135**: 397-403

Wada, A., E. Seaki, T. Takeuchi and A. Watanabe (1989). Development of unbonded brace, A Nippon Steel Publication. **115:** 12

Watanabe, A., Y. Hitomi, E. Saeki, A. Wada and M. Fujimoto (1988). Properties of brace encased in buckling-restraining concrete and steel tube. Ninth World Conference on Earthquake Engineering, Tokyo-Kyoto

Watanabe, A., Y. Hitomi, E. Yaeki, A. Wada and M. Fujimoto (1973). Experimental study of elasto-plastic properties of precast concrete wall panels with built-in insulating braces. Summaries of technical papers of annual meeting, . Tokyo, Japan, Architechural Institute of Japan**:** 1041-1044.(in Japanese)

Watanabe, A. N., H. (1992). Study on the behavior of buildings using steel with low yield point. Proceedings of Tenth World Conference on Earthquake Engineering. Rotterdam**:** 4468-4468

Westeneng, B., C.-L. Lee and G. A. MacRae (2016). Prevention of gusset plate out-of-plane sway buckling failure in buckling restrained braced frames. 2016 New Zealand Society of Earthquake Engineering Conference. Christchurch, New Zealand, NZSEE

Wigle, V. R. and L. A. Fahnestock (2010). Buckling-restrained braced frame connection performance. Journal of Constructional Steel Research **66**: 65-74

Wijanto, S. and G. C. Clifton (2014). Experimental testing and design of BRB with bolted and pinned connections. Bulletin of NZSEE **47**: 264-274

Yam, M. C. H. and J. J. R. Cheng (2002). Behavior and design of gusset plate connections in compression. Journal of Constructional Steel Research **58**: 1143-1159

Zaboli, B., G. C. Clifton and K. Cowie (2018). BRBF and CBF gusset plates: Out-of-plane stability design using a simplified notional load yield line (NLYL) method. SESOC Journal **28**: 531-551

Zhao, J., B. Wu and J. Ou (2011). A novel type of anlge steel buckling-restrained brace: cyclic behavior and failure mechanism. Journal of Earthquake Engineering and Structural Dynamics **40**: 1083-1102

2 EVIDENCE COLLECTED FOR PEER REVIEW OF BUCKLING-RESTRAINED BRACES MANUFACTURED IN NEW ZEALAND

Buckling-restrained braces (BRBs) form a bracing system that provides lateral strength and stiffness to a building. These systems have been shown to provide more stable energy dissipation in severe earthquake events compared to concentrically and eccentrically braced frames (CBFs and EBFs). However, unlike CBFs and EBFs there is no guidance document or specific instructions in regulatory standards for the design of buckling-restrained braced frames (BRBFs) in New Zealand. This means structural designs that include BRBFs require a peer-review. Currently the American standard ANSI/AISC 341-16 is the adopted document used in New Zealand for guidance in how to collect evidence showing a BRBF system will perform as intended. This chapter discusses the intentions of ANSI/AISC 341-16 and applicability to New Zealand conditions. Specifically, the recommended testing and results that help gain building compliance. By way of example, this chapter presents the experimental test process and results acquired from prequalification testing of five different commercially available BRB designs. The BRBs presented, represent the only braces commercially manufactured in New Zealand. One test failed prematurely due to global buckling. The likely cause was a manufacturing error. All other BRBs performed well, meeting the acceptance criteria and have now been installed in medium to high-rise buildings throughout New Zealand. Project specific subassemblage testing to assess the performance of a BRB and its frame components was not conducted as part of gaining building compliance.

2.1 **Introduction**

As BRBs are relatively new to the New Zealand market, there is not yet any documented guidance or specific instructions in regulatory standards for the design of BRBFs. This makes it difficult for engineers to anticipate all the possible stability and strength issues within a system and actively mitigate them in each design. To help ensure BRBF designs perform as intended, a peer review and physical testing are currently required to gain building compliance in New Zealand. The American standard of seismic provisions for structural steel buildings (ANSI/AISC 341-16) is the commonly adopted document that describes how to conduct testing and present evidence to show that each BRB system will perform as required. Firstly, BRB prequalification testing is conducted to ensure each BRB specimen is suitably designed and manufactured to perform effectively in design level earthquake events. This type of testing isolates the performance of a BRB by applying a cyclic uniaxial loading protocol with displacement increments based a building projects design storey drift.

Results from prequalification testing according to ANSI/AISC 341-16 should show the brace can reach displacements equal to two times the design storey drift ($2\Delta_{bm}$) and dissipate energy equivalent to 200 times yield strain displacement ($200\Delta_{by}$) without failure. Testing also determines the yield strength and over-strength factors required for the design loads of connecting elements (beam, column, gusset plate). Other protocols used for brace prequalification testing worldwide include EN 15129 as a part of the European Standards (CEN 2010), which use similar displacement targets as ANSI/AISC 341-16. Whereas, recommendations made by European Convention for Constructional Steelwork (ECCS 1986) specify displacement targets based on increments of yield strain instead of design storey drift. Other countries such as in Japan are again different, where target displacements are defined as average strain, this being a percentage of the yielding length of the core. The advantage of using average strain as a basis for target displacements is that a BRB can be tested and approved for use within a set strain-range limit. Then for each specific building project, the structural engineer can simply check if the demand falls within the approved strain range by dividing the design storey drift target by the yielding length. The overstrength factors required to design BRB connecting elements can be determined by interpolating between data points from the original testing. This approach puts more onus on the suppliers up front, but means testing for each building project is not required. Rather, each customer takes advantage of the initial testing.

Major designers and manufacturers of BRBs include CoreBrace in the United States, Nippon Steel in Japan and NCREE in Taiwan. Due to the confidential and proprietorial nature of BRBs test data from prequalification testing are rarely made available to the public. The financial cost and limited availability of capable laboratories mean testing of every BRB architype and variation is not viable. Commonly BRB

manufactures test a selection of BRBs and extrapolate results between sizes. However, the complex behaviour exhibited in BRBs makes it difficult to interpolate results between different BRB sizes accurately.

Market rates for accredited prequalification testing are approximately $8-10k (USD) depending on testing demand, with subassemblage testing costing more. In New Zealand, this cost and the financial pressures inherent in commercial projects has meant uniaxial testing is favoured without project specific subassemblage testing. Alternatively, building designers rely on BRB suppliers to instil confidence, this could mean results from other full frame or subassemblage tests are used to demonstrate performance. However, BRBF building design in New Zealand allows for a large variation of connections zones, with connections often being more flexible than those tested. Also, unlike Japan and Taiwan where BRBFs are often used as a supplemental damper, New Zealand uses BRBFs as the primary lateral supporting system. Without test results that incorporate the full spectrum of BRBF combinations or without the limitations imposed on BRBF design such as those in Japan and Taiwan there is a level of uncertainty regarding the seismic performance of these systems. In addition, the confidential and proprietorial nature of commercial building and BRB designs limit the availability of BRB test data, making it difficult for the New Zealand engineering community to determine best practice.

By way of example, this chapter presents the experimental test process and results from prequalification testing of five BRBs. As part of a peer review, these tests provided the evidence needed to gain building compliance. These BRBs represent the only braces commercially manufactured in New Zealand and have now been installed in commercial buildings throughout New Zealand. This information is valuable since test data for BRBs relevant to the New Zealand construction environment are not publically available, with many research projects restricted to the study of relatively small braces.

2.2 **BRB Specimens tested**

Five tested BRB designs were reviewed. Each BRB investigated was assigned a Brace ID during testing. The BRBs selected encompass a variety of BRB options on the market and represent the only braces commercially manufactured in New Zealand. The displacement loading test requirements are based upon the design storey drift of the frame each BRB was intended for. The angle of inclination (angle the brace is connected diagonally into corner gussets of a frame) influences the amount strain the brace will experience over its length. Details of each brace are shown in Table 2-1, with material properties in Table 2-2. Solid model images and selected shop drawings of each BRB are presented in Figure 2-1 through to Figure 2-5. Appendix 8.1 through to Appendix 8.5 contains the full set of shop drawings and tensile material test data of these BRBs.

Table 2-1. Details of BRB specimens investigated

Brace ID	**Total Length [mm]**	**Connection type**	**Installed angle of inclination [^{0}]**	**Core Area [mm]**	**Design Yield Force [kN]**
BRB 6.5a	7238	Pinned	24.7	25x140	1221.5
BRB S3	3812	Bolted	43.15	12x55	204
BRB C6	6566	Pinned	32.9	50x85	1445
BRB 9.5	7592	Pinned	28.9	32x176	1726
BRB 2A	4025	Pinned	36.8	12x30	118

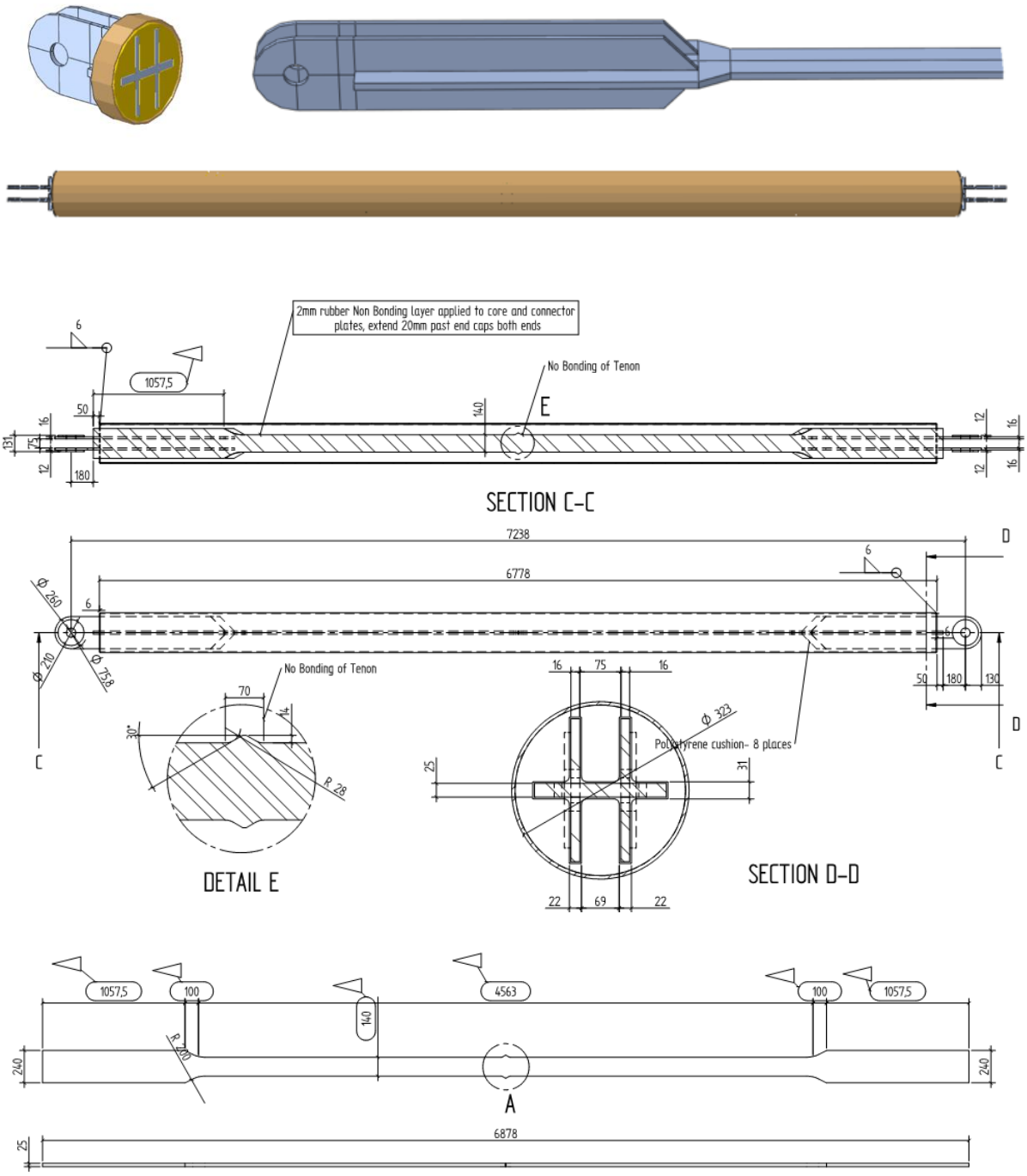

Figure 2-1. Solid model images and shop drawings (BRB 6.5a)

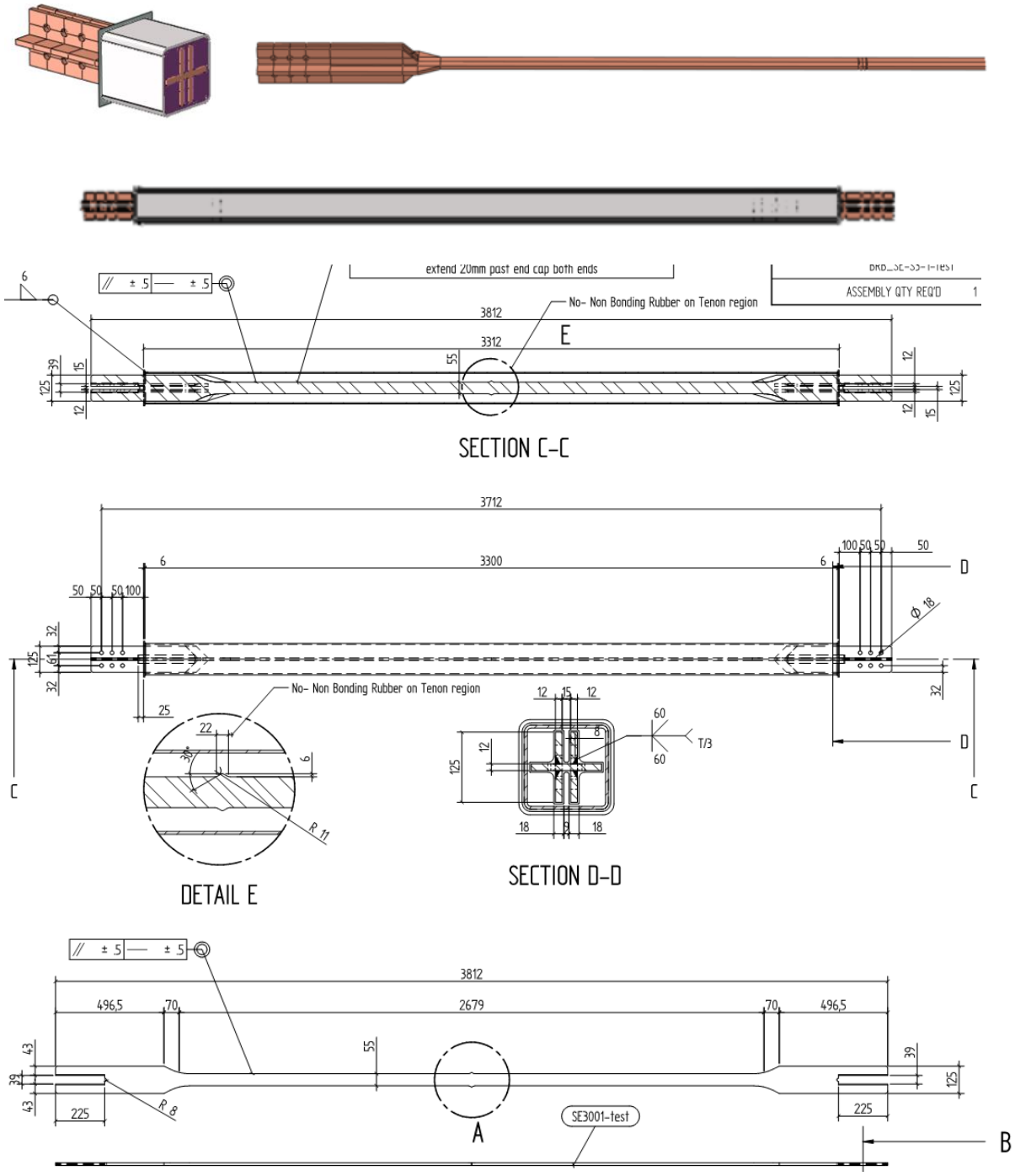

Figure 2-2. Solid model images and shop drawings (BRB S3)

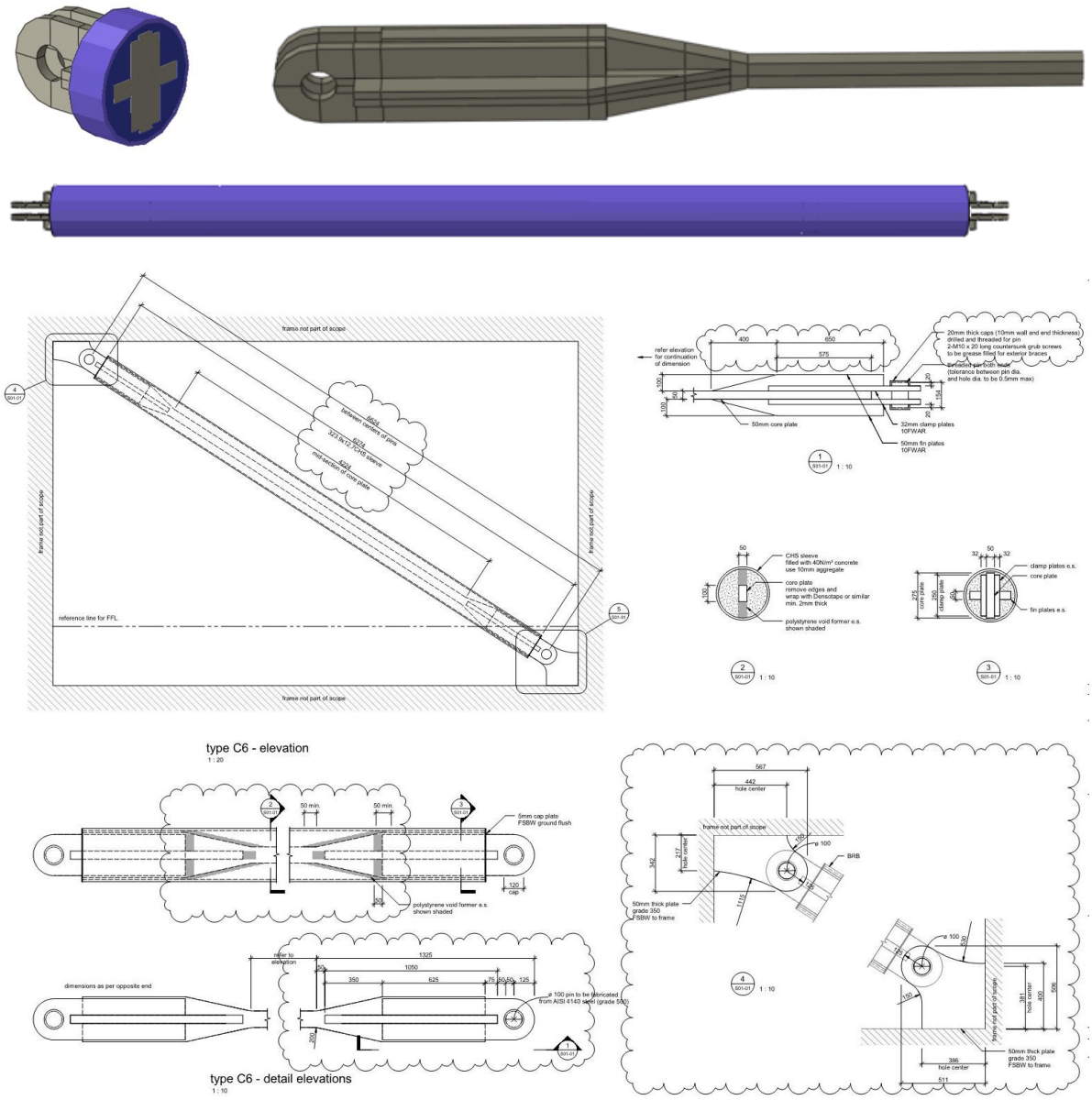

Figure 2-3. Solid model images and shop drawings (BRB C6)

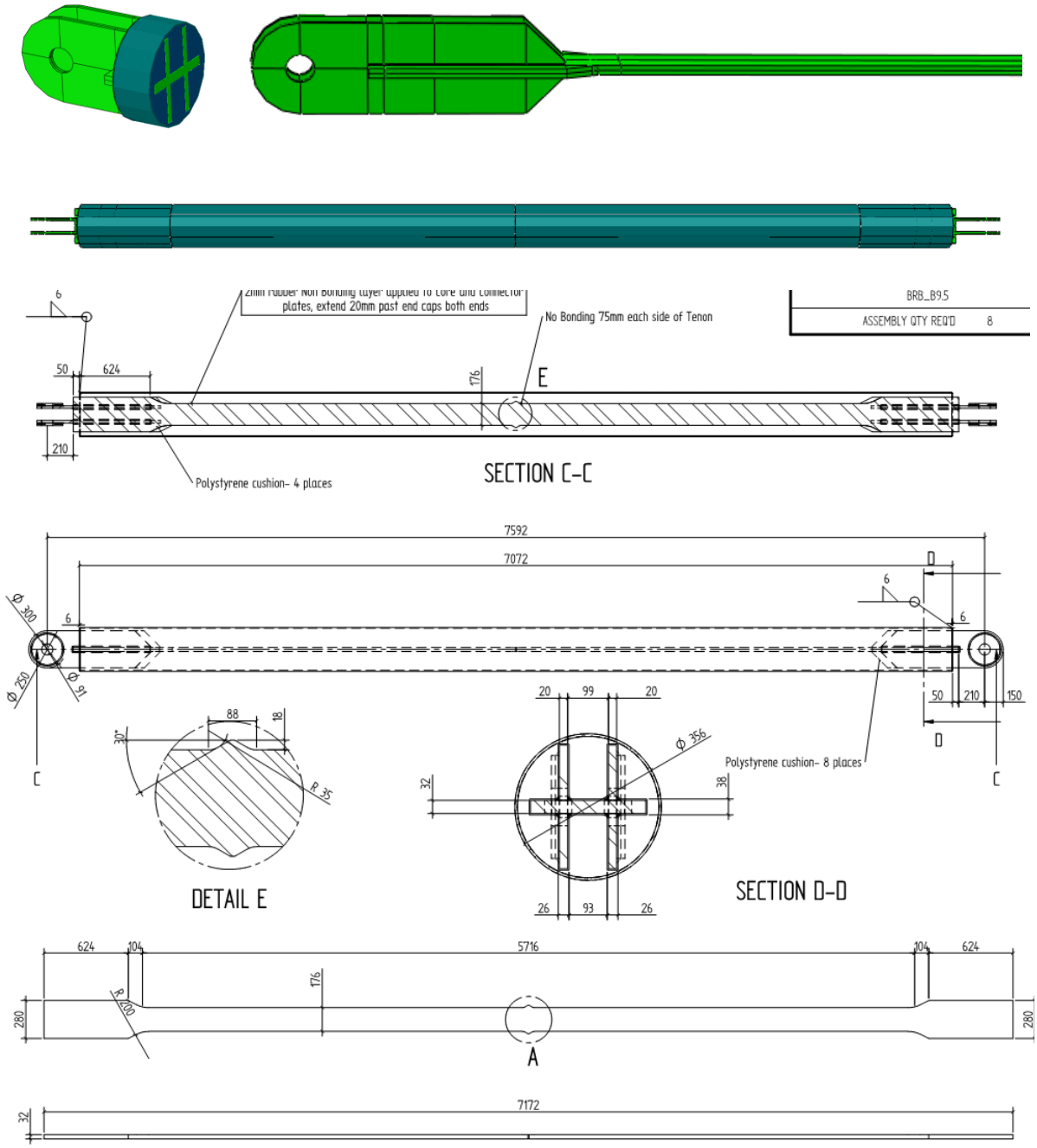

Figure 2-4. Solid model images and shop drawings (BRB 9.5)

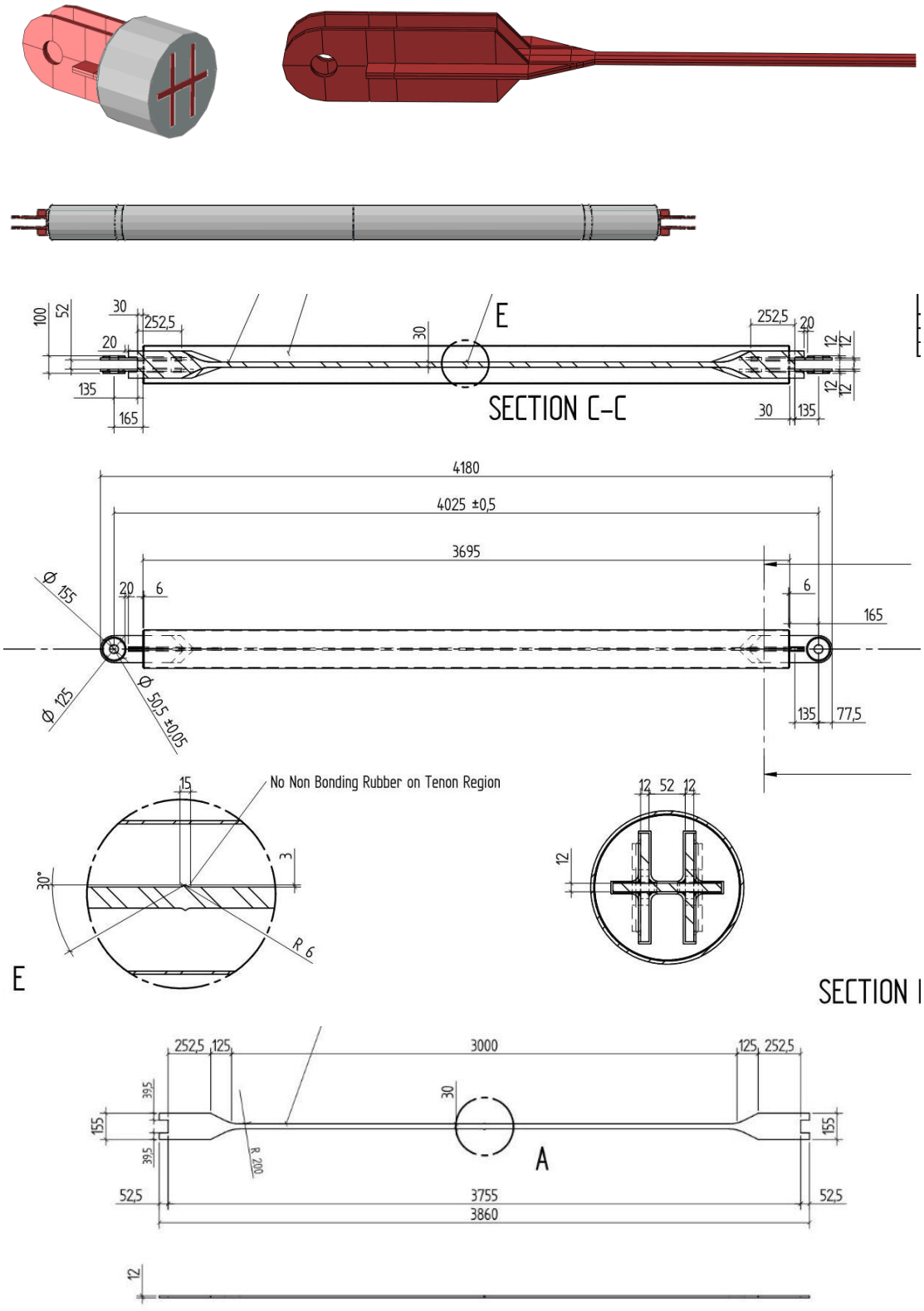

Figure 2-5. Solid model images and shop drawings (BRB 2A)

Table 2-2. Material details of BRB specimens investigated

	Core plate			Restrainer	
Brace ID	**Material Grade**	**Yield stress [MPa]**	**Ultimate stress [MPa]**	**Material Grade**	**Size [mm]**
BRB 6.5a	300	346	499	350	ϕ 323 x 6.4 CHS
BRB S3	300	311	409	350	125 x 125 x 6 RHS
BRB C6	300	342	408	350	ϕ 323 x 12.7 CHS
BRB 9.5	300	326	497	350	ϕ 356 x 6.4 CHS
BRB 2A	300	328	434	350	ϕ 219 x 4.8 CHS

The testing of the BRBs described in Table 2-1 took place within an IANZ accredited testing laboratory (Holmes Solutions 2014). The test apparatus is presented in Figure 2-6. An example of a bolted connection used in the test apparatus is shown in Figure 2-7.

Figure 2-6. A tension/compression capable horizontal test machine (Holmes Solutions 2014)

Figure 2-7. Gusset connection installed in test apparatus (load cell end) (Holmes Solutions 2014)

Each BRB was oriented in a horizontal direction during testing. This orientation induces an initial curvature due to flexure of the BRB under gravity, similar to in-service conditions. Testing was completed by imposing displacements to each BRB in predetermined increments up to a maximum displacement equivalent to twice the design storey drift ($2\Delta_{bm}$) for the intended building.

2.3 **Experimental testing methodology**

Uniaxial testing was used to assess the performance of each BRB specimen. This type of cyclic testing acts to induce a continually increasing axial strain within the BRB core, without the application of a bending moment. Test loading occurs in a cyclic manner, inherently subjecting the BRB core to varying cycles of tensile and compressive strains.

During testing, the gusset plates were bolted to the mounting platens of the test apparatus. An actuator was then extended to a position where the BRB could be installed without preload. Imposed displacements, based upon the design storey drift (where each BRB was intended for), were applied to one end of the BRB via a hydraulic actuator in accordance with the loading protocol.

2.3.1 **Loading protocol**

Test loading was applied in accordance with ANSI/AISC 341-16 Section K3 'Cyclic Tests for Qualification of Buckling Restrained Braces', with loading as prescribed in Section K3.4.c 'Loading Sequence' (ANSI/AISC 2010).

During the first load cycle of the test, an initial displacement is made in a positive drift direction (tension) until the force verse displacement response plot exhibited the occurrence of yielding. Yielding is defined as a distinct reduction in the stiffness. Once the initial tension yield displacement was discovered, the direction of loading was reversed in the opposite direction to an equal value of force (induced compression).

All subsequent cycles of loading were applied to pre-determined levels of displacement in both the tension and compression loading directions. At each level of drift displacement, the specimen was cycled from tension into compression, for two complete cycles before incrementing to the next drift displacement level. At the request of the engineer of record, additional cycles were applied to BRB S3 and BRB C6. An example of a loading protocol is presented in Figure 2-8.

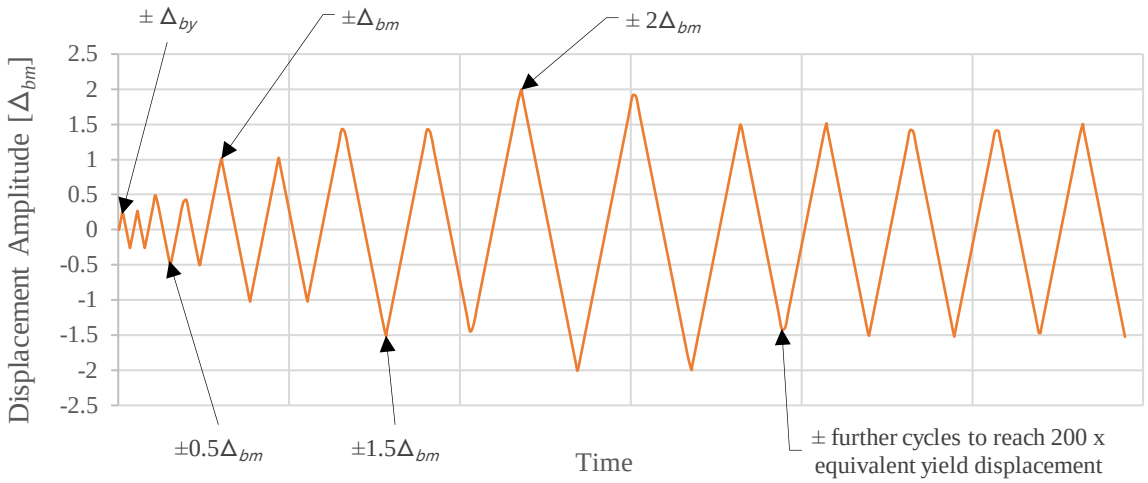

Figure 2-8. Loading regime for uniaxial cycle BRB testing as per ANSI/AISC 341-16 Manual (ANSI/AISC 2016)

The displacement amplitudes of each loading cycle are dependent on multiples of design storey drift that each brace is designed for. The following notations are used to represent the level of deformation and load each brace experiences.

Δ_b The level of displacement (drift), imposed on the test specimen.

Δ_{by} The level of displacement, Δ_b (drift), at the first significant yield of the test specimen.

Δ_{bm} The level of displacement, Δ_b (drift), corresponding to the design storey drift.

2.4 **Test procedure**

Cyclic testing begins by putting the brace into tension. The displacement of the actuator was computer servo controlled. A string pot displacement sensor recorded displacement of the brace. The string pot was attached between two jigs fastened around the centroid of the connection to each clevis. A four cell load array at one end of the test rig recorded the axial force throughout each test. To capture an accurate yield point and to reduce post yield displacement on the first cycle an initial rate of displacement of 0.5 mm/sec was used. Following this first target, the remaining amplitude targets did not require real-time interpretation so the loading rate was increased to 5mm/sec to reduce overall testing time, while remaining at a pseudo-static rate. Figure 2-9 shows BRB C6 installed in the testing apparatus prior to testing.

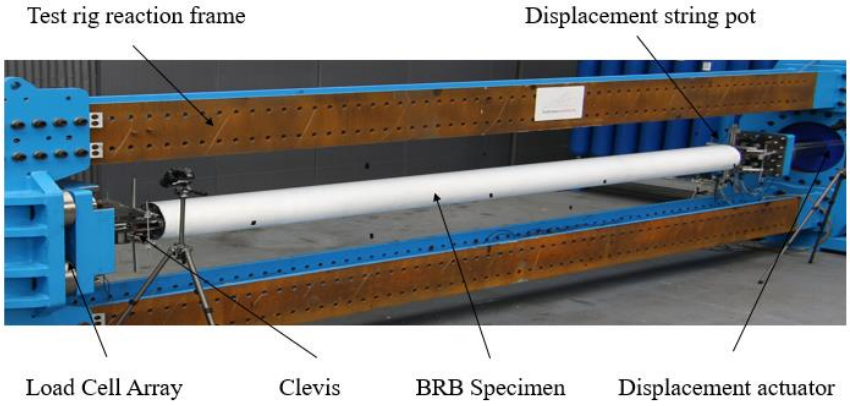

Figure 2-9. Physical specimen (BRB C6) in testing apparatus (Holmes Solutions 2014)

2.5 **Testing criteria and acceptance**

Prequalification testing serves several purposes. It confirms the BRBs yield load and adjustment factors required for connection design. It also tests the BRB ability to sustain axial strains expected in a design level earthquake event. Acceptable performance is demonstrated through stable hysteretic behaviour without failure. Results are judged according to the following acceptance criteria in ANSI/AISC 341-16:

- Display stable, repeatable load - displacement history with positive incremental stiffness.
- No rupture, brace instability or brace end connection failure during testing protocol.
- The maximum tension and compression force during each subsequent cycle after yield shall be no less than the yield force.
- The ratio of maximum compression to tension force during each subsequent cycle after yield shall not exceed 1.3

2.6 **Test results**

The loading protocol and results of the five BRB prequalification tests are presented in Figure 2-10 through to Figure 2-21. The loading protocol for each test is shown in terms of displacement and displacement relative to design storey drift (Δ_{bm}). This is followed by the force response of each specimen to its displacement loading protocol. For comparison the force response is also shown in terms of the overstrength ratio (force/yield force).

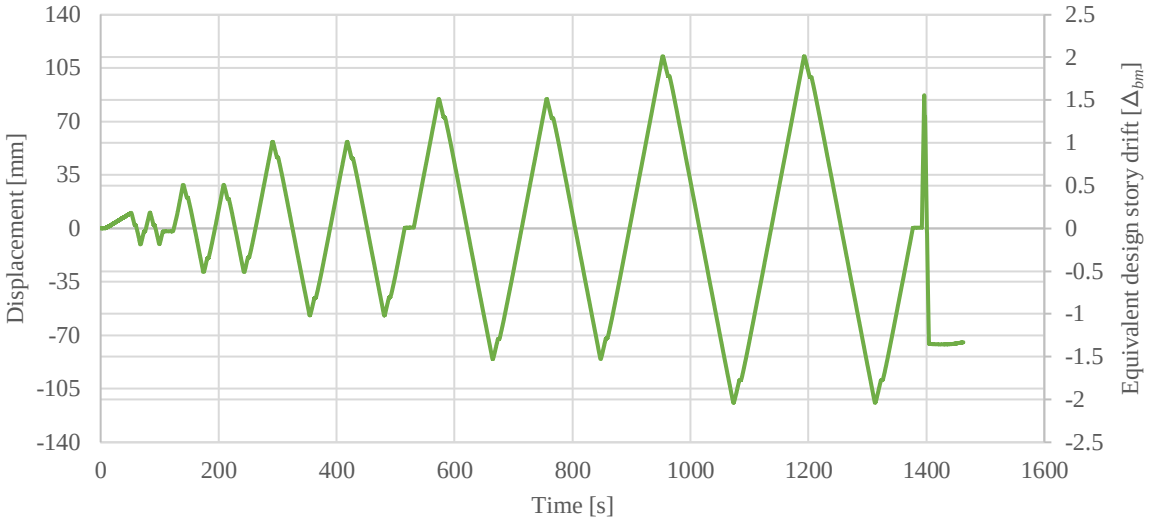

Figure 2-10. Loading protocol for BRB 6.5 (displacement - time domain)

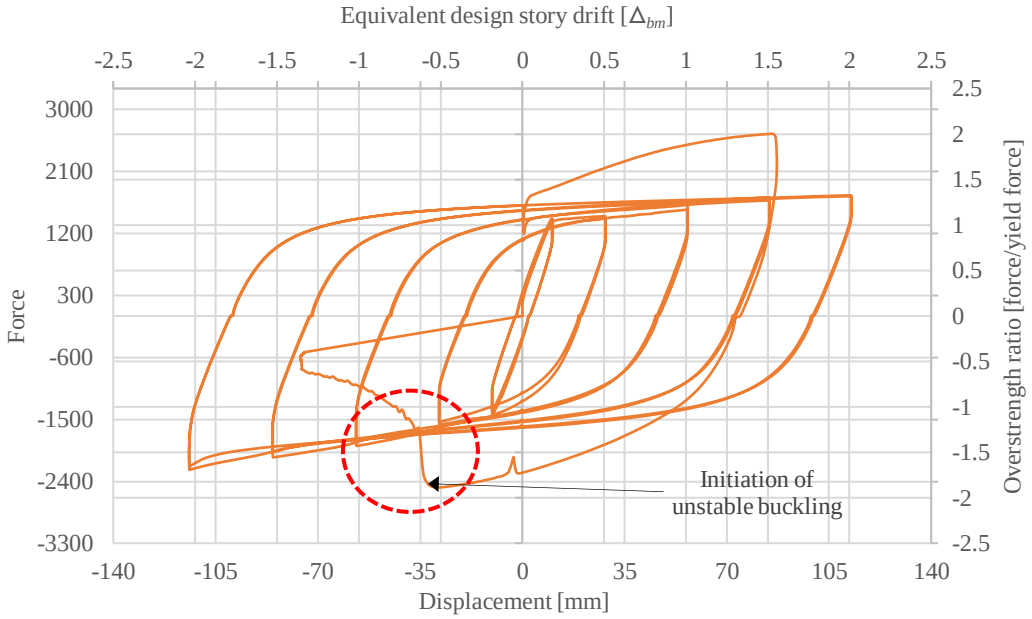

Figure 2-11. Experimental results for BRB 6.5 (force - displacement domain)

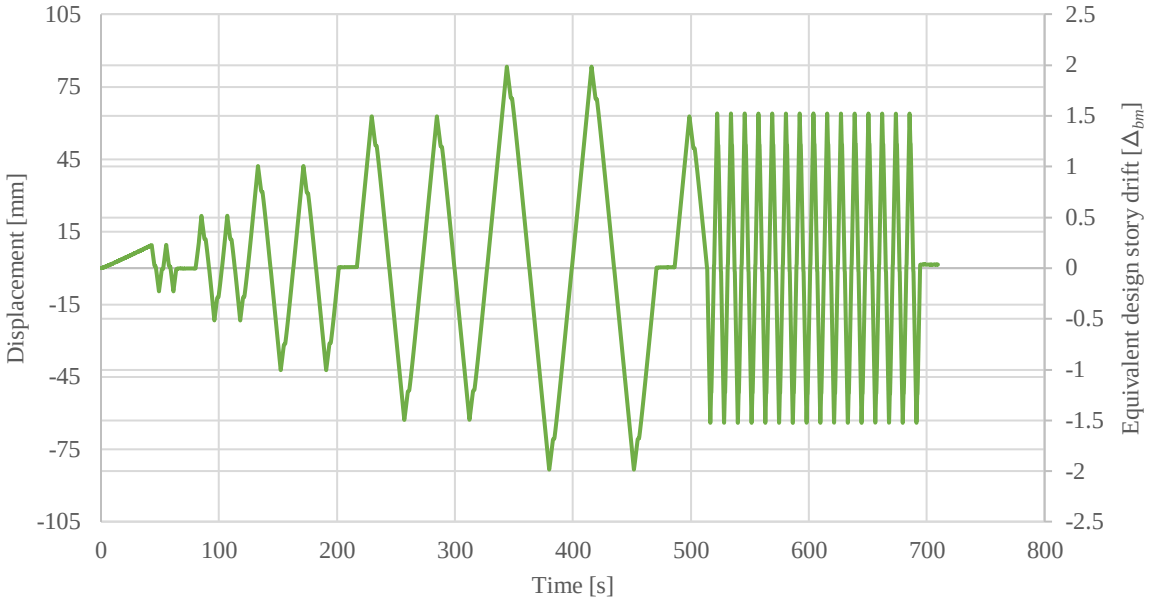

Figure 2-12. Loading protocol for BRB 6.5A (displacement - time domain)

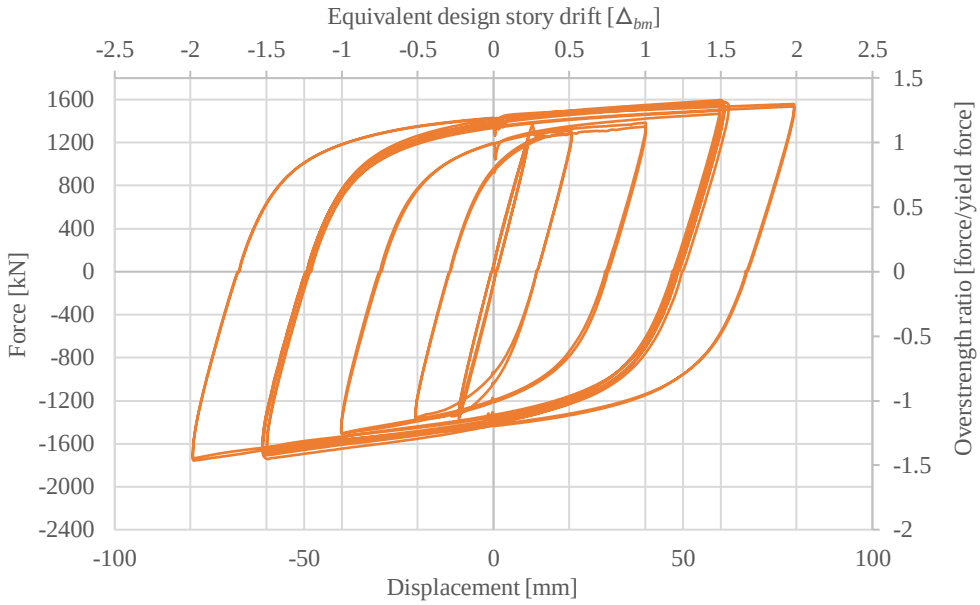

Figure 2-13. Experimental results for BRB 6.5a (force - displacement domain)

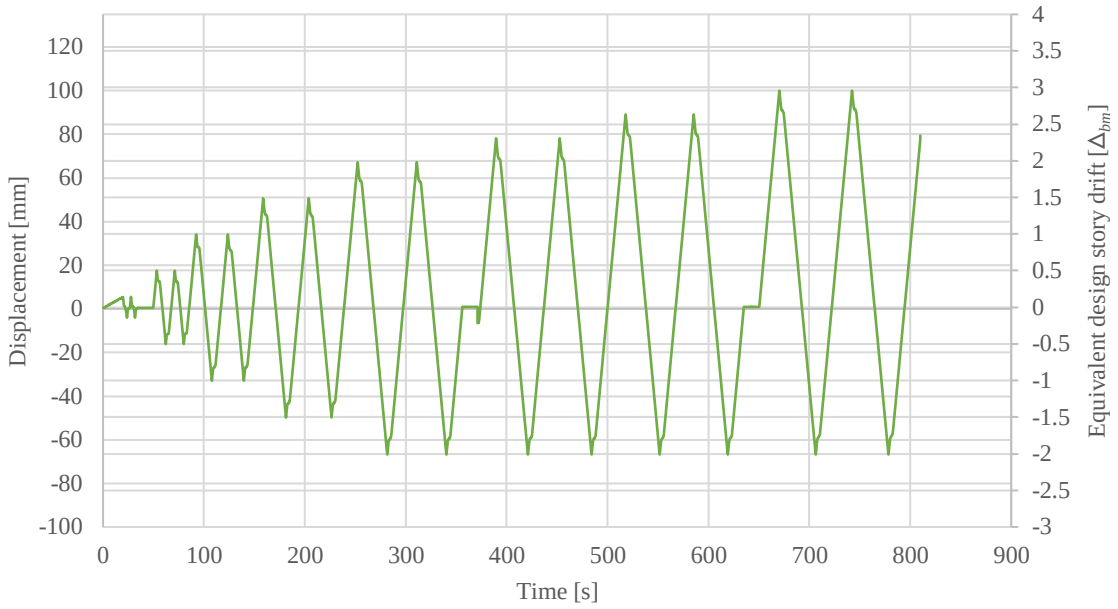

Figure 2-14. Loading protocol for BRB S3 (displacement - time domain)

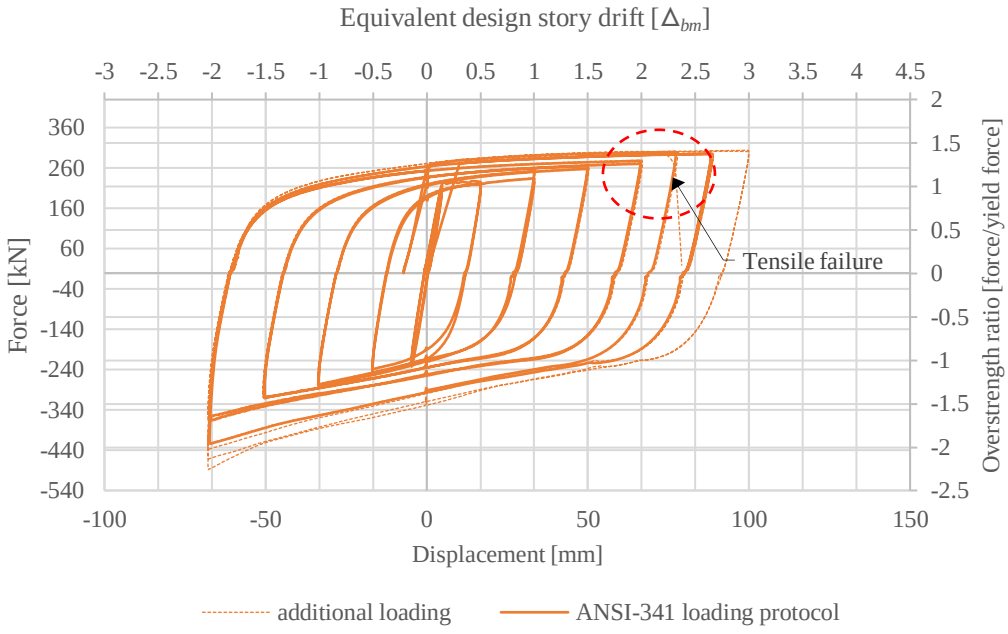

Figure 2-15. Experimental results for BRB S3 (force - displacement domain)

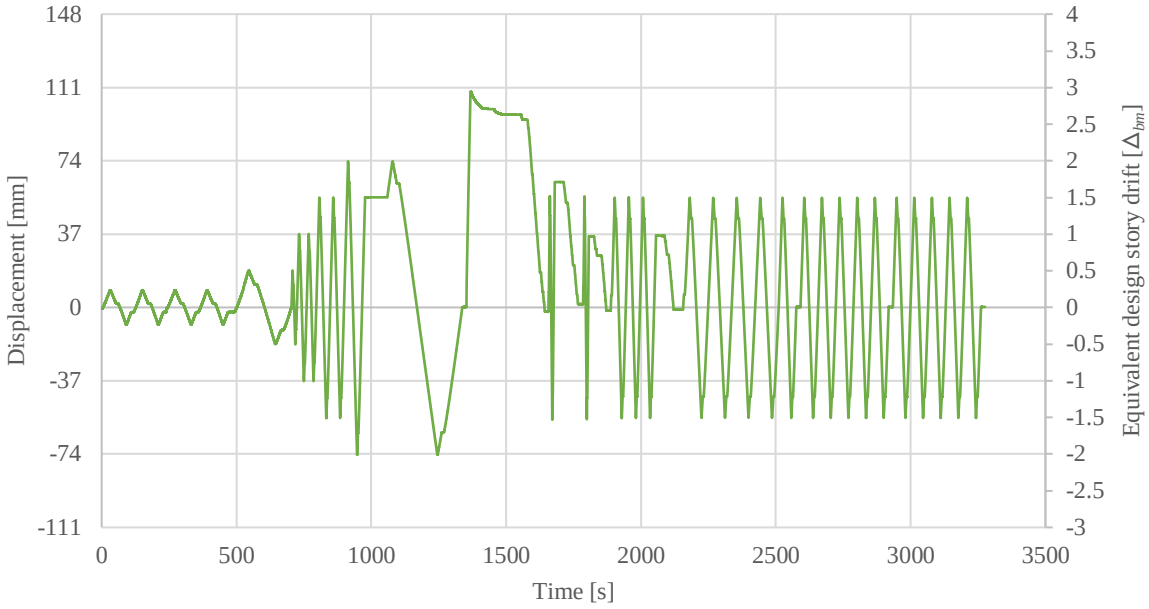

Figure 2-16. Loading protocol for BRB C6 (displacement - time domain)

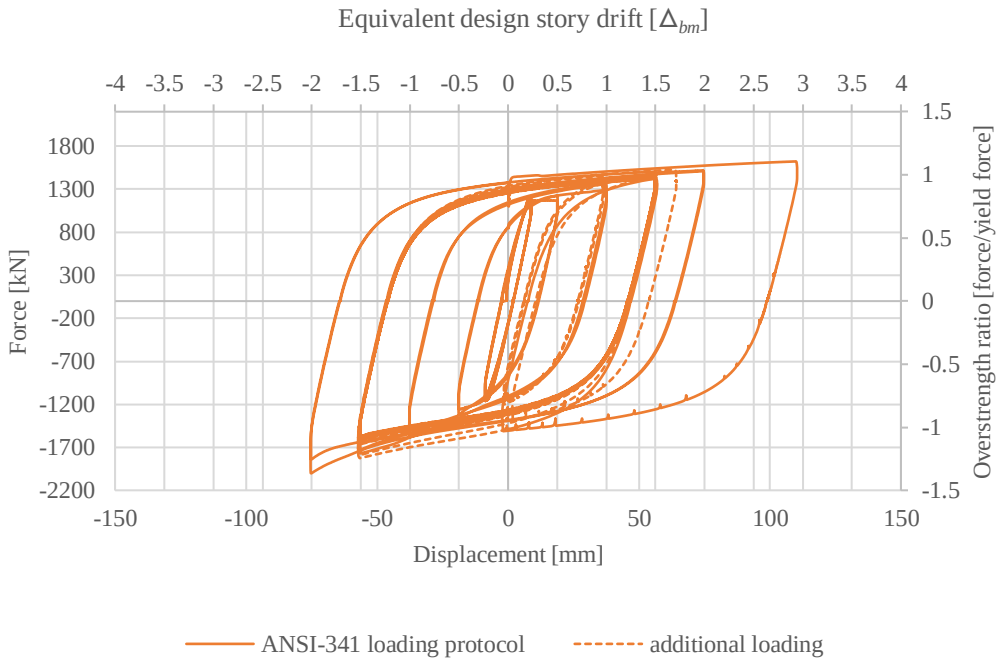

Figure 2-17. Experimental results for BRB C6 (force - displacement domain)

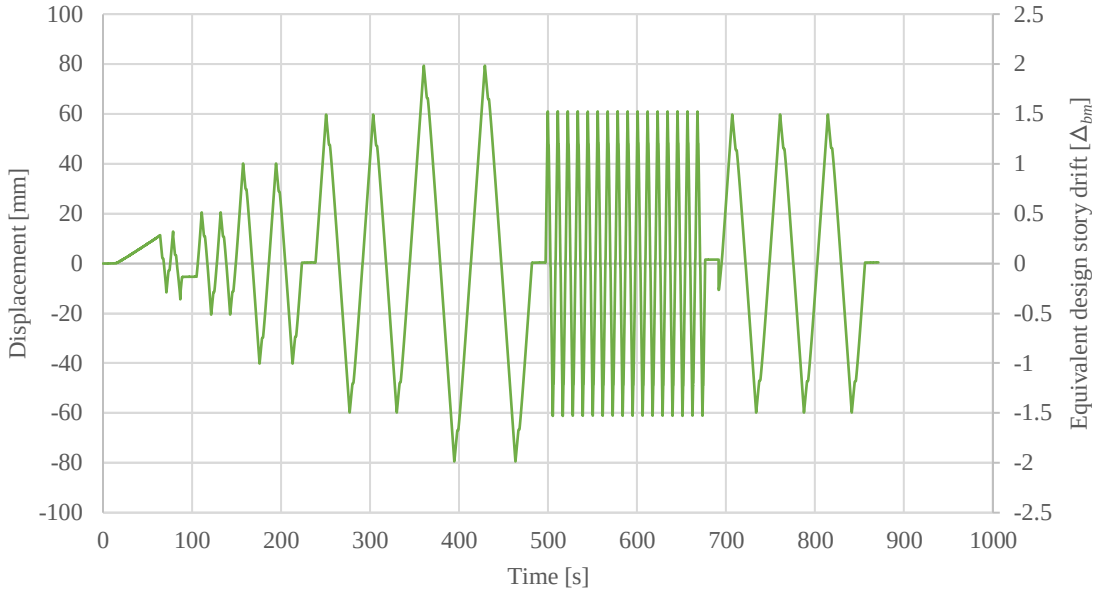

Figure 2-18. Loading protocol for BRB 9.5 (displacement - time domain)

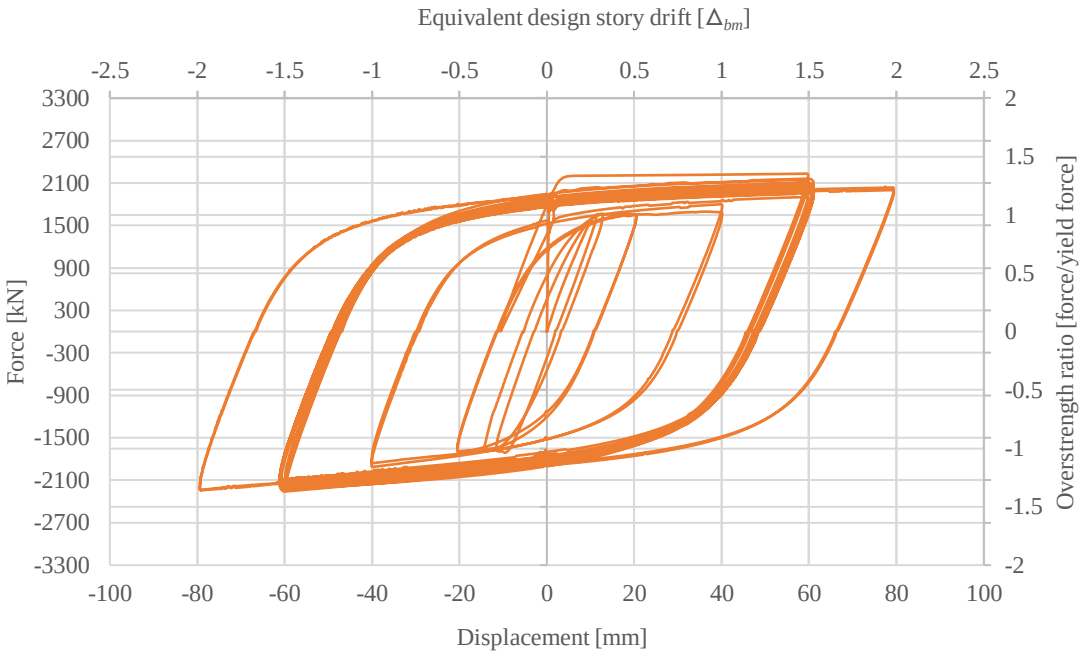

Figure 2-19. Experimental results for BRB 9.5 (force - displacement domain)

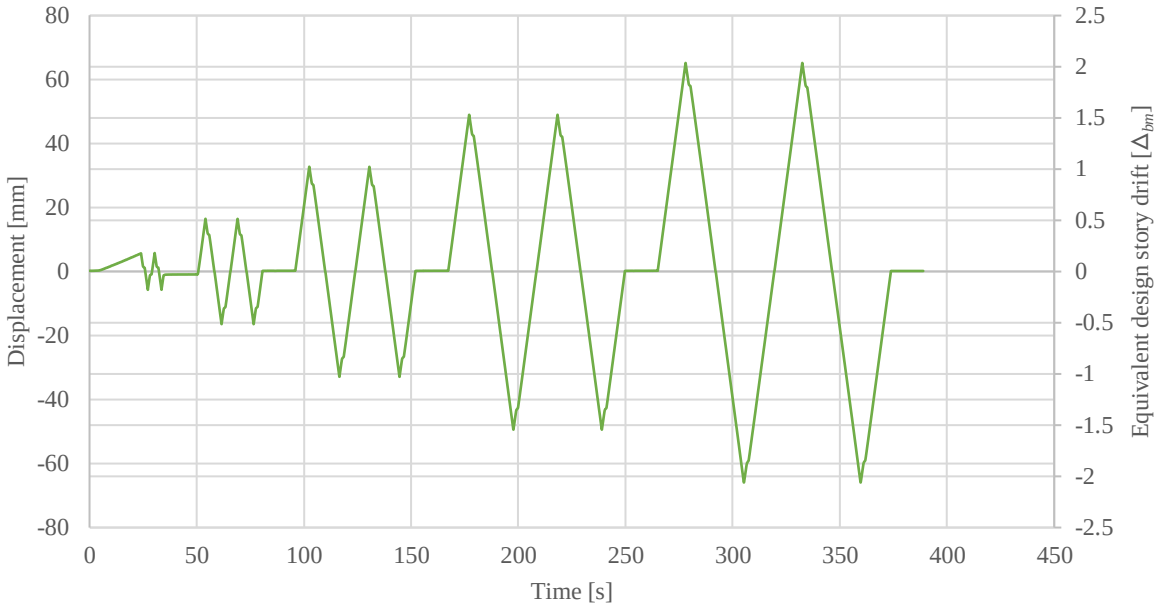

Figure 2-20. Loading protocol for BRB 2A (displacement - time domain)

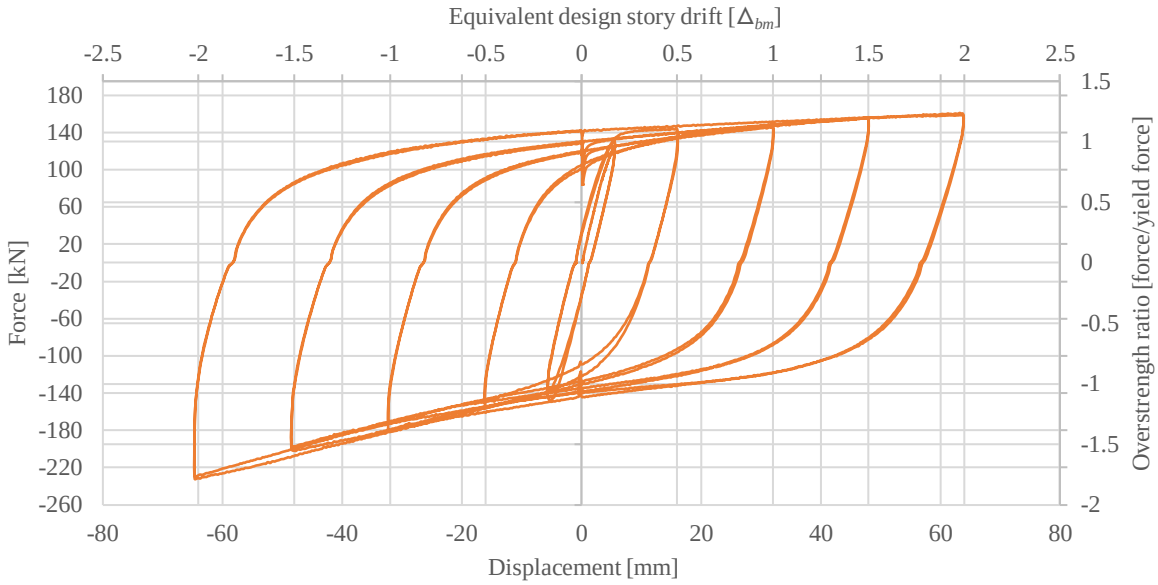

Figure 2-21. Experimental results for BRB 2A (force - displacement domain)

2.7 **Post test observations and discussion**

Following testing of the five braces presented in this chapter, it is of interest to compare results and observations between the different specimens.

2.7.1 **BRB 6.5**

This brace displayed stable hysteretic behaviour up to $\pm 2\Delta_{bm}$. This corresponds to an average strain of 2.3%. The specimen required additional cycles to achieve the cumulative strain requirement of 200 times yield displacement. However, upon the first additional cycle it failed.

The failure mode was consistent with global buckling. Initially, the core seems to catch or bind inside the restrainer causing a spike in the load response during the tension cycle. Upon load reversal, this occurs again in compression, quickly followed by a degradation in stiffness associated with buckling collapse. Figure 2-22 shows the brace after testing with the global buckling shape clearly visible.

Figure 2-22. Global buckling in prequalification testing of BRB 6.5 (Holmes Solutions 2014)

The force-displacement response in Figure 2-11 supports this behaviour, showing a sharp reduction in stiffness just prior to the peak load in the final compression cycle. Deconstruction of the specimen took place after testing. By cutting into the restrainer, it was revealed the core of the BRB was not running through the direct center of the restrainer. Figure 2-23 and Figure 2-24 show the location of the core relative to the restrainer.

Figure 2-23. Post-test examination of BRB 6.5, showing cracking underneath steel casing

Figure 2-24. Post-test examination of BRB 6.5, showing location of BRB core inside restrainer

One theory for this defect occurring, is that during construction the brace was orientated horizontally, allowing gravity to act along the length of the steel tendon. This caused the core to sag while the grout cured inside the restrainer. It is also possible that injection of the viscous grout further pushed the core to one side.

This failed test lead to a review of the construction process. To ensure the core remains in the center of the BRB during fabrication, the following steps were added. 1) Before filling the restrainer with grout, the welded section of core is hung vertically and tensioned slightly. Secondly, the steel casing is fixed with temporary props with the core in the center. It is important to note, that New Zealand does not yet have any regulations or guidance document for the fabrication or use of BRBs, so prototype testing (such as the ones described here) help to develop standard procedures for good practice.

With these steps added to the fabrication process, the same design was tested at a later date. Results showed this brace to perform well and able to meet all the acceptance criteria in ANSI/AISC 341-16. Full cycles to a displacement corresponding to $2\Delta_{bm}$ were achieved. This corresponds to an average strain (displacement/core yield length) of 1.7%.

2.7.2 **BRB S3**

This brace achieved the full loading protocol set out in ANSI/AISC 341-16 without core rupture or any signs of progressive reduction in load carrying capacity. When subjected to further loading cycles, BRB S3 continued to respond with positive stiffness for each increased displacement target until failure occurred. Displacement amplitudes corresponding to $3\Delta_{bm}$ in tension and $2\Delta_{bm}$ drift in compression were achieved. This corresponds to an average strain of 3.7%. Upon initiation to a target displacement of $3.5\Delta_{bm}$ in tension, core rupture was observed. This corresponded to a sudden loss of load carrying capacity and an audible noise typical to that of a steel tensile failure. This is in agreement with hysteresis plot in Figure 2-15. Deconstruction of this specimen did not take place after testing.

2.7.3 **BRB C6**

The expected yield load was 1445 kN but physical testing indicated yielding occurred at 1150 kN, demonstrated by a sustained period of elongation without increase in load. The expected yield load is calculated using the yield stress from material testing, and the cross sectional area of the core. However, testing appeared to show that BRB C6 yielded at 80% of expected yield load. The reason for the difference is unclear and no investigation took place at the time of testing. A sample taken from the non-yielding section of the BRB may have confirmed what caused this discrepancy. If the theoretical load of 1445 kN was used in design, BRB C6 fails to meet the acceptance criteria. As such, the design yield load was adjusted to 1150 kN. Following this, BRB C6 achieved the full loading protocol without core rupture or any signs of progressive reduction in load carrying capacity. Cycles reaching a displacement corresponding to $3\Delta_{bm}$ in tension and $2\Delta_{bm}$ in compression were achieved. This corresponds to an average strain of 2.6%. BRB C6 sustained further loading, in addition to the required loading protocol. Twenty additional cycles targeted $\pm 1.5\Delta_{bm}$. With this additional loading, accumulated displacement equivalent to 650 times displacement at yield ($650\Delta_{by}$) was achieved.

Upon completion of testing of BRB C6, the specimen was removed from the test apparatus and deconstructed to expose the core section. With the outer BRB casing removed, several cracks within the grout sleeve were discovered. Two longitudinal cracks were present, as well as a multitude of circumferential cracks, as can be seen in Figure 2-25. Upon removal of the grout sleeve no observable defects to the core were visible.

Figure 2-25. Post-test examination of BRB C6, observed cracks in grout with outer shell removed

2.7.4 **BRB 9.5**

This brace achieved the full loading protocol set out in ANSI/AISC 341-16 without core rupture or any signs of progressive reduction in load carrying capacity. Displacement amplitudes corresponding to $2\Delta_{bm}$ in tension and $2\Delta_{bm}$ in compression were achieved. This corresponds to an average strain of 1.4%. Deconstruction of this specimen did not take place after testing.

2.7.5 **BRB 2A**

This brace also achieved the full loading protocol set out in ANSI/AISC 341-16 without core rupture or any signs of progressive reduction in load carrying capacity. Displacement amplitudes corresponding to $2\Delta_{bm}$ in tension and $2\Delta_{bm}$ in compression were achieved. This corresponds to an average strain of 2.2%.

All cycles with a drift of $1.5\Delta_{bm}$, or less, resulted in the ratio of compression to tensile force not exceeding the allowable value of 1.3. However, all cycles conducted at $2\Delta_{bm}$ exceeded the allowable ratio, with a ratio of 1.4.

Prior to testing, it was thought that the restrainer may be contributing to the increased compressive effects. As such, strain gauges were attached to the outer steel casing in four locations in the middle of the BRB (top, bottom, left and right). Each strain gauge recorded strain in the longitudinal direction. Figure 2-26 shows where the strain gauges were attached.

(a) (b)

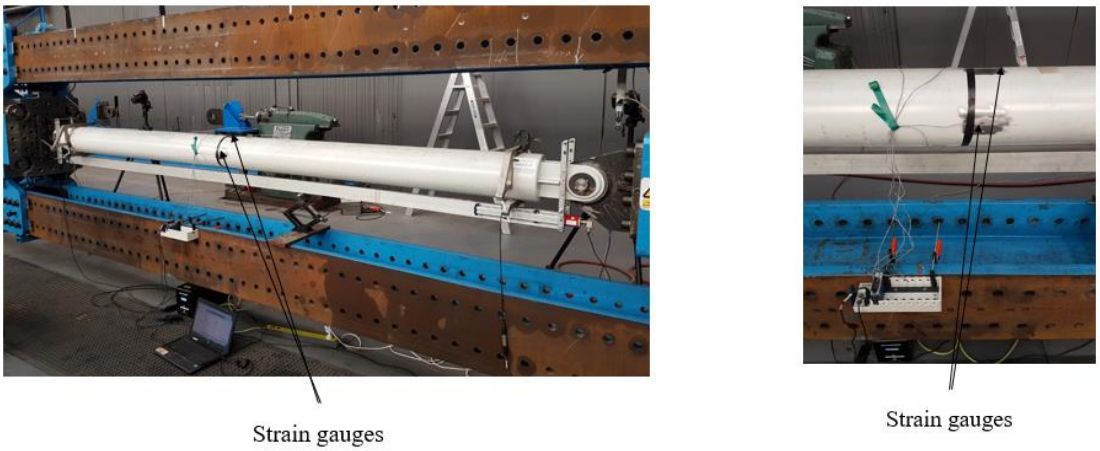

Figure 2-26. Location of strain gauges on outer surface of restrainer for BRB 2A
(a) wide view, (b) close up

Figure 2-27 shows the readings from four strain gauges evenly spaced around the center of the restrainer. The strain gauge data indicates that the welded core section transfers load to the restrainer in both tension and compression cycles. The spike in strain seen in the compressive cycles at $2\Delta_{bm}$ suggest the restrainer to core interaction influenced the higher compression to tension ratio for this cycle. This confirms the notion that significant axial force can be transferred through to the restrainer. In addition, each strain gauge appears to dip in strain twice within each cycle. This happens shortly after the transition from compression to tension and again shortly after the transition from tension to compression. This may be a result of stick-slip action between the core and restrainer.

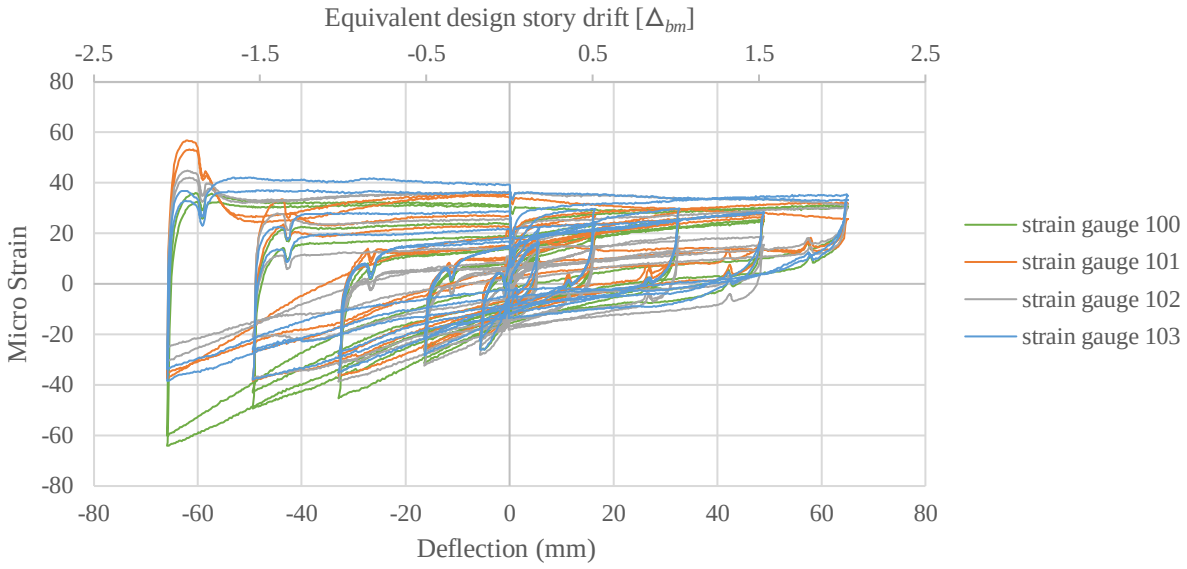

Figure 2-27. Strain readings from outer surface of restrainer for BRB 2A

2.7.6 **Comparison of overstrength factors**

To restrict weld tearing and connection zone failure, design loads for BRB frame elements are based on the post-yielding strength of the BRB core, when displacements equal $2\Delta_{bm}$ (Figure 1-23). Prequalification testing determines load adjustment factors. In tension, the design load for connecting elements is the product of the core area, yield strength and is multiplied by a strain hardening adjustment factor. In compression, a strain hardening and a compressive adjustment factor are multiplied by the core area and yield strength. Upon comparing the hysteresis plots between each brace, in was found that BRB S3, BRB C6 and BRB 2A had a higher compression adjustment factor (β) compared to BRB 6.5 and BRB 9.5. According to ANSI/AISC 341-16, this is acceptable if the ratio between tension and compression cycles does not exceed 1.3.

2.7.7 **Debonding material**

The debonding material between the core and the concrete restrainer is a key feature in BRB design. The debonding material is a thin film-like material that provides a low friction sliding interface between the core and the restrainer. This interface minimizes axial load transfer between the core and the restrainer. The thickness can vary depending on the debonding material used, but is generally 2.0 mm running the entire length of the restrainer. During compression cycles, significant normal forces develop at this interface and the core can deflect in either direction. The actual behaviour of the debonding material deforming inside the restrainer is very complex. The material heats up due to the plasticity of the steel core. This combined with the bending and stretching behaviour of the core, forces the material between the restrainer and the core in a fluid-like way. Physical observations of the material extruding out of the ends of the restrainer is evidence of this. Specific properties of the debonding material in commercial BRBs are generally confidential. However, information from a supplier suggest it is a type of butyl rubber. Figure 2-28 shows how the debonding material has extruded from the end of the restrainer.

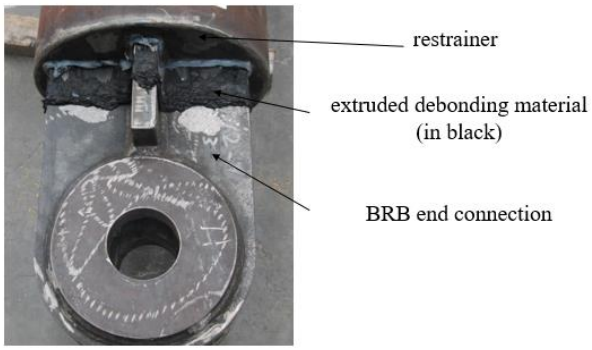

Figure 2-28. Post-test observation of dedonding material (BRB 6.5)

2.7.8 **Statistical considerations**

Most prototype structural products need at least three nominally identical tests to be undertaken, to enable a mean value and standard deviation to be evaluated. However, the cost associated with this type of testing meant each of the five BRBs were only tested once. Variation between results of the same BRB design are expected. FEA model development suggests the variations in the mild steel used in the core of the BRB is a leading cause of variation between BRBs of the same design. This means, that in theory, if FEA models calibrate the material model using brace specific material test data, this variation can be largely accounted for. For this to work, other factors that could influence test results need to be minimised. For example the fabrication process would need to be repeatable and with good quality controls. To reduce the expected variation of structural characteristics between test conditions and on-site performance, the displacement targets used in testing are based on project specific design targets. In addition, the yield load used in design is calculated from material test data, and verified against the BRB prequalification test results.

2.8 **Conclusion**

In New Zealand there is currently no standard or regulation on how to incorporate BRBFs in commercial building design. This makes it difficult for engineers to anticipate all the possible stability and strength issues within a system and actively mitigate them in each design. To help ensure BRBF designs perform as intended, a peer review and physical testing are currently required to gain building compliance in New Zealand. Details from the American standard (ANSI/AISC 341-16), that explain how to collect this evidence and why it is important is discussed. Specifically ANSI/AISC 341-16 prescribes two forms of testing.

1) Brace prequalification testing is conducted to ensure each BRB specimen is suitably designed and manufactured to meet earthquake design limits. This type of testing isolates the performance of a BRB by applying a cyclic uniaxial loading protocol.

2) Subassemblage testing investigates the performance of the system, specifically to ensure stability is maintained during design level earthquake events.

By way of example, this chapter presents the experimental test process and prequalification results of five commercially available BRBs manufactured in New Zealand. Testing was required as part a peer review to gain building code compliance. The first test of BRB 6.5 showed pre-mature failure. Post-test observations confirmed manufacturing errors led to global buckling failure. Each remaining BRB specimen achieved the full loading protocol, without core rupture or any signs of progressive reduction in load carrying capacity. Strain gauges attached to the casing of BRB 2A confirmed load is transfer through the restrainer. This information is valuable since test data for BRBs relevant to the New Zealand construction environment are not commonly available, with many experiments in New Zealand restricted to relatively small braces.

2.9 **References**

ANSI/AISC (2010). Seismic provisions for structural steel buildings - ANSI/AISC. One East Wacker Drive, Suite 700, Chicago, Illinois 60601-1802, American Institute of Steel Construction

ANSI/AISC (2016). Seismic provisions for structural steel buildings - ANSI/AISC. One East Wacker Drive, Suite 700, Chicago, Illinois 60601-1802, American Institute of Steel Construction

CEN (2010). European Committee for Standardization (CEN) EN15129:2010 Anti-seismic devices, CEN

ECCS (1986). Seismic design, recommended testing procedure for assessing the behaviour of structural steel elements under cyclic loads, European convention for constructional steelwork - Technical Committee 1. **Structual saftey and loadings - Technical working Group 1. -**

Holmes Solutions (2014). Buckling-Restrained Brace Testing. 5 Canterbury Street, Christchurch, New Zealand, Holmes Solutions Testing Laboratory

3 FEA STRATEGY FOR REALISTIC SIMULATION OF BUCKLING-RESTRAINED BRACES.

Buckling-restrained braces (BRBs) are seismic devices that provide structures such a buildings and bridges with lateral support, dissipating more energy than traditional bracing. Large-scale laboratory testing to assess every buckling-restrained braced frame (BRBF) is desirable but cost prohibitive. Computer simulation that incorporates realistic BRB mechanical behaviour is an attractive option to supplement such testing. Of particular interest is predicting the cyclic response, and to ensure stability following severe earthquake events. A finite element analysis (FEA) strategy that can model the testing of BRBs was developed using Abaqus®. The development of nonlinear material and contact models are important aspects that affect accuracy and convergence in each model. The Chaboche method, using six backstress curves is used to characterize the combined kinematic and isotropic hardening exhibited in a BRBs steel core. A simplified approach was developed to model the contact interaction between the restrainer and the core. Each model captures important frictional dissipation as well as lateral motion and bending associated with higher-order constrained buckling of the core in both the strong and weak axis. At the same time, the methodology sought to minimize computational expense for this highly nonlinear system. The strategy was validated by comparing cyclic axial force versus displacement predictions to experimental data for three different BRB designs. The strategy was then tested through blind prediction of two other BRBs without the use the experimental data for callibration, keeping all modelling features the same aside from the shop drawings and the available material test data. Results from these blind predictions showed good agreement with experimental data.

3.1 **Introduction**

The interaction of the core and the restrainer is a complex nonlinear phenomena that has limited the development of detailed FEA models. It involves a combination of instability effects, nonlinear constitutive laws and frictional contact. These behaviours play a significant role in the performance of the BRB system. The restrainer is designed to confine transverse displacements of the core and prevent global buckling of the BRB assembly. However, transverse displacements are caused by the slender nature of the core that can lead to constrained buckling at very low axial compressive loads (less than yield). Simplified approaches are traditionally used to model the features related to this behaviour. For example, Chou et al. (2012) used shell elements to represent a BRB within a frame and then simplified this to investigate only the connection zone including the end of the BRB, gusset plate and beam-column-joint. Material non-linearity was represented as a bi-linear curve using the yield and ultimate stress. A frictionless contact with no gap was used to model the restrainer and BRB core. This model reasonably predicted the ultimate load of the connection. However, it has not been validated over a range of experiments and does not help researchers understand the internal behaviour of different BRB designs. In addition, these simplifications render such models ineffective for predicting local deformation.

Another approach to modelling a BRB using FEA is presented by Chou et al. (2009) who uses a truss element to represent the BRB. As truss elements cannot represent bending, there is no need for modelling a restrainer, thus reducing computational demand. Material nonlinearity was approximated using a bilinear stress-strain relationship. A more sophisticated approach by Westeneng (2016) used two beam elements, one to represent the BRB core and the second to represent the restrainer. The two beam elements are coupled together at pre-selected degrees-of-freedom, constraining all but translation in the longitudinal direction of the beam. This allows sliding of the core inside the restrainer to occur but does not allow frictional contact and restricts buckling to one mode shape. Westeneng states that this modelling method makes it difficult to accurately predict the hinging behaviour that has been observed at the BRB end. Both of these methods are appealing as they significantly reduce computational demand. The sacrifice, however, is they lack of fidelity and therefore a lack of representation of realistic local deformation.

Zsarnozay (2013) and Budaházy (2015) developed a more complex BRB model that captures elements of the behaviour of the core inside the restrainer. This was achieved by using a newly developed enhanced material model based on the Chaboche model (Budaházy et al. 2013), solid elements and contact interactions. These modelling features resulted in increased computational cost and convergence issues. To achieve viable numerical processing times, Budaházy (2015) resorted to modelling half of the BRB. The

complexity of this type of modelling and associated computational demand is the main reason why this level of modelling detail has seldom been used. In addition, Zub et al. (2020) developed a set of complex solid models of their in-house BRB designs. These designs had yield capacities of 150kN-840kN and their FE models used an explicit solver. There is the need for high-fidelity models that capture realistic behaviour of the core inside the restrainer but with reduced model development time and computational cost. This will enable engineers and researchers to analyse subassemblage and complete system interactions. Computational resources are becoming increasingly available and due to the large number of variables and types of non-linear behaviour observed in BRBs, FEA is the best tool to conduct analysis for this application.

In building and bridge design, FEA is commonly used to build models of entire structural systems with the purpose of checking and verifying structural design limits. These limits are often associated with post-yield and collapse behaviour as well as system-level behaviour and performance such as the response to seismic or gravity loads. Common software analysis tools such as Sap2000 (Computers and Structures Inc. 2004), ETABS (Computers and Structures Inc. 2016), Opensees (Mazzoni et al. 2007) and Perform3D (Computers and Structures Inc. 2011) make simplifying assumptions about rigidity of connections, stiffness of members, and plasticity, either in distributed plasticity models, (where plane sections remain plane), or lumped plasticity models. Continuum modelling such as that used in this paper, captures local deformation with minimal simplifying assumptions. Continuum modelling can be used to inform and calibrate the assumptions made by structural level analysis tools to more accurately represent components and therefore global behaviour.

Subassemblage testing is highlighted in the seismic provisions of ANSI/AISC 341-16 as an important aspect in demonstrating a BRB will perform as intended. This is to verify the BRB core can accommodate the combined axial and rotational deformation demands without failure. It is recognized that subassemblage testing is more difficult and expensive then uniaxial BRB testing. For these reasons non-linear FEA in combination with uniaxial testing has been approved as an alternative to subassemblage testing (ANSI/AISC 2010).

To capture the stress-strain development of a BRB core and connection zone, this paper describes a strategy to model BRBs in FEA. This captures the deforming behaviour of the core as it interacts with the restrainer. The modelling strategy takes into account the development and computational cost of each modelling feature and the sensitivity each has on predicting important aspects of the cyclic response. The key areas discussed regarding the FEA model development are; defining material properties of the core and grout, the contact relationship between the BRB core and the restrainer, and methods used to overcome

convergence issues. Specifically, the definition of these material and contact models provides suitable accuracy of the cyclic behaviour while minimising development and computational cost. Validation is demonstrated through comparing simulated results to experimental uniaxial testing of three BRBs designed by engineers in Taiwan at the National Center for Research on Earthquake Engineering (NCREE 2020). Results show that these features are required for FEA to accurately determine the acceptance criteria and overstrength factors of BRBs needed for design of BRB frame elements. For completeness, summary statements are made about other generic modelling selections.

3.2 Material modelling

3.2.1 Mild steel plasticity

The plasticity of mild steel, such as that used to fabricate the core of BRBs, is well studied. The following sub-sections explain behaviours observed when mild steel is subjected to cyclic loading. Due to the cyclic nature of earthquake loads it is important to understand and capture these. Two distinct changes to the yield surface occur during plasticity, these being isotropic and kinematic hardening. Isotropic hardening describes the uniform expansion of the yield surface in stress space. Kinematic hardening describes the translation of the yield surface. Both hardening behaviours happen simultaneously and are defined as functions of plastic strain.

For numerical simulations to make accurate predictions of cyclic loading they need to account for observed material behaviours. The Baushinger effect is characterised by a reduced yield stress upon load reversal following plastic deformation. Kinematic hardening captures this behaviour. Research shows this phenomenon saturates the initial yield stress and yield plateau within the first few cycles and decreases with continued cycling (Budaházy et al. 2013). The cyclic loading protocol for prequalification of BRBs results in many cycles and strain ranges much larger than the yield plateau. This means the transition phase of the Bauschinger effect from first yield has a negligible effect on overall cyclic behaviour. Figure 3-1 shows how the Baushinger effect saturates within a few cycles.

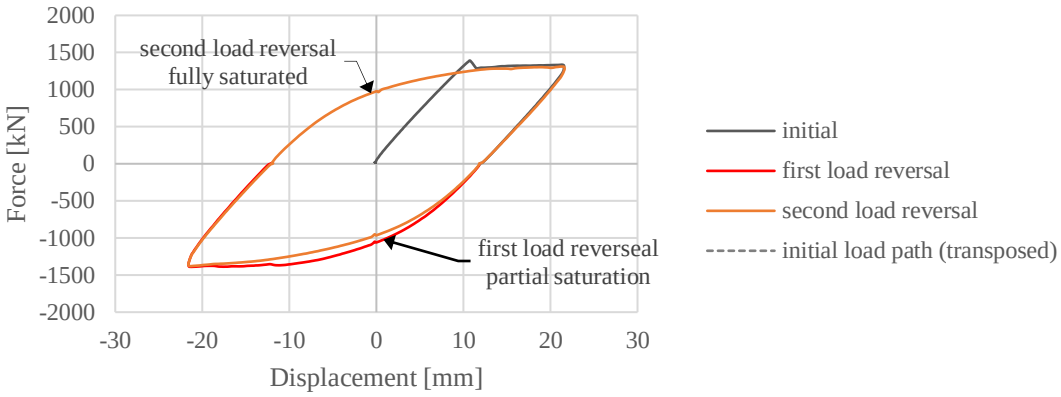

Figure 3-1. Schematic of Bauschinger effect

Other material characteristics effecting BRB behaviour include plastic shakedown and ratcheting. Plastic shakedown describes the tendency for ductile metals to harden toward a stable limit. This is easily observed in symmetric strain-controlled experiments. Ratcheting or “creep” is caused when cyclic loading is unsymmetrical, where the mean stress between compression and tension is non-zero. This can happen in

discrete zones of a BRB if combined bending and axial stresses are present, even though axial displacements applied to the entire BRB are equal and opposite. A schematic of these characteristics, plastic shakedown and ratcheting are presented in Figure 3-2a and Figure 3-2b respectively.

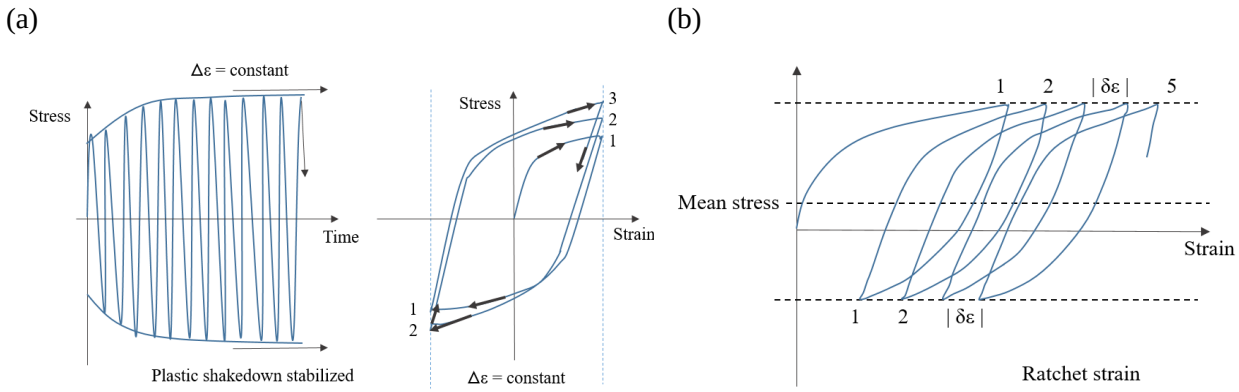

Figure 3-2. Schematic of non-linear material behaviors in mild steel (a) plastic shakedown (b) ratcheting (Lemaitre et al. 1990)

3.2.2 **The Chaboche method**

FEA packages facilitate different methods of modelling ductile steel, such as that used in the core of BRBs. The Chaboche method (Broggiato et al. 2008) forms the basis for the material model used here. The Chaboche method is a refinement of the Fredrick-Armstrong (F-A) method. It uses an exponential function to form a backstress curve $\boldsymbol{\alpha}$ that models the change of the yield surface. Figure 3-3 shows how the F-A method describes 3-D stresses in principal stress space ($\boldsymbol{\sigma_1}$, $\boldsymbol{\sigma_2}$ and $\boldsymbol{\sigma_3}$) in a stress-strain curve.

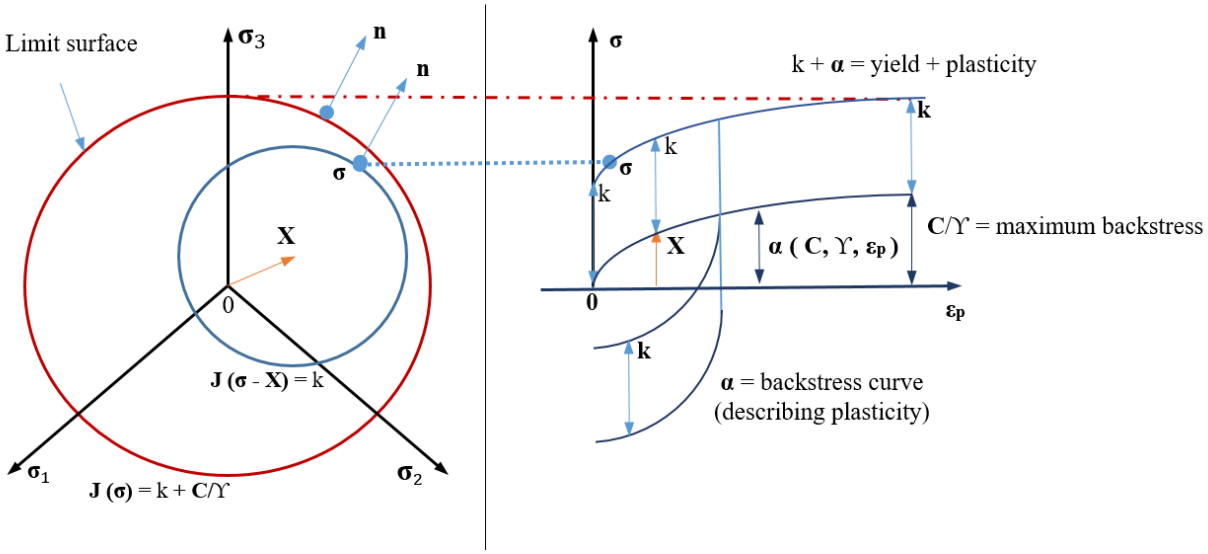

Figure 3-3 Behavior of Frederick-Armstrong Model (Lemaitre et al. 1990)

In Figure 3-3 (on the left), the yield surface ***J (σ-X)***, in principal stress space ($\boldsymbol{\sigma_1}$, $\boldsymbol{\sigma_2}$ and $\boldsymbol{\sigma_3}$), can translate by ***X*** (kinematic) or uniformly expand (isotropic) to the limit surface ***J (σ)***. The F-A method (on the right) uses two parameters to describe kinematic hardening in stress-strain space. The first being an initial hardening modulus ***C*** and the second, a recovery parameter Υ. The recovery parameter defines fading from the initial modulus ***C*** to a tangent stiffness that plateaus (zero gradient) at a stress value of $\boldsymbol{C/\Upsilon}$. By removing the elastic limit ***k***, the F-A method models this behaviour with exponential functions and they are referred to as backstress functions. The Chaboche method builds on the F-A method by providing the option to sum together several backstress curves to better define the overall non-linear behaviour. Presented in equation (1) is how a backstress develops over a plastic strain range $\boldsymbol{\varepsilon}_{\text{pl}}$, where k denotes the k^{th} backstress. Figure 3-4 is a graphical representation of how several backstresses sum together to form the overall non-linear backstress as shown in Figure 3-3 (on the right).

$$\boldsymbol{\alpha}_k = {}^{\boldsymbol{C}_k}/_{\boldsymbol{\gamma}_k} \left(1 - e^{-\gamma_k \varepsilon_{pl}} \right) \tag{3.1}$$

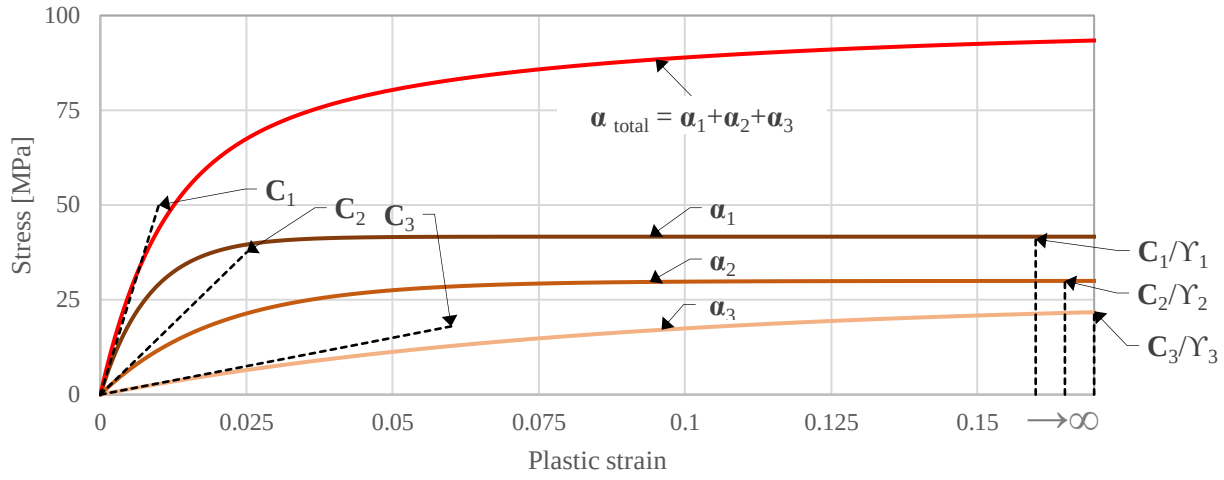

Figure 3-4. Development and summation of Chaboche backstress curves

Chaboche also provides a method to model the expansion in the yield surface (isotropic hardening) controlled by accumulated plastic strain and temperature. To numerically model this form of hardening, it is advantageous to express it in the same exponential form as equation (1). Therefore, equation (2) is also an exponential function describing how isotropic hardening $\boldsymbol{\sigma_{iso}}$ changes with plastic strain $\boldsymbol{\varepsilon_{pl}}$, where $\boldsymbol{Q_\infty}$ is the asymptotic stress value and b is known as the velocity of stabilisation.

$$\boldsymbol{\sigma_{iso}} = \boldsymbol{Q_\infty}\,(1 - e^{-b\,\boldsymbol{\varepsilon_{pl}}}) \tag{3.2}$$

Cyclic experimental test data of the material is required to construct these backstress curves. Through iteration, the parameters defining each backstress can be determined to achieve a good fit to the experimental data. As the Chaboche method describes material plasticity of steel, if the same material is used for different BRB architypes and sizes, then calibration only needs to be conducted once for numerical modelling. The F-A and Chaboche methods are well documented. Further background to the development and history of these methods is provided by (Budaházy 2015).

3.2.3 **General limitations of the Chaboche model.**

A summary of the general limitations of the Chaboche model is presented here.

1) It cannot accurately predict fading memory behaviour.

Fading memory behaviour is observed when a single cycle of high strain occurs, followed by cycles of lower strain. The effect of the maximum strain fades during subsequent stress-strain cycles. This is observed to occur in a preloaded experimental test. The Chaboche method does not have a specific feature to account for this behaviour. However, using several non-linear kinematic backstresses helps to capture it. When simulating BRB prequalification testing, this phenomenon is not present as load cycles are symmetrical. However, this needs to be considered in realistic earthquake loading as a large pulse load may be followed by smaller amplitude ground motions.

2) It can overestimate ratcheting effects.

Ratcheting or creep is caused when cyclic loading is unsymmetrical, when the mean stress between compression and tension is non-zero. Generally, this phenomenon is observed to reduce to zero if there is a low mean stress but continues to increase if there are high mean stresses. When modelling this material behaviour, a single non-linear kinematic curve results in constant ratchet strain. To improve modelling accuracy, isotropic hardening can be used to reduce the ratcheting effect. Also, employing several kinematic curves with one being linear or nearly linear can improve overall predictions and increase the ratcheting effect at higher mean stresses (Dassault Systems 2014)[1].

3) It cannot describe the yield plateau.

For low carbon steel, such as that used to fabricate the core of a BRB, a yield plateau is a prominent feature upon initial yielding that is particularly evident in tensile testing and the Chaboche model does not represent this behaviour. However, in a cyclic loading environment (such as BRB testing), this feature goes away in subsequent cycles and it only occurs at low strains within the first few cycles. As such, it has little effect on predicting overall cyclic BRB behaviour including overstrength factors.

4) It may not take into account all the components of isotropic hardening

Experimental testing has shown isotropic hardening appears as two components. Isotropic hardening distinctively develops within the first few load cycles and then stabilizes at a maximum strain of 8%. The second depends on accumulated plastic strain and always increases (Budaházy 2015). The method employed in this strategy uses one exponential curve to capture both components of isotropic hardening.

3.2.4 **Calibrating the Chaboche model**

The BRB test results used for validating the strategy presented in this paper were initially only intended for use in commercial building projects. Therefore, the material testing required to calibrate the non-linear material parameters in the Chaboche model were not conducted. As such, these parameters were obtained through iteration. Calibrating this way is time consuming and requires iteration to match BRB test data. For these reasons, this section describes how to conduct material tests and use test data to calibrate each of the non-linear parameters without the need for testing BRBs. As common testing standards do not specify cyclic loading protocols for investigating steel, this section describes a selection of recommendations made by Budaházy (2015).

Although the Chaboche method with non-linear isotropic hardening has limitations, it only requires two forms of cyclic testing to adequately model the cyclic response of BRBs. Also, as this material model is embedded within Abaqus it is a cost effective option and easier to implement then more complex models such as the PRESCOM model (Budaházy 2015).

The stress-strain backstress produced from each cyclic material test to represent kinematic hardening can be calibrated to the Chaboche method using the curve fitting algorithm provided by Abaqus. This typically fits three kinematic curves which sum together to match the experimental dataset. However, by having five user-defined backstresses the Chaboche method has been found to capture phenomena not observed in these loading protocols, such as ratcheting. This can also ensure positive stiffness over the desired strain zone meaning an ill conditioned stiffness matrix is avoided.

First, to determine yield and ultimate strength, and to ensure the required ductility, a monotonic tensile test should be conducted. Procedures set out in AS 1391 2007 (Standards Australia 2007) should be followed for this type of testing. For modelling purposes, the initial yield stress is adjusted to better match the value where the linear-elastic range finishes once stabilized cycles are reached. This is expected to be between 50%-70% of the initial yield strength of the first cycle, depending on the grade of steel (Budaházy et al. 2013).

Second, two uniaxial cyclic tests should be conducted. Strain gauges should be attached along the length of the gauge section, on each flat side of the specimen. The specimen for each test should be sized as shown in Figure 3-5. This specimen design reduces the likelihood of buckling due to it chubbier shape due to the short length compared to the transverse dimensions.

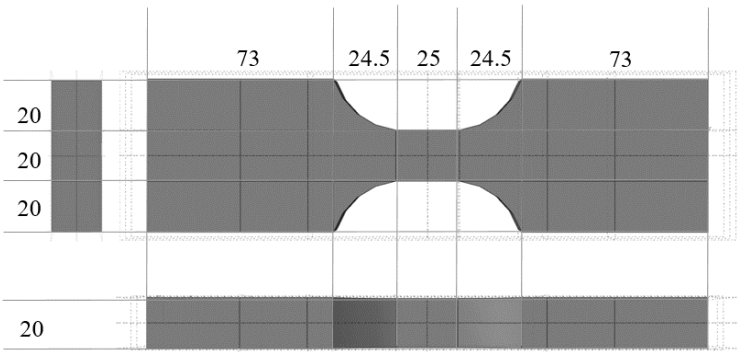

Figure 3-5. Cyclic uniaxial specimen (Budaházy 2015)

3.2.4.1 Calibration of Kinematic Hardening

To identify kinematic hardening, the strain history shown in Figure 3-6 should be followed. This is a symmetric strain-controlled experiment with constant increase in amplitude cycle-to-cycle. The idealised response to this loading is presented in Figure 3-7.

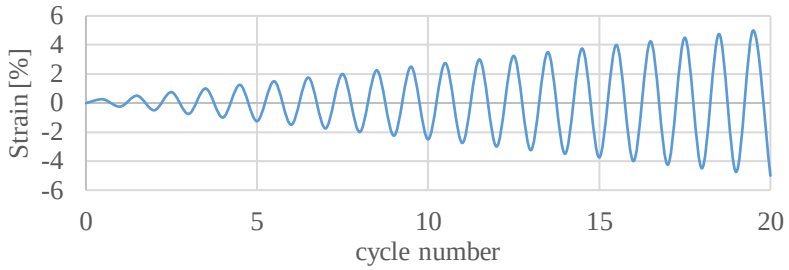

Figure 3-6. Symmetric strain-controlled experiment with increasing amplitudes

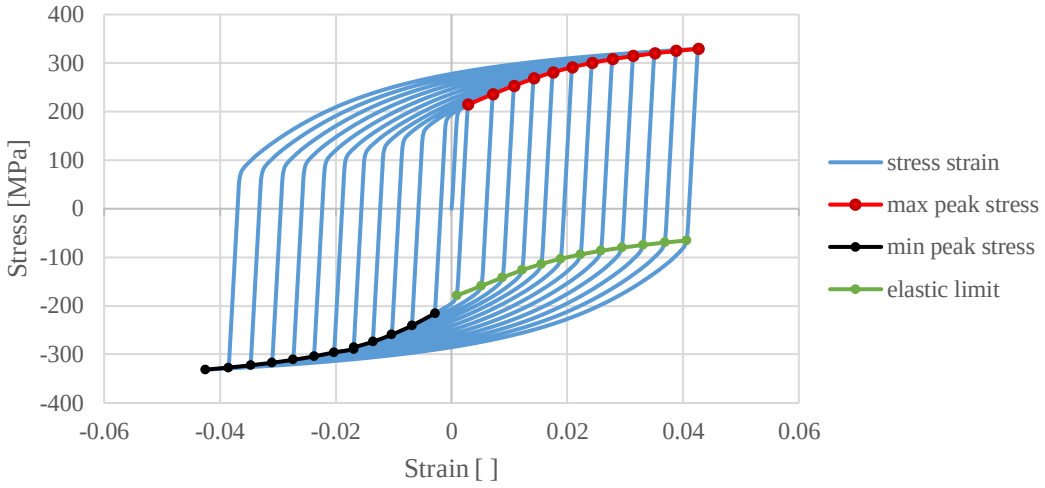

Figure 3-7. Identifying kinematic hardening from cyclic material test data

This cyclic stress-strain plot is used to determine the overall kinematic backstress curve ($\boldsymbol{\alpha}$) using equation (3.3). This requires the total stress $\boldsymbol{\sigma}_i^{total}$ for each the loop to be calculated using equation (3.4). This is the average of the peak compression and tension stresses for each cycle. Next, the peak yield stress or elastic limit $\boldsymbol{\sigma}_i^{elastic}$ upon load reversal needs to be identified. For each cycle, this is the point where the gradient of the curve falls below 90% of the elastic modulus attained in the tensile testing.

$$\boldsymbol{\alpha}_i = \frac{\boldsymbol{\sigma}_i^{total} + \boldsymbol{\sigma}_i^{elastic}}{2} \tag{3.3}$$

$$\boldsymbol{\sigma}_i^{total} = \frac{\boldsymbol{\sigma}_i^{max} - \boldsymbol{\sigma}_i^{min}}{2} \tag{3.4}$$

The superposition of several backstress curves is generally required for good results. Figure 3-8 shows results from the present work for different numbers of backstress curves. It was found that using five curves achieved good representation of cyclic BRB behaviour using the Chaboche method. Additional backstress curves had minimal effect.

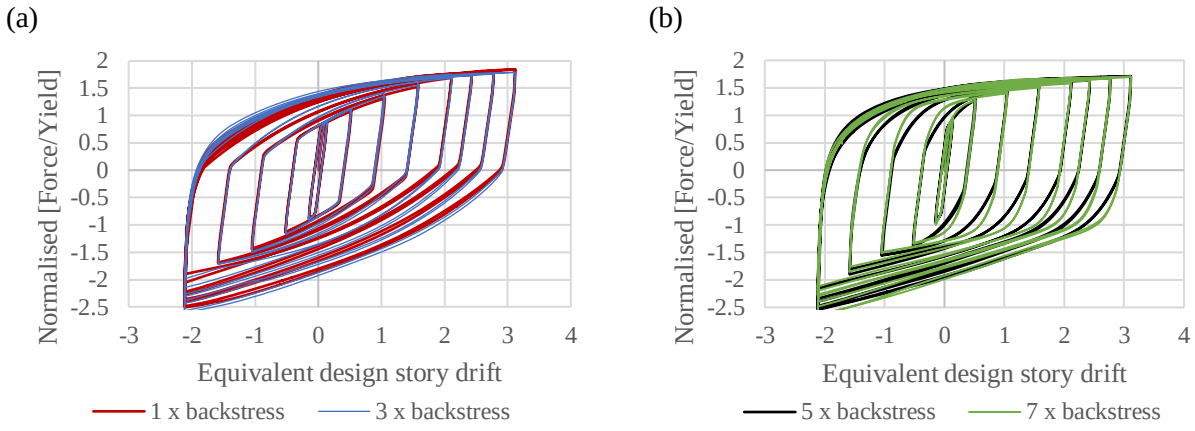

Figure 3-8. Effect of using multiple Chaboche backstress curves for modelling BRBs
(a) 1 x & 3 x backstress curves, (b) 5 x & 7 x backstress curves

By using the following recommendations to calibrate five kinematic backstresses to the overall backstress from testing, a suitable definition can be achieved quickly. To represent the Baushinger effect, the first backstress should have an initial gradient of ~ E/3 and should stabilise (~zero gradient) at plastic strains as low as 0.5%. This should be used in conjugation with the reduced yield stress. The next two backstresses should have initial gradients $\mathbf{C}_k$ ranging from approximately E/15 - E/50 and should stabilize between 0.5% and strain at ultimate stress (as per tensile testing) approximately 8%. The fourth and fifth backstress should be linear or near linear ($\Upsilon << \mathbf{C}$) representing the true stress-strain after the ultimate stress. These gradient and stabilization targets are similar to Zub et al. (2019), who developed a method to calibrate the Chaboche material model using only tensile coupons tests. They were able to capture necking behaviour for several tensile tests, which translated to their BRB models. However, their method was only tested against one loading variation.

3.2.4.2 Calibration of Isotropic Hardening

An additional backstress describes the uniform change in the size of the yield surface due to accumulated plastic strain. A test protocol with cyclic loads between a low strain amplitude of ±0.5% for 20 cycles is recommended, as opposed to fewer cycles with larger strain increments. To show how to extract isotropic hardening from test data, a schematic of a stress-strain response to this loading is presented in Figure 3-9 .

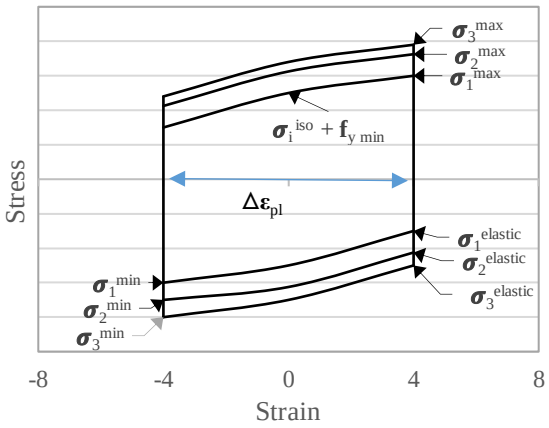

Figure 3-9. Identifying isotropic hardening from cyclic material test data (Lemaitre et al. 1990)

For each cycle (*i*), the increment in isotropic hardening is determined by subtracting kinematic hardening stress increment ($\boldsymbol{\alpha}_i$) and the minimum yield stress ($\boldsymbol{f}_{y\,min}$) from the total stress ($\boldsymbol{\sigma}_i^t$) as shown in equation (3.5). Both kinematic hardening and total stress are defined previously in equation (3.3) and equation (3.4). The associated equivalent plastic strain for each cycle is then calculated using equation (3.6).

$$\boldsymbol{\sigma}_{\mathrm{i}}^{iso} = \boldsymbol{\sigma}_i^t - \boldsymbol{\alpha}_i - \mathbf{f}_{y\,min} \tag{3.5}$$

$$\boldsymbol{\varepsilon}_{pl\,i} = \frac{1}{2}(4i-3)\Delta\boldsymbol{\varepsilon}_{pl\,i} \tag{3.6}$$

By plotting this stress-strain pair, it becomes easy to calibrate $\boldsymbol{Q}_\infty$ (the asymptotic stress value) and b (velocity of stabilisation) for isotropic hardening in equation (3.2).

3.2.5 **Concrete material model**

High strength concrete using cement based grout is commonly used for restraining the core of a BRB from global buckling. High strength concrete provides increased stiffness and strength compared to traditional concrete. The BRBs involved in this study used Sika-Grout 212 (Sika 2018) to form the restrainer. An advantage of high-fidelity BRB models as described here, is that prediction of complex phenomena like bulge failure of the restrainer in Lin et al. (2016) become possible. To capture effects of cyclic loading on the concrete restrainer the concrete damaged plasticity model provided by Abaqus (Dassault Systems 2014)[1] was used.

The plasticity input parameters required for this model are presented in Table 3-1. The elastic modulus of concrete is calculated using equation (3.7) (Park et al. 1975). The compressive behaviour was defined using Popvics model (Maekawa et al. 1983) with the concrete strength f'_c taken from the product data sheet (Sika 2018). The tensile behaviour was defined using a tension softening model (Gopalaratnam et al. 1985) with the tensile strength f'_t determined as per equation (8) (Standards New Zealand 2006). The remaining parameters follow those recommended by Aslani et al. (2012), which are default options prescribed by Abaqus.

$$E_c = 3320\sqrt{f'_c} + 6900 \tag{3.7}$$

$$f'_t = 0.36\sqrt{f'_c} \tag{3.8}$$

Table 3-1. Numerical concrete model inputs

E_c [MPa]	f'_c [MPa]	f'_t [MPa]	Dialation angle [φ]	Eccentricity	F_{b0}/F_c	K	Viscosity parameter
34500	70	3	30	0.1	1.16	0.667	0

3.2.6 **Modelling of BRB core to restrainer interface (debonding material)**

As discussed in Section 2.2.7, between the core and the concrete restrainer is thin-film-like material that runs the entire length of the restrainer. It provides a low friction sliding interface between the core and the restrainer minimizing axial load transfer between them. During compression cycles, significant normal forces develop at this interface. The load transfer between the core and concrete was modelled as a gap with a nonlinear deflection-contact pressure relationship. This allowed realistic lateral deflections of the core relative to the restrainer so that associated constrained buckling could be predicted. A friction coefficient allows for axial load transfer that is significant during compression loading.

The softened contact pressure-overclosure relationship, used to model the soft, thin layers of the debonding material between the core and restrainer, makes the contact non-linearity less severe than for the hard contact modelling option in Abaqus, thus reducing computational demand. At the same time it is consistent with observations that the debonding material is pushed around (flows) during loading. Figure 3-10 presents the general exponential pressure-overclosure relationship provided in Abaqus. Where $\mathbf{P}_0$ is the pressure upon contact and $\mathbf{C}_0$ is the clearance when all pressure has diminished.

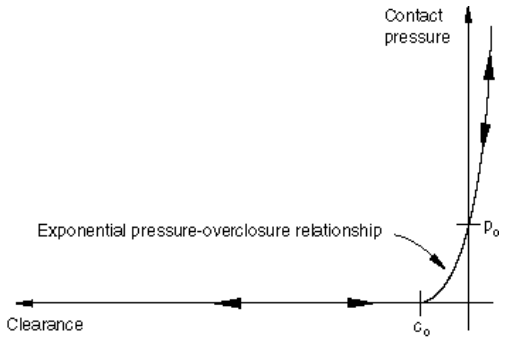

Figure 3-10. The exponential pressure-overclosure relationship (Dassault Systems 2014)

Generally, the thickness of the debonding material is 2.0 mm. This results in a maximum of 4.0 mm clearance under deformation, neglecting Poisson effects. A linear piecewise function was developed that is similar to the exponential function provided by Abaqus but with improved convergence time. Figure 3-11 presents the pressure-overclosure relationship used.

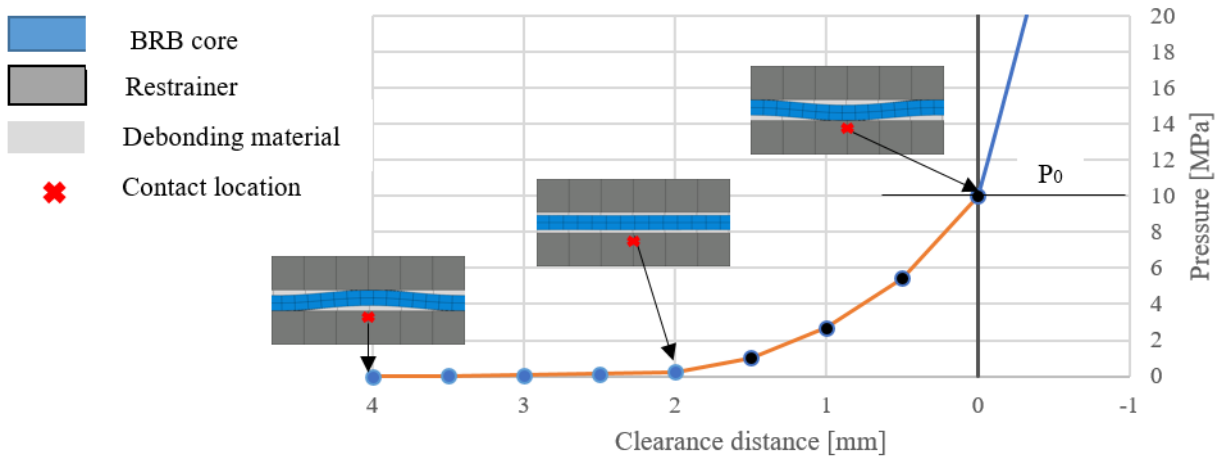

Figure 3-11. Formation of stepwise exponential pressure-overclosure relationship

This relationship takes into account the total possible separation between the core and the restrainer while keeping pressures low for the initial clearance of 2.0 mm or larger. Several combinations were trialed with the ideal combination ensuring 1) validation against experimental results, 2) the pressure upon contact is $\boldsymbol{P}_0$ is low as to not restrict deformation and 3) computational cost is kept to a minimum.

3.3 **Mesh quality**

FE mesh quality can play a significant role in both accuracy and convergence of results. To capture cyclic load histories, large numbers of load increments are necessary. When this is combined with convergence iterations for the nonlinear solution, the computational cost becomes high. Because of this it is important to optimize mesh parameters so that a good solution is obtained with a minimal number of elements. Generally, low order fully integrated quadrilateral element types are most efficient for models with material nonlinearity. However, fully integrated elements are susceptible to 'locking' behaviour, both in shear and in volume (Dassault Systems 2014)[2]. The Abaqus software offers an incompatible mode element (C3D8I) that eliminates locking behaviour. In addition, quadrilateral elements work best when minimally distorted from the ideal rectangular shape. To control the mesh density and allowing for significant variations without badly distorted elements, partitioning of the solid model was used to break the geometric domain into simpler volumes conducive to regular meshes. In addition, the geometry of the restrainer where the polystyrene spacer is located was simplified. This zone lets the core and end connection move back and forward. As there is no axial force applied directly to the restrainer this geometric simplification has little to no effect on results. However, a significant improvement in computational efficiency is achieved. Figure 3-12a presents the actual shape made by the spacer, and how this has been simplified. Figure 3-12b shows how this looks in the assembly and locations where partitioning has been used and also shows partition lines applied to help control the meshing.

(a)

(b)

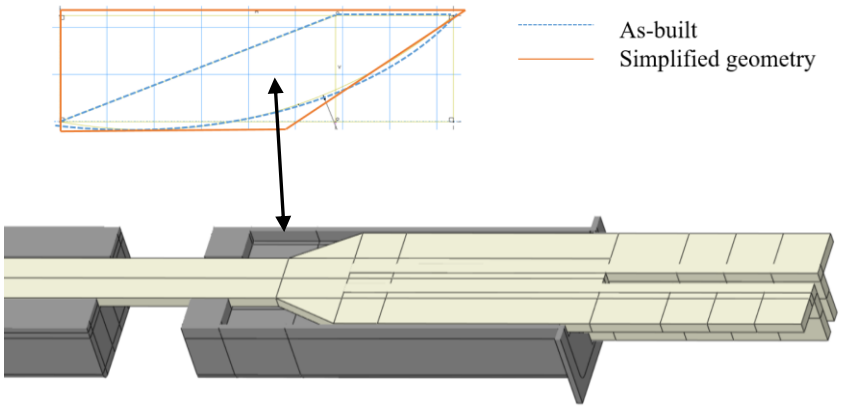

Figure 3-12. Representation of geometric simplification
(a) as-built and simplified shape, (b) FEA solid model assembly (cut view)

3.4 **Overcoming convergence issues and reducing computational cost**

Specific to BRBs, as compressive axial displacement increases, the core progresses through several mode shapes of constrained buckling. Each buckling mode results in a ‘snap through’ of momentary instability while the structure transitions from one equilibrium configuration to another without a global collapse. Each mode shape of buckling is controlled, with relatively little transverse displacement before it arrives at a new equilibrium configuration when the lateral support becomes active (gap closes). For a static solver this leads to convergence issues. Figure 3-13 presents a schematic of this buckling phenomena and the negative stiffness that occurs during this transition.

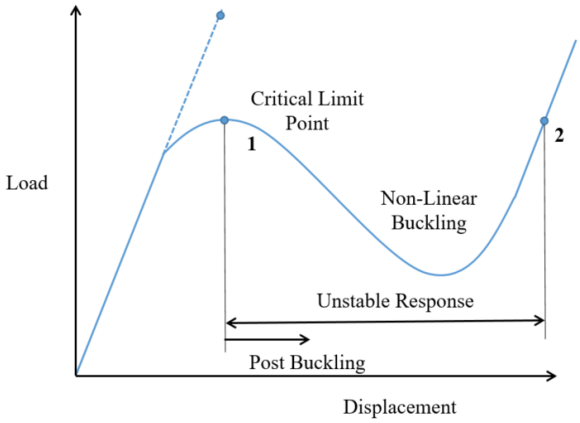

Figure 3-13. Schematic example of 'snap through' due to buckling

The very nature of BRBs and the higher mode buckling that can occur in the restrainer, means that within each time step the solver has to deal with negative eigenvalues. Selecting an appropriate solver type helps reduce convergence issues. The direct-integration dynamic procedure provided in Abaqus (Dassault Systems 2017) offers a choice of implicit operators for integration of the equations of motion. The operator-matrix is inverted, and the set of nonlinear equilibrium equations is solved at each time increment. The quasi-static application of the implicit solver was found to work well for this problem. It can regularize unstable behaviour and also takes large time increments when possible, thus improving run-times. This generally occurs in the tension cycles where bending and contact of the core against the restrainer is reduced.

The geometric features three BRB designs (Chapter 2) were used as a basis for the BRBs modelled. In this study, the clevis and test rig was not modelled. Instead the inner surface of either the pin or bolts was coupled to a center node. Each of these center nodes was fixed in translation degrees of freedom but were free to rotate was (like a pin or bolt). This assumption reduced the amount of interactions and number of elements.

Parallel processing was used to shorten run times. However, implicit parallel solvers generally realize significant benefit only from relatively small numbers of processors. For the present model it was found that additional processes beyond eight provided minimal reductions in run-time. A typical simulation took 30 hours to complete with eight processes/cores. The relationship between numbers of processes and runtime is illustrated in Figure 3-14.

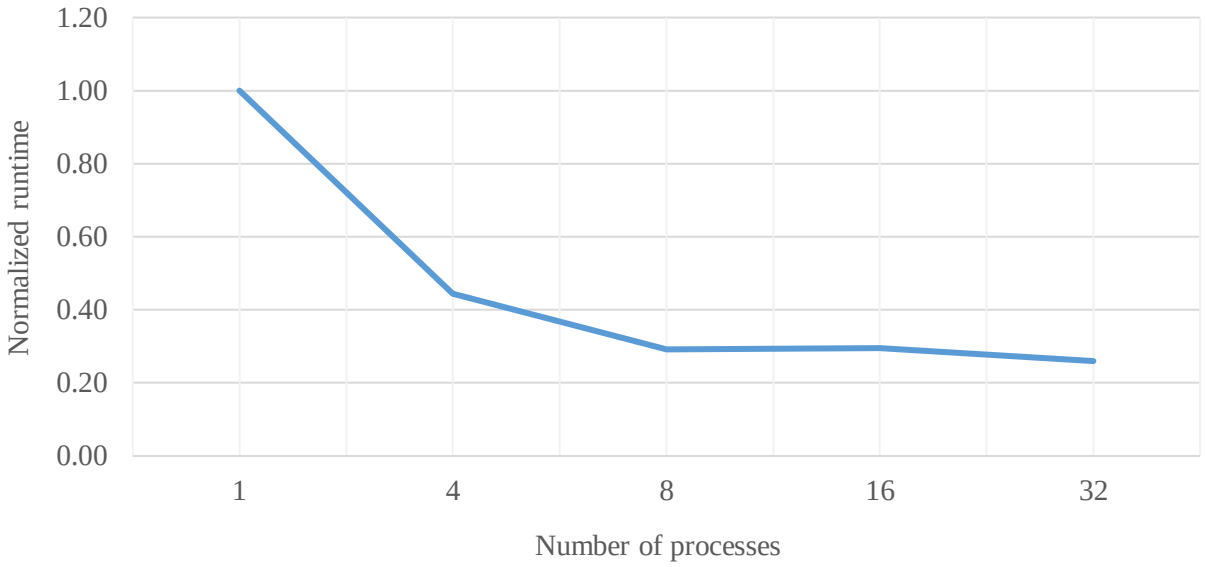

Figure 3-14. Run time performance with increasing number of CPUs

3.5 **Geometric imperfections**

Initial geometric imperfections of BRBs can arise from: the shape of the steel core (misalignment of the core and non-yielding components, core off-centering relative to steel tube) and those of the steel tube (bow imperfections and misalignment of connections). Takeuchi et al. (2017) states imperfections in BRBF can easily be in order of 1% of the length of the BRB.

In structural analyses, initial geometric imperfections are added to a model to reflect the possible effects of all types of imperfections (geometrical misalignments, loading eccentricities). However, imperfections of each BRB were not measured at the time of testing. As such, an initial equivalent geometrical bow imperfection (Figure 3-15) was introduced into each BRBF model. This bow imperfection was based on the first mode of elastic buckling. The maximum point (e_0) was equal to 1 mm (Figure 3-15), with each remaining node distributed according to the shape of the bow imperfection. The displacement of each node was then multiplied by a factor equal to the length of BRB divided by 500. Noting that construction tolerances of eccentricity normally target a limit equal to the length of BRB divided by 1000.

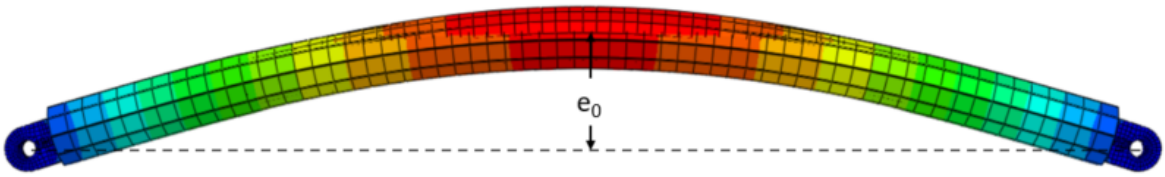

Figure 3-15. Modelled geometric bow imperfection (BRB C6)

3.6 **Validation of Models**

Validation of the FEA strategy was achieved through the modelling the prequalification testing of three brace designs. These braces were first presented in Section 2.2. Physical testing of these braces was for the purposes of use in commercial building projects. Engineers from Taiwan at NCREE designed the BRBs. The BRBs encompass a variety of BRB options on the market, making them suitable for validation. A summary description of the BRBs used for validation has been taken from Table 2-1 and is presented here again. To visualize the modelling conducted, Figure 3-16 shows specimen 'BRB C6' in the experimental set up, alongside its corresponding finite element model.

Table 3-2. BRB specimen specifications

Brace ID	Total length [mm]	Connection type	Core area [mm]	Design yield force [kN]
BRB S3	3812	Bolted	12x55	204
BRB 6.5a	7238	Pinned	25x140	1221.5
BRB C6	6566	Pinned	50x85	1445

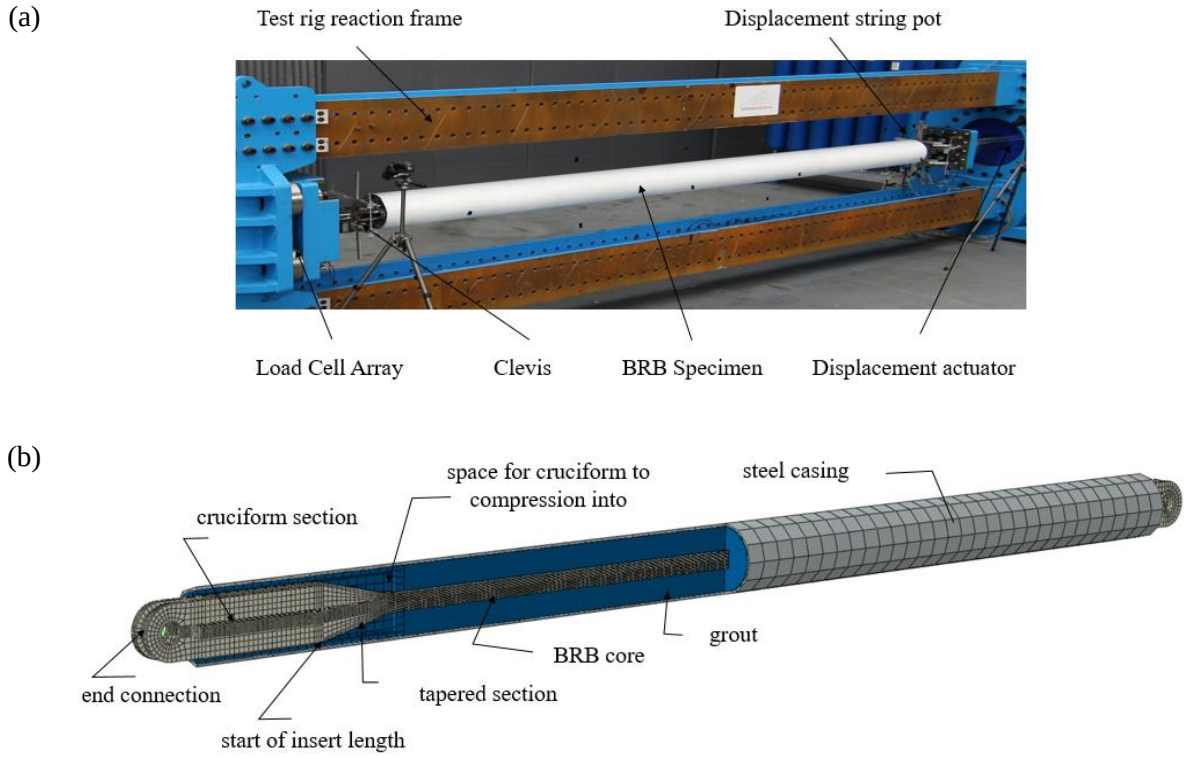

Figure 3-16. BRB C6 (a) experimental set up (Holmes Solutions 2014), (b) meshed assembly in FEA

In accordance with the requirements of each commercial building project, uniaxial testing was used to assess the performance of each BRB type. This type of testing continually increases axial strain within the BRB core element. Test loading was applied in accordance with ANSI/AISC 341-16 Section K3 'Cyclic Tests for Qualification of Buckling Restrained Braces', with loading as prescribed in Section K3.4.c 'Loading Sequence'. Dynamic loading is not prescribed in this standard, as the available research on dynamic loading effects on steel test specimens have not demonstrated a compelling need for such testing (ANSI/AISC 2016). Nominally, each BRB follows the same loading protocol as defined in ANSI/AISC 341-16. However, in order to achieve 200 times yield displacement, the amplitude and number of additional cycles vary between brace types. The loading requirements are based on a study in which a series of nonlinear dynamic analyses were conducted on model buildings and the ductility capacity requirement represents a mean of response values (Sabelli et al. 2003). Figure 3-17 illustrates the comparison of predicted and measured hysteresis loops. In addition to the hysteresis loops, presented in Table 3-3 is the ratio of peak tension load to the yield load, and the ratio of peak compression to peak tension for first eight cycles for both experimental (EXP) and simulated results (SIM). Good agreement is observed for all three BRB types.

(a)

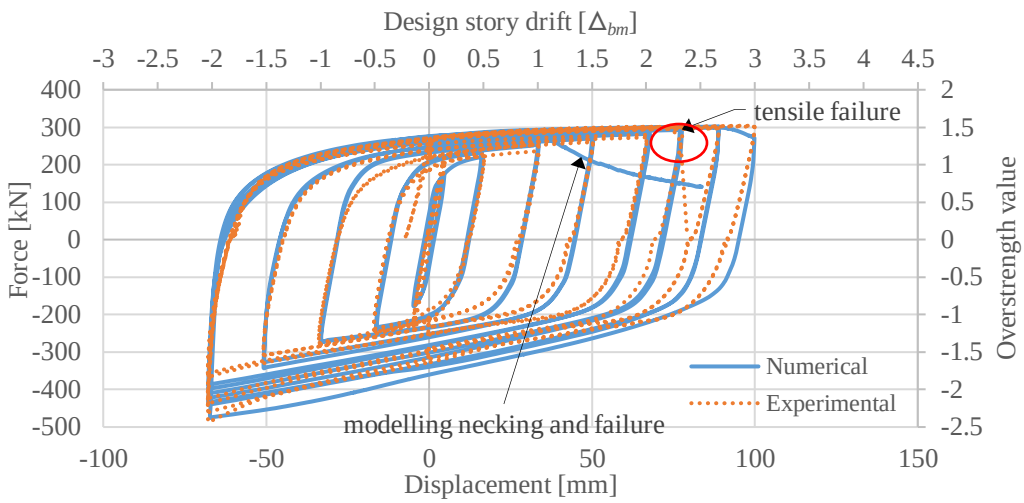

(b)

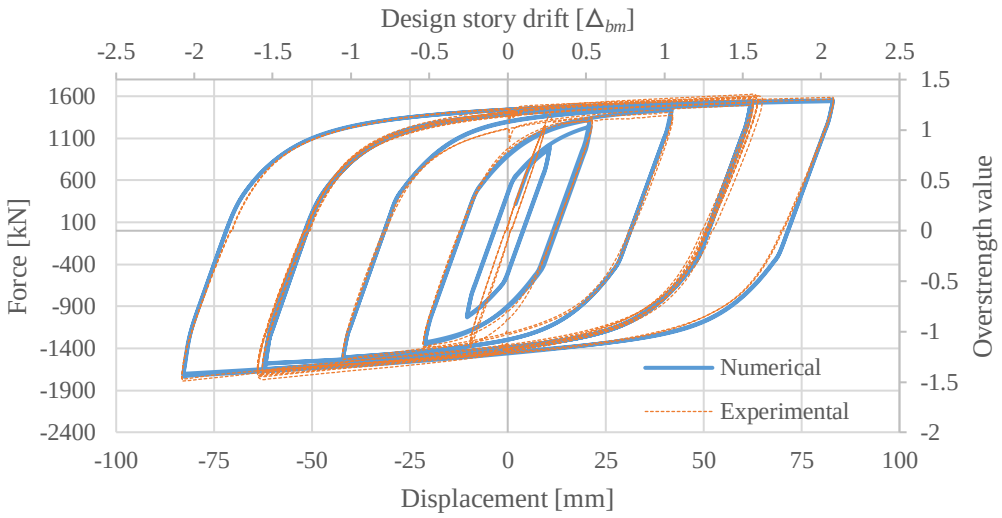

(c)

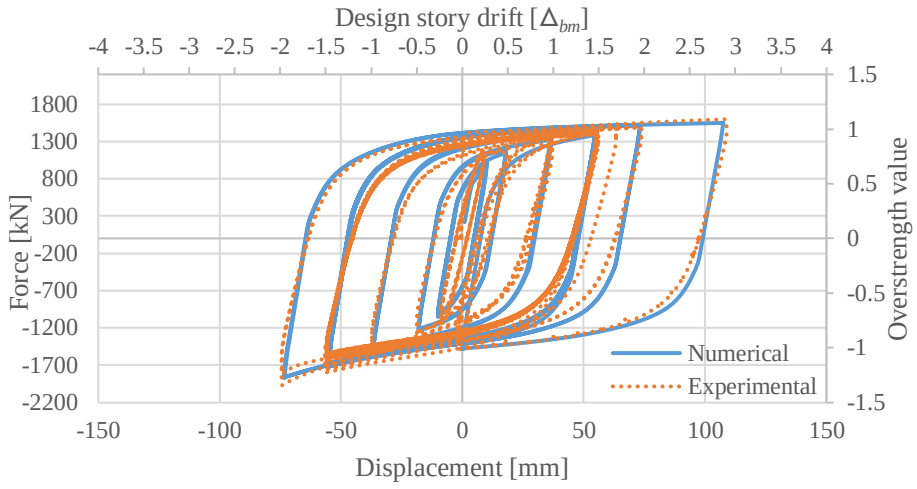

Figure 3-17. Numerical and experimental hysteresis plots (axial force-displacement domain) (a) BRB S3, (b) BRB 6.5a, (c) BRB C6

Table 3-3. Ratio of peak tension load to the yield load and the ratio of peak compression to peak tension for first eight cycles.

Target			BRB S3		BRB 6.5a		BRB C6	
			EXP	SIM	EXP	SIM	EXP	SIM
$\pm \Delta_b = 0.5\Delta_{bm}$	1	**T**	1.12	1.10	1.09	1.02	1.08	0.99
		C	1.08	1.05	1.04	1.07	1.00	1.06
	2	**T**	1.09	1.14	1.07	1.08	1.04	1.04
		C	1.07	1.03	1.05	1.02	1.08	1.04
$\pm \Delta_b = 1.0\ \Delta_{bm}$	1	**T**	1.16	1.22	1.12	1.18	1.09	1.15
		C	1.19	1.07	1.11	1.05	1.24	1.11
	2	**T**	1.24	1.25	1.15	1.2	1.14	1.21
		C	1.08	1.05	1.1	1.03	1.11	1.08
$\pm \Delta_b = 1.5\ \Delta_{bm}$	1	**T**	1.27	1.31	1.22	1.23	1.22	1.27
		C	1.19	1.17	1.13	1.05	1.23	1.15
	2	**T**	1.31	1.34	1.25	1.24	1.24	1.29
		C	1.16	1.21	1.09	1.04	1.19	1.13
$\pm \Delta_b = 2.0\ \Delta_{bm}$	1	**T**	1.34	1.38	1.28	1.26	1.29	1.31
		C	1.3	1.34	1.14	1.1	1.3	1.23
	2	**T**	1.37	1.4	1.3	1.27	1.29	1.32
		C	1.31	1.37	1.11	1.11	1.22	1.22

3.6.1 **Non-linear parameters for the Chaboche method**

The non-linear material parameters required to model the steel material in the core of each BRB as per equation 3.1 – 3.6 are presented here in Table 3-4. The differences in values are a result of different heats of steel being used for the fabrication of each brace.

Table 3-4. Material properties of non-linear hardening model

			BRB specimen		
	Symbol	Units	S3	6.5a	C6
Material Properties	$\boldsymbol{\sigma}_y$	[MPa]	311	346	342
	$\boldsymbol{\sigma}_u$	[MPa]	409	499	527
	E	[MPa]	205 000	205 000	205 000
Calculated Properties	$\boldsymbol{\sigma}_{y'}$	[MPa]	210	220	157
Kinematic Hardening	$\mathbf{C}_1$	[MPa]	66 000	72 000	60000
	Υ_1		1150	850	1200
	$\mathbf{C}_2$	[MPa]	10500	12600	10000
	Υ_2		420	245	300
	$\mathbf{C}_3$	[MPa]	4000	4500	3000
	Υ_3		45	80	70
	$\mathbf{C}_4$	[MPa]	225	300	200
	Υ_4		1.3	1.3	1.3
	$\mathbf{C}_5$	[MPa]	170	245	200
	Υ_5		1	1	1
Isotropic Hardening	$\mathbf{Q}_\infty$	[MPa]	50	48	65
	b		35	75	20

3.6.2 **Calibrating friction between the core and the restrainer**

The properties of debonding materials used in commercial BRBs are often confidential. This makes modelling this material difficult. To assess the effect of friction a sensitivity study was performed that calibrated a friction coefficient to the overall structural test data. This is shown in Figure 3-18. The comparison with experimental data shows that a friction coefficient of 0.15 provides good agreement with the test data of all three BRBs. The model assumes the coefficient to be constant, therefore being representative of the average frictional behaviour that would be variable along the length of the core depending on local stress and material conditions.

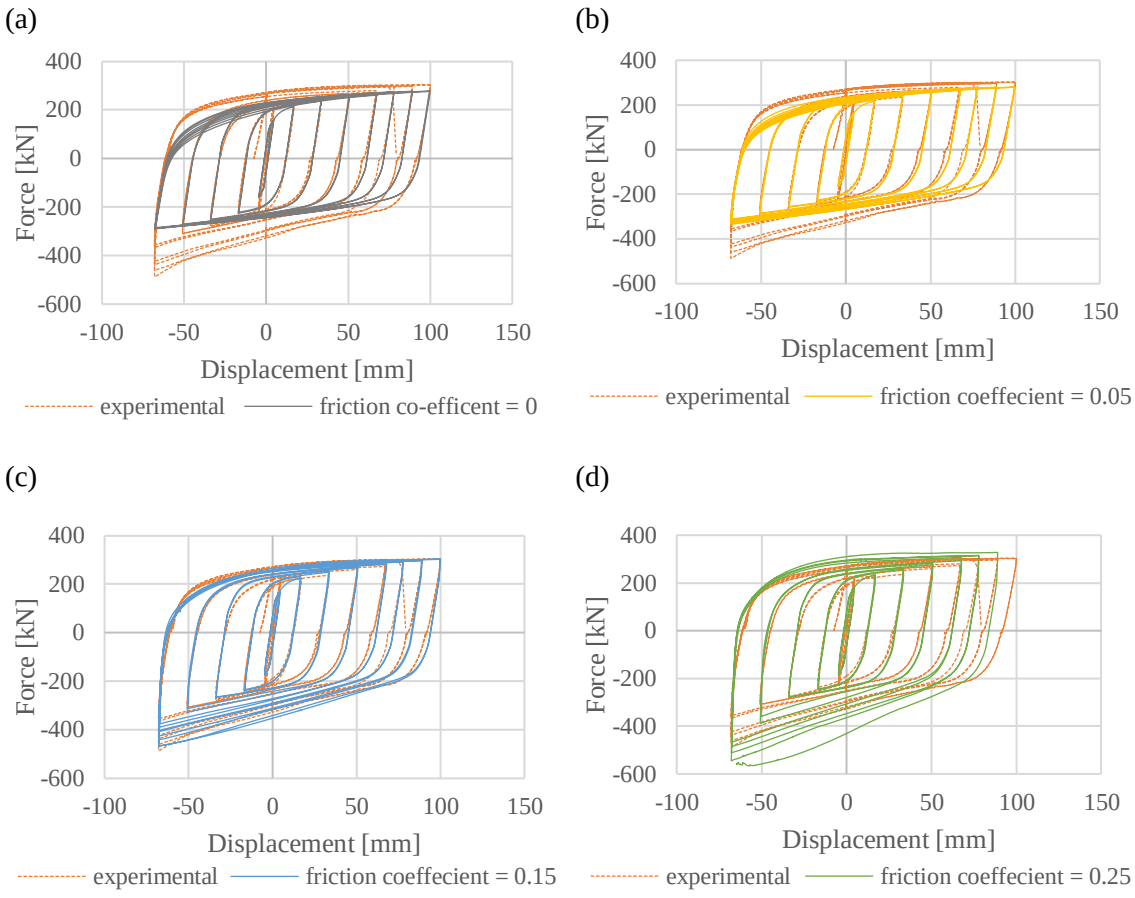

Figure 3-18. Sensitivity study results (friction coefficient)
(a) $\mu = 0$, (b) $\mu = 0.05$, (c) $\mu = 0.15$, (d) $\mu = 0.25$

In tension, it is noted frictional effects are also present. This is likely because as the core transitions from being dilated and deformed in compression, it rubs against the restrainer as it unbinds in tension. The deformation and strain profile along the core become varied as it progresses through each loading cycle. Observation from FEA results suggest in some locations the core is still bound up in a higher mode buckling shape while being stretched out in others. Figure 3-19 presents a snap shot of the scaled deformation of core inside the restrainer at the peak tension displacement. This highlights the contact of the core to the restrainer in tension cycles. When applying this strategy to other BRB types, if a different debonding material is used then re-calibration is recommended.

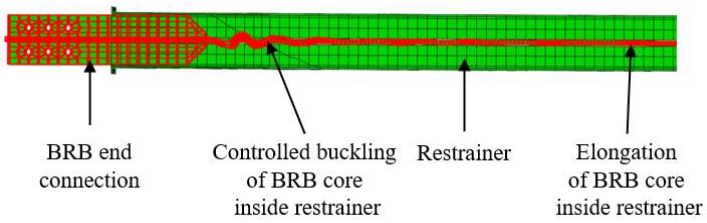

Figure 3-19. Shape of BRB core at peak tension displacement (BRB S3) deformation scale = 2 (to highlight contact zones)

3.6.3 **Comparison of models with experimental testing**

As per criteria set out in ANSI/AISC 341-16, the peak loads within each cycle are key data points used to determine prequalification (ANSI/AISC 2016). To highlight the accuracy of the simulations Figure 3-20 shows the ratio of predicted peak forces (SIM) versus experimental (EXP) peak forces.

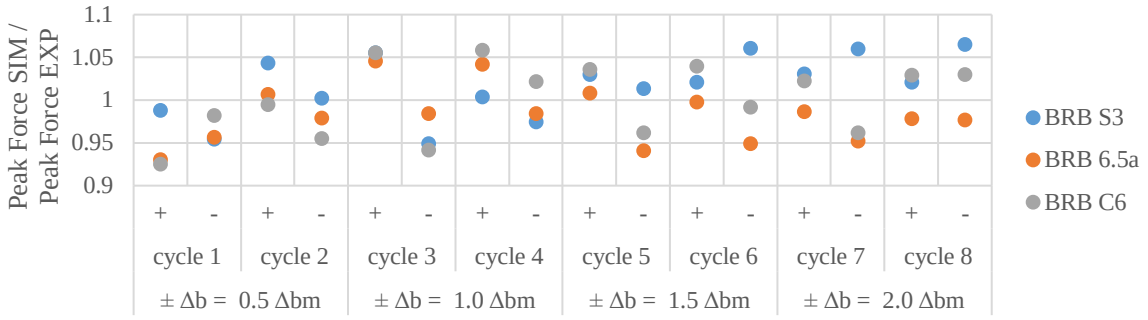

Figure 3-20. Ratio of predicted peak force at each cycle to measured peak force for 8 cycles (simulation/experimental)

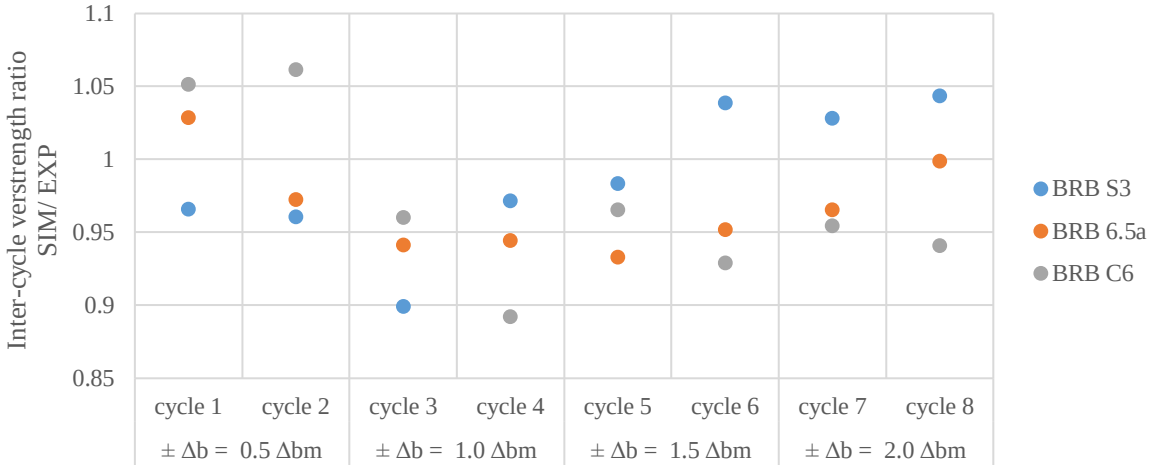

Figure 3-21. Ratio of predicting inter-cycle ratios to measured inter-cycle ratios for 8 cycles (simulation/experimental)

The inter-cycle ratio for each cycle is calculated by dividing the peak compression force by the peak tensile force. Figure 3-21 shows how the simulations correspond to experimentally measured overstrength ratios. Both plots show predictions are within 10% of the experimental results. This suggests the FEA modelling strategy can be used to accurately predict cyclic BRB behaviour. It is notable that the overstrength ratio at $-2.0\Delta_{bm}$, which is used to generate the compressive adjustment factor (β) for the design of BRB frame elements, are within 6% of experimental data.

3.7 **Discussion**

Having validated the FEA strategy presented in this paper, it is of interest to explore the capability of the modelling predictions produced. The difficulty to capture stress-strain data inside the restrainer during physical testing means there is a lack of understanding of how strain develops along the core. Table 3-3 shows that BRB S3 and BRB C6 had a higher compression adjustment factor (β) compared to BRB 6.5a. FEA modelling results were used to investigate this, and it was found that the relative lengths of the polystyrene spacer is the main contributing factor. The length of the spacer used in BRB S3 and BRB C6 was 50% less than that used in BRB 6.5a. A shorter spacer means more axial stress is exerted on the restrainer as the transition zone of the BRB core pushes up into the void. This action occurs at each end, so as compressive displacements increase, the restrainer begins to contribute to a higher compressive load. This idea is supported by looking at the stress concentration in this zone when the spacer pushes against the restrainer. Figure 3-22 shows the stress concentration is higher for both BRB S3 and BRB C6 compared to BRB 6.5a, when displacements = $-2.0\Delta_{bm}$, where grey and red indicate higher levels of stress and blue indicates low levels of stress.

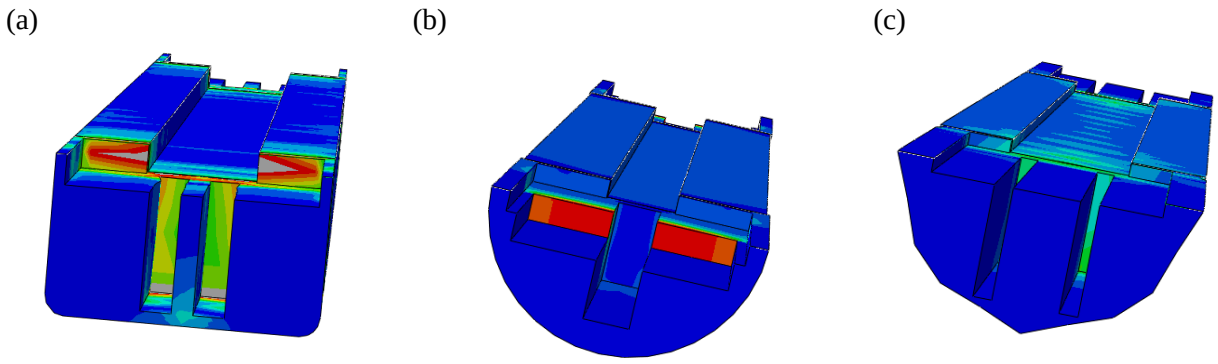

Figure 3-22. Von Mises stress in the concrete restrainer of each BRB when target displacement = $-2.0\Delta_{bm}$ (a) BRB S3, (b) BRB C6, (c) BRB 6.5a

The frictional sensitivity presented in this chapter showed that without the correct friction coefficient the overstrength predictions are in error as much at 40%. This error is largest for large displacement compressive cycles when the contact normal forces are high. As illustrated in Figure 3-18, friction between the core and the restrainer contributes significantly to overall BRB cyclic behaviour and therefore the overstrength factors required for design of BRB frame elements are sensitive to this parameter. For validation purposes a friction coefficient of μ = 0.15 showed good agreement with BRB test data. By comparison, this is larger than μ = 0.1 as described by NCREE (Tsai et al. 2014). In contrast, Budaházy (2015) found the effect of friction increases over time, where after continued cycles the steel begins to damage the surface of the concrete. To account for this damage mechanism, he developed a more

complicated friction model using an initial friction co-efficient of μ = 0.35 that increases to maximum of μ = 0.5.

The actual behaviour of the debonding material deforming inside the restrainer is very complex. The material heats up due to the plasticity of the deforming steel core. This combined with the bending and stretching behaviour of the core, forces the material in and out of voids between the restrainer and the core in a fluid-like way. Physical observations of the material extruding out of the ends of the restrainer support this. Figure 3-23 presents evidence of the debonding material extruding from the end of the restrainer during testing. The approach adopted to model this behaviour, in which a gap with pressure-overclosure relationship was implemented, is a coarse approximation but it allows for the type of core movement associated with flow of debonding material. Close comparison of simulations to experimental data suggest it is a suitable approximation for predicting overall BRB behaviour.

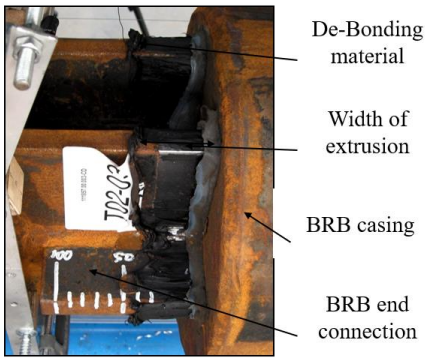

Figure 3-23. Physical observation of debonding material extruding from end of restrainer (BRB 6.5)

The steel plasticity model employed captures ratcheting, which occurs in discrete zones of a BRB due to combination of bending, and axial stresses, even though axial displacements applied to the entire BRB are equal and opposite. However, one shortcoming of the material model is the inability to capture behaviour unique to the first cycle. For example, the cyclic material model dictates an artificial reduction in initial yield stress that results in more strain for the first cycle compared to experimental results. This is readily observed for BRB 6.5a in Figure 3-17b. By reducing the initial yield value, the first cycle exhibits more strain compared to experimental testing. However, by the second cycle the simulated results more closely match experimental data.

Another observation from simulations shows the development of bending moments at the end connections. This is attributed to the bending and buckling of the core inside the restrainer. Figure 3-24 illustrates the buckling and bending that occurs in both planes along the length of the core.

(a)

(b)

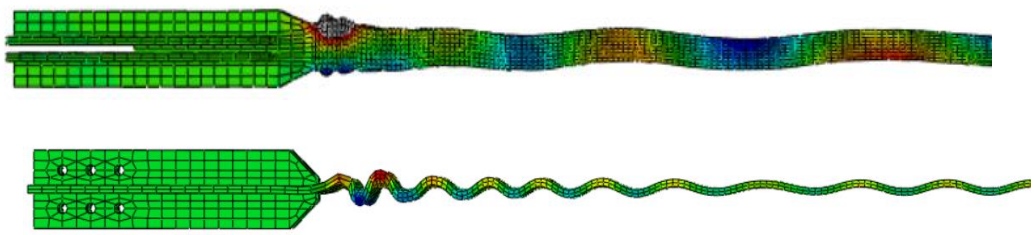

Figure 3-24. Buckling observed along core within the restrainer (BRB S3)
(a) buckling about the strong axis, (b) buckling about the weak axis
(displacements magnified for clarity – scale factor = 5)

This bending behaviour results from the core to the end connection being forced off-center creating a moment transmitted through the end connection. This is not a concern in the strong axis of a gusset plate, however observations show if the BRB core is orientated in the same plane as the gusset plate then moment transfer was higher in the weak plane, which may contribute to overall instability. Figure 3-25a illustrates the lateral movement and associated bending moment. Figure 3-25b shows that these two behaviours occur at the same intervals throughout the simulation.

(a)

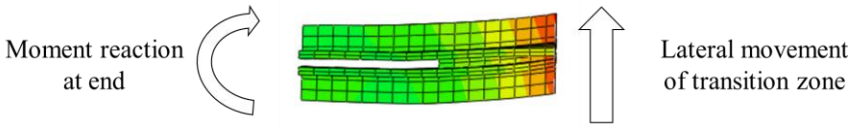

(b)

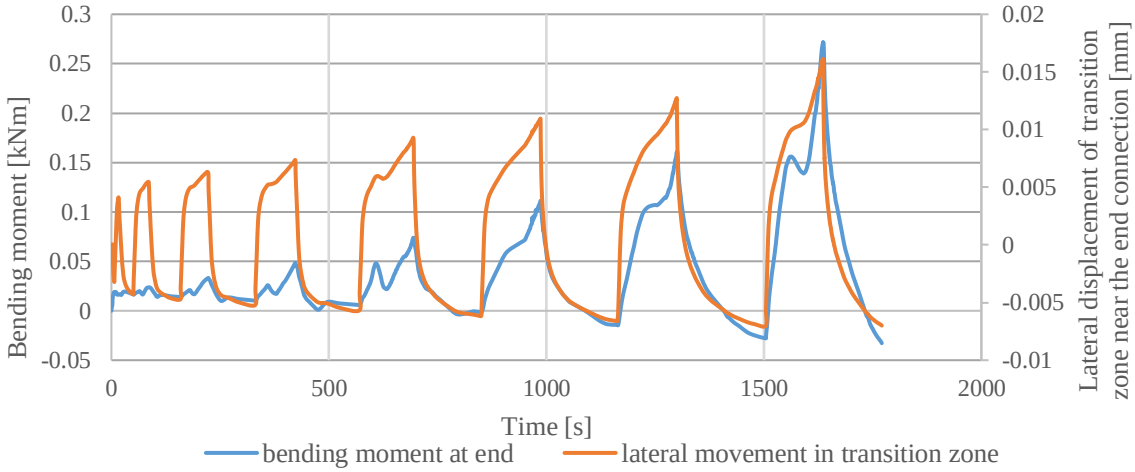

Figure 3-25. Bending moment at end connections and lateral movement of transition zone of BRB S3
(a) location of reactions, (b) relationship during simulation

Most prototype structural products need at least three nominally identical tests to be undertaken, to enable an estimate of mean value and standard deviation. However each of the five BRBs were tested only once in the test programme due to the cost associated with this type of testing. To reduce the expected variation of structural characteristics between test conditions and on-site performance project specific displacement targets are used, and the design yield load from material test data are verified against the BRB test results. The various sensitivity studies show that calibrating the material model correctly is the largest influence on accuracy. This means, that in theory the models can be built with only geometric and material test data with variation of 5-10% expected as shown in Figure 3-20 and Figure 3-21.

With a validated method for modelling realistic BRB behaviour it is of interest to explore the applicability of the strategy to other BRB designs. Following an earthquake event, detailed BRB models could be used to provide evidence on weather replacement is required by estimating the residual strain capacity. As such, BRB 9.5 and BRB 2A (as detailed in Chapter 2) were modelled without the use the experimental data for callibration, keeping all modelling features the same aside from the shop drawings and the available material test data. Preliminary results as per Figure 3-26 support the notion that other generic BRBs can be modeled using this approach. Differences in experimental to numerical values are thought to be caused by not having cyclic material test data available for calibration.

(a)

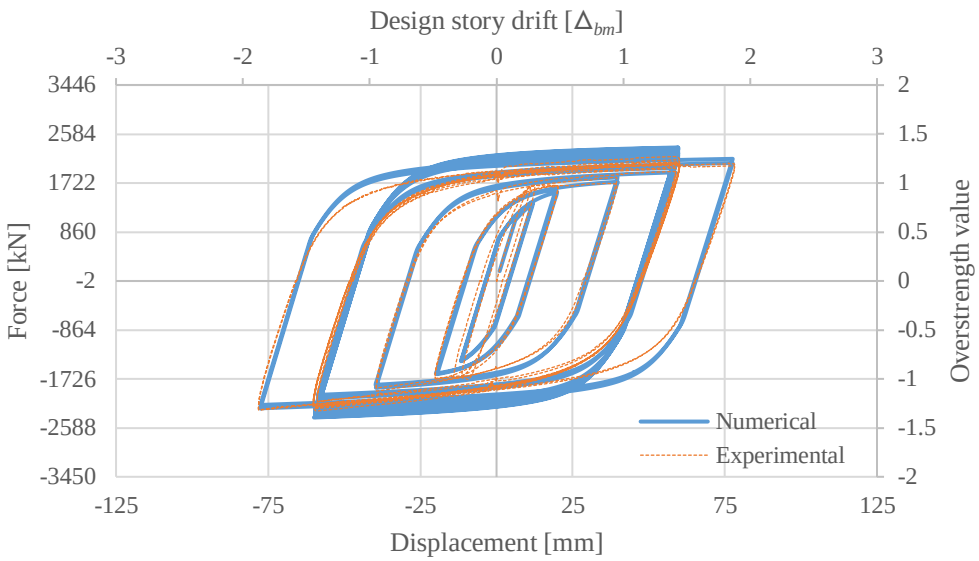

(b)

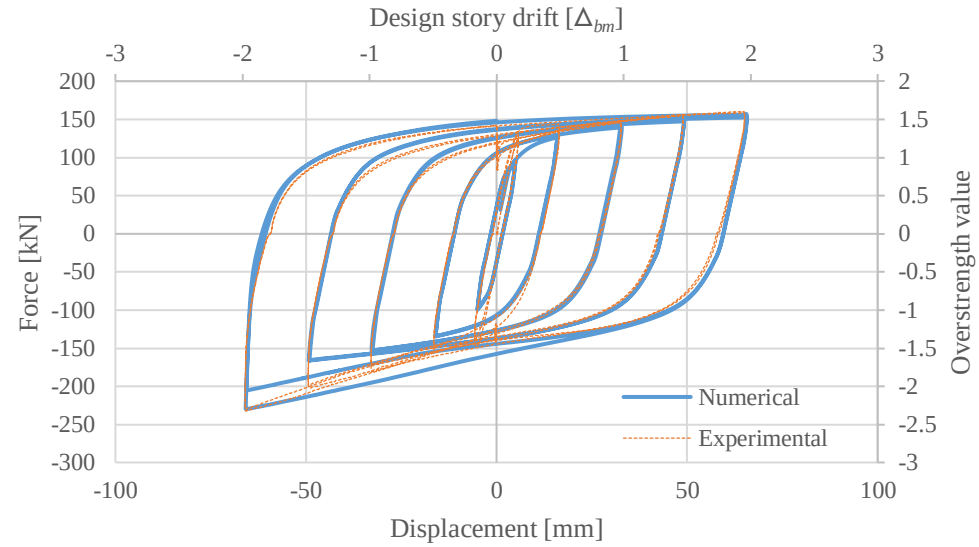

Figure 3-26. Numerical and experimental hysteresis plots (axial force-displacement domain) (a) BRB 9.5, (b) BRB 2A

It is also of interest to study how other generic BRB designs interact within complete structural frames. The most complicated aspects of modeling a BRB is capturing the non-linear material, contact, and non-linear geometric effects of the BRB core interacting with the restrainer. The type of modeling presented in this paper gives us clues about what may be occurring inside the restrainer. The difficulty to capture stress-strain data inside the restrainer during physical testing means there is a lack of understanding of how strain develops along the core of a BRB. The restrainer is designed to confine transverse displacements of the core and prevent global buckling of the BRB core. However, the slender nature of the core causing transverse displacements that can lead to constrained buckling at very low axial compressive loads and can progress through several buckling modes. The greater the curvature associated with the constrained

buckling, the higher the local strains are, which could lead to tensile failure. Being able to estimate the onset and degree of higher mode buckling could help BRB designers select geometries that minimize this effect and therefore reduce these high concentrations strain (associated with failure). The ratio of the thickness of the debonding material and the thickness of the BRB core is thought to be a key factor. As a final example, strain at the peak tensile and compressive displacement loads was recorded along a path running the length of the BRB core on the outer top surface. Figure 3-27 illustrates where along the core of BRB 6.5a the logarithmic strain recordings were taken from.

(a)

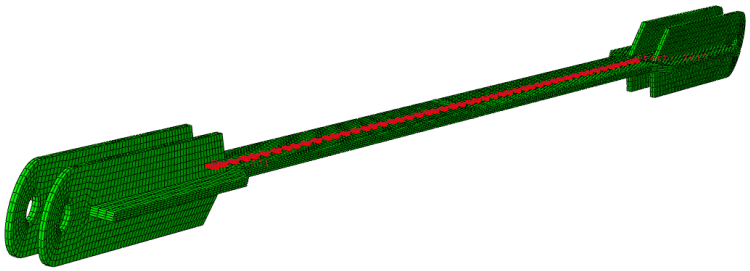

Figure 3-27. Strain recordings along core at first cycle of each target displacement (BRB 6.5a) path of elements where strain was recorded

Figure 3-28a and Figure 3-28b graph the logarithmic strain recordings as per the locations shown in Figure 3-27, for BRB 6.5a and BRB 2A respectively. Both graphs indicate that friction mutes the compressive strains at core mid-length and that high levels of strain occur closer to the ends. This high level of strain is associated to the bunching of constrained buckling similar to that shown in Figure 3-19 and Figure 3-24. This suggests failure is likely to occur near the ends for this specimen. Figure 3-28a predicted the strain profile for BRB 6.5a has the maximum strain on 8%, where as Figure 3-28b indicates high levels of strain (up to 25%) for BRB 2A. Suggesting this BRB 6.5a is less likely to fail in tension compared to BRB 2A.

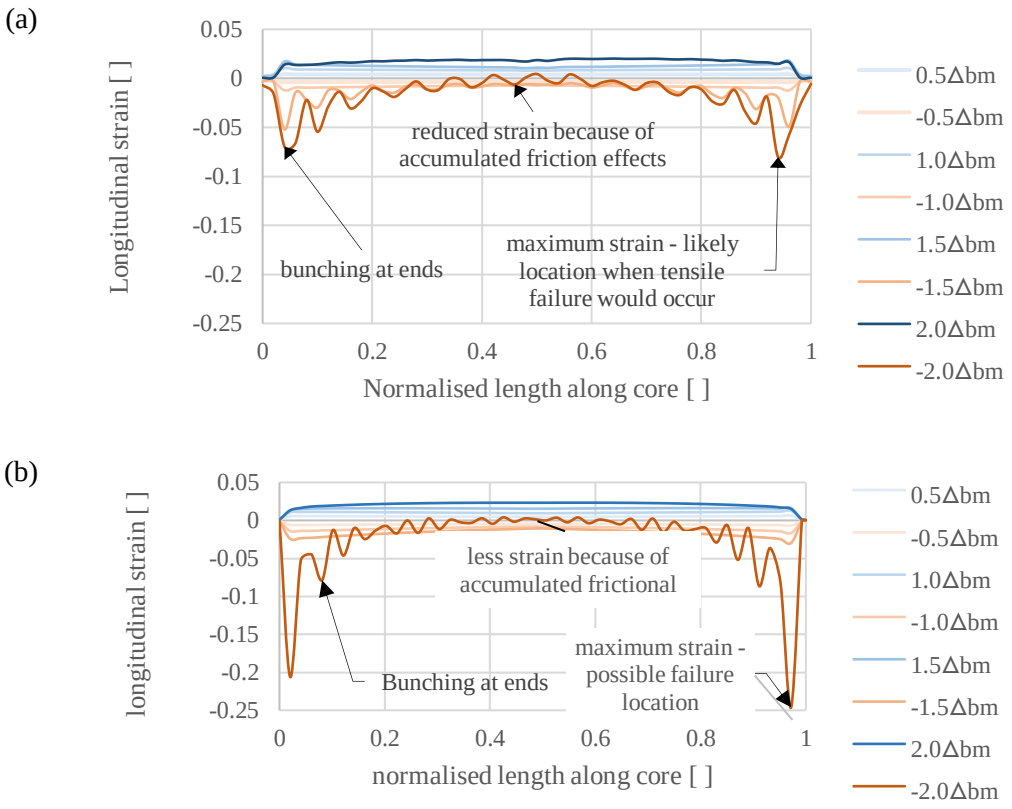

Figure 3-28. Strain profile along core at first cycle of each target displacement (a) BRB 2A, (b) BRB 6.5a

The failure exhibited in BRB S3 gives one opportunity to investigate the capability of the model to capture tensile failure as localized necking. Figure 3-29 shows the necking behaviour captured in the BRB S3 model as associated with Figure 3-17a. Although necking failure appeared approximately at the point in the cyclic load history where BRB S3 failed, these models have not been validated by any kind of blind prediction for other failed BRB tests. However, one small measure of validation is that this adjusted material model (calibrated to the failure of BRB S3) did not result in necking failures, corresponding with observed behaviours, for either BRB 6.5a or BRB C6.

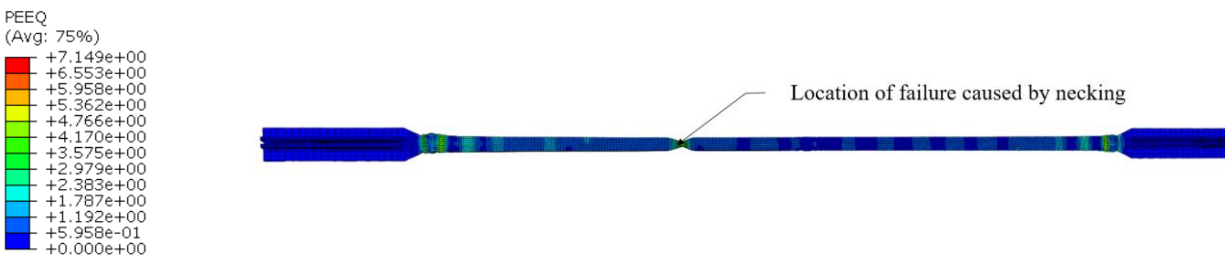

Figure 3-29. Location of failure caused by necking in model of BRB S3

Neither BRB 6.5a nor BRB C6 experienced failure during testing; this provides another opportunity for each model to investigate the maximum displacement limits and failure mode of these braces. As such, each model was re-run to investigate that maximum displacement and possible failure mode. To achieve this, each followed a loading protocol that increased in amplitude after every two cycles until failure.

BRB 6.5a was predicted to have positive stable hysteresis up to displacement equivalent to three times the design storey drift. On the first cycle targeting 3.5 Δ_{bm}, the brace successfully went through the tension cycle but was predicted to fail in compression at 2.8Δ_{bm} as shown in Figure 3-30. When we examine the solid model at this point, it appears the core initially buckled inside the transition zone (where the polystyrene space is located) as shown in Figure 3-31. This action caused the core and restrainer to bind at one end. This meant the other end of the BRB core quickly ran out of room to compress into, and caused the axial load to be transferred through the concrete restrainer and the tapered section of the BRB pushed against the restrainer.

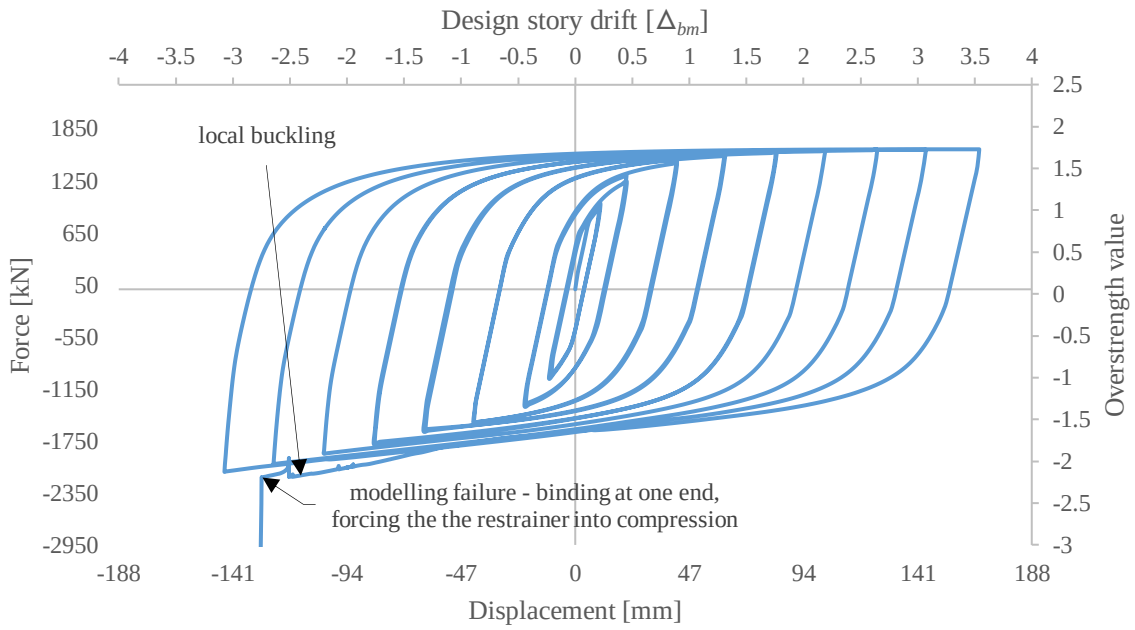

Figure 3-30. Extended modelling of BRB 6.5a

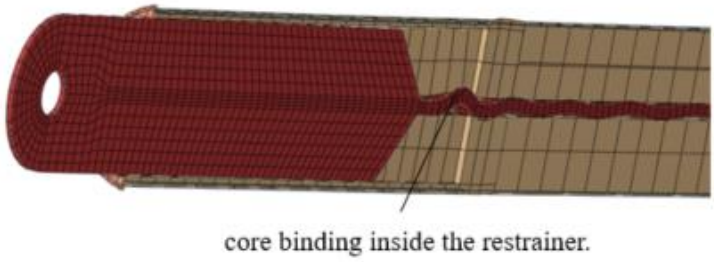

Figure 3-31. Model showing point at failure (BRB 6.5a)

BRB C6 also demonstrated positive stable hysteresis up to displacement equivalent to three times the design storey drift. On the first cycle targeting 3.5 Δ_{bm}, the brace successfully went through the tension cycle but failed in compression at 3.1Δ_{bm} as shown in Figure 3-32. When we examine the solid model at this point, it appears the tapered section at each end of the BRB ran out of space to compress into and means the BRB end plates push against the restrainer from each end. This action causes the axial load to be transferred through the concrete restrainer, as well the core as shown in Figure 3-33.

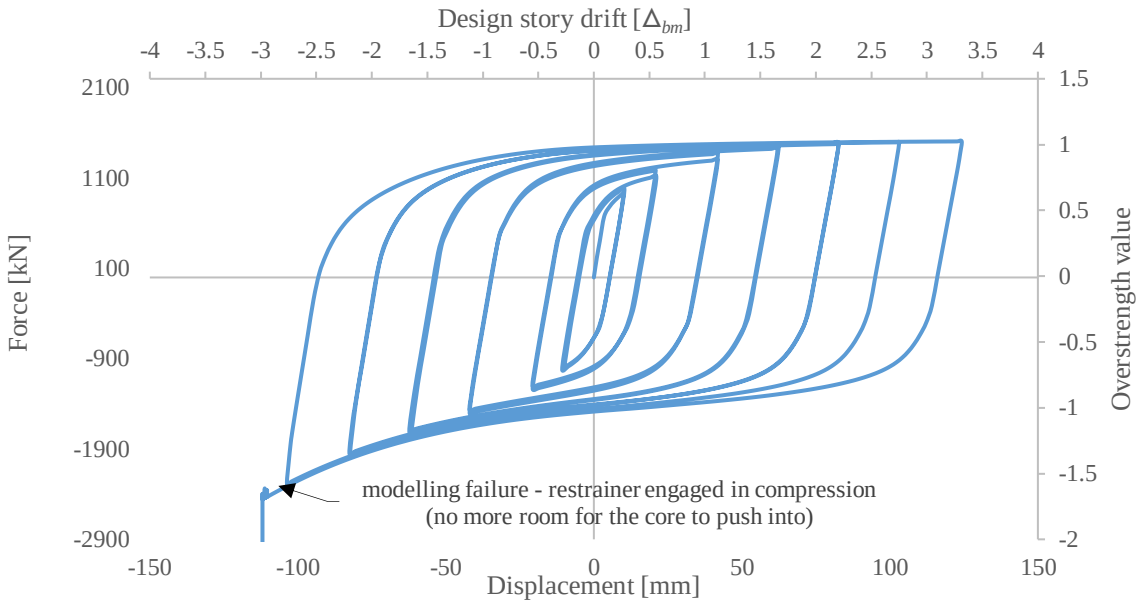

Figure 3-32. Extended modelling of BRB C6

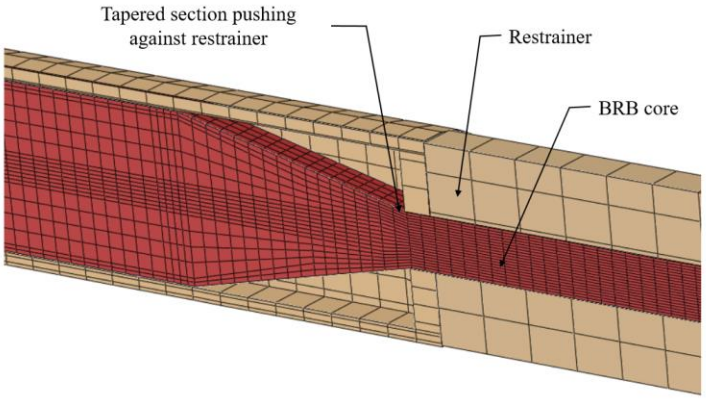

Figure 3-33. Model showing point at failure (BRB C6)

Although each model has the ability to simulate necking and core binding failure modes, this is clearly not a validated failure prediction capability. For example, it is unknown if the predicted location of the failure in BRB S3 is correct. Also, tests to failure were not conducted for either BRB 6.5a or BRB C6. No blind predictive capability has been demonstrated. Proper development of a failure prediction capability would require a combination of cyclic uniaxial testing and BRB testing that somehow collects data on the spatial variation in strain along the core. This poses a significant challenge as, for example, traditional methods for fastening strain gauges are likely to not survive the interaction between the BRB core, debonding material and restrainer.

Moving forward, the overall modelling approach described in this paper can be used to study and better understand the local and global behaviour of a BRB, which could include developing a predictive capability for modelling failure. This would require a significant experimental program.

3.8 **Conclusion**

Presented is a strategy for developing complex models of typical BRBs in Abaqus® which could be applied using similar FEA codes. Of particular interest is accurately predicting the cyclic response of BRBs to deduce the overstrength factors required for structural design. Prequalification testing can cost $8-10k (USD), so to determine these overstrength factors manufacturers test a selection of BRBs and extrapolate results between sizes. However, the complex behaviour of BRBs, particularly in compression, can make extrapolation of test results between different sizes difficult. This chapter proposes a modelling strategy to supplement testing to estimate brace specific overstrength factors for all types and sizes and to quantify performance and under varying loading scenarios. An obvious application is to improve the design of BRBs. Alternatively, this can also aid researchers in understanding the strength failure hierarchy of complete BRBF systems, or for checking specific designs where this system is used in an unconventional way. Furthermore, this strategy can inform or validate assumptions adopted in simpler models applied, for example in simulation of complete building structures.

The following observations/conclusions are made about the BRB modelling strategy presented in this paper.

- In defining the material model, for the steel of a BRB core, a minimum of six backstress curves (five kinematic and one isotropic) are needed to accurately represent experimental data.

- A simplified approach was developed for modelling the frictional contact interaction between core, debonding material and the restrainer. This approach uses a softened contact relationship using a piecewise linear piecewise function, similar to the exponential function provided by Abaqus but with improved convergence characteristics. Along with a friction coefficient of 0.15, good agreement was achieved with BRB experimentally determined hysteretic behaviour.

- The modelling strategy was validated by good agreement with physical test data. The overstrength ratio for all cycles were within 8% and the predictions at $2.0\Delta_{bm}$ are within 6% of the experimental data for all three BRB designs (Court-Patience et al. 2021).

- The present models are not without limitations for predicting BRB structural behaviour. In addition to the limitations of the Chaboche plasticity model discussed in Section 2.2.1, rupture of the core, low cycle fatigue failure has not been validated and large brace sizes have not yet been considered.

3.9 **References**

ANSI/AISC (2010). Seismic provisions for structural steel buildings - ANSI/AISC. One East Wacker Drive, Suite 700, Chicago, Illinois 60601-1802, American Institute of Steel Construction

ANSI/AISC (2016). Seismic provisions for structural steel buildings - ANSI/AISC. One East Wacker Drive, Suite 700, Chicago, Illinois 60601-1802, American Institute of Steel Construction

Aslani, F. and R. Jowkarmeimandi (2012). Stress-strain model for concrete under cyclic loading. Magazine of Concrete Research **64**(8): 673-685

Broggiato, G. B., F. Campana and L. Cortese (2008). The Chaboche nonlinear kinematic hardening model: calibration methodology and validation. Meccanica **43**: 115–124

Budaházy, V. (2015). Uniaxial cyclic steel behavior and model for dissipative structures. Doctoral thesis, Department of Structural Engineering at Budapest University of Technology and Economics.

Budaházy, V. and L. Dunai (2013). Parameter-refreshed Chaboche model for mild steel cyclic plasticity behaviour. Periodica Polytechnica Civil Engineering **57**: 139-155

Chou, C.-C. and P.-J. Chen (2009). Compressive behavior of central gusset plate connections for a buckling-restrained braced frame. Journal of Constructional Steel Research **65**: 1138-1148

Chou, C.-C. and J.-H. Liu (2012). Frame and brace action forces on steel corner gusset plate connections in buckling-restrained braced frames. Earthquake Spectra **28**(2): 531-551

Computers and Structures Inc. (2004). SAP2000, linear and nonlinear static and dynamic analysis and design of three-dimensional structures. Berkley, California, USA

Computers and Structures Inc. (2011). User guide Perform-3D. Berkeley, California, USA

Computers and Structures Inc. (2016). ETABS - integrated building design software, user's guide. Berkeley, California, USA

Court-Patience, D. and M. Garnich (2021). Evidence collected for peer review of BRBFs in New Zealand. Bulletin of the New Zealand Society for Earthquake Engineering **(in press)**

Dassault Systems (2014). ABAQUS 6.14 Analysis User's Guide, Volume III: Materials

Dassault Systems (2014). ABAQUS 6.14 Analysis User's Guide, Volume IV: Elements

Dassault Systems (2014). ABAQUS 6.14 Analysis User's Guide, Volume V: Prescribed conditions, constraints and interations

Dassault Systems (2017). Abaqus 2017, SIMULIA

Gopalaratnam, V. S. and S. P. Shah (1985). Softening response of plain concrete in direct tension. Journal of American Concrete Institute **82**(May-June): 310-323

Holmes Solutions (2014). Buckling-Restrained Brace Testing. 5 Canterbury Street, Christchurch, New Zealand, Holmes Solutions Testing Laboratory

Lemaitre, J. and J.-L. Chaboche (1990). Mechanics of solid materials, Cambridge University Press.

Lin, P.-C., K.-C. Tsai, C.-A. Chang, Y.-Y. Hsiao and A.-C. Wu (2016). Seismic design and testing of buckling-restrained braces with a thin profile. Earthquake Engineering & Structural Dynamics **45**: 339-358

Maekawa, K. and H. Okamura (1983). The deformation behaviour of constitutive equation of concrete using the elasto-plastic and fracture model. Journal of the Faculty of Engineering at the University of Tokyo **37**(2): 253-328

Mazzoni, S., F. McKenna, M. H. Scott and G. L. Fenves (2007). Opensees command language manual. University of California, Pacific Engineering Research Center

NCREE. (2020). "National Center for Research on Earthquake Engineering - https://www.ncree.narl.org.tw/." Retrieved 04/29/2021.

Park, R. and T. Paulay (1975). Reinforced concrete structures, John Wiley & Sons.

Sabelli, R., S. Mahin and C. Chang (2003). Seismic demands on steel braced frame buildings and buckling-restrained braces. Engineering Structures **25**: 665-666

Sika (2018). Product Data Sheet version no: 03/18 SikaGrout - 212 HP

Standards Australia (2007). Metallic materials - Tensile testing at ambient temperature AS 1391

Standards New Zealand (2006). NZS 3101: Part 1 Concrete Structures Standard. Wellington, New Zealand, Standards New Zealand

Takeuchi, T. and A. Wada (2017). Buckling-restrained braces and applications. Tokyo, Japan, The Japan Society of Seismic Isolation.

Tsai, K.-C., A.-C. Wu, C.-Y. Wei, P.-C. Lin, M.-C. Chuang and Y.-J. Yu (2014). Welded end-slot connection and debonding layers for buckling-restrained braces. Earthquake Engineering Structural Dynamics: 785–1807

Westeneng, B. (2016). Buckling behaviour of gusset plates in buckling-restrained braced frames. Masters of Engineering, University of Canterbury.

Zsarnozay, A. (2013). Experimental and numerical investigation of buckling-restrained braced frames for Eurocode conform design procedure development. PhD, Budapest University of Technology and Economics.

Zub, C. I., D. Dubina and A. Stratan (2019). Calibration of parameters of combined hardening model using tensile tests. P. U. o. Timisoara

Zub, C. I., A. Stratan and D. Dubina (2020). Prequalification of a set of buckling restrained braces: Part II - numerical simulations. Steel and Composite Structures **34**: 561-580

4 BUCKLING ANALYSIS OF GUSSET PLATES WITH BOLTED CONNECTIONS USING FINITE ELEMENT MODELLING

Gusset plates connect lateral bracing to a building by fixing two perpendicular edges into the corners of a frame. This means that along the length of a gusset plate the cross sectional area is not uniform and causes make the stress distribution through a gusset plate difficult to predict. This has motivated design methods to approximate the yield force of gusset plates. The Whitmore width method (1952) is a widely adopted method used to estimate the yielding area of gusset plates in tension or those that do not buckle in compression. When considering buckling, design codes prescribe equations that calculate the compressive strength of gusset plates. These equations reduce the yielding capacity of the gusset plate by a factor based on slenderness. However, the reduction factor is based on column buckling behaviour and are not specific to gusset plates. This study uses finite element modeling to study the development of yielding and plastic behaviour of a brace end bolted to a series of corner gusset plates. In total, 184 variations of gusset plate geometries were modelled in Abaqus®. The FEA modelling assumed an initial imperfection and applied a monotonic uniaxial load. Upon comparing results to current design methods, it was found that the Whitmore width method is generally un-conservative in predicting initial yielding of gusset plates. To improve accuracy and safety in the design of gusset plates, modifications to current design methods for calculating the yield area and compressive strength curve for gusset plates is proposed.

4.1 **Introduction**

In seismic building design, gusset plates connect lateral bracing within a structural frame along primary load paths. The type of braced frame selected (i.e. SCBF, EBF or BRBF) dictates the gusset plate design to achieve the desired behaviour. As gusset plates are connected into the corners of a frame, the perpendicular boundary conditions mean stress distribution through the connection zone (beam, column, brace and gusset) is complex and difficult to predict. Until 1952, beam formulas were used in the design of gusset plates (Whitmore 1952, Birkemoe et al. 1969, Vasarhelyi 1971, Gaylord et al. 1972). These beam formulas checked the stress limits along various sections of a connection zone. To examine the validity of this approach, Whitmore investigated the stress distribution of an aluminum gusset plate within a truss. He found beam formulas to be inaccurate and founded an alternative method (the Whitmore width method (AISC 1974)). He concluded that an effective normal stress, transferred from the end of a member into the plate could be estimated adequately by assuming the force was distributed uniformly over an effective area. This area was obtained by multiplying the thickness of the plate by an effective width. The effective width is presented in equation (4.1).

$$b_e = b_{bolt\ array} + 2\, L_{bolt\ array}\, tan\ 30^0 \tag{4.1}$$

Where, $b_{bolt\ array}$ and $L_{bolt\ array}$ is the width and length of the bolt array. Figure 4-1 illustrates how the effective width is calculated. This is achieved by tracing lines 30º from the outer bolts of the first row, to a perpendicular line passing through the bottom row of bolts (ANSI/AISC 2016). This effective width is multiplied by the thickness and yield strength to calculate the sections force capacity of the gusset plate.

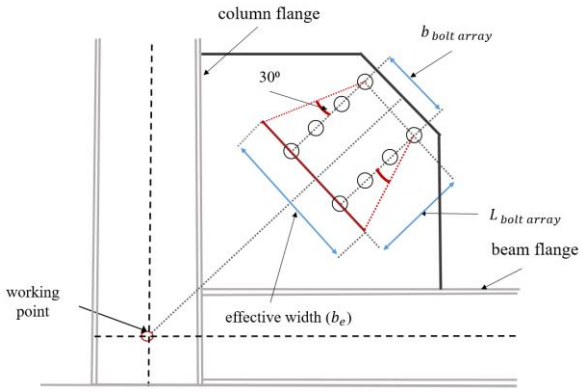

Figure 4-1. Schematic of Whitmore width (b_e) (ANSI/AISC 2016)

Initially, the Whitmore width method was used to estimate peak axial stresses at the end of the joints. This seems reasonable as it provided a good fit to the results of the aluminum gusset plate – frame joint experiment. However, the spectra of gusset plate geometries used today means the ability of the Whitmore width method to predict the onset of yielding for all scenarios should be questioned. This is a problem when designing gusset plates using capacity based design philosophy, which relies on being able to predict yielding of each member.

Seismic design requires engineers to consider both tension and compression demands. In tension, energy dissipates through yielding and plastic flow. In compression, braces are susceptible to global buckling behaviour, meaning energy dissipates through combined axial and bending deformation. Under compression braces are also susceptible to hinging. If the brace buckles out-of-plane, hinging within the gusset plate should be the primary load transfer mechanism. To encourage this mechanism, seismic provisions in AISC and NZS3404 prescribe a minimum clearance of two times the thickness from the end of brace, parallel with the corner of the shortest free edge of the gusset plate as per Figure 4-2(a-b) (Standards New Zealand 1997, ANSI/AISC 2016). This approach results in relatively large section sizes that are not desirable.

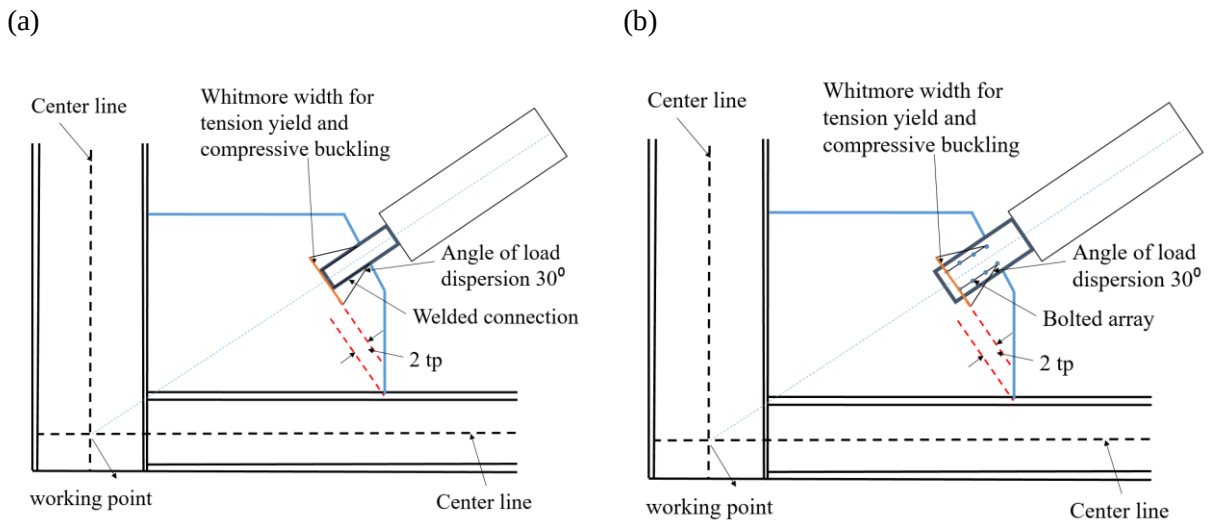

Figure 4-2. Schematic of gusset plate geometries allowing for end rotation
(a) 2tp clearance on welded connection, (b) 2tp clearance on a bolted connection

To achieve smaller section sizes, designers can use tapered sections. Alternatively, Roeder et al. (2011) introduced another approach which assumes the gusset plate can bend about an elliptical line pattern. Figure 4-3 (a-b) illustrates the linear clearance approach with a tapered section and the elliptical clearance approach respectively.

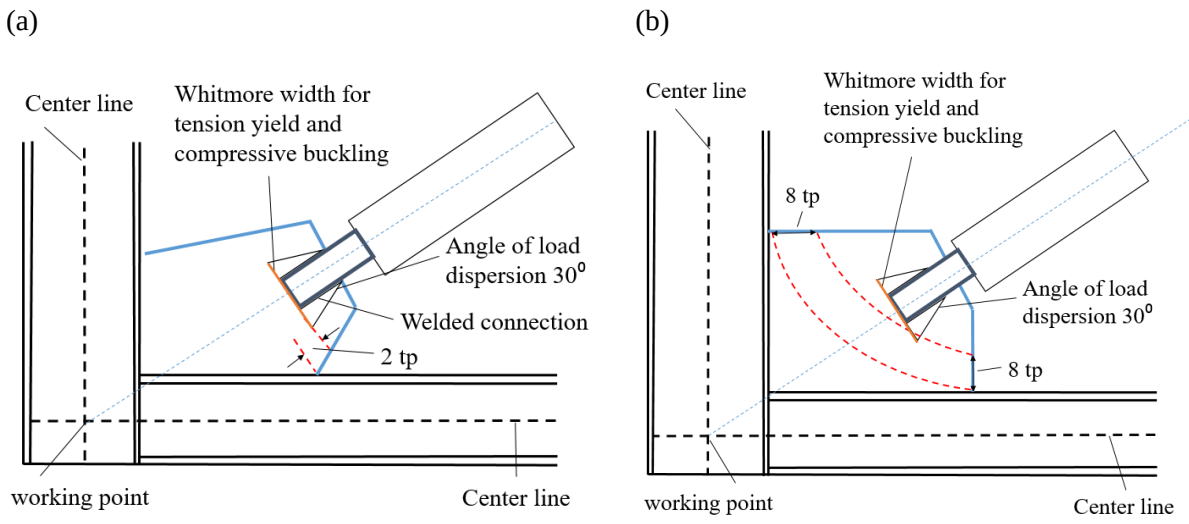

Figure 4-3. Schematic of gusset plate geometries allowing for end rotation
(a) 2tp clearance with tapered gusset, (b) Elliptical clearance with rectangular gusset

Different to traditional braced frames (SCBFs and EBFs) are buckling-restrained braced frames (BRBFs). BRBFs dissipate energy in the core of the brace while encased in a restrainer. The restrainer prevents the global buckling exhibited in traditional bracing to achieve plastic flow in a larger volume of material. Unlike traditional bracing, hinging about the gusset plate is not encouraged and more compact gusset plates are desirable. To prevent local instability or plastic collapse of the gusset plate, design equations are used to predict compressive strength. These equations reduce the effective yield capacity of the gusset plate based on its slenderness. However, this reduction is based upon column buckling behaviour and simplify gusset plates according to an equivalent column.

Internationally, design codes have adopted this approach with variations on how to construct the effective column and reduction factor. Thornton (Thornton 1984) initially proposed the equivalent column approach. To construct the equivalent column, he approximated the buckling length by the distance from the end of the bolt array, in the middle of the Whitmore width, along the load path, to either the beam or the column flange along the load path. This is considered the maximum unsupported length but was deemed too conservative. He then proposed the buckling length as the average of three lengths, equally spaced along the Whitmore width as shown in Figure 4-4.

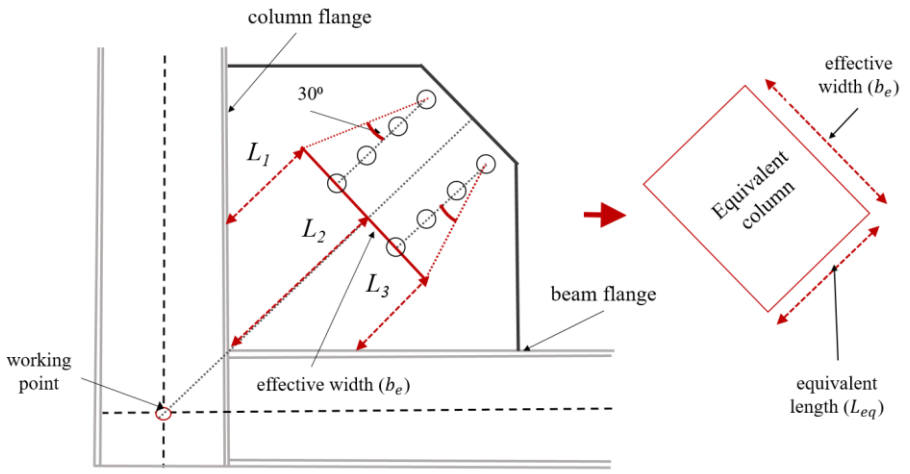

Figure 4-4. Schematic of Whitmore Width (b_e) and Thornton Lengths (L_1, L_2 and L_3)

Thornton also developed a unique strength curve to describe buckling behaviour of columns. This method built on Euler's column buckling theory that is limited to elastic buckling behaviour of columns. Thornton's method reduces the section capacity described by Equation (4.2). The section capacity is the strength of a very short column that cannot undergo overall member buckling. Unlike Euler buckling, it aims to account for inelastic and second order effects such as initial geometric imperfections and residual stress. Thornton applied this to gusset plates using the equivalent column dimensions described in Figure 4-4. This method separates the overall strength curve into two components, inelastic/nonlinear buckling as per Equation (4.3) and elastic buckling as per Equation (4.4). Both equations (4.3) and (4.4) use a slenderness parameter, defined by Equation (4.5).

$$\boldsymbol{N}_s = b_{e\,30}\ t_g\ \boldsymbol{\sigma}_y \tag{4.2}$$

$$\boldsymbol{P}_{cr} = (0.658)^{\lambda_c{}^2}\ \boldsymbol{N}_s \qquad \lambda_c \leq 1.5 \tag{4.3}$$

$$\boldsymbol{P}_{cr} = \left(0.877/\lambda_c{}^2\right)\ \boldsymbol{N}_s \qquad \lambda_c > 1.5 \tag{4.4}$$

$$\lambda_c = \frac{K_e L_{avg}}{\pi r}\ \sqrt{\frac{\boldsymbol{\sigma_y}}{\boldsymbol{E}}} \tag{4.5}$$

In equations 4.2-4.5, K_e = effective length factor; L_{avg} = the average Thornton length; r = the radius of gyration for a plate ($t/\sqrt{12}$); $\boldsymbol{\sigma_y}$ = yield stress of the material, $\boldsymbol{E}$ = the elastic modulus, $b_{e\,30}$ = Whitmore width (with a load dispersion angle of 30º), and t_g = gusset plate thickness. Figure 4-5 shows the construction of the Thornton method using equations (4.3) and (4.4), presented as a function of geometric

slenderness L_{avg}/r. All critical load values are normalised by the critical load when λ_c = 1.5, and will be used to normalise all strength curves herein. Note that λ_c = 1.5 represents the elastic limit as proposed by the Thornton method but may not be a true representation for all methods.

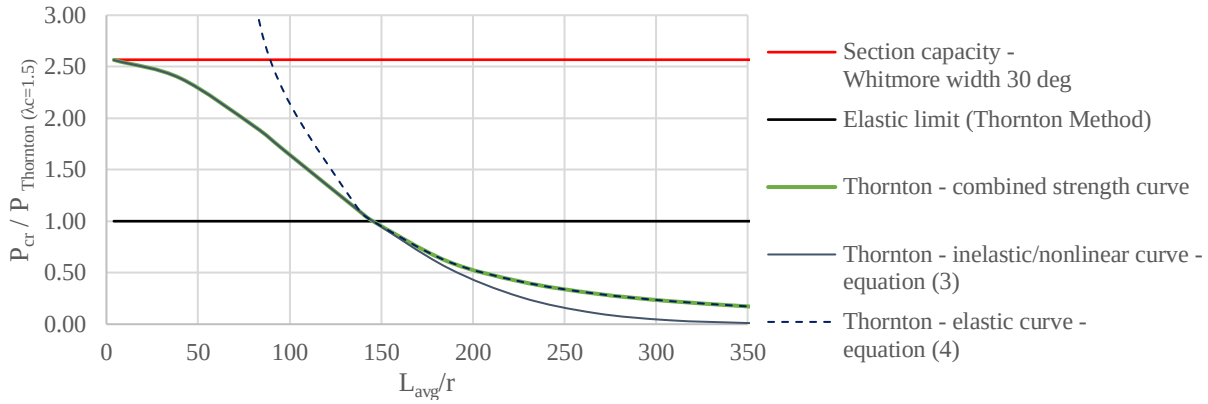

Figure 4-5. Thornton method for predicting buckling capacity

Thornton did not provide any experimental results to support and validate the application of this method. Subsequent experimental testing has since found this method to be too conservative in some cases (Yam et al. 1993) (Gross 1988). Yam and Gross proposed a change to reduce excessive oversizing of gusset plates. Specifically, they suggest the thickness of the plate be reduced by assuming the effective width is larger. This is achieved by changing the dispersion angle as per the Whitmore width method, from 30º to 45º, as shown in equation (6).

$$b_{e\,45} = b_{\,bolt\ array} + 2\,L_{\,bolt\ array}\ tan\ 45^{0} \tag{4.6}$$

The modified Thornton method uses Equation (4.6) to calculate the load bearing capacity of a gusset plate, and replaces equation (4.2) in the Thornton method. This change accounts for greater assumed load redistribution (spreading) after initial yielding in the gusset plate. However, further research showed this method to be un-conservative for many larger/stocky gusset plates.

In another study, Sheng et al. used results from validated finite element modelling to predict inelastic compressive buckling of gusset plates and developed a new design method using prescribed tables (Sheng et al. 2002). However, this method was only validated for a small number of variations. Similar numerical studies include Williams (1986), Hu (1987) and Brown (1988).

To date, the response of relatively slender gusset plate connections has not been adequately studied. As such, Fang et al. (2015) recently presented a numerical study on the post buckling behaviour of slender gusset plates connections. Different grades of steel were modelled to study the effect strain hardening has on post buckling behaviour. The results were used to determine the appropriateness of using high grade steel in gusset plate design. Each model demonstrated stable post-buckling equilibrium paths, and two design approaches to predict ultimate strength are proposed. The two approaches include a Column Buckling Approach, which is also based on a modified column analogy from common design practice, and a Plate Buckling Approach, which is based on a plate analogy and modified Winter formulae. Although this study is helpful for predicting the ultimate strength of slender gusset plates, more studies are required to confirm the application of this approach outside of conditions modelled.

A method similar to the Thornton method is prescribed in the New Zealand Steel Structures Standard (NZS 3404) (Standards New Zealand 1997). Here again, the gusset plate is treated as an equivalent column, using the average Thornton length and Whitmore width (with a load dispersion angle 30 degrees). Like the Thornton method, the compressive strength is calculated by reducing the section capacity based on slenderness. To account for the different cross-sectional shapes and fabrication methods of typical columns, the NZS 3404 defines five different strength curves to describe buckling (McGuire 1968, Rotter 1982, Rasmussen et al. 1989, Trahair et al. 1991). These account for different load distribution, and magnitudes of residual stress among sections. These curves require a more comprehensive set of equations compared to the Thornton method, so to reduce manual calculations a set of design tables were also developed (section 6.3.4 of NZS 3404 – Appendix B). Gussets plates are not specifically accounted for in these strength curves but are treated as a 'H' or 'I' column section with a thickness up to 40mm. Figure 4-6 displays the method of gusset plate design set out in NZS3404, for comparison the Thornton method and Euler buckling method are also plotted alongside this is. In general, for the same gusset plate the NZS3404 method predicts a lower capacity compared to the other methods presented.

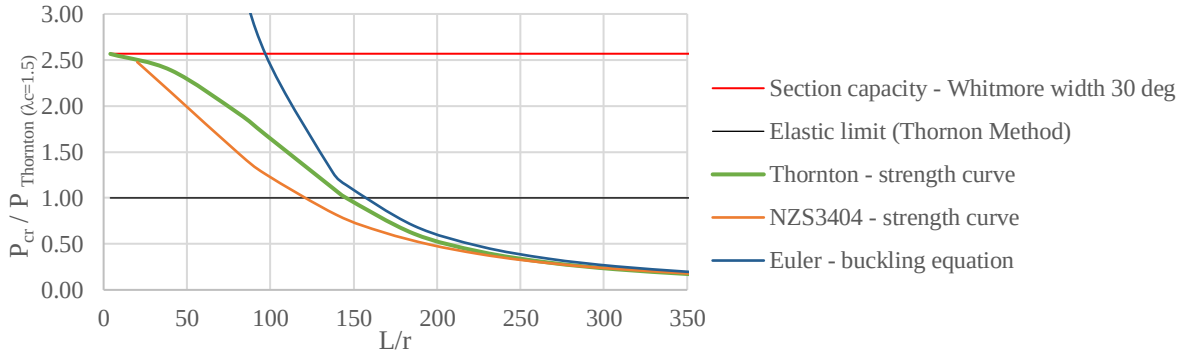

Figure 4-6. The Thornton and NZS3404 Method used to predict column buckling

Several researchers have reviewed the accuracy of these methods. One study (Westeneng 2016) compared the Thornton and NZS3404 method, against 30 experimentally tested gusset plates. This helped identify the overall level of safety provided by design codes. Although in general these methods were conservative, it also showed some experimentally tested gusset plates can fail at a lower strength than those predicted (Westeneng 2016).

In 2007, the Interstate 35W (I-35W) bridge in Minnesota, USA, collapsed, resulting in 13 deaths and more than 100 injuries. The collapse was caused by overstressed and buckled gusset plates (Berman et al. 2011), This incident resulted in extensive experimental and numerical investigations being undertaken to better understanding of the behaviour of gusset plate connections (Lehman et al. 2008, Martinez-Saucedo et al. 2008, Chou et al. 2009).

The above statements suggest the need to identify which geometries and simplifying features are at higher risk of failing before design loads calculated from existing methods. In general, the equivalent column approach has been shown to be conservative but varying levels of safety prescribed by these methods suggest the underlying assumptions of these models, such as initial yield area, yield development and slenderness are only accurate for particular range of gusset plate designs. Ideally, gusset plates in BRBF are compact and stiffened to reduce local and global instability. However, internationally, few design codes enforce this, which has led to a large range of gusset plate variations on the market.

Although significant experimental and numerical investigations have been conducted on the compressive strength of gusset plates, it appears there has been limited progress in the developing new analytical models for the predicting buckling and plastic collapse behaviour specific to gusset plate connections. This study involves the use of finite element analysis (FEA) to investigate the yielding and plastic behaviour of gusset plates with bolted connections considering both slender and compact designs. The models predict the initial yield area, the elastic buckling length and critical compressive load for 184 gusset plate designs. Of interest is how different design parameters, such as the size of the connection area, load angle, thickness, length and shape of the gusset plate affect performance. Based on the observations from FEA modelling, changes to the current methods used to predict the yield area, length and compressive capacity of a gusset plate are suggested.

4.2 **Finite element model development**

The non-uniform geometry and variations in gusset plate designs make it difficult to predict how stresses distribute through a gusset plate and connection zone. This is because the yielding of the material develops in different sections of the gusset plate as loading increases. The Whitmore width method approximates this yielding behaviour in an average sense over a hypothetical section area. Since the conception of the Whitmore width method (1952), advances in FEA now enable detailed analysis of stress-strain behaviour and the onset of elastic-plastic buckling-like collapse. To study the yielding and buckling behaviour of different gusset plates, a series of finite element models were developed using Abaqus®. All models were the same except for geometric dimensions. Each model included a brace end connected to a gusset plate. Solid (C3D8I) elements were used to capture the stress-strain response through the thickness of each member (Dassault Systems 2014). To capture buckling behaviour, non-linear geometric analysis was performed.

Slenderness of a gusset plate influences the type of compressive failure. More slender gusset plates tend to show sway failure and more compact gusset plates tend to crush. This varying behaviour makes it difficult to select the appropriate boundary conditions. In this study, the gusset plate to beam-column boundary was idealised as being fixed. The gusset plate to brace end boundary was idealised as a pin-roller. These assumptions approximate the actual behavior but have the advantage of coinciding with the effective length factor k_e = 0.7 as per NZS 3404 and ANSI 341-16 recommendations (Standards New Zealand 1997, ANSI/AISC 2016). Surface-surface contact between the gusset plate and brace end connection was included in the FEA models. Each bolted connection was approximated using a coupling constraint, which coupled the inner surface of each bolt hole to a centre node. To capture local bolt bearing deformation, only half the inner surface of each bole hole was constrained to this centre node. To represent S235 grade steel, an elastic modulus of 205 GPa and a yield strength of 350 MPa was used alongside a tabulated multi-linear isotropic hardening material model as per Table 4-1 (Yam et al. 1993). This was deemed suitable as only monotonic axial loading was applied.

Table 4-1. Isotropic material model – S235 grade steel

Yield stress [MPa]	305	310	400	460	480
Plastic strain	0	0.0125	0.04	0.1	0.15

Each model included an initial imperfection of 2 mm in the lateral out-plane direction. This offset represents any initial geometric imperfections, residual stress and eccentricity associated with a BRBF under compression. In a BRBF, eccentricity to largely influenced by core to restrainer interaction. Generally, the debonded gap between the end section of a restrainer is 1-2 mm. A 4 mm imperfection was also investigated. Although the effect of increasing the imperfection was more noticeable in 6 mm plates compared to 32 mm plates, only a slight reduction (<6%) in yield and ultimate load was observed. Validation of these modeling selections is shown through direct simulation of the experimental testing conducted by (Yam et al. 1993). Figure 4-7 presents the experimental setup and finite element model of the test.

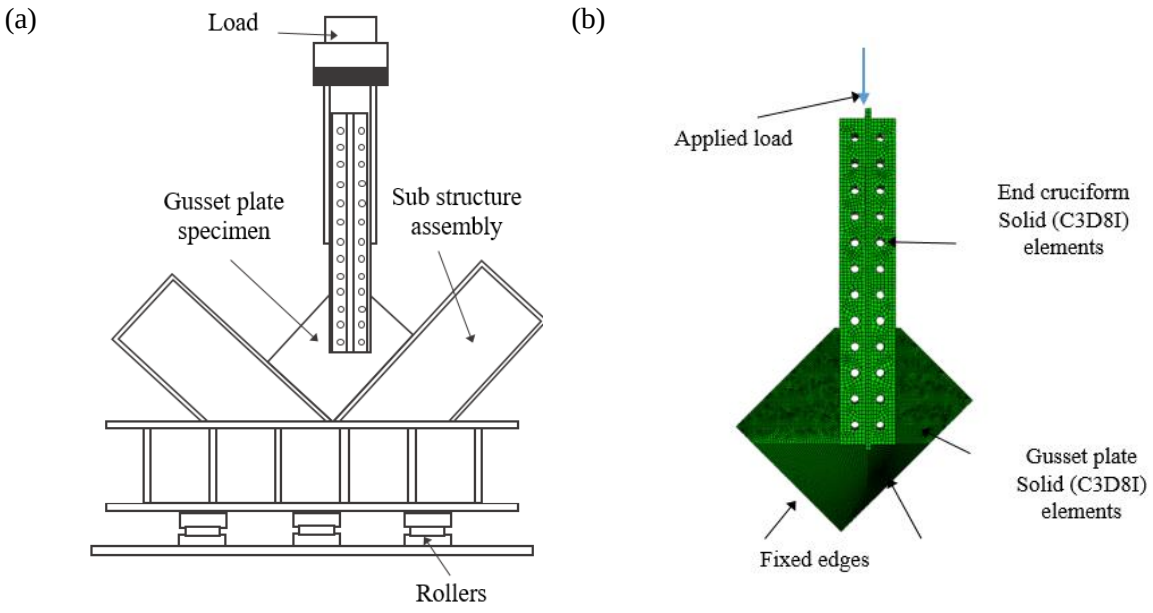

Figure 4-7. Comparison of experimental test set up and FEA model
(a) experimental test setup (Yam et al. 1993), (b) visualization of FEA model

Three gusset plates (GP1, GP2 and GP3) were selected from Yam et al. (1993) for validation. The peak loads for both simulated and experimental results are shown in Table 4-2, showing simulated results to be within 5% of experimental results.

Table 4-2. Peak axial loads of gussets plates used for validation

	Ultimate load (EXP) [kN]	Ultimate load (SIM) [kN]	Percentage difference [%]
GP1	1956	2050	4.8
GP2	1356	1421	4.8
GP2	742	725	2.3

Direct comparison of force-displacement plots was not suitable as each experiment only captured the stroke of the hydraulic ram in the vertical direction. However, Yam et al. (1993) also used more precise LVDTs to measure the out of plane displacements in each gusset plate test. The location of the LVDTs is shown in Figure 4-8a. Modelling showed reasonable replication to the out-of-plane displacements captured in the experiments. Figure 4-8b shows the comparison between the measured (EXP) and simulated (FEA) out-of-plane displacements for GP2.

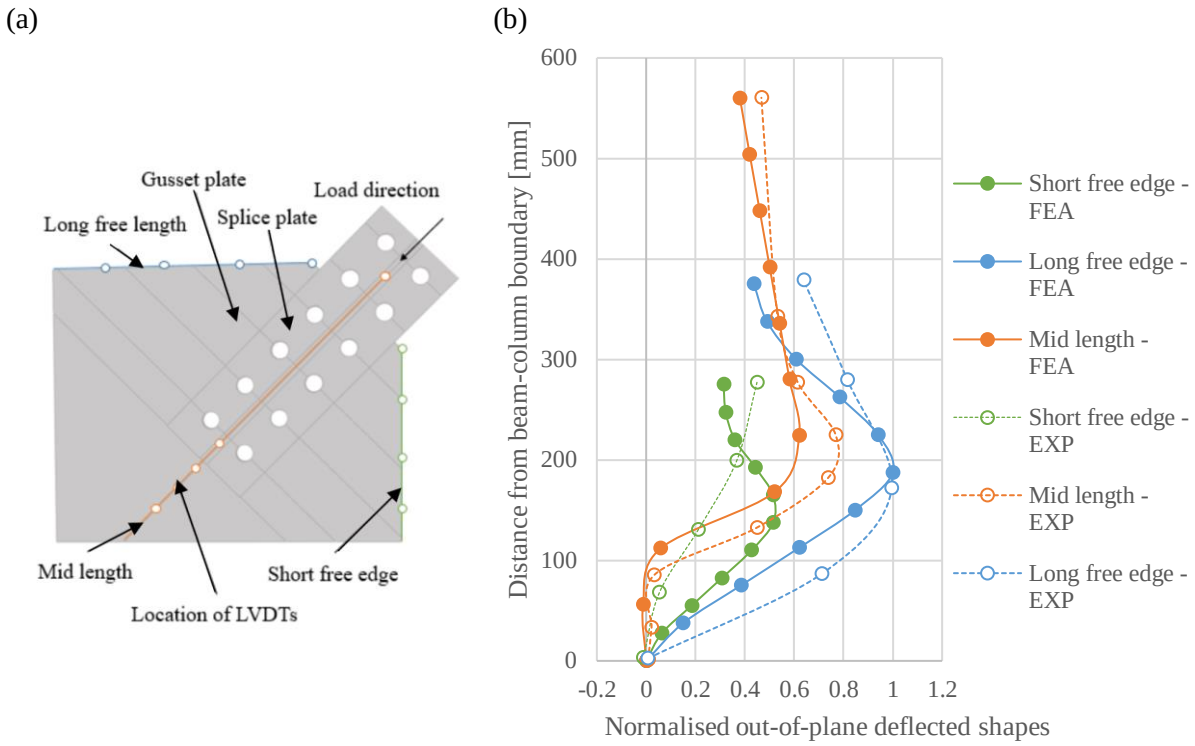

Figure 4-8. (a) Location of LVDTs on gusset plate specimen (Yam et al. 1993)
(b) Comparison of out-of-plane displacements (FEA vs EXP)

Following validation, a total of 184 gusset plate models were developed in Abaqus®. Common gusset plate designs guided the selection of geometries investigated (such as the tapered examples shown in Figure 4-9 (a-b)). Variations include square/rectangular and tapered designs, the size of the bolted connection and number of bolts, angle of inclination, gusset plate thickness and length of bolted connection from the working point. Table 4-3 presents a summary of all the variations investigated accompanied by Figure 4-10 showing each of the geometric parameters. These parameters combine to create 512 possible variations. Of those, 184 were deemed practical and realistic of industry practice.

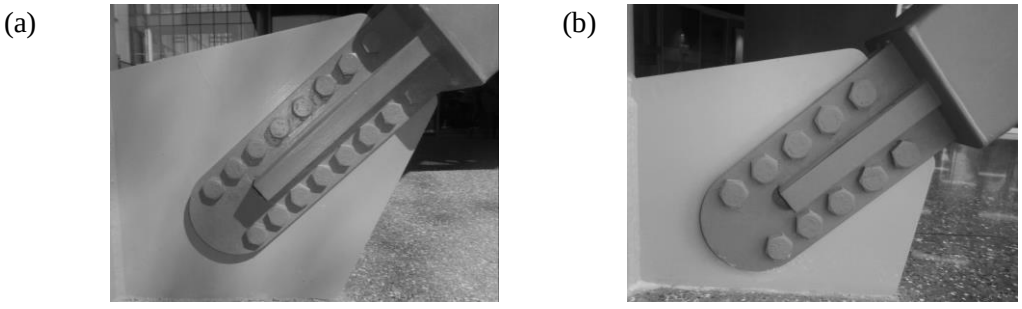

Figure 4-9. Various lengths of bolted connection arrays used in BRBF design
(a) 16 bolt array (b) 10 bolt array

Table 4-3. Variations in gusset plate geometries investigated

Geometric description	Values/types
Shape of gusset plate	Regular
	Tapered (with a cut at 22.5º on each edge)
Size of bolted connection - # of bolts	4 bolts (125mm x 210mm)
(Length of bolt array x Width of bolt array)	6 bolts (125mm x 210mm)
	6 bolts (61mm x 100mm)
	8 bolts (125mm x 210mm)
	10 bolts (125mm x 210mm)
	12 bolts (250mm x 436mm)
	14 bolts (250mm x 436mm)
	16 bolts (250mm x 675mm)
Angle of inclination	22.5^0 45^0
Thickness	6mm, 15mm, 25mm, 32mm
Length	100mm, 300mm, 500mm, 1000mm

(a) (b)

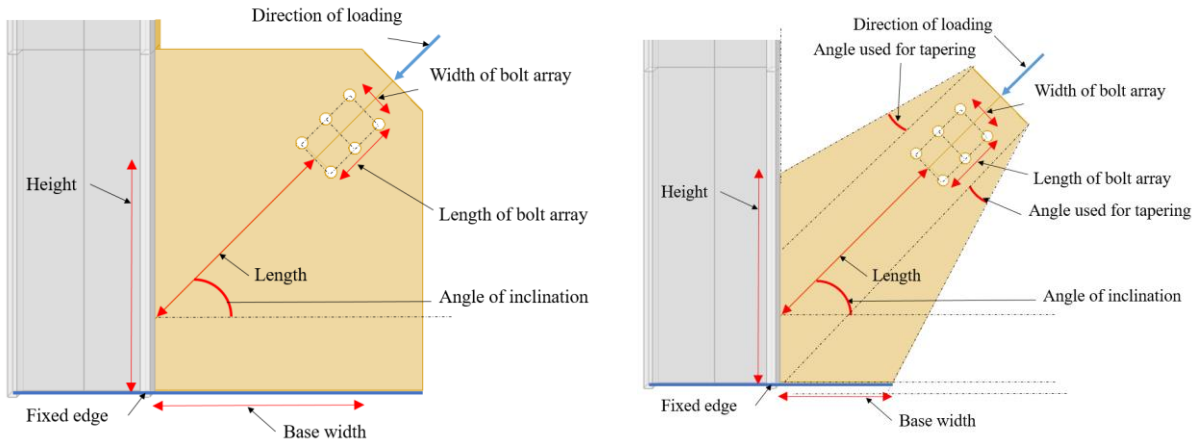

Figure 4-10. Geometric parameters used in variations of gusset plates
(a) regular design (b) tapered design

Figure 4-11 illustrates three examples of the gusset plate models described in Table 4-3. These vary in geometric slenderness (L/r) from 60, being very slender to 2, being compact.

(a) (b) (c)

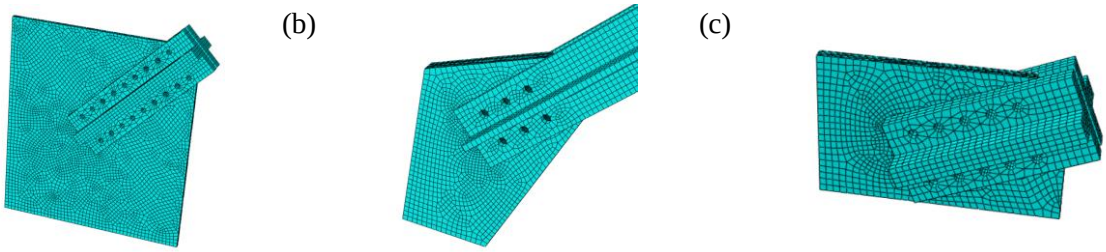

Figure 4-11. Example of gusset plates modelled in FEA
(a) 16 bolt array – 45 ^{o}- non tapered – L/r = 60, (b) 6 bolt array - 45 ^{o}- tapered – L/r = 13
(c) 10 bolt array – 22.5 ^{o}non tapered – L/r = 2

4.3 **Gusset plate yield area**

Finite element modelling enables close examination of stress-strain behaviour. This can be used to study how yielding initiates and develops through a gusset plate under loading. Generally, slender sections are governed by elastic buckling. However, the majority of gusset plate designs are compact and the likelihood of elastic buckling is low. In these cases, the design is governed by yielding and non-linear buckling and plastic collapse.

In simple uniform axial loaded structural members, the yield area is simply the cross-sectional area. However, the geometric features of a gusset plate, and diagonal brace connection cause a non-uniform distribution of stress under compressive loading. This has motivated methods for estimating an effective yield area. At the one end of the gusset plate, a brace connects diagonally by an array of bolts. At the opposite end, a gusset plate has two edges fixed to the beam and column flanges of a frame at perpendicular angles. This means the cross-sectional area varies along the axis of loading. To illustrate this, Figure 4-12 displays a schematic of gusset plate with several cuts made perpendicular to the direction of brace which corresponds to the direction of loading. It is easy to see that these cuts are all different lengths. In addition, the load is transferred from the brace to the gusset plate through a rectangular array of bolts. These complexities make it difficult to accurately estimate the "effective" cross-sectional area upon yielding.

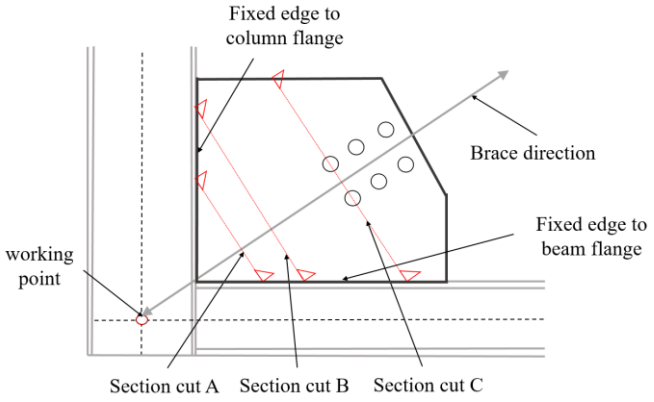

Figure 4-12. Schematic showing change in cross-section width of a gusset plate

Figure 4-13(a)-(c) shows an example of how von Mises stress develops through a gusset plate under loading where red and grey indicate yielding/plastic deformation and blue indicates low levels of stress. These images represent snapshots within the load history. This shows that yielding does not occur over the entire cross section evenly, and that it has a complex spatial evolution.

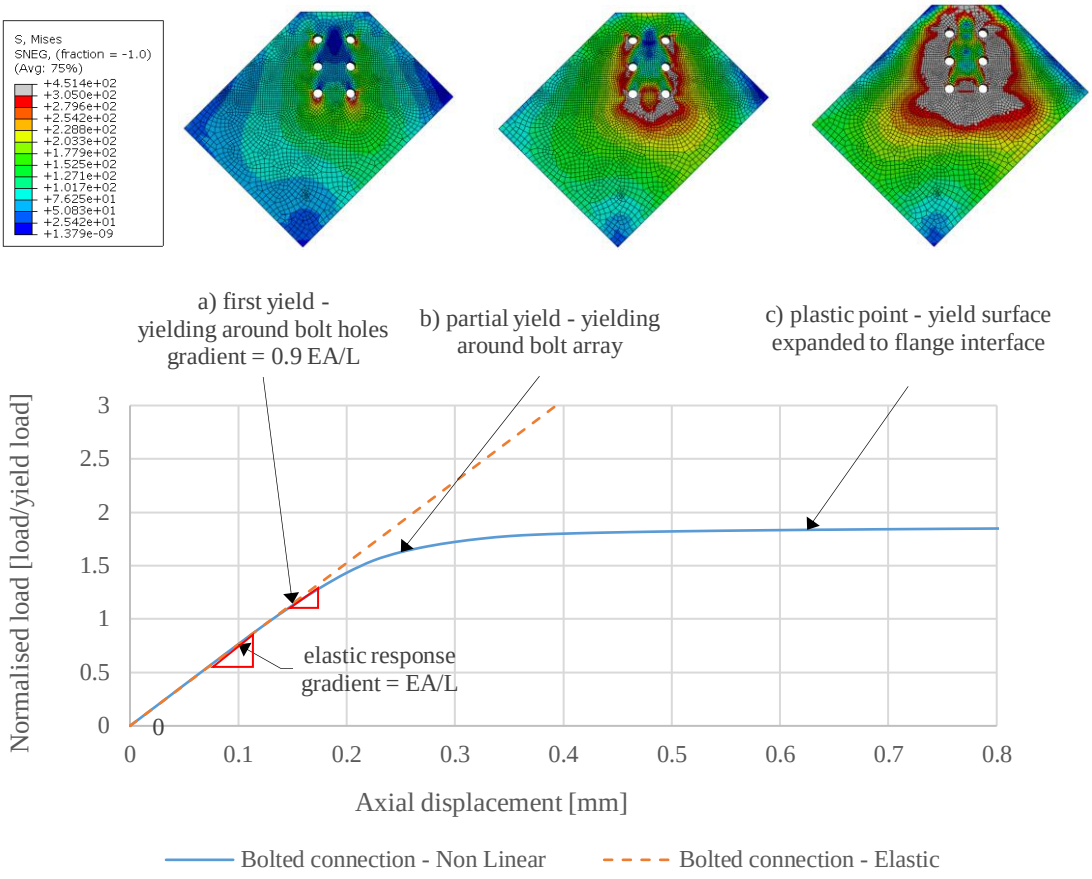

Figure 4-13. Force vs displacement response of an axially loaded gusset plate (showing the response locations associated with yielding images)

Although the Whitmore width method is used estimate general yielding of a gusset plate, there is no standardised method to establish the initial yield load of a gusset plate. Identifying yield is important as it defines the end of the elastic response. The analysis in this study detects yielding to begin around the bolts. This is difficult to observe in experiments due to the brace end obscuring this zone, and is unique to gusset plates with bolted connections. Analysis of simulated data showed this point (where yielding is first detected around the bolts) is closely affiliated to the point where the stiffness reduces to 90% of its initial linear-elastic value on the force-displacement plot.

Defining an initial yield load for gusset plates is difficult. This is because the selection of both the effective cross-sectional area and elastic buckling length of a gusset plate can be debated. As such an offset, using the point where the stiffness reduces to 90% of its initial linear-elastic value is proposed. This method is analogous to using the 0.2% offset method for defining yield strength. It identifies the end of the elastic response in a consistent way that is less sensitive to system parameters than, for example, the proportional limit. By defining a first yield point, an effective first yield area can be calculated by dividing the first yield

load by the yield strength of the material. Then an effective width associated with first yield can be calculated by dividing the effective yield area by its thickness.

By using the FEA results, we can calculate the effective yield width between each gusset plate model and compare these to the Whitmore width method. We can also investigate how different gusset plate features such as angle of inclination, length and tapering influence the initial yielding. Displayed in Figure 4-14 are FEA results, showing the effective first yield width calculated for the different sizes of bolted connections modeled. These are all presented as a function of the perimeter of each bolt array. The perimeter of each bolt array connects the centers of all the outer edge bolts.

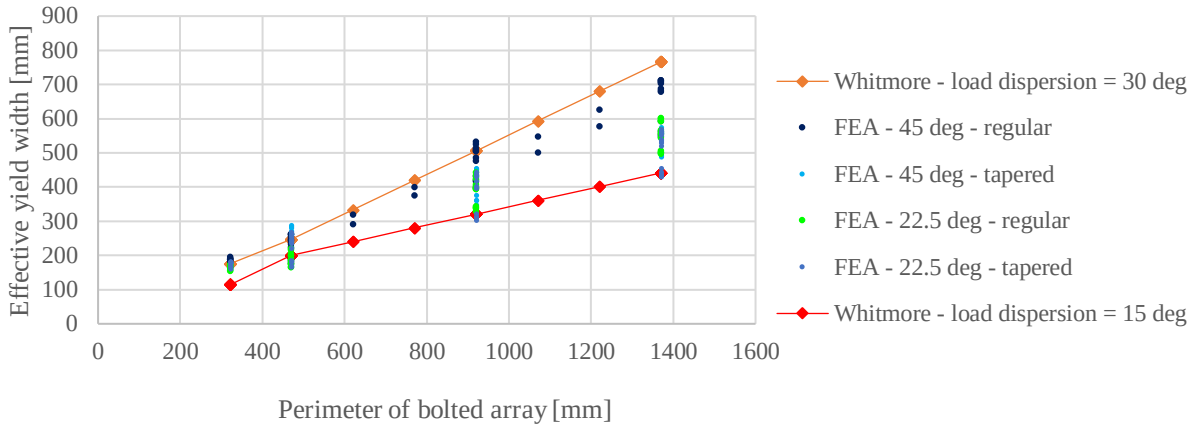

Figure 4-14. Gusset plate width (at first yield)

It was found that the Whitmore width method generally overestimates the initial yielding width compared to FEA results, especially for gusset plates with larger connections. By simply changing the load dispersion angle to 15º instead of 30º, as per equation (4.7), the prediction of initial yield width generally became conservative.

$$b_{e\,15} = b_{bolt\ array} + 2\,L_{bolt\ array}\ tan\ 15^{\circ} \tag{4.7}$$

Important to note: Bolted arrays can have different length-width ratios while having the same perimeter lengths. As the Whitmore width method is a function of this length-width ratio, the orange and red lines shown in Figure 4-14 may very slightly if additional gusset plate designs are investigated.

4.4 Length of a gusset plate

The length of a column is a key parameter in predicting buckling. This is generally the physical length between the each end. For gusset plates, the length between each end is ill-defined because of the way a gusset is welded into the corners of a frame. This complexity motivates methods for estimating an effective length. The most commonly adopted method for calculating an effective length of a gusset plate is the Thornton length method. As illustrated previously in Figure 4-4, the Thornton length approximates the buckling length by using the average of three physical lengths between the Whitmore width (using a load dispersion of 30º), and the beam or column flange interface. In this study, the elastic buckling length is calculated using the elastic stiffness (EA/L) generated from the axial-force displacement responses from the series of gusset plates modelled in this study. Then by using the initial yield force (Figure 4-13) and the elastic modulus, an effective buckling length can be estimated. Figure 4-15 shows the elastic member stiffness in the axial-force (F) displacement (U) response, and equation (4.8) and equation (4.9) show how to determine the elastic buckling length of a member.

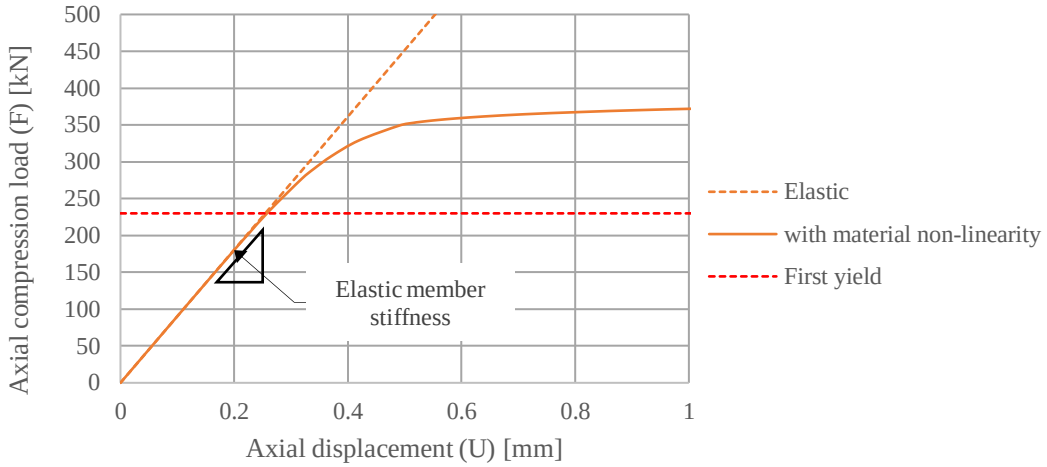

Figure 4-15. Axial force-displacement of gusset plate under ideal loading conditions

$$F/U = EA/L_{el} \quad \text{(Elastic axial stiffness of member)} \tag{4.8}$$

$$L_{el} = E\, b_e\, t_{gp}\, U/F \tag{4.9}$$

To easily distinguish between all the types of length variables used in gusset plate design, the following notations are used hereinafter.

L_2 The mid length, using the Thornton length method.

$L_{1,3}$ The outer lengths as per the Thornton length method.

L_{avg} The Thornton length.

L_{el} The elastic buckling length from FEA, determined from the elastic axial stiffness from the axial force-displacement response from each simulation.

Following the analysis of the gusset plate models in this study, the elastic length was compared to the average Thornton length method as displayed in Figure 4-16.

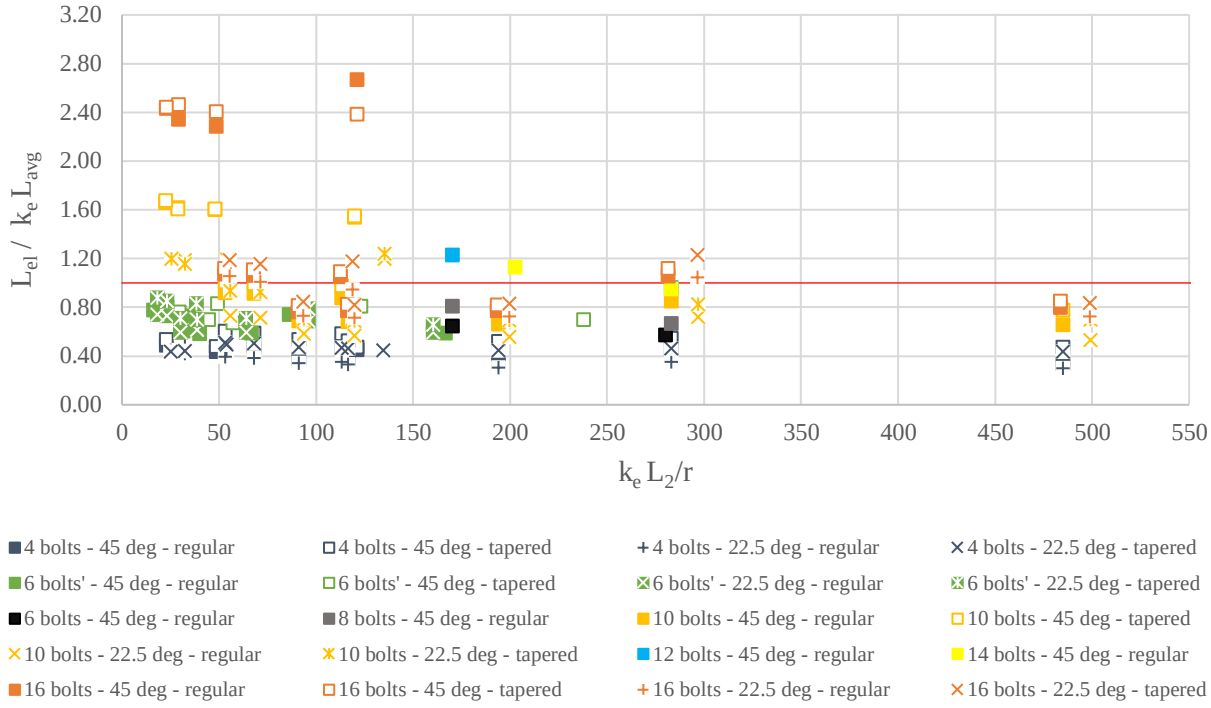

Figure 4-16. Comparing elastic length from FEA to the average Thornton length

Results show the ratio of the elastic FEA length and the average Thornton length (with a load dispersion angle of 30 degrees) ranges from 0.3 to 2.7. The spread of results suggest the Thornton length is not accurate for all gusset plate designs. Figure 4-16 also suggests that the average Thornton method underestimates the buckling length for many gusset plates. This is indicated by all the values above 1.0 (red line). In design, when a shorter length is applied to a formula predicting strength, the buckling capacity could be higher than it should be, therefore overestimating its strength and could result in an un-conservative design.

Instead of using the average Thornton length, this study found that using the middle Thornton length as the basis for estimating the elastic buckling length is advantageous. This is because the mid length gives a conservative approach for all types of gusset plates (indicated when ratios < 1.0). This reduces the scatter

of results seen in Figure 4-16, and is simpler for designers to calculate. Figure 4-17 shows the ratio between elastic length (identified through FEA) and the mid length (using the Thornton's approach) in terms of slenderness.

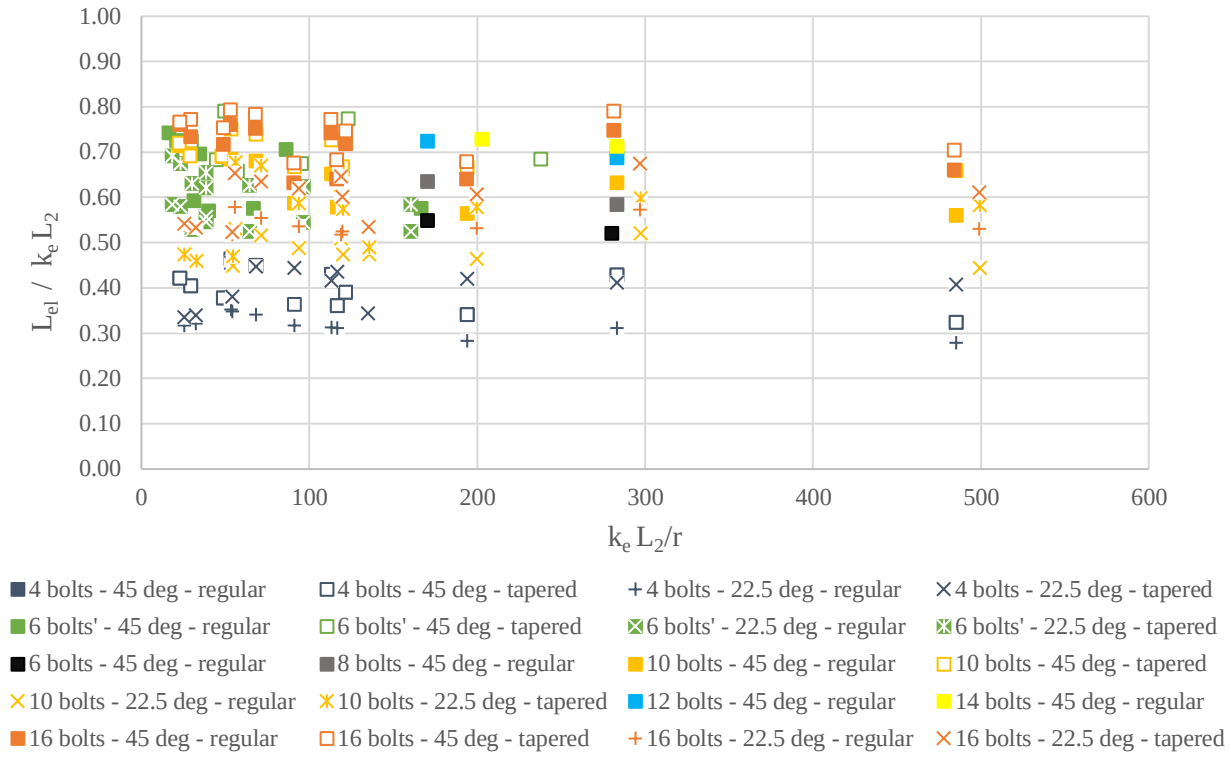

Figure 4-17. Elastic length compare to geometric slenderness using L2

In general, as the size of the bolted array gets larger, the closer the elastic FEA length and the mid length become. However, this is not the case for every size, so it is difficult to find an adjustment that further reduces the scatter; as such, a simple approach that approximates the elastic buckling length of a gusset plate is proposed in equation (4.10).

$$L_{gp} = 0.8 \, . \, L_2 \tag{4.10}$$

Equation (4.10) is a lower bound approach. Other factors that influence the elastic length include tapering, which extends the elastic length on average by 5%, and reducing angle of inclination, which decreases the elastic length by approximately 10%. However, to maintain simplicity these parameters are not explicitly taken into account in the proposed method.

4.5 **Buckling capacities**

Analytical methods used to predict load capacity of a gusset plate, first calculate the section capacity, Equation (4.2), which corresponds to the strength of a very short column not susceptible to buckling. To account for buckling, the section capacity is reduced as a function of its slenderness. The amount of reduction is based on observations of column buckling behaviour. These simplifications are a coarse approximation of the actual elasto-plastic behaviour of gusset plates under compression (as previously displayed in Figure 4-13). By using the FEA modelling results we can study the buckling behaviour of gusset plates and propose improvements upon methods used in current design codes. Figure 4-18 shows the normalised critical buckling loads from simulations alongside the predictions provided by the Thornton and NZS 3404 method. These are plotted in terms of the geometric slenderness (using the mid Thornton length) and normalised by the load at first yield (previously illustrated in Figure 4-13). However, it is noted that average Thornton length method was used in both the Thornton and NZS 3404 methods to calculate each compressive reduction factor.

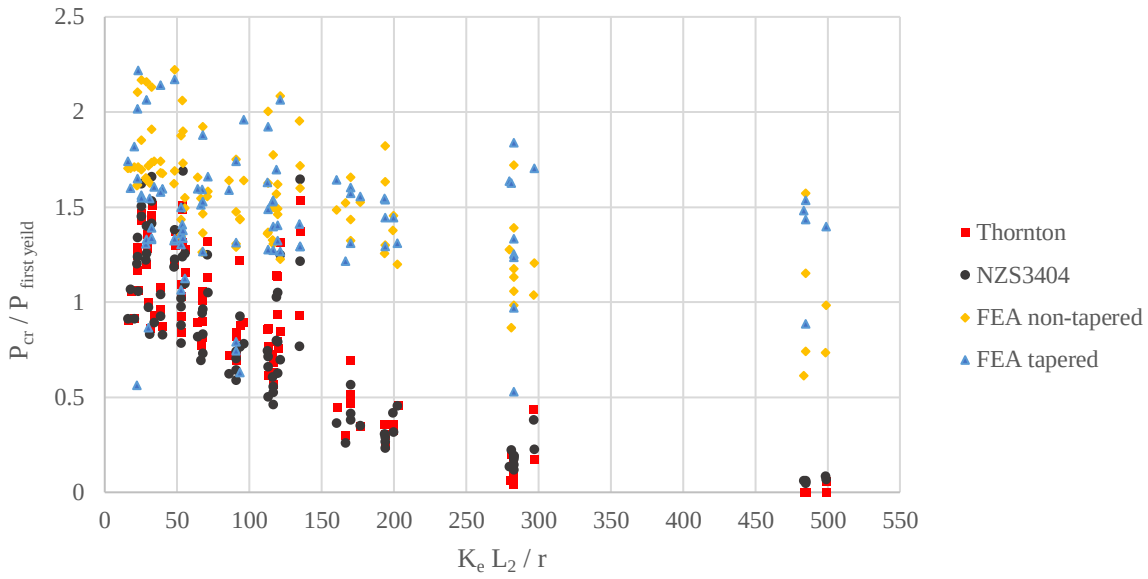

Figure 4-18. Normalised critical load from FEA compared with the Thornton and NZS3404 methods

While Figure 4-18 is useful when isolating and investigating each specific design, it is difficult to make observations about the overall level of safety provided by both the Thornton and NZ 3404 methods. However, by dividing the critical load obtained from FEA, by the design load using the Thornton and NZS 3404 we get an indication on the level of safety/accuracy provided by these methods (Figure 4-19).

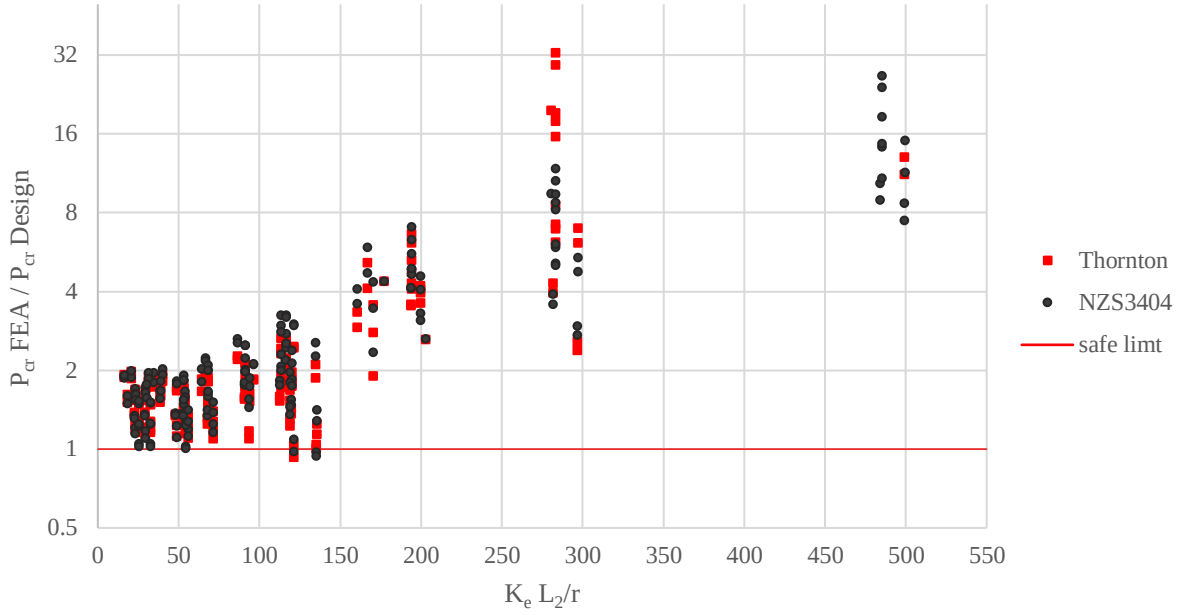

Figure 4-19. Factor of safety provided by the Thornton and NZS3404 method

Figure 4-19 clearly demonstrates that generally both the Thornton and NZS 3404 method are conservative. However, the level of safety varies from being un-conservative in a few cases, where data points fall below the red line, to providing a factor of safety of 32+ for a number of cases. This study found that some simple modifications can improve the Whitmore width and Thornton methods, to help ensure safe design for all gusset plates and to reduce excessive oversizing. The modifications used curve fitting of the different FEA studies presented in this study, with a shift to capture the lower bound results to ensure a conservative approach. First, let us recall that currently the Whitmore width method defines the section capacity for both tension and compression. This study proposes a different section capacity for tension and compression. For tension, the effective width ($b_{e\,15}$) should be used as per Equation (4.6). By multiplying $b_{e\,15}$ by the thickness and yield strength, we define the section capacity in tension as per Equation (4.11). This reduces overestimates of the yield area (shown in Figure 4-14).

In compression, the progression from first yield load to complete yield (plastic point) needs to be considered. This can be achieved by setting the section capacity at plastic point to 120% of the section capacity at first yield load, as per Equation (4.12). This represents gusset plates with the lowest ratio of plastic point to first yield load. To illustrate this, Figure 4-25 presents the load at the plastic point ($P_{y\,max}$) as a ratio of the initial yield load for all the gusset plates in this study. Results show that the plastic point load can vary between 1.2 - 2.2 times the initial yield load for gusset plates with the same bolted array design. This improves the level of safety for designs highlighted as un-conservative in Figure 4-19.

The Thornton method is then modified to construct a strength curve describing the compressive failure of gusset plates as a function of slenderness. The nonlinear/inelastic component of the Thornton method is kept the same, (Equation 4.13), but the adjusted section capacity (Equation 4.12) is used. Then, Equation 4.14 is used to describe the elastic buckling component. This changes the curve from being parabolic to being a linear function. This reduces excessive oversizing of longer gusset plates by accounting for the load redistribution as highlighted in (Sheng et al. 2002). Lastly, the average Thornton length is substituted for the equivalent length of a gusset plate as proposed in Equation (4.10) when calculating the slenderness parameter as per Equation (4.15).

$$\boldsymbol{N_{st}} = b_{e\,15}\, t_g\, \boldsymbol{\sigma_y} \tag{4.11}$$

$$\boldsymbol{N_{sc}} = 1.2\, \boldsymbol{N_{st}} \tag{4.12}$$

$$\boldsymbol{P_{cr}} = (0.658)^{\lambda_c{}^2}\ \boldsymbol{N_{sc}} \qquad \lambda_c \leq 1.5 \tag{4.13}$$

$$\boldsymbol{P_{cr}} = (-0.06\,\lambda_c + 0.68)\ \boldsymbol{N_{sc}} \qquad \lambda_c > 1.5 \tag{4.14}$$

$$\lambda_c = \frac{K_e\, L_{gp}}{\pi r} \sqrt{\frac{\sigma_y}{E}} \tag{4.15}$$

In the above, $\boldsymbol{N_{st}}, \boldsymbol{N_{sc}}$ are the respective section capacities for a gusset plate in tension and compression.

When we apply these modifications to the Thornton method and compare them to the FEA results in this study, the new level of safety provided shows all designs are conservative while excessive conservatism in slender gusset plates is significantly reduced. Figure 4-20 shows the improved accuracy this modified Thornton method has in estimating design loads for gusset plates. Included is a linear curve fit and R^2 value.

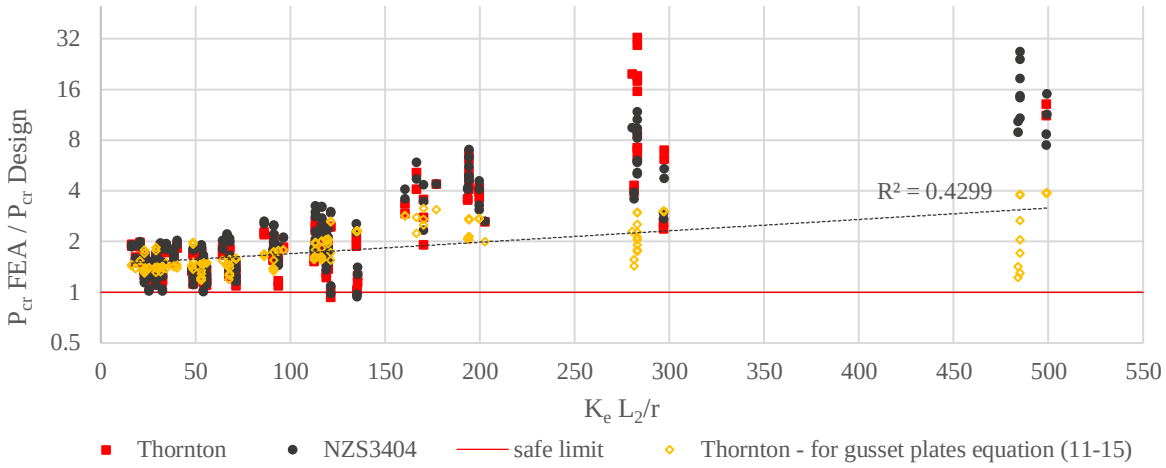

Figure 4-20. Comparison of buckling equations for gusset plates relative to slenderness

4.6 **Discussion**

Having performed FEA modelling for 184 gusset plates, how different geometric features influence the onset of yielding and buckling behaviour was investigated. Of interest is how these results compare to the current and proposed methods for designing gusset plates. Observations from FEA show that in general, tapered gusset plates have a reduced elastic axial stiffness, and a reduced initial yield load compared to rectangular plates. It is intuitive that tapering increases the elastic buckling length and the FEA results confirm that. Tapering is common among gusset plate designs. It helps accommodate bending and can improve the aesthetic nature of the design. However, the effect this has on yielding and buckling is not considered in design codes. Figure 4-21 shows two gusset plates, one rectangular and one tapered.

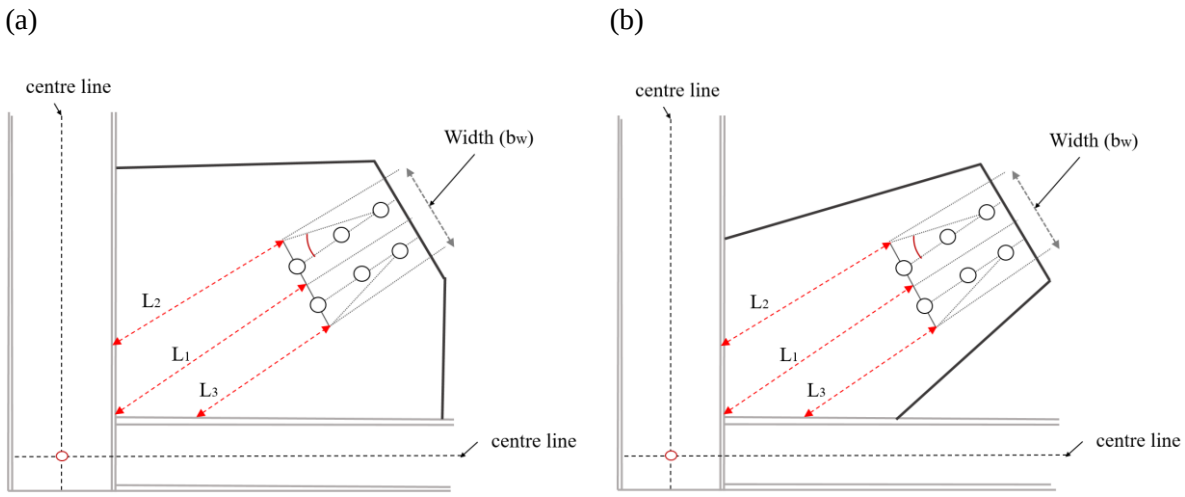

Figure 4-21. Two gusset plates with different areas but considered the same using the Whitmore width and Thornton length methods (a) rectangular, (b) tapered

The proposed equivalent length defined by Equation (4.10) also assumes rectangular and tapered designs have the same buckling length and axial stiffness. This is because not all designs are affected by tapering and that results varies between designs, particularly between designs that have different sized bolted connection zones and different gusset plate length. Figure 4-22 shows the effect tapering has on the elastic buckling length for the designs investigated in this study.

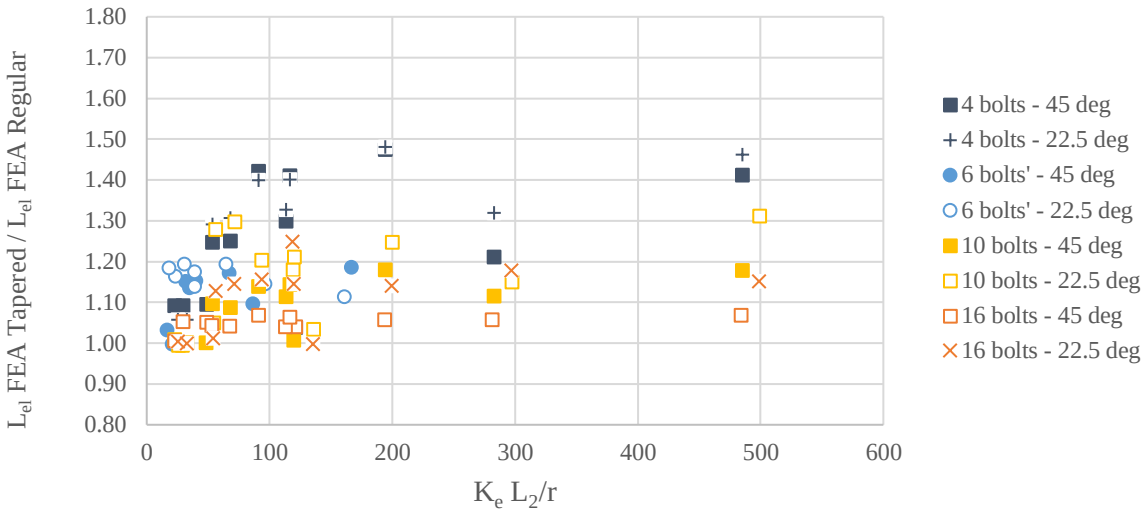

Figure 4-22. Effect tapering has on buckling length of gusset plate obtained from FEA

Figure 4-22 shows that tapering does not affect all gusset plates the same, and that tapering has little to no effect on gusset plates with particularly larger connections i.e 16 bolts. In addition, as form of tapering is stipulated by the architect or engineering, the proposed method would require additional data and complexity to account for the variety of designs.

Another geometric feature of a gusset plate is the angle of inclination. The dimensions of a frame (bay) within a commercial building govern this angle. Commonly, this angle ranges from 22.5 degrees, being a relatively wide frame, to 45 degrees, being a square frame. In general, as the angle of inclination reduces, the initial yield area reduces particularly for compact designs. By changing the angle of inclination, the overall size of the gusset plate changes. This effects how stress distributes through a gusset plate. With a smaller angle of inclination, the stiffness of gusset plate, from the end of brace to the working point is less symmetrical. As stress flows through the stiffest path, it travels to the closest weld zone creating a reduced effective yield area than if it was symmetrical. Figure 4-23 (a-b) illustrates this by showing how Von Mises stress distributes differently between a gusset plate that has a load angle of 45 degrees, and one that has a load angle of 22.5 degrees, where red and grey indicate yielding/plastic deformation and blue indicates low levels of stress. Figure 4-24 compares the force-displacement response of two gusset plates that have the same bolted array but at different angles of inclination. This figure shows the initial yield point and maximum load are reduced when the angle of inclination reduces but that the elastic response is very similar. However, similar to tapering, the effect that the angle of inclination has on different gusset plates designs varies, noting that it is particularly less prominent for larger gusset plates.

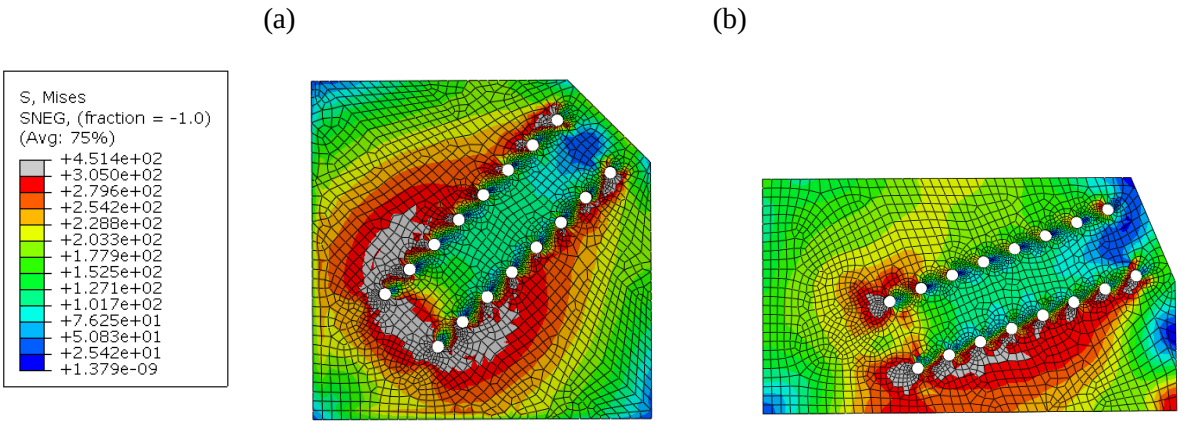

Figure 4-23. Illustrating stress distribution in gusset plate
(a) angle of inclination at 45 degrees (b) angle of inclination at 22.5 degrees

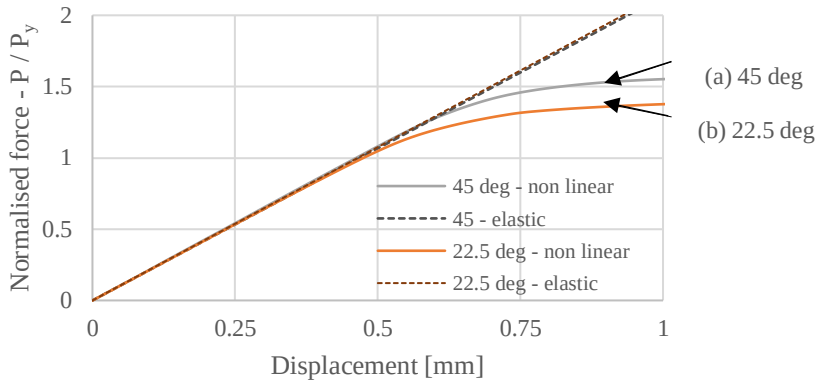

Figure 4-24. Force-displacement plot comparing response of two designs with different angles of inclination

When we examine the applicability of both the Thornton and NZS3404 methods to gusset plate design, we must first acknowledge that these are based on column buckling behaviour. To account for different types of columns i.e. pipe, I-section, square, flat plate etc., these methods prescribe each type of column a different buckling strength curve. However, this approach assumes the cross-sections are uniform for each type of column. Because gusset plates have a non-uniform cross-section, yielding first develops in a small area and spreads through the plate engaging more material until an equilibrium is reached in an elasto-plastic like manner.

Non-linear/inelastic buckling is governed by this spread of stress from initial yield to the plastic point when plastic deformation spans the cross section. Inelastic buckling is more difficult to predict for members that have non-uniform cross-sections like gusset plates as shown in by Figure 4-25. In this figure, results show

that the plastic point can vary between 1.2 - 2.2 times the initial yield load, even for gusset plates with the same bolted array (# of bolts and spacing). Figure 4-25 also shows that initial yield load does not predict the plastic point load. This is because the initial yield is largely influenced by the size of bolted array, where the plastic point is a function of the size and shape of the gusset plate.

The FEA results suggest that in general, as the bolted array gets larger and longer the plastic point load decreases. As part of the proposed changes to the Thornton method, the maximum buckling limit (section capacity in compression) is set to 1.2 times initial yield (a lower bound solution). To further reduce the scatter in Figure 4-25, a more sophisticated solution is needed.

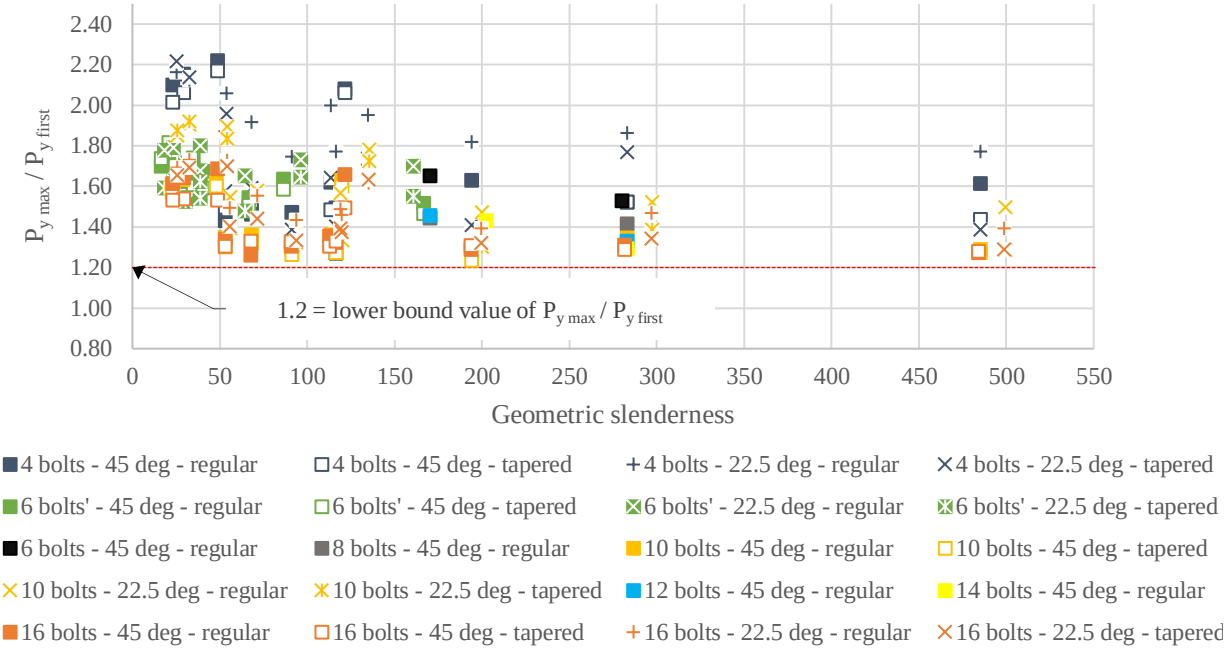

Figure 4-25. Maximum yield capacity of gusset plates

For slender gusset plates that are governed by elastic buckling, FEA results suggests both the Thornton and NZS3404 method result in excessive over-sizing. Unlike columns, the cross-sectional area of a gusset plate changes as the gusset plate gets longer. By applying elastic column buckling theory to gusset plates, we assume that as the length increases, the buckling load decreases exponentially. However, unlike classic column theory, increasing the effective length of a gusset plate generally coincides with increased height and width of the gusset. Although this effect is reduced through tapering and reducing the angle of inclination, the exact implications this has on the length and stiffness of gusset plate is largely unknown. The gusset plate resistance to buckling changes as a relatively complex function of these variables. It is not surprising that existing methods, that are not specific to gusset plates, are not accurate for a large range of

gusset plate configurations. This is the motivation for proposing a new equation to predict the elastic buckling component of a gusset plate, as per Equation (4.14). This modification aims to better represent the elastic behaviour of gusset plates as a function of slenderness.

The boundary conditions for each FEA model were idealised. The gusset plate to beam-column boundary was fixed, and the gusset plate to brace end boundary was idealised as a pin-roller. These assumptions approximate the actual behavior but have the advantage of coinciding with the effective length factor k_e = 0.7 as per NZS 3404 and ANSI 341-16 recommendations (Standards New Zealand 1997, ANSI/AISC 2010). For future predictions it is recommended to use k_e = 1.2 for slender gusset plate designs that are expected to fail in sway mode buckling.

Equation (4.11) through to Equations (4.15) sets out the proposed changes to the Thornton method to better describe gusset plate behaviour. Figure 4-26 presents the combination of these equations (as a function of slenderness) and compares this to the Thornton and NZS3404 methods. When compared to both the Thornton and NZS3404 methods, this new method reduces the expected buckling capacity for stocky members (making them safer) and assumes more slender members have more capacity, therefore reducing excessive oversizing as was illustrated in Figure 4-20.

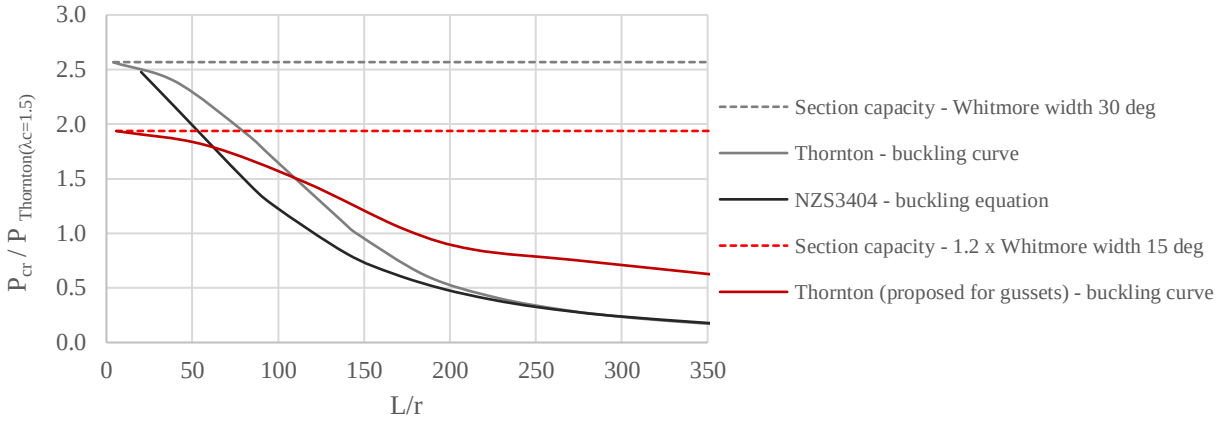

Figure 4-26. Methods used to predict gusset plate buckling

FEA results suggest the proposed set of changes to the Thornton method provide a more safe and economic design when compared to existing design methods. However, as they are based on lower bound results, they are still likely to be overly conservative for many designs. Although this study investigated 184 different gusset plates with a variety of features, to develop a more comprehensive and exact method for predicting buckling behaviour and associated stiffness parameters, a larger dataset is required. Such a study would include more sizes, and could also investigate parameters that effect connection zone rigidity such as stiffeners, ratio of gusset plate to web thickness, diaphragm connections and the incorporation of moment

releases. To improve the design of these connection zone we need a better understanding of these relationships. This is important as gusseted connection zone are expected to undergo significant plastic deformation in severe earthquake events as part of the primary load path of the building.

4.7 **Conclusion**

FEA was used to study the effect that several geometric features have on the yielding and buckling behaviour of gusset plates. FEA was necessary as investigating the detailed stress-strain behaviour of gusset plates in experiments is too difficult. In total 184 variations of gusset plate were investigated. The FEA modelling assumed an initial imperfection and applied a monotonic uniaxial load through a brace end connection via a bolted connections. Results were compared to the Thornton and NZS3404 gusset plate design methods. Based on the results the following observations and recommendations are made:

- The Whitmore width method does not compare well with the initial yielding of the gusset plates modeled in FEA, particularly for gusset plates with larger connections. This study assumes initial yield is defined as the point where the stiffness reduces to 90% of its initial linear-elastic value. This study found that by modifying the load dispersion angle in the Whitmore width method from 30º to 15º, generally the Whitmore method can make a conservative prediction of the effective width associated with the initial yield load as defined by FEA results. It is suggested that the Whitmore width method using a load dispersion angle of 15º, should be used to calculate the section capacity of a gusset plate in tension.

- The elastic buckling length of the gusset plates modelled did not match well with values calculated by the average Thornton length (using the Whitmore width method with a load dispersion angle of 30 degrees), particularly designs that are stocky. A generalized approach equal to 80% of the mid Thornton length is proposed and is shown to be in better agreement with the FEA predictions based on the elastic stiffness of each force-displacement.

- When designing a gusset plate in compression, in most cases both the Thornton and NZS3404 method were found to be conservative when compared to the simulated results. However, the level of safety is inconsistent and varies from being un-conservative in a few cases to providing a factor of safety of 32+ in some cases. Both the Thornton and NZS3404 methods predict the compressive capacity based on column buckling behaviour. To improve upon these gusset plate design methods, modifications to the Thornton method, based on curve fitting FEA results are proposed. These include: 1) Setting the section capacity of the gusset plate in compression to 1.2 times the section capacity in tension, and 2) the elastic function of the Thornton buckling curve is adjusted to $P_{cr} = -0.06\,\lambda_c + 0.68\,b_e t_g f_y$ when $\lambda_c > 1.5$. When these modifications are applied to the Thornton method, and compared to the simulated test results in this study, the new level of safety shows all designs are conservative and that excessive oversizing is significantly decreased.

4.8 **References**

AISC (1974). Guide to design criteria for bolted and riveted joints. One East Wacker Drive, Suite 3100, Chicago, IL 60601, American Institute of Steel Construction (AISC).

ANSI/AISC (2010). Specification for structural steel buildings - ANSI/AISC

ANSI/AISC (2016). Seismic provisions for structural steel buildings - ANSI/AISC. One East Wacker Drive, Suite 700, Chicago, Illinois 60601-1802, American Institute of Steel Construction

Berman, J. W., B. S. Wang, O. A., C. W. Roeder and D. E. Lehman (2011). Simple check for yielding in truss bridge gusset plate connections. In: Struct congress ASCE**:** 1027-1035

Birkemoe, P. C., R. A. Eubanks and M. W.H. (1969). Distribution of stresses and partition of loads in gusseted connections. Structural Research Series - Department of Civil Engineering University of Illinois Urbana(Report 343)

Brown, V. L. (1988). Stability of gusseted connection in steel structures. PhD dissertation, University of Delaware.

Chou, C.-C. and P.-J. Chen (2009). Compressive behavior of central gusset plate connections for a buckling-restrained braced frame. Journal of Constructional Steel Research **65**: 1138-1148

Dassault Systems (2014). ABAQUS 6.14 Analysis User's Guide, Volume IV: Elements

Fang, C., M. C. H. Yam, X. Zhou and Y. Zhang (2015). Post-buckling resistance of gusset plate connection: Behaviour, strength and design considerations. Engineering Structures **99**(9-27)

Gaylord, E. H. and C. N. Gayloard (1972). Design of steel structures second edition. New York, McGraw-Hill.

Gross, J. L. C., G. (1988). Experimental study of gusseted connections for laterally braced steel building. Gaithersburg, U.S Deparment of Commerce

Hu, S.-Z. (1987). Compressive behavior of gusset plate connections. Master of Science, The University of Alberta.

Lehman, D. E., C. W. Roeder, D. Herman, S. Johnson and B. Kotulka (2008). Improved seismic performance of gusset plate connections. Journal of Structural Engineering **134**: 890-901

Martinez-Saucedo, G., J. A. Packer and C. Christopoulos (2008). Gusset plate connections to circular hollow section braces under inelastic cyclic loading. Journal of structural Engineering ASCE **137**

McGuire, W. (1968). Steel structures. New Jersey, Prentice Hall.

Rasmussen, K. J. R. and G. J. Hancock (1989). Compression tests of welded channel section columns. Journal of Structural Engineering ASCE **115**: 789-808

Roeder, C. W., E. J. Lumpkin and D. E. Lehman (2011). A balanced design procedure for special concentrically braced frame connections. Journal of Constructional Steel Research **67**: 1760-1772

Rotter, J. M. (1982). Multiple column curves by modifying factors. Journal of the Structural Division ASCE **108**: 1665-1669

Sheng, N., C. H. Yam and V. P. Iu (2002). Analytical investigation and the design of the compressive strength of steel gusset plate connections. Journal of Constructional Steel Research **58**

Standards New Zealand (1997). NZS 3404:1997 Steel Structures Standard. Wellington, New Zealand

Thornton, W. A. (1984). Bracing connection for heavy construction. Engineering Journal **21**: 139-148

Trahair, N. S. and M. A. Bradford (1991). The behaviour and design of steel structures Rev. 2nd edition. London, Chapman and Hall.

Vasarhelyi, D. D. (1971). Tests of gusset plate models. Journal of the Structural Division ASCE **97**

Westeneng, B. (2016). Buckling behaviour of gusset plates in buckling-restrained braced frames. Masters of Engineering, University of Canterbury.

Whitmore, R. E. (1952). Experimental investigation of stresses in gusset plates. University of Tennessee Bulletin **No.16**

Williams, G. C. R., R.M. (1986). Steel connection design based on inelastic finite element analysis. Department of Civil Engineering and Engineering Mechanics, The University of Arizona

Yam, M. C. H. and J. J. Roger Cheng (1993). Experimental Investigation of the compressive behavior of gusset plate connection, University of Alberta, Department of Civil Engineering. **Structural Engineering Report No. 194**

5 STABILITY OF DIAGONAL BRBFS WITH BOLTED END CONNECTIONS

Bolted connections are a popular and common connection type used in buckling-restrained braced frame (BRBF) design. Global out-of-plane stability tends to govern the design for this connection type. Numerous studies have highlighted the risk of global out-of-plane buckling initiated by softening due to inelasticity in the gussets, neck of the BRB end and/or restrainer ends (Saeki et al. 1995), (Tsai et al. 2002, Tsai et al. 2008). Japan has developed an alternative approach to subassemblage testing and incorporated it in their design codes. The approach uses an analytical method to assess the stability of a BRBF system under different collapse mechanisms by focusing on moment transfer. Strict design criteria for BRBF design in Japan is required to work within the limits set by this method. Structural building design codes in New Zealand, Europe and the United States do not yet provide an analytical method to assess BRB and connection stability, with prototype testing used as the primary means of evidence needed to gain building compliance. This makes the method used in Japan (Takeuchi's method), an attractive option for other countries to use as an alternative to full-scale testing in combination with prequalification testing. However, available publications only provide a limited amount of validation of this method. As such, there is a need to investigate the capability of this method using; BRBs designs and gusset plate designs that represent those used outside of Japan (including unstiffened gusset connection zones). This chapter demonstrates the capability of detailed finite element analysis (FEA) modelling to investigate the cyclic response and a subassemblage test – resembling that of a ground storey frame with a diagonal BRB with bolted connections. Initially a total of eight BRBF variants were modelled in Abaqus®. To capture the different failure mechanisms identified in Takeuchi et al. (2017), these designs varied the length that the cruciform (non-yielding) section inserts into the restrainer. It was found that increasing the thickness of the gusset plates according to modifications discussed to the Thornton method (Chapter 4), improved overall performance for most variants. The effect of bi-directional loading was also evaluated and was not found to significantly affect global out-of-plane stability. FEA results were compared against Takeuchi's method for assessing the out-of-plane stability of BRBFs. Generally, Takeuchi's method was found to be conservative. The accuracy of Takeuchi's method improved when using eigenvalue analysis of the FEA models to calculate the global elastic bucking load, and when assumptions on which failure mechanism were adjusted.

5.1 **Introduction**

A BRB connects to a frame via pins, welds or a bolted array. Greater construction tolerances and cheaper on-site costs mean bolted connections are a favored connection type in New Zealand. Bolted connections also allow for ease of replacement following a severe earthquake. In general, BRBF designers must anticipate a range of strength and stability considerations, including both local and global effects. However, global stability tends to govern the designs with bolted connection (Takeuchi et al. 2017). While BRB stability calculations have traditionally been limited to the restrainer design, numerous studies have highlighted the risk of global out-of-plane buckling initiated by a stiffness reduction due to inelasticity in the gussets and the BRB end and/or restrainer ends (Saeki et al. 1995, Tsai et al. 2002, Tsai et al. 2008). This type of failure is distinct from local gusset plate buckling, global restrainer buckling and restrainer bulging. Figure 5-1 highlights the different BRB strength and stability considerations in orange.

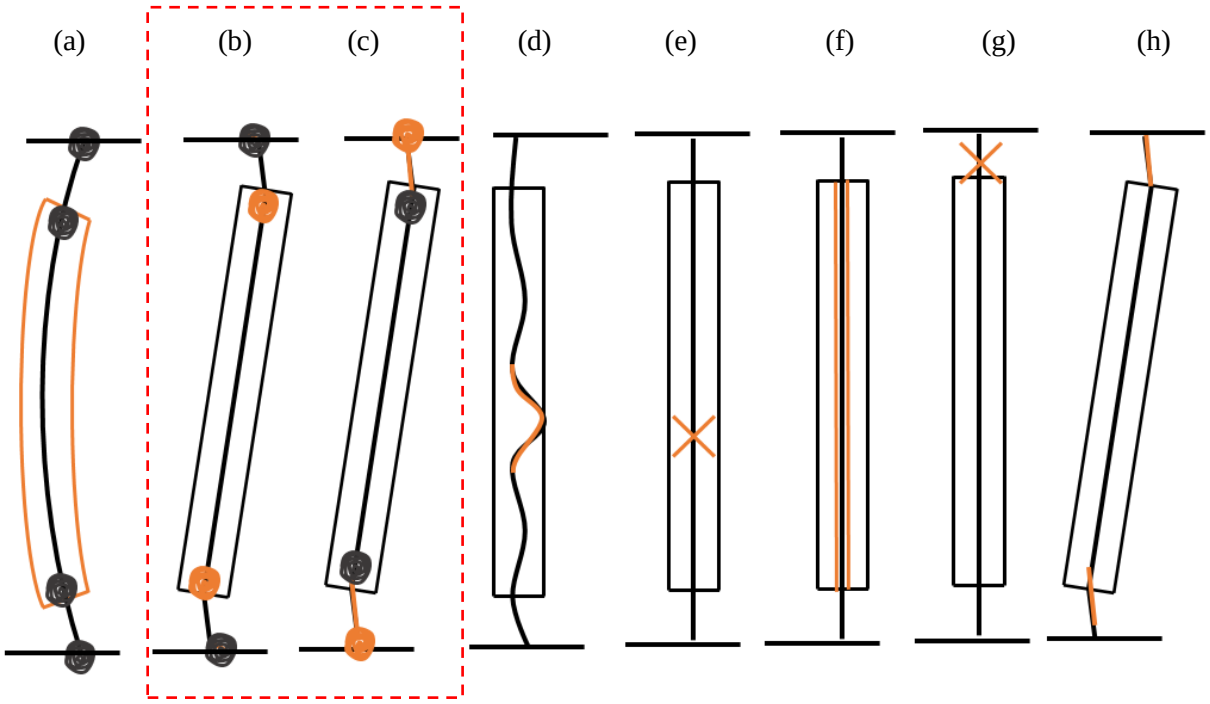

Figure 5-1. BRB strength and stability considerations (Takeuchi et al. 2017)
(a) global stability – restrainer, (b) global stability – restrainer end, (c) global stability – connections, (d) higher mode buckling and bulging, (e) low cycle fatigue and fracture , (f) compression/tension ratio, (g) connection strength, (h) rotation compatibility due to in-plane frame deformation

The ultimate strength of a BRB core can be obtained from prequalification testing and is commonly approximated to 1.5 times the yield force of the BRB core ($N^{core}_{ultimate}$). A BRBF should be able to reach the ultimate strength of the BRB core before global instability occurs. This is achieved by ensuring the beam-column joints, gussets, restrainer and cruciform section of the BRB are proportioned correctly.

Tsai et al. (2002) proposed the first method to estimate the out-of-plane stability limit of a BRBF. The method uses the Cantilever Connection Concept shown in Figure 5-2a. This concept simplifies a BRBF system to a fixed-pin ended column system. The beam-column joint, where the gusset is connected to, is represented by the fixed end. A member with uniform flexural stiffness represents the exposed BRB cruciform end and gusset. A pinned joint represents the interface of the exposed cruciform end and restrainer. Other parts of the BRBF are not considered. The elastic buckling limit uses the cruciform section of the BRB, with an effective length twice the distance from the restrainer end to the intersection at the flange edge of the beam-column joint. To check stability, the elastic buckling limit of this simplified system is compared against the maximum expected axial load ($N^{core}_{ultimate}$).

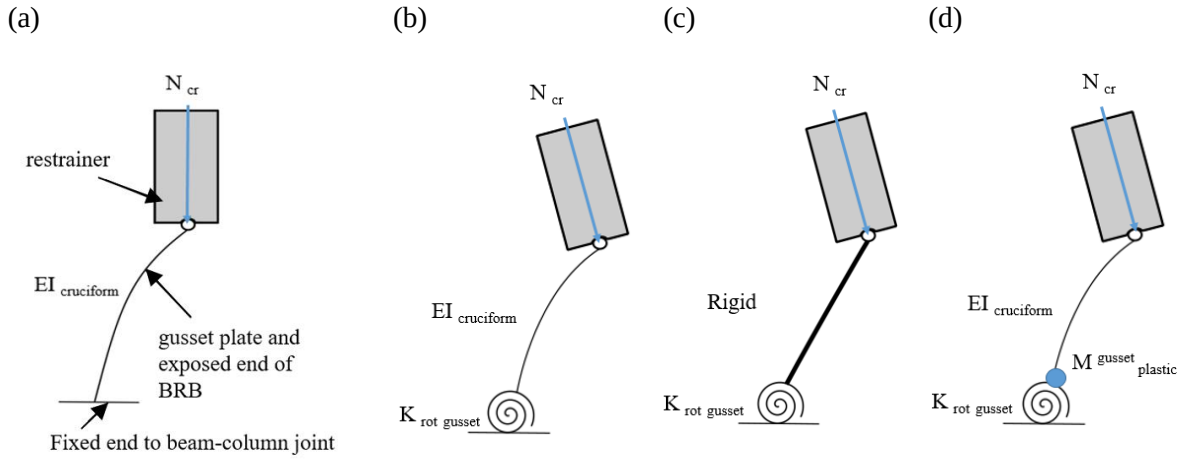

Figure 5-2. Cantilever Connection Concepts
(a) Tsai et al. (2002), (b) Koetaka et al. (2008), (c) Hikino et al. (2013), (d) Takeuchi et al. (2013)

Koetaka et al. (2008) proposed a similar method (Figure 5-2b), by using a rotational spring to represent the interface of the beam-column joint to the gusset plate. It assumes the restrainer can also rotate at the pinned end. Hikino et al. (2013) then proposed a method with similar boundary conditions as Koetaka et al. (2008) but modelled the restrainer and connection segments as rigid bodies.

Takeuchi et al. (2013) recognised these methods (Figure 5-2(a-c)) would often require stocky frame elements, stiffened gussets and stocky BRB end zone. As stocky sections are more susceptible to non-linear buckling, Takeuchi et al. (2013) proposed using code column equations curves to account for the expected inelasticity of the BRB cruciform and gusset plate. Equation (5.1) describes the elastic buckling of Takeuchi's method in Figure 5-2d.

$$N^{R}{}_{cr} = (1 - 2\xi').\frac{\pi^2 \Upsilon_J EI_B}{(2\xi L_0)^2}.\frac{\xi\kappa_{Rg}}{\xi\kappa_{Rg}+\frac{24}{\pi^2}} \tag{5.1}$$

$$\xi\kappa_{Rg} = \frac{K_{Rg}\,\xi L_0}{\Upsilon_J EI_B} \tag{5.2}$$

Where, L_0 = the total diagonal length (working point to working point), ξ' = total length of the cruciform of BRB divided by the total diagonal length, ξ = exposed length of the cruciform of BRB divided by the total diagonal length, EI_B = the flexural stiffness of the restrainer (grout + steel casing), Υ_J = flexural stiffness of cruciform divided by flexural stiffness of restrainer and $\xi\kappa_{Rg}$ = normalised rotational stiffness of the gusset.

A generalised equivalent slenderness covering all gusset plate designs is given by Equations (5.3 – 5.5)

$$\lambda = \frac{L_e}{i_g} \tag{5.3}$$

$$i_g = \sqrt{\frac{I'}{A'}} \tag{5.4}$$

$$L_e = 2\xi' L_0.\frac{\Upsilon_J I_r}{I'}\sqrt{\frac{\xi\kappa_{Rg}+\frac{24}{\pi^2}}{(1-2\xi')\xi\kappa_{Rg}}} \tag{5.5}$$

Where, λ = slenderness ratio, L_e = the effective length, i_g = the radius of gyration of the gusset plate, I' = the second moment of area of the gusset an A' = area of the effective yielding section of the gusset.

Westeneng (2016) proposed an alternative to the Cantilever Connection Concepts. The GP-BRB system stability method accounts for the different stiffness properties associated with the gusset plate and BRB cruciform section. The method uses stability functions from elastic analysis, and considers beam-column joints, gusset plates, cruciform end section and the restrainer. However, lack of appropriate experimental data has meant this method is yet to be validated. In addition, the method does not yet include the effect of out-of-plane storey drift.

Methods that use pinned boundary simplifications at the restrainer to cruciform interface or elastic analysis, mean stocky and stiffened sections are required to ensure stability conditions are met. To permit more flexibility in gusset plate design and adjacent framing of a BRBF, Takeuchi et al. (2013) proposed a new method based on the Restrainer Continuity Concept (Figure 5-3). As it is more economical to have unstiffened gusset plates and frame sections, Takeuchi's new method offers one way to assess the out-of-plane stability of less rigid/stocky BRBFs design without the need for full-scale full frame testing. This analytical method uses a set of equations to assess the out-of-plane stability of a BRBF under different collapse mechanisms by focusing on moment transfer.

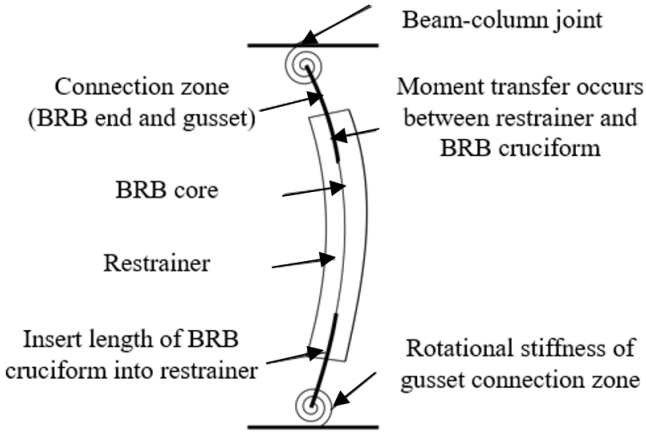

Figure 5-3. Restrainer Continuity Concept (Takeuchi et al. 2013)

5.1.1 **Out-of-plane stability (based on the Restrainer Continuity Concept)**

Takeuchi's method for assessing the out-of-plane stability of BRBFs (based on the Restrainer Continuity Concept), idealises a BRBF system as a model using prismatic elements and springs (Figure 5-4). The critical hinges are assumed to be in the connection regions, where the cross sectional area changes. These changes occur at the transition of cruciform to restrainer end, and intersection of the cruciform to gusset plate.

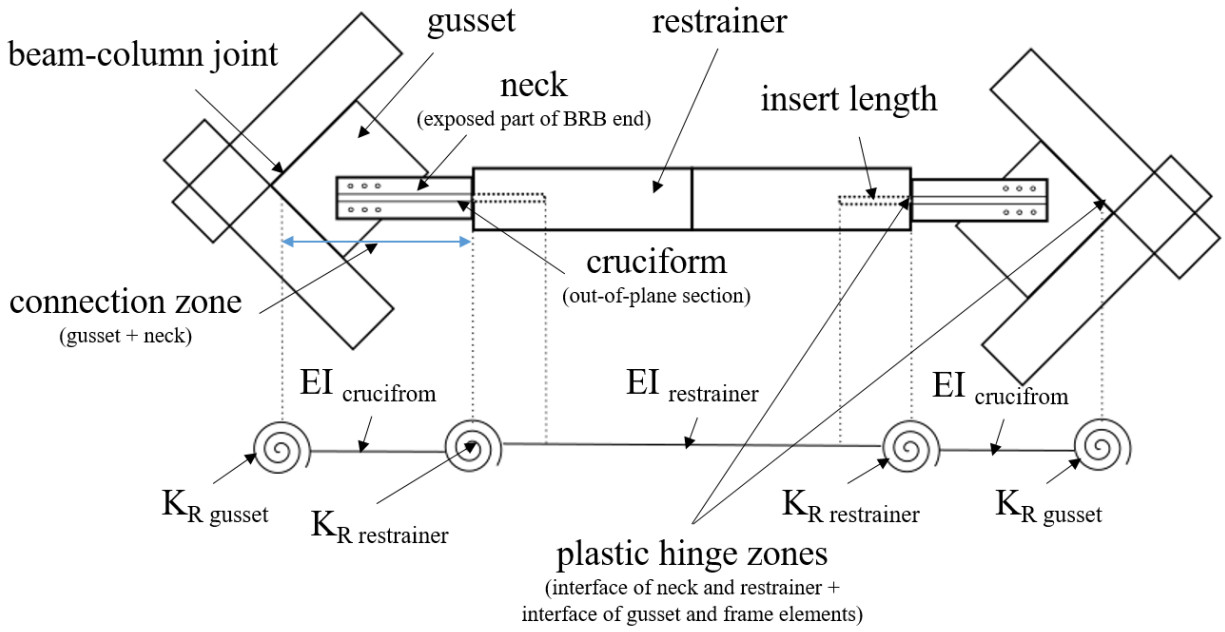

Figure 5-4. Idealised model of a BRB using prismatic elements and springs

Takeuchi's method first evaluates the elastic buckling load of the idealised model (Figure 5-4) under the different collapse mechanisms in Figure 5-5. The elastic buckling load of each mechanism needs to be evaluated in order to determine which mechanism governs the design.

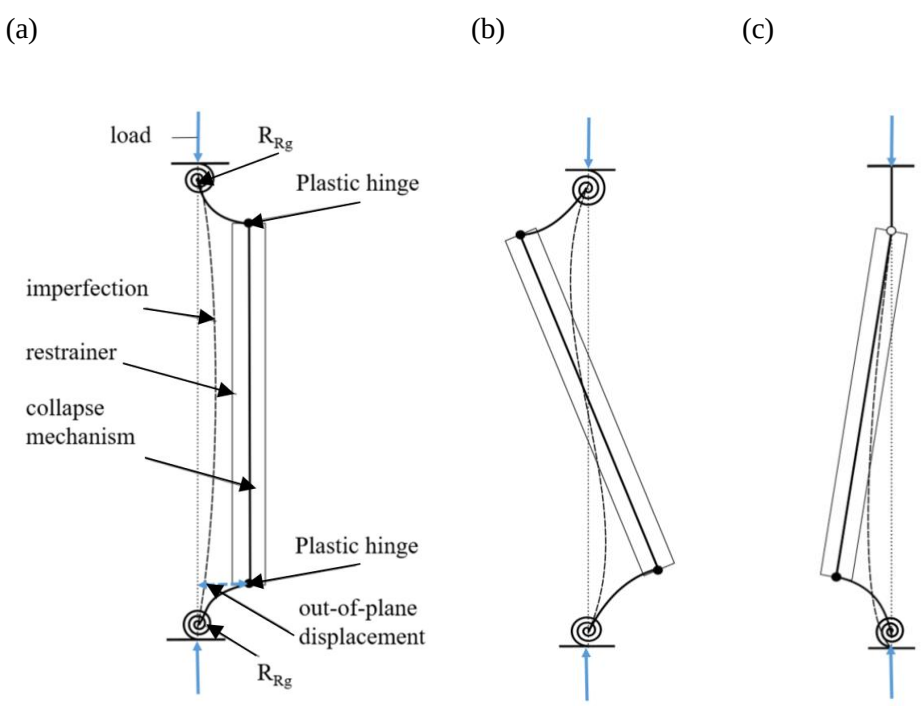

Figure 5-5. Collapse mechanism with rotational springs as gusset plates (a) symmetrical, (b), asymmetrical and (c) one-sided

Each mechanism occurs as a result of critical Pδ moments where 'δ' is the maximum local out-of-plane deflection of the BRB. This maximum out-of-plane deflection develops at the restrainer end for all the collapse mechanisms, being the location of the critical hinges (Figure 5-5). This out-of-plane deflection is initially caused by geometric imperfections which increase with compressive loading.

Takeuchi's method utilises the elastic load-deflection path (elastic path) of the idealised BRB system (Figure 5-4), and the compressive and flexural strength of the critical hinge zones of the connection zone (neck + gusset). The stability limit is deemed as the intersection of the elastic buckling path and the ultimate N-M capacity of the connection zone and critical hinge zones. Instability is predicted to govern failure if the stability limit is less than the ultimate strength of the core ($N^{core}_{ultimate}$). This stability limit concept is depicted in Figure 5-6.

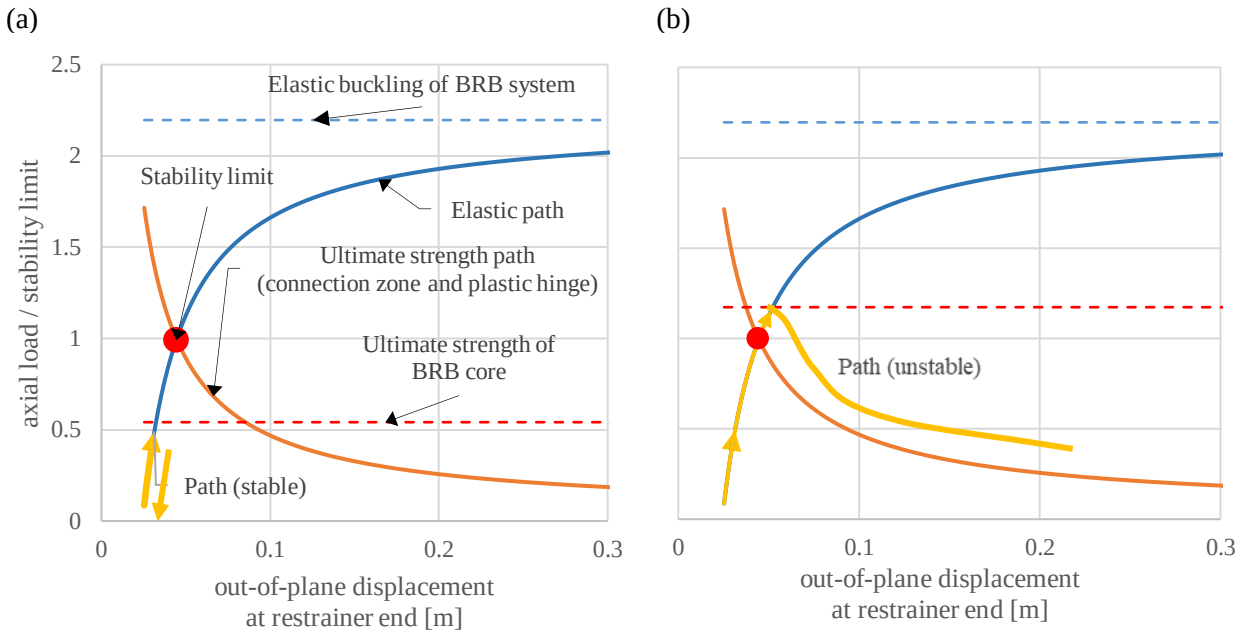

Figure 5-6. BRBF stability limit concept (Takeuchi et al. 2017)
(a) Stable (N_{cu} < stability limit), (b) Unstable (N_{cu} < stability limit)

As out-of-plane displacement increases, the force-deflection (elastic path) begins to stabilize (*blue lines* in Figure 5-6). Matsui et al. (2010) calculates the maximum elastic buckling capacity using equations derived from the differential equation method proposed by Timoshenko et al. (1965). These equations assess the idealised model (Figure 5-4) in either a symmetric or anti symmetric buckling mode (Appendix D). Other methods such as stability functions (Westeneng 2016) or eigenvalue analysis in FEA can also be used. The elastic path is described by Equation (5.6)

$$N = \frac{y_r}{y_r + a_r} N^B_{cr} \tag{5.6}$$

Where, a_r = the initial imperfection at the restrainer end, y_r = additional out-of-plane displacement due to compressive loading, N^B_{cr} = maximum elastic buckling capacity.

The path of the N-M capacity is called the ultimate strength path and is described by the *orange lines* in Figure 5-6. This ultimate strength path is calculated using Equation (5.7). This ultimate strength path describes the combined compressive strength of the connection zone, and the plastic moment capacity of the plastic hinge (either steel casing or cruciform) divided by out-plane displacement at this point. As the out-of-plane displacement reaches infinite, the path stabilises to the axial load capacity of the cruciform end.

$$N = N_{cr}^{r} + \frac{M_p^r - M_0^r}{y_r + a_r} \tag{5.7}$$

$$\lambda_r = \frac{2\xi' L_0}{i_c} \cdot \sqrt{\frac{\xi \kappa_{Rg} + {}^{24}/_{\pi^2}}{(1-2\xi')\xi\kappa_{Rg}}} \tag{5.8}$$

Where, N_{cr}^{r} = the inelastic compressive capacity of the BRBs end connection, calculated using the equivalent slenderness ratio of Equation (5.8) in a column buckling curve, M_p^r = plastic moment capacity of the limiting failure mechanism (Takeuchi et al. 2013), i_c = radius of gyration of the connection zone.

5.1.2 **Geometric imperfections**

The restrainer of a BRB constrains core buckling. For the restrainer to engage/support the core, the cruciform section undergoes some rotation as it compresses into the debonding material causing eccentric loading. This behaviour influences the eccentric loading that reduces the critical buckling load of the system. Therefore understanding the factors that contribute to these imperfections is important. Equation (5.9) presents a conservative approximation of the geometric imperfections as proposed by Takeuchi et al. (2013). This is used to calculate the different load paths is assessing out-of-plane stability in Figure 5-6.

$$a_r = e + s_r + \xi L_0 \left(\emptyset_0 + \frac{2s_r}{L_{in}}\right) \tag{5.9}$$

Where, a_r = total initial geometric imperfection, e = eccentricity of the load, s_r = thickness of debonding material or gap between core and restrainer at rest, L_0 = total length of BRB, ξ = ratio of exposed length of BRB to total length, $\emptyset_0$ = construction tolerance, L_{in} = insert length of the cruciform section as shown in Figure 5-7.

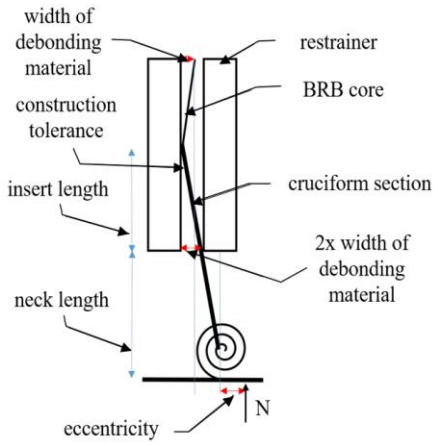

Figure 5-7. Causes of geometric imperfections in a BRB

5.1.3 **Interaction of the cruciform section and restrainer**

The suitability of a gusseted connection zone (specifically its rigidity) depends on the ability of the BRB to transfer moment from the restrainer to the neck (exposed end of the BRB). Flexural continuity between the restrainer and neck of the BRB occurs when the side of cruciform section bears up against the restrainer under compressive loading. Matsui et al. (2010) found that the ability for a BRB to transfer a moment from the restrainer to the neck relates to how much the cruciform section is inserted into the restrainer and suggests this governs which component is likely to fail first. As a general rule, shorter insert lengths cause damage the restrainer because of larger localized bearing forces (Figure 5-8b), where longer insert lengths enable the cruciform to reach its plastic moment (Figure 5-8c). In addition, the ratio of the insert length (L_{in}) to the width of cruciform section (B_{cruc}) provides an easy way to predict which component governs the maximum moment.

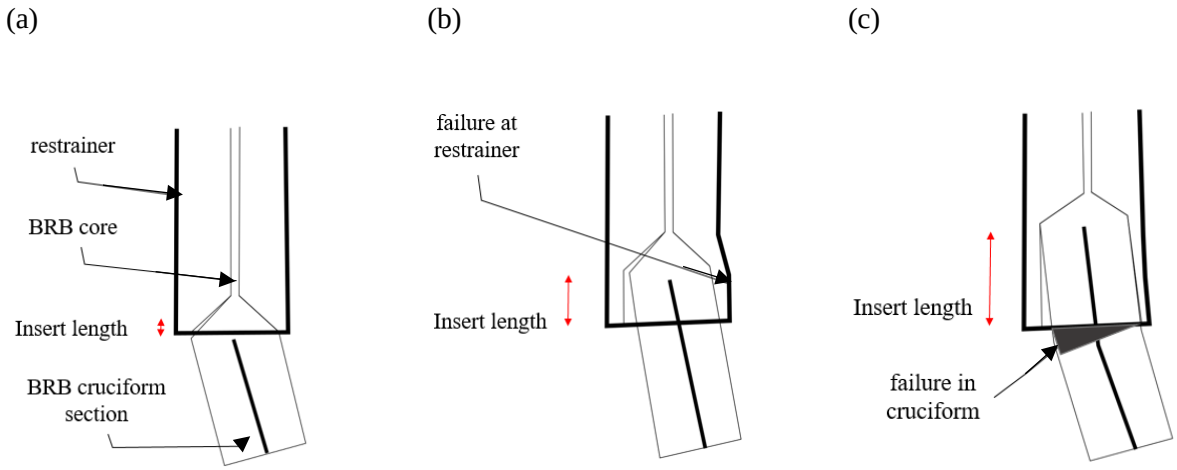

Figure 5-8. Moment transfer between restrainer and cruciform end
(a) $L_{in}/B_n<1$ = no moment transfer (very stiff gusset plates and frames elements required)
(b) $1 \leq L_{in}/B_{cruc} \leq 2$= moment transfer exists (M_p^r=restrainer)
(c) $L_{in}/B_{cruc} > 2$= moment transfer exists (M_p^r=cruciform)

5.1.4 **Stiffness of gusseted connection zones**

Takeuchi's method requires the rotational stiffness of the gusset plates and their adjacent frames elements.

Kinoshita et al. (2008) describes a method to approximate the moment carrying capacity and out-of-plane rotational stiffness of stiffened gussets. However, this only applies to edge stiffened gusset plates. In general, defining the rotational stiffness of a gusseted connection zone not straightforward and generally requires physical testing or finite element modelling.

Takeuchi et al. (2017) believes the type and amount of stiffeners are the main contributors to rotational stiffness regardless of shape and slenderness. As such, only four types of gusset plate design (Figure 5-9 a-d) are considered. As a general rule, stiff gusset plates (like Figure 5-9c and Figure 5-9d) are required to meet the stability conditions set out in the simpler Cantilever Connection Concept method. Whereas, at least partially stiffened gusset plates (Figure 5-9b) are required to meet the stability conditions set out in the Restrainer Continuity Concept. Unstiffened gusseted connection zones (like those modelled in Chapter 4 Figure 4-9) represented by Figure 5-9a, are likely to create unstable conditions (Takeuchi et al. 2017) . However, Takeuchi et al. (2017) only uses two gusset plate designs in their validation, so even though unstiffened gusset plates are not recommended, further validation may demonstrate that particular unstiffened designs may still provide stable conditions.

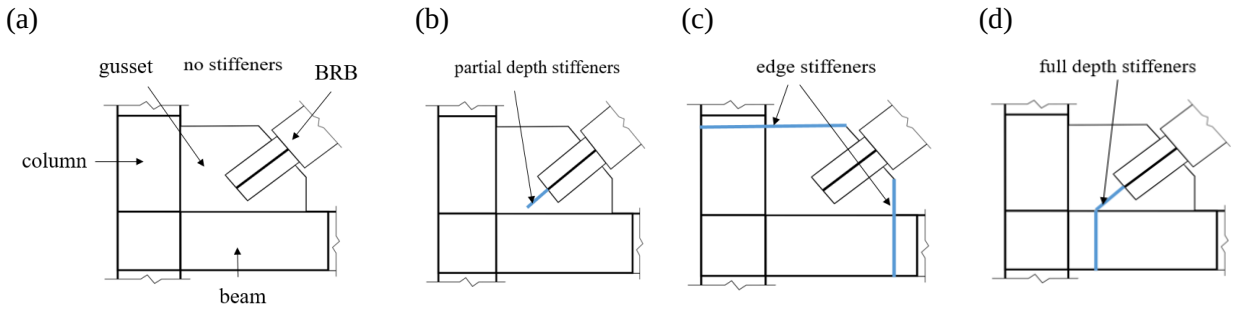

Figure 5-9. Diagonal gusset plates with different levels of out-of-plane stiffness
(a) and (b) low stiffness, (c) and (d) high stiffness

Matsui et al. (2010) tested and modelled six different gusset plates to determine their rotational stiffness using FEA. All these specimens had some level of stiffeners but not enough information is provided to expand upon this study. This makes it particularly challenging to define the rotational stiffness of the gusseted connection zone and therefore to implement the Restrainer Continuity method for other BRBF designs. Ida et al. (2013) reports that the normalised rotational stiffness of the gusset plate zone to be distributed between 0.2 and 1.0 in actual connections.

5.1.5 **Magnitude and direction of loading**

Out-of-plane drift due to bi-directional loading or torsional effects also contribute to the stability limit of a BRBF. Takeuchi's method calculates the additional moment demand caused by out-of-plane drift by using equation (5.10). This moment reduces the moment carrying capacity of the restrainer mechanism.

$$M^r{}_0 = (1 - 2\xi)K_{Rg}\left[\frac{\delta_0}{L_0} - \frac{2s_r(1-2\xi)}{L_{in}}\right] \tag{5.10}$$

Where, $M^r{}_0$ = bending moment due to out-of-plane drift, δ_0 = out-of-plane displacement, s_r = width of debonding material or gap between core and restrainer at rest, L_{in} = insert length of the cruciform section as shown in Figure 5-10.

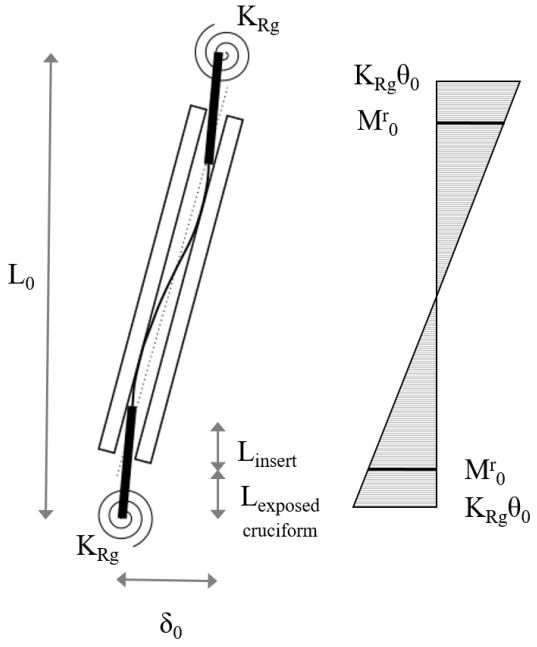

Figure 5-10. Bending moment due to out-of-plane drift

However, out-of-plane drift may have a larger impact on the ground storey where the base of the connections are fixed in both directions. This is unlike other levels that generally rotate less relative to each other when the building moves laterally. As the building moves out of plane, a flexural demand develops about the weak axis of the gusset plate. Figure 1-16 (in Chapter 1) presents a schematic of in-plane and out-of-plane displacements.

5.1.6 **Stability limits**

With the stability limit calculated, the load limit paths can be calculated. To determine each load limit path, Takeuchi et al. (2017) analysed each of collapse mechanisms using an energy method. The first load limit path (Equation 5.11) assumes the gusseted connection remain elastic. Essentially, the first load limit path is constructed by shifting the ultimate strength path. The original intersection of the elastic and ultimate strength path is shifted such that it passes through a_r instead of a_r+y_r (Figure 5-11).

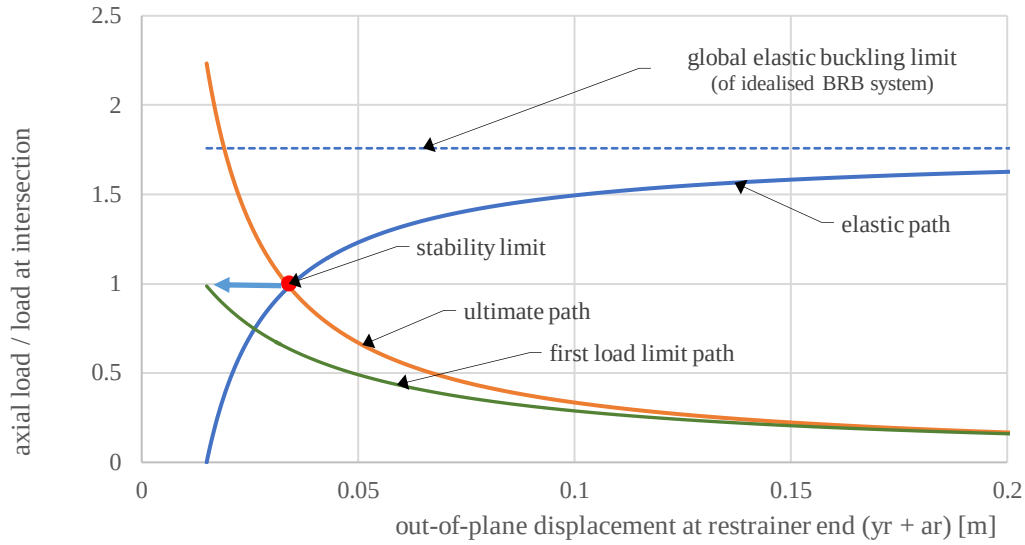

Figure 5-11. Takeuchi's BRB stability model with stability limits (based on moment continuity concept)

$$N_{lim1} = \frac{\left(M_p^r - M_0^r\right) / a_r + N_{cr}^r}{\left(M_p^r - M_0^r\right) / a_r \, N_{cr}^B + 1} > N_{cu} \tag{5.11}$$

Where, M_p^r = the plastic moment of either the restrainer or cruciform (Figure 5-8) (Appendix F), M_0^r = bending moment due to out-of-plane drift (Figure 5-10), a_r = the initial geometric imperfection (equation 5.1), N_{cr}^r = the inelastic compressive capacity of the BRBs end connection, calculated using the equivalent slenderness ratio of Equation (5.8) in a column buckling curve, N_{cr}^B = elastic buckling of BRB system (Figure 5-6) (Appendix D) and N_{cu} = the ultimate strength of the BRB core. The first stability limit path assumes the gusset plates remain elastic under collapse.

When plastic hinges occur in the gusset plates a different global buckling mode occurs. Takeuchi expresses this condition as the second load limit path (Equation 5.12). The amount the second load limit path reduces from the first load limit path depends on the ratio of stiffness between the strength gusset plate and the neck of the BRB, where if the gusset plate has a low compressive strength compared to the neck of the BRB then the effect of the gusset plate is hinging is less (Figure 5-12). The least of the two failure forces along each path is considered to be the stability limit.

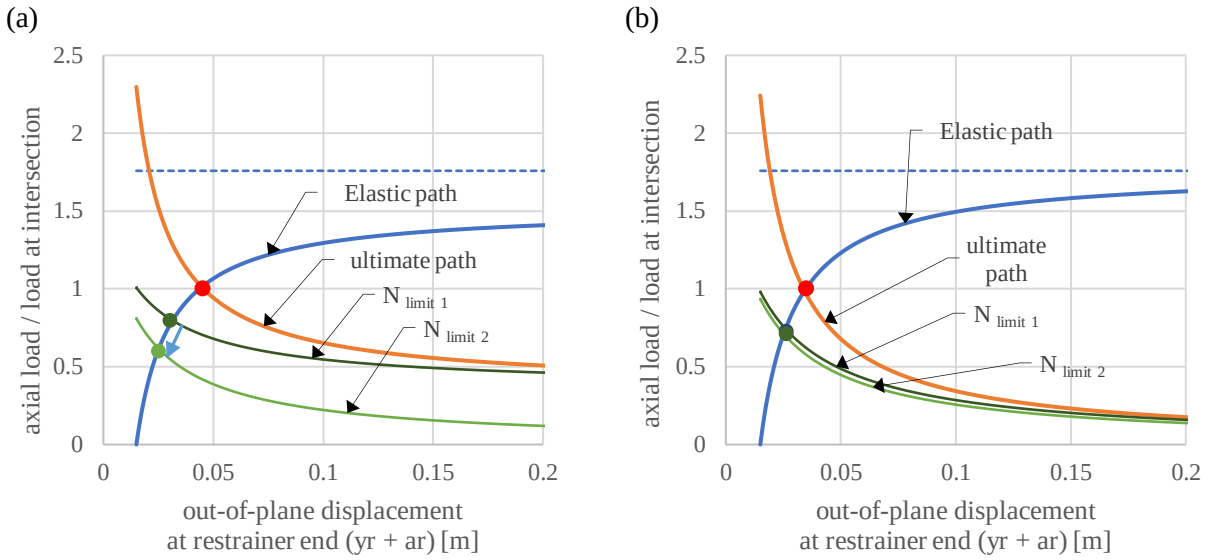

Figure 5-12. BRBF stability limit concept – development of load limit 2 (Takeuchi et al. 2017)
- ratio of stiffness of gusset plate to stiffness of the neck of the BRB
(a) higher ratio, (b) lower ratio

$$N_{lim2} = \frac{\left[(1-2\xi)M_p^{\mathrm{g}} + M_{\mathrm{p}}^r - 2M_0^r\right] / a_r}{\left[(1-2\xi)M_p^{\mathrm{g}} + M_{\mathrm{p}}^r - 2M_0^r\right] / (a_r \mathrm{N}_{\mathrm{cr}}^{\mathrm{B}}) + 1} > N_{cu} \tag{5.12}$$

Where, M_p^g = the plastic moment of the gusset plate and ξ = connection zone length ratio to total length.

5.1.7 **Numerical modelling of BRBFs**

To evaluate Takeuchi's method with numerical modelling, each model needs to capture the behaviours that contribute to stability conditions. Specifically the interaction of the core and cruciform section, with the restrainer as the BRB stretches and compresses. These interactions play a significant role in the defining stability of a BRBF system. The complex nonlinear phenomena associated with these interactions has limited the development of detailed FEA models of BRBFs. Simplified approaches are traditionally used to model the features related to this behaviour. For example, Mahin et al. (2004) presents modelling a BRBF in LS-DYNA (Field 2003). This modelling approach used shell elements to represent all the components neglecting the interaction of BRB core and restrainer as shown in Figure 5-13.

(a)

(b)

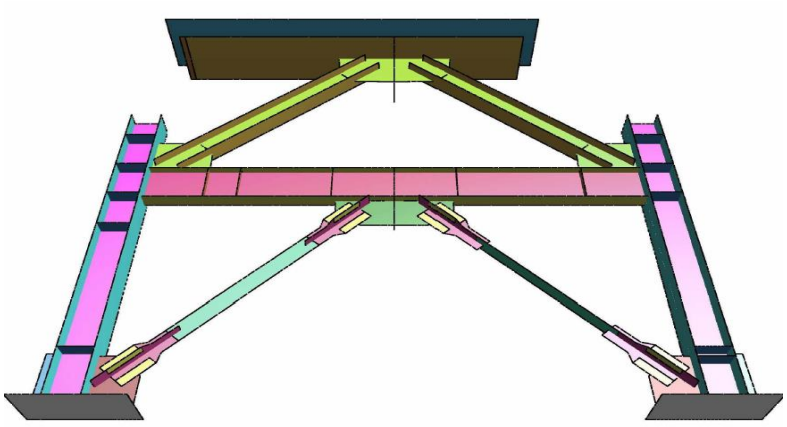

Figure 5-13. Modeling of BRBF (Mahin et al. 2004)
(a) experimental setup, (b) numerical model

Another approach published in Chou et al. (2012) used shell elements to represent a BRB within a frame and then simplified this to investigate only the connection zone including the end of the BRB, gusset plate and beam-column-joint. Material non-linearity was represented as a bi-linear curve using the yield and ultimate stress. A frictionless contact with no gap was used to model the restrainer and BRB core. This model reasonably predicted the ultimate load of the connection. However, it has not been validated over a range of experiments and does not help researchers understand the internal behaviour of different BRB designs. In addition, these simplifications render such models ineffective for predicting local deformation.

(a) (b)

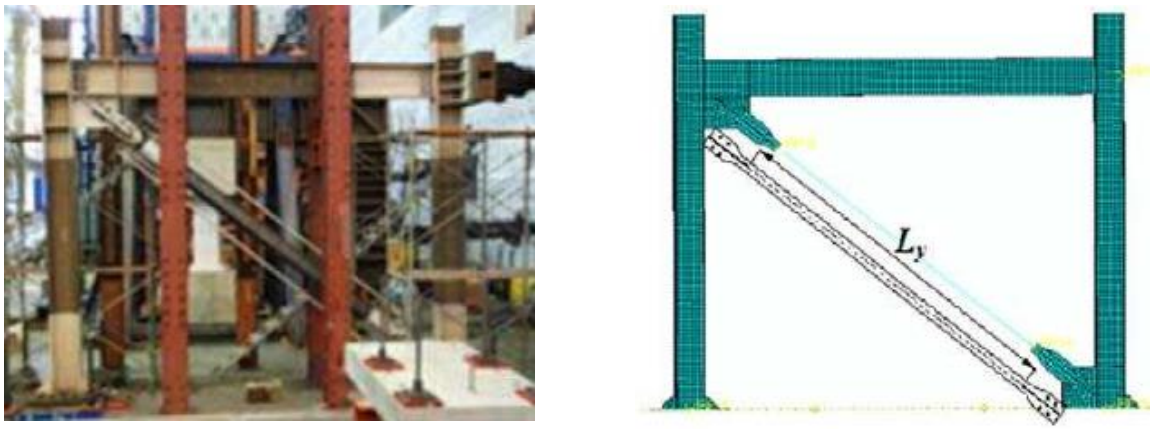

Figure 5-14. Modelling of BRBF (a) experimental setup, (b) meshed assembly (Chou et al. 2012)

A slightly more sophisticated approach to modelling the experimental set in Figure 5-14a is presented in Westeneng (2016). This approach uses two beam elements, one to represent the BRB core and the second to represent the restrainer. The two lines of beam elements are coupled together at 16 evenly spaced nodes along the length of the restrainer. Each location of coupling has pre-selected degrees-of-freedom, constraining all but translation in the longitudinal direction of the BRB. This allows sliding of the core inside the restrainer to occur but does not allow frictional contact and restricts buckling to one mode shape. Westeneng states that this modelling method makes it difficult to predict the hinging behaviour that has been observed at the BRB end. Both of these methods are appealing as they significantly reduce computational demand. The sacrifice, however, is a lack of fidelity and therefore less realistic local deformation is captured.

A more recent study published by Tsai et al. (2018) modelled a two storey BRBF with welded end slot connections and reinforced concrete frame elements Figure 5-15. This model used shell elements to represent the gussets and beam elements for the BRB and frame components. Upon comparison of the modelling results to experimental testing, the model was able to capture base shear and gusset plate interface forces to satisfactory level. In addition, the model was able to capture buckling of the first-storey upper gusset. Takeuchi's method for evaluating out-of-plane stability for the first floor was also compared against results. It was found that by using a thickened gusset plate or adding edge stiffeners meant the first-storey upper gusset plate buckling could be prevented.

(a) (b)

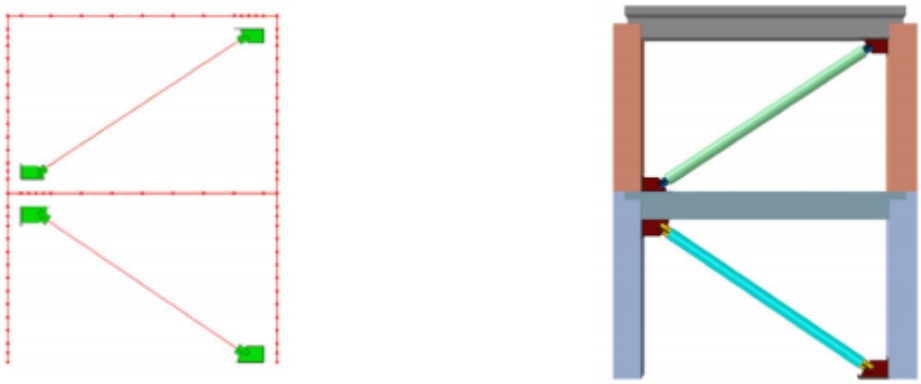

Figure 5-15. Model of two storey BRBF (Tsai et al. 2018)
(a) elements used in BRBF model, (b) elements with sections displayed.

Although modelling a BRBF with beam or shell elements is attractive due to significantly reduced model development and processing times. These simplifications mean the interaction of the core and cruciform section with the restrainer as the BRB stretches and compresses are negated. However, these interactions play a significant role in the defining stability of a BRBF system. Continuum modelling described here captures local deformation with minimal simplifying assumptions. Continuum modelling is important to accurately represent components and therefore many types of global behaviour.

5.1.8 **Summary**

Publications from Architectural Institute of Japan offer the most detailed analytical/closed form treatment for evaluating the out-of-plane stability of BRBFs as per Takeuchi's proposal (Architectural Institute of Japan (AIJ) 2009, Architectural Institute of Japan (AIJ) 2013, 2014). Japans building design code (BCJ) uses this evaluation which supplements prequalification assessments of individual BRBs. This is unlike structural building codes in New Zealand, Europe and the United States that do not yet provide alternative methods to assess BRB and connection stability, with prototype testing used as the primary means of certification. This makes the method used in Japan (Takeuchi's method), an attractive option for countries of high seismicity to use as an alternative to full-scale testing in combination with prequalification testing.

As a quick check, Takeuchi et al. (2017) states out-of-plane stability is unlikely to be a problem if the following conditions are met.

- The ratio of the exposed cruciform section to the total length is < 0.2.
- The flexural stiffness of the cruciform section of the BRB is > 0.5 of the flexural stiffness of the restrainer and steel casing.
- Gusset plates have high stiffness as per Figure 5-9c or Figure 5-9d.

However, BRBs manufactured outside of Japan often fail these quick check conditions. Also, the amount of information regarding the validation of this method is limited. Available publications only describe validation for one type of BRB design. This BRB would also be considered particularly small in New Zealand, with a total length of 2.4 m and a maximum axial load of 400 kN.

Modern Japanese building designs are recognised for being relatively stiff compared to New Zealand designs (Pettinga et al. 2019). In addition, buildings in New Zealand are expected to perform without instability beyond levels of ultimate limit state (ULS). This means that for the same level of earthquake, buildings in New Zealand can generally expect more lateral displacement compared to buildings in Japan.

The role BRBs play in earthquakes is also different for Japan and New Zealand. In Japan, BRBs are commonly used a supplemental damper. Whereas in New Zealand, BRBs are designed to be the primary horizontal load carrying structural member. This means that in New Zealand, buildings with BRBs are at greater risk of collapse if BRBF instability occurs, when compared to Japan.

As such, any likely candidates to supplements full-scale testing (such as the Takeuchi method) should be evaluated using BRB designs and connection detailing that represent those in use (including unstiffened gusset connection zones). In addition, approved design combinations should be tested to levels beyond ultimate limit state (ULS).

Subassemblage testing or full-frame testing would be the ideal method to assess Takeuchi's method in more detail. However, large BRBs and full-frame designs make experimental testing expensive. This makes detailed FEA an attractive alternative. ANSI/AISC 341-16 also recognizes the cost of subassemblage testing and has approved non-linear FEA in combination with uniaxial testing as an alternative to subassemblage testing (ANSI/AISC 2010). However, the complexities of BRB behaviour has limited the development of such modelling efforts.

To evaluate the performance and stability of a diagonal ground storey BRBF, this chapter uses detailed FEA to study the behaviour of ground storey diagonal BRBFs with bolted connections. To overcome the traditional challenges of detailed BRB modelling, the validated strategy for modelling uniaxial BRB tests (presented in Chapter 3) will be used as a foundation. To capture the realistic behaviour of a BRB within a frame, boundary conditions are adjusted and frame elements are added (which have relatively simple geometry and no contact conditions). Results are used to evaluate; Takeuchi's method for assessing the out-of-plane stability of BRBFs, the effect of bi-directional loading on ground storey BRBFs, and the suitability of using different gusset plate designs in these systems (discussed in Chapter 4).

5.2 **Model description**

To evaluate the performance and stability of a diagonal ground storey BRBF, a series of finite element models were developed using Abaqus®. All the finite element models were the same except for selected geometric dimensions. Each model included a complete BRB, modelled as per the details explained in Chapter 3 with each BRB connected to corner gussets of a steel frame. All frame elements were modelled using shell (S4R) elements (Dassault Systems 2014). To capture buckling behaviour, non-linear geometric analysis was performed.

The geometric features of BRB 6.5a (Chapter 2 and 3) were used as a basis for the BRBs modelled. To capture the different failure mechanisms (Figure 5-8), four BRB variants were modelled. These varied the length that the cruciform section inserts into the restrainer. In addition, the connection type was changed to a bolted array, as global stability tends to govern BRBFs with bolted connections (Takeuchi et al. 2017). Geometric details of the BRBs modelled are shown in Table 5-1 and Table 5-2. These geometric features are highlighted in Figure 5-16. Where L_g = the mid length of the gusset, using the Thornton length method, L_{neck} = the exposed cruciform length, L_{in} = the insert length of the cruciform section into the restrainer, L_{rest} = the length of the restrainer, L_{total} = the total length of the BRB (end to end), and B_{cruc} = is the width of the cruciform.

Initially, each BRB variant was matched with each a compact or semi-slender gusset plate design (Table 5-3). These combine to make a total of eight BRBF variants modelled using Abaqus®. In order to accommodate the various BRB and gusset plate lengths, the sizes of the frame elements were adjusted in each model, while keeping the BRB core length constant. However, should the total length remain constant, then the yielding length would need to change. This means modelling results cannot be compared directly against each other. However, this does not affect the ability to assess Takeuchi's method when calculating the stability limit.

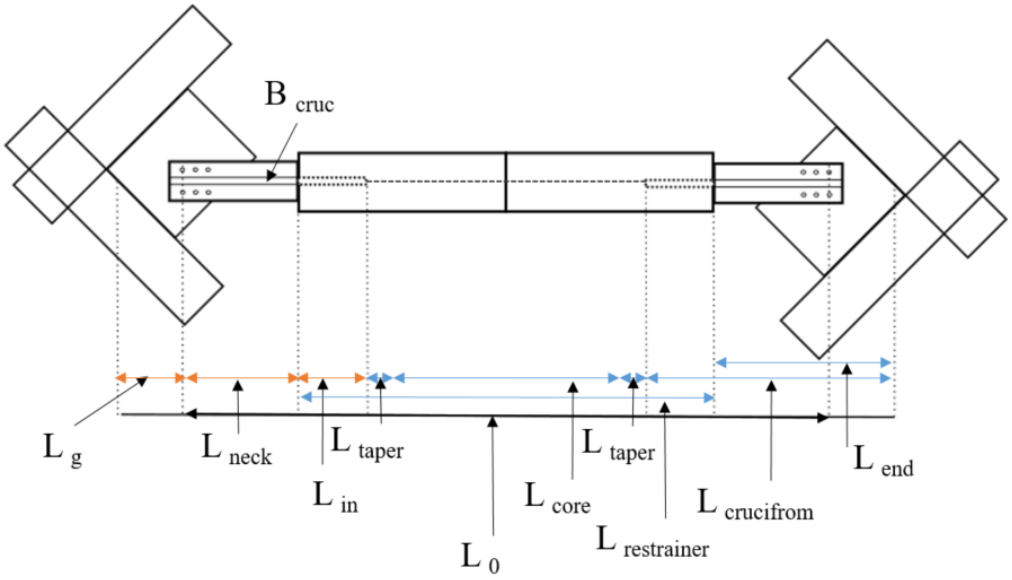

Figure 5-16. Geometric dimensions of BRB and connections

Table 5-1. BRB geometric parameters held constant

Beam	Column	B_{cruc} [mm]	L_{core} [mm]	L_{neck} [mm]	L_{taper} [mm]	A_{core} [mm x mm]	A_{grout} [mm^2]	A_{casing} [mm x mm]	Angle of inclination [θ]
310UC 118	310UC 118	240	4563	550	100	140 x 25	71400	323 x 6.4	33

Table 5-2. Combinations of BRB geometric parameters applied in the FE models

Model ID	L_{in} [mm]	L_{in}/ B_{cruc}	L_0 [mm]	$L_{restrainer}$ [mm]
D6.5b_0.5	120	0.5	6509	5409
D6.5b_1.5	360	1.5	6749	5649
D6.5b_2.5	600	2.5	6989	5889
D6.5b_4.0	1000	4.1	7389	6289

Two gusset lengths representing both compact and semi-slender gusset plate options were chosen. For each of these two lengths, the thickness was initially determined by following instructions as per NZS 3404. Because the ground storey bay was modelled, the two gusset plates varied slightly between the ground and first level. The dimensions of each gusset plate design are defined in Table 5-3, with the geometric parameters shown in Figure 5-17. In this study, surface-to-surface contact modelling between the gusset plate and brace end connection was included in the FEA models, and the gusset plate to beam-column boundary was idealised as being fixed. Each bolted connection was approximated using a coupling constraint, which coupled the inner surface of each bolt hole to the center point of the hole.

(a) (b)

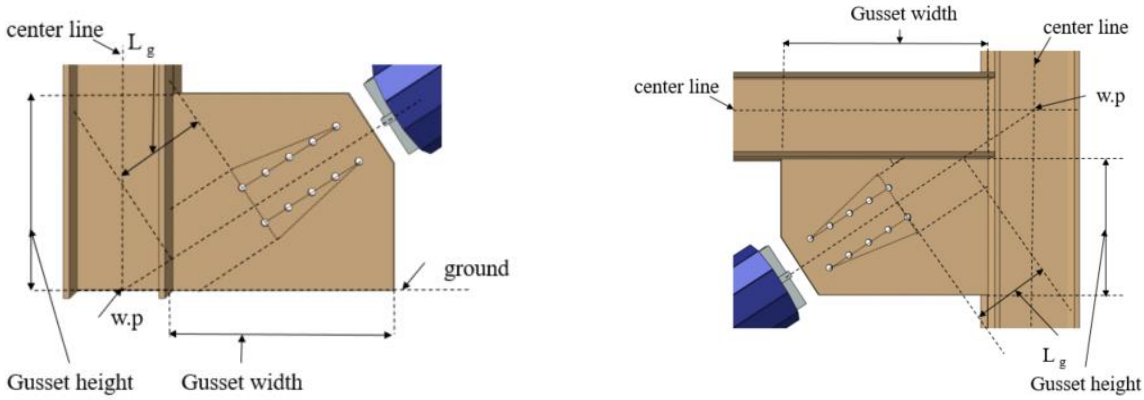

Figure 5-17. Geometric parameter definitions of each gusset plate (a) G, (b) L1

Table 5-3. Geometric variables details of each gusset plate

Model ID	Position	L_g [mm]	K_eL_e [mm]	t [mm]	L/r	Area [mm x mm]
GP1G	G	300	117	13	25	613 x 689
GP2G	G	800	467	22	27	1107 x 885
GP1L1	L1	300	97	13	67	774 x 511
GP2L1	L1	800	447	22	66	1194 x 783

5.3 **Boundary conditions and loading**

The boundary conditions of each BRBF model are shown in Figure 5-18. These boundary conditions aim to represent conditions of a ground storey BRBF. Each model was subjected to a displacement based cyclic loading protocol at the loading point. To capture the effect of the floor diaphragm, the loading point was coupled to the mid-section of the beam. This means the red surface (Figure 5-18), effectively moves as a rigid member.

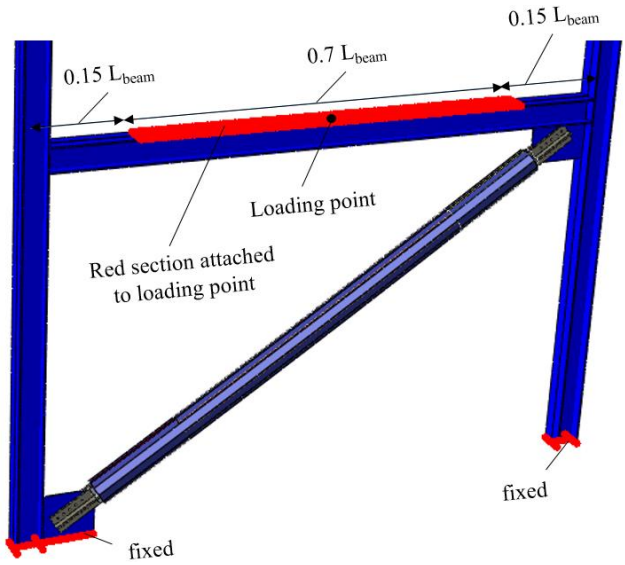

Figure 5-18. Boundary conditions for each BRBF model

To investigate the effect of bi-directional loading, each model was subjected to displacement based cyclic loading in both in-plane and combined in-plane and out-of-plane directions. The oblique (combined loading) direction was set to a 45 degree offset from the in-plane direction. The magnitude of loading remained the same for both directions of loading. For the combined case, this means the in-plane component of loading is about 71% of the in-plane loading only. The loading protocol used in this study is a reduced version to that used for prequalification testing, where increasing amounts of cyclic loading are applied, targeting displacements relative to the design story drift (Figure 5-19), and while free to move in the vertical direction. This reduced loading protocol was used to reduce the computer processing time of each model while still providing a valid basis for comparison between the BRB design variants.

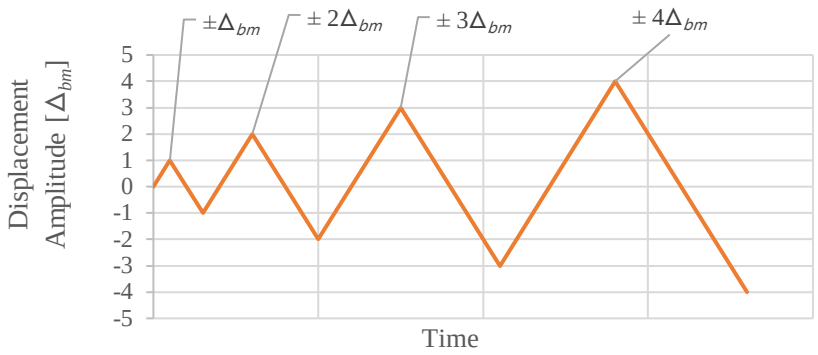

Figure 5-19. Loading protocol for each BRBF model

Initial geometric imperfections of BRBFs can arise from the shape of the steel core (misalignment of the core and non-yielding components, core off-centering relative to steel tube) and those of the steel casing (bow imperfections and misalignment of connections), frame and ground connection alignments. Takeuchi et al. (2017) states imperfections in a BRBF can easily be in order of 1% of the length of the BRB. As such, an initial equivalent geometrical bow imperfection (Figure 5-20) was introduced into each BRBF model (similar to Chapter 3). This bow imperfection was based on the first mode of elastic buckling. The maximum point (e_0) was equal to the 0.5% of length of the BRB (Figure 5-20) with each remaining node distributed according to the shape of the bow imperfection.

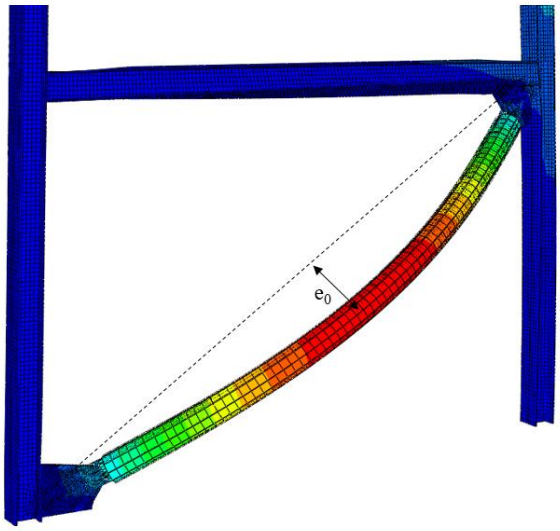

Figure 5-20. Equivalent geometric bow imperfection (exaggerated for clarity) in BRBF models

5.4 **Results**

The in-plane and bi-directional responses of each specimen are presented in Figure 5-21 through Figure 5-24. In each figure, part (a) shows results for designs with compact gussets (GP1G and GP1L1) and part (b) show results for designs with semi-slender gussets (GP2G and GP2L1). Results are shown in terms of overstrength ratio (force/yield force) and displacement relative to design storey drift (Δ_{bm}). In each graph the blue curve represents results for inplane loading and the orange curve represents results for bi-directional loading. The inset FE images show deformed configurations associated with local losses in stability as predicted by the FEA.

As a benchmark, a BRBF that maintains stability at interstory drifts up to $\pm 3\Delta_{bm}$ is deemed to have performed well. For the cases with compact gusset plates (denoted GP1G and GP1L1 in Table 5-3) and L_{in}/B_w ratio < 1, bending initiated early in the restrainer/cruciform. For all other models with compact gusset plates, softening first occurred in the BRB core between $3\text{-}4\Delta_{bm}$. This was followed by bending of either the cruciform or gusset plate upon load reversal. For gusset plates with semi-slender gusset plates, all models displayed instability at lower displacements. Again, when $L_{in}/B_w < 1$, bending initiated early in the restrainer/cruciform. For all other designs, gusset plate bending limited performance. Of all the models with semi-slender gusset plate, D6.5b_4.0 performed the best. When comparing results of in-plane loading to bi-directional loading for the same magnitude, bi-directional loading achieved the same or even higher relative displacements for most cases.

(a)

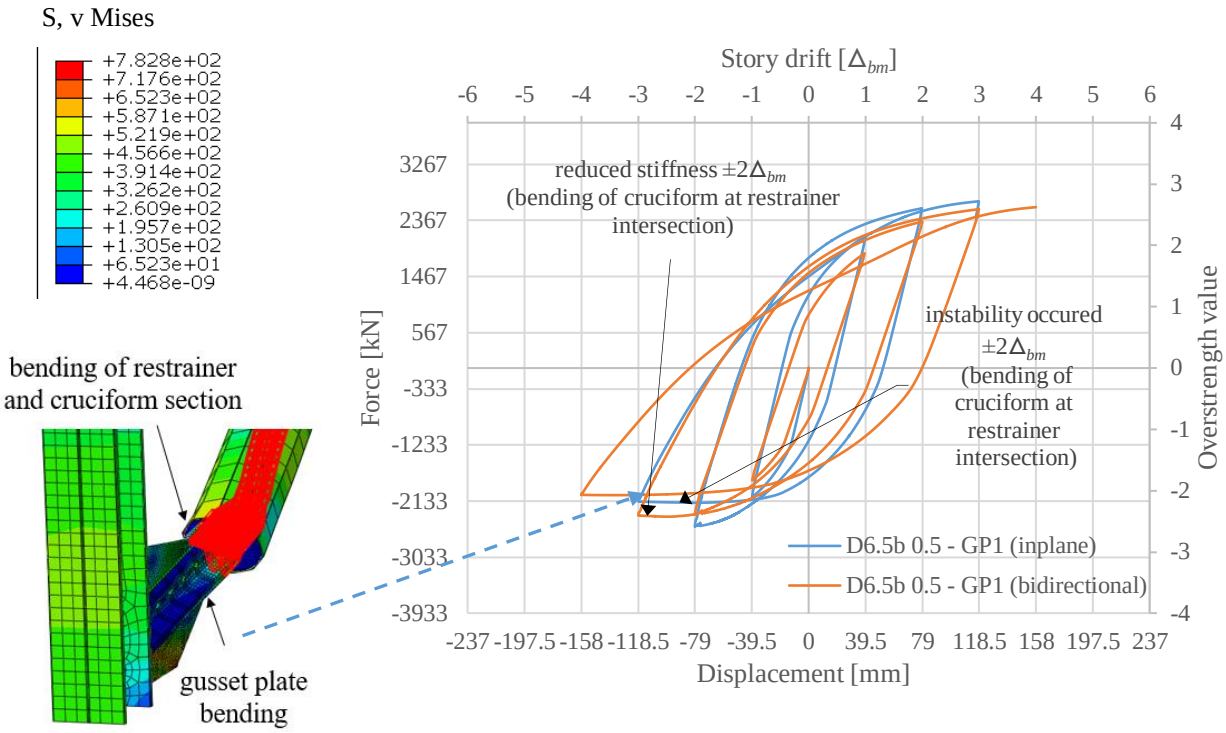

(b)

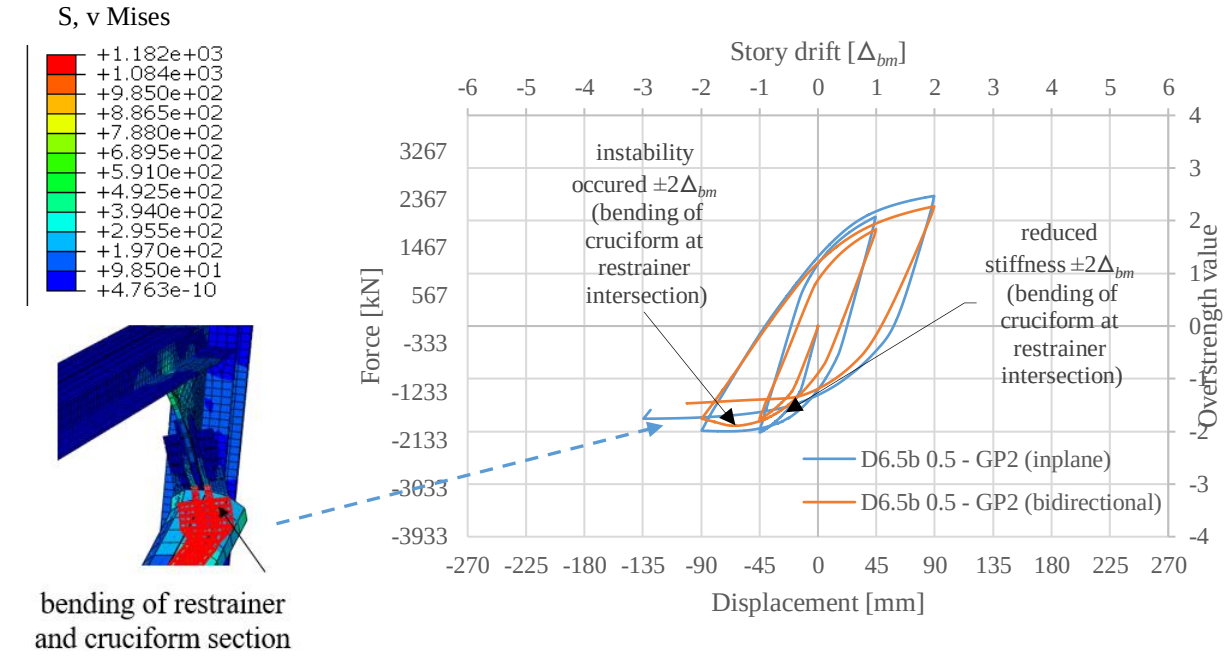

Figure 5-21. Lateral force-displacement history of BRBF D6.5b_0.5 (insert length ratio L_{in}/ B_{cruc} = 0.5) (a) GP1 (compact), (b) GP2 (semi-slender)

(a)

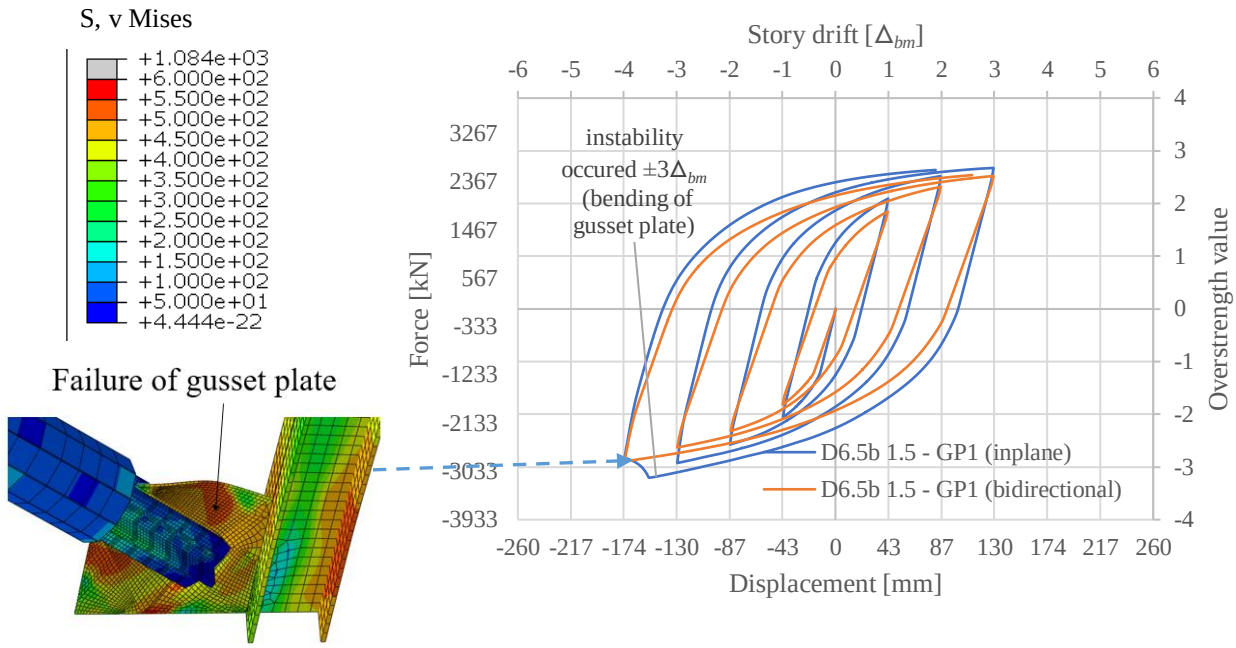

(b)

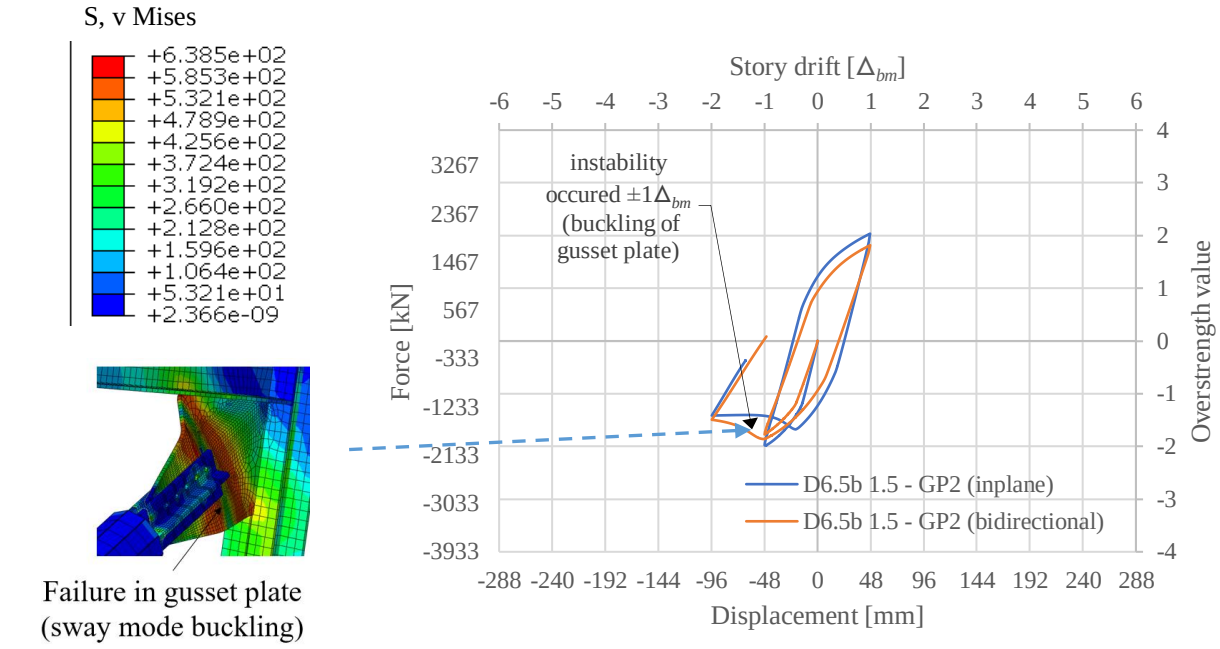

Figure 5-22. Lateral force-displacement history of BRBF D6.5b_1.5 (insert length ratio L_{in}/B_{cruc} = 1.5) (a) GP1 (compact), (b) GP2 (semi-slender)

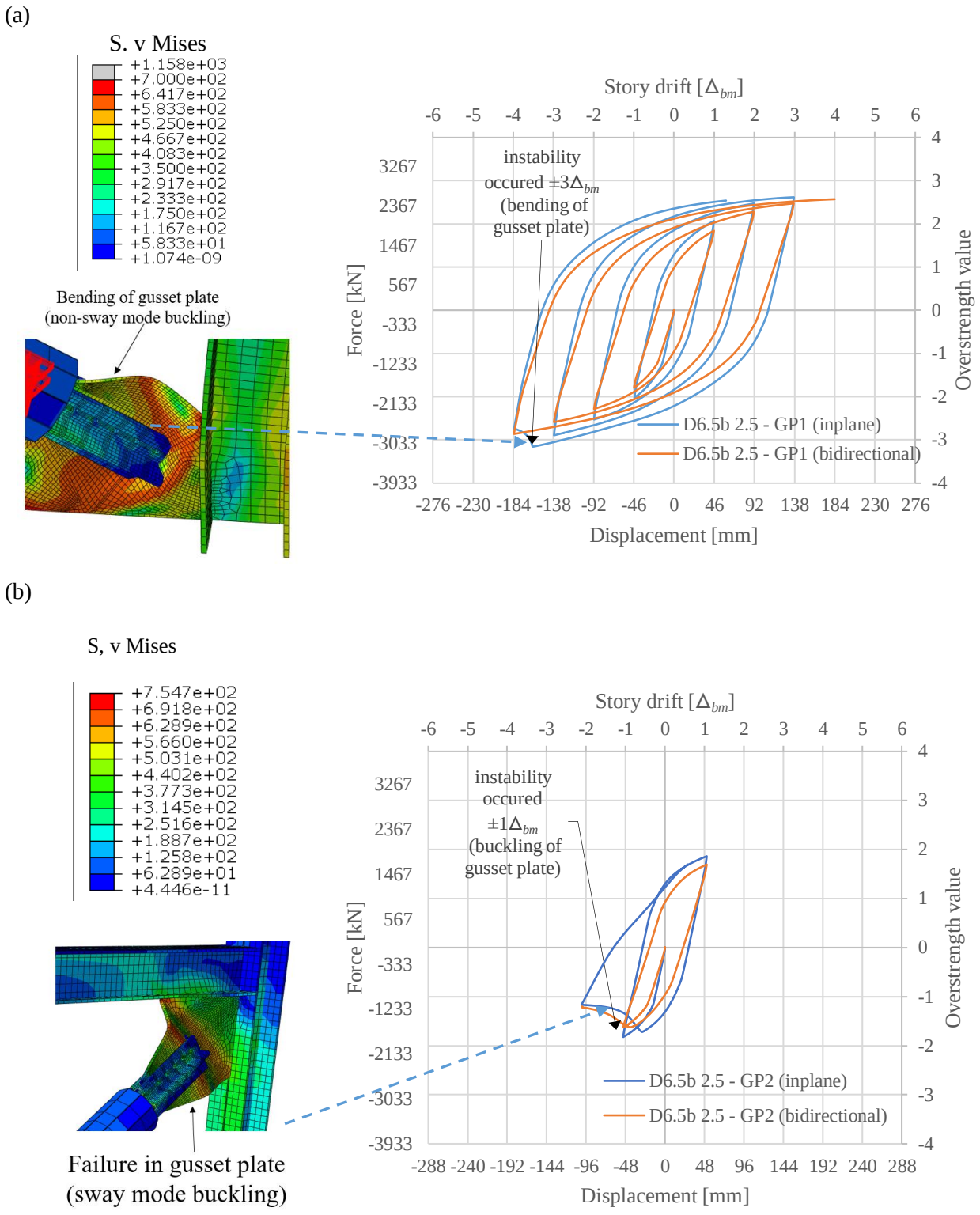

Figure 5-23. Lateral force-displacement history of BRBF D6.5b_2.5 (insert length ratio L_{in}/B_{cruc} = 2.5) (a) GP1 (compact), (b) GP2 (semi-slender)

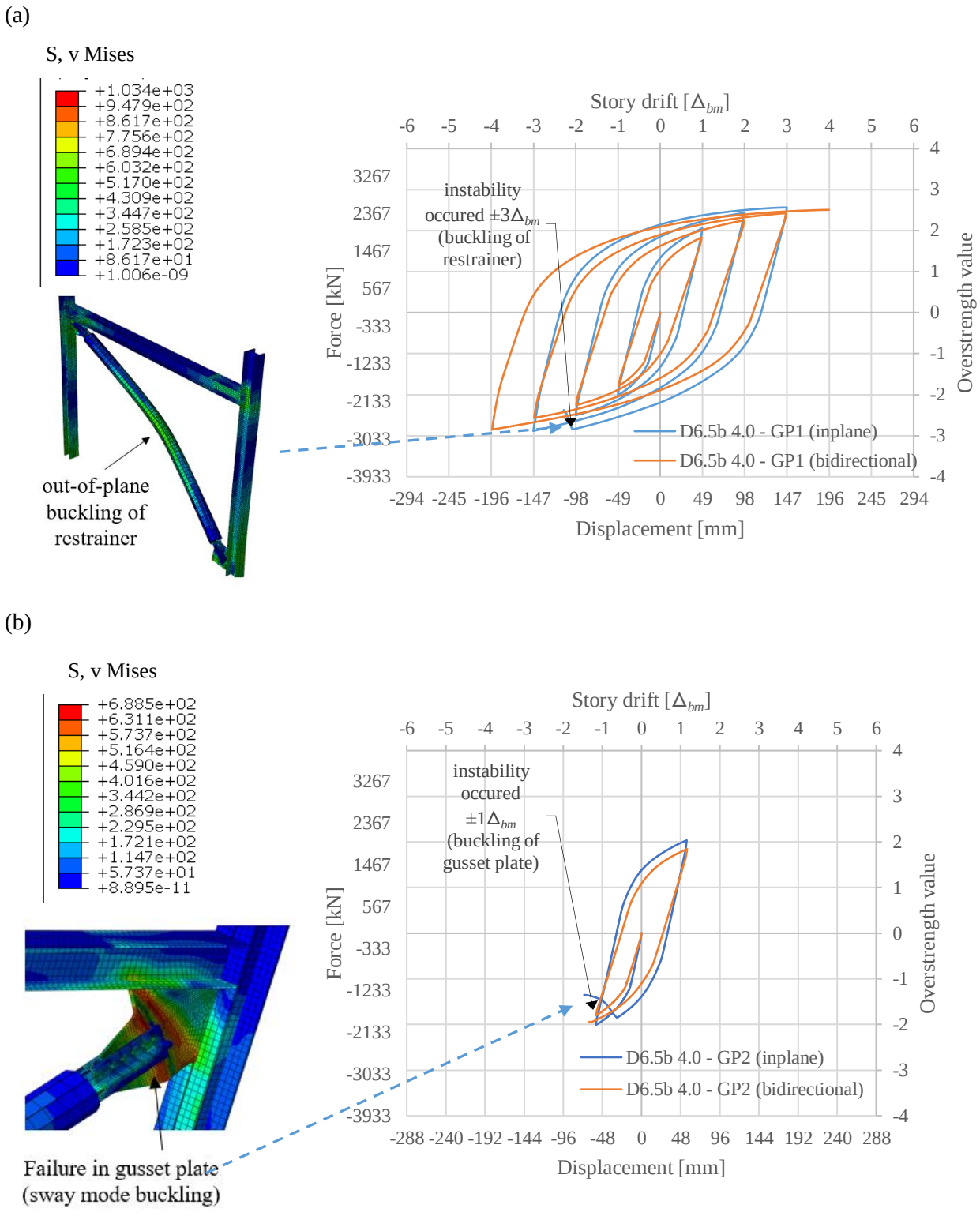

Figure 5-24. Lateral force-displacement history of BRBF D6.5b_4.0 (insert length ratio L_{in}/B_{cruc} = 4.0) (a) GP1 (compact), (b) GP2 (semi-slender)

Following the initial set of simulations, it was of interest to explore alternative gusset plate designs that may improve performance, particularly for the models that showed instability before achieving drifts up to $\pm 3\Delta_{bm}$. It was also of interest to compare predictions made by FEA to Takeuchi's method, and to discuss the limitations of this method and the modelling used in this study.

5.5 **Improvements to connection design**

Observations from FEA results show that gusset plate bending and buckling was a limiting feature in most of the BRBF models. Takeuchi et al. (2017) recommends some form of out-of-stiffeners on the gusset plates and frame elements to avoid this problem. However, as it is more economical to have unstiffened gusset plates, it is of interest to explore if stability can be maintained without the use of gusset plate stiffeners. Following the baseline analyses presented so far, a modification was made to the two gusset plate designs. The same set of BRB variants and gusset plate lengths were modelled, but the gusset plate thickness was calculated using Thornton's method for gusset plates as described in Court-Patience (2020). In addition, to account for the sway mode failure observed in the semi-slender gusset plates (denoted as GP2G and GP2L1), the effective length factor was increased from 0.7 to 1.2. Table 5-4 presents geometries for the modified gusset plates.

Table 5-4. Geometric dimensions of the modified gusset plate designs

Model ID	Position	Design	L_g [mm]	L_e [mm]	K_eL_e [mm]	t [mm]	L/r
GP1'G	G	NZS3404	300	240	288	19	53
GP2'G	G	NZS3404	800	640	768	28	95
GP1'L1	L1	NZS3404	300	240	288	19	53
GP2'L1	L1	NZS3404	800	640	768	26	95

For each of the modified designs, the force response to the inplane cyclic loading protocol is presented in Figure 5-25 and Figure 5-26. For ease of comparison, results for each simulated test are shown (in green) alongside the original models (in blue) with thinner gusset plates. As before, results are shown in terms of overstrength ratio (force/yield force) and displacement relative to design storey drift (Δ_{bm}). These figures show improved performance for all cases.

(a)

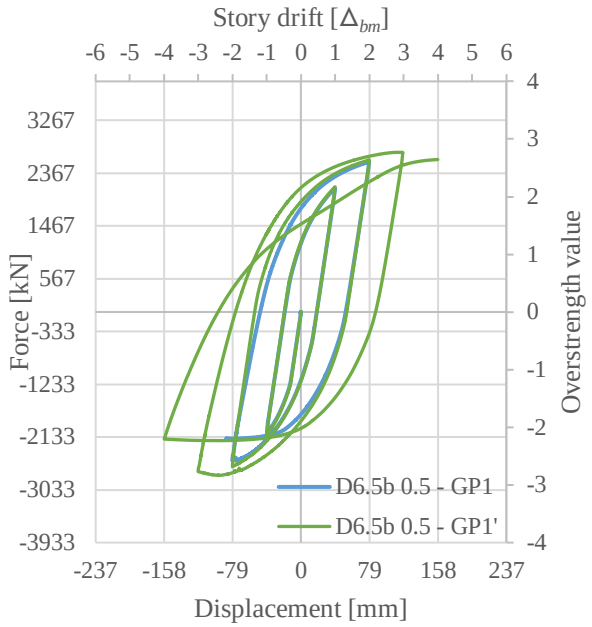

(b)

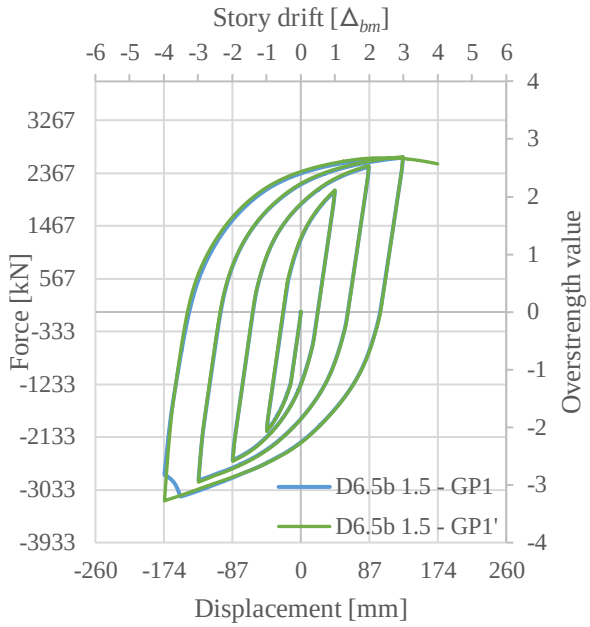

(c)

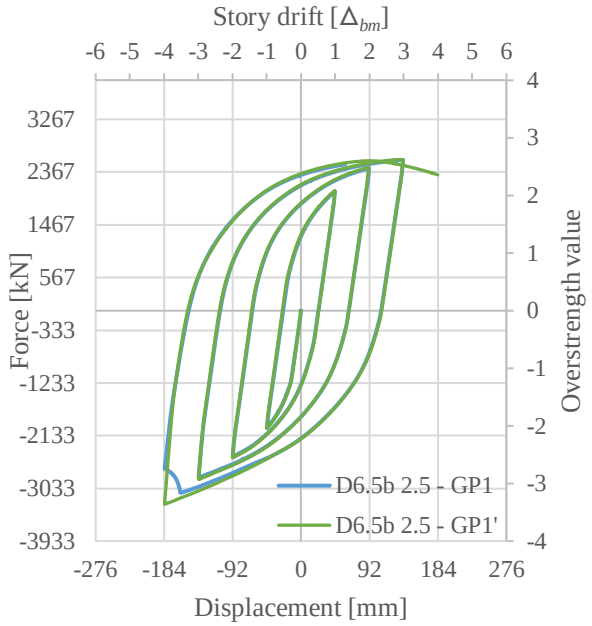

(d)

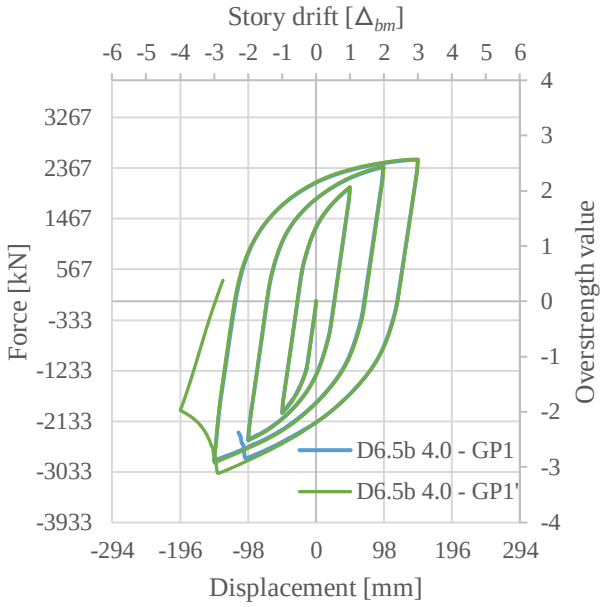

Figure 5-25. Lateral force-displacement history of BRBF with compact gusset plates
(a) L_{in}/B_{cruc} = 0.5, (b) L_{in}/B_{cruc} = 1.5, (c) L_{in}/B_{cruc} = 2.5, (d) L_{in}/B_{cruc} = 4.0

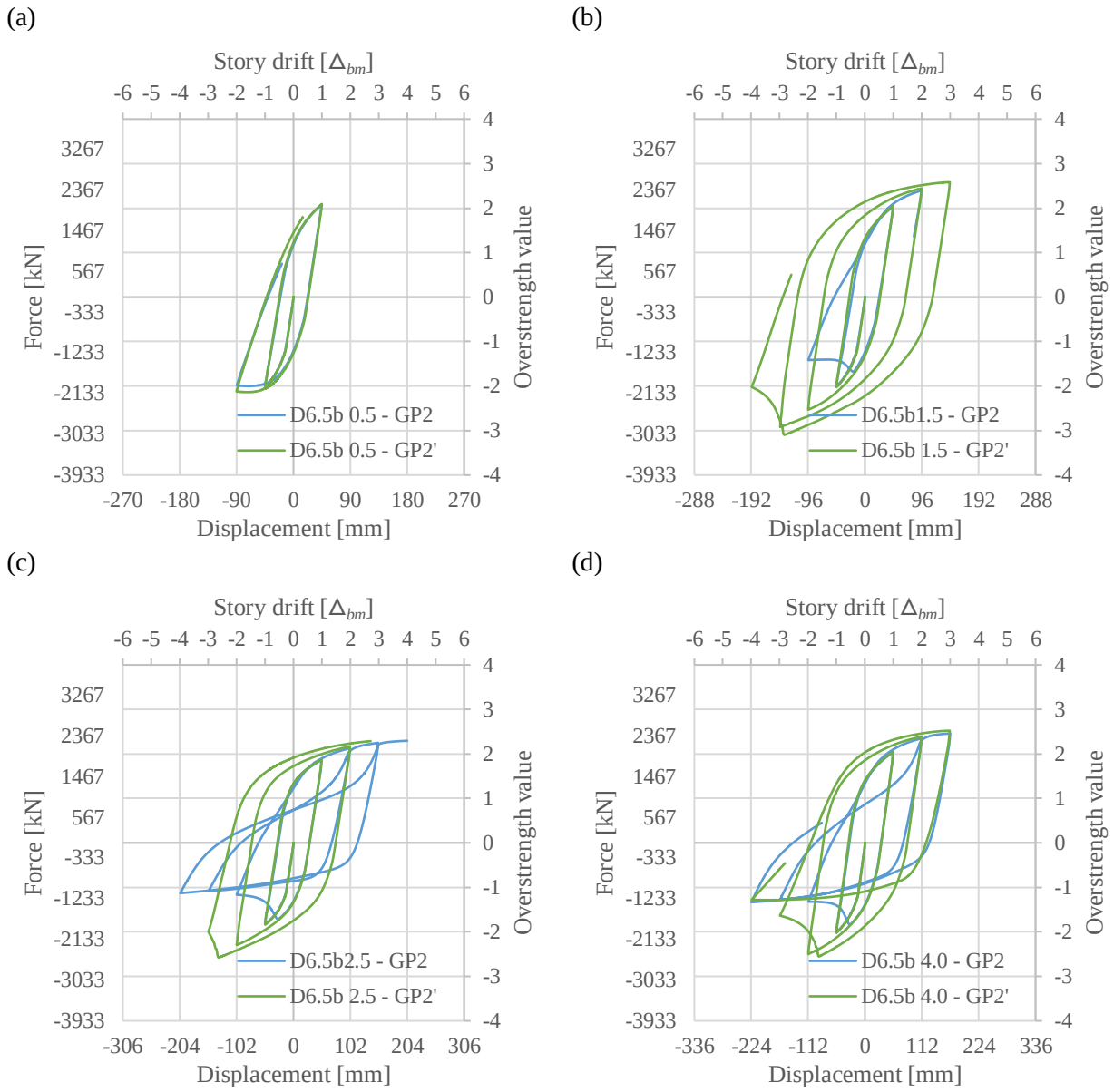

Figure 5-26. Lateral force-displacement history of BRBF with semi-slender gusset plates
(a) L_{in}/B_{cruc} = 0.5, (b) L_{in}/B_{cruc} = 1.5, (c) L_{in}/B_{cruc} = 2.5, (d) L_{in}/B_{cruc} = 4.0

5.6 **Improvements to Takeuchi's method**

Takeuchi's method is an attractive option to use as an alternative to full-scale testing (in combination with prequalification testing of BRBs). However, available publications only provide validation of this method over a limited range of BRBF designs. As such, Takeuchi's method was evaluated against a set of detailed BRBF models. Four BRB variants of the same design were modelled with different ratios of L_{in}/B_{cruc} with unstiffened gusset plate designs. Generally, Takeuchi's method was found to be conservative. However, validating all the evaluations (load paths) in Takeuchi's method is difficult, particularly those that have values above the ultimate compressive load of the BRB core.

To summarise, Takeuchi's method sets out equations to determine a stability limit of an idealised BRB system. The idealised BRB system is modelled using prismatic elements and springs where critical hinges are assumed to be in the connection regions, where the cross sectional area changes. These changes in cross sectional area occur at the transition of cruciform to restrainer end, and intersection of the cruciform to gusset plate.

Takeuchi's method first evaluates the global elastic buckling load of the idealised model under the different collapse mechanisms. Each mechanism occurs as a result of critical P-δ moments where 'δ' is the maximum local out-of-plane deflection of the BRB and P is the axial load. This maximum out-of-plane deflection develops at the restrainer end for all the collapse mechanisms considered, being the location of one of the critical hinges. This out-of-plane deflection is initially caused by geometric imperfections which increase during compressive loading.

According to Takeuchi's method, the maximum stability limit is deemed as the intersection of two constructed load paths (the elastic path and the N-M ultimate path in Figure 5-27). The elastic path is the elastic load-deflection path of the idealised BRB system. And the N-M ultimate path is the function of the combined compressive and flexural loading strength of the connection zone (neck + gusset) in terms of out-of-plane deflection.

With the maximum stability limit established, the load limit paths can be calculated. The first load limit path (N_{lim1} in Figure 5-27) assumes the gusseted connection remains elastic. When plastic hinges occur in the gusset plates a different global buckling mode occurs. Takeuchi expresses this condition as the second load limit path (N_{lim2} in Figure 5-27). The amount the second load limit path reduces from the first load limit path depends on the ratio of stiffness between the gusset plate and the neck of the BRB, where if the gusset plate has a low compressive strength compared to the neck of the BRB then the effect of the gusset plate hinging

is less. The governing stability limit is considered to be the lower of the two forces, where each load limit path intersects with the elastic path.

(a) (b)

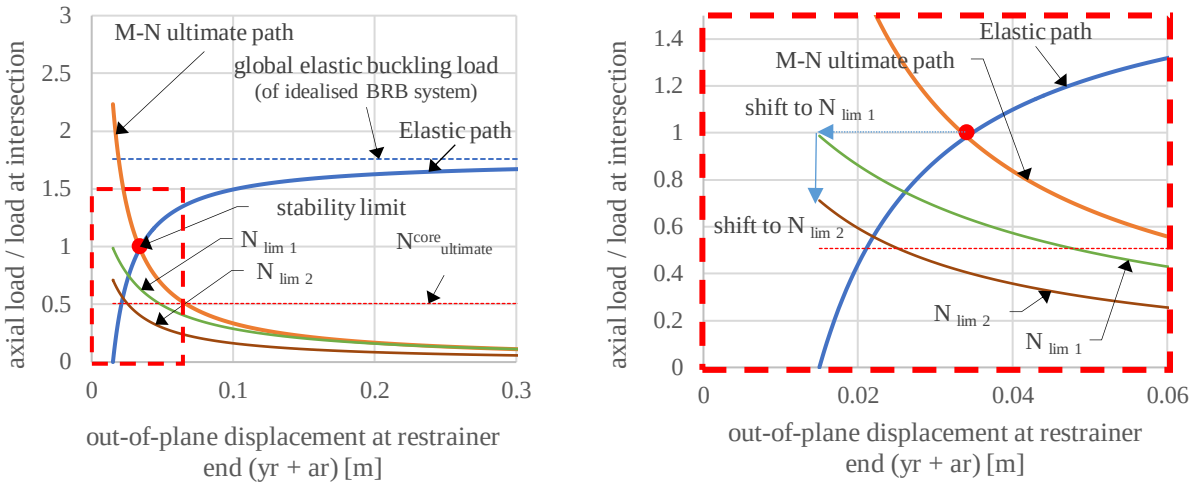

Figure 5-27. Takeuchi's equations for evaluating BRB stability model, based on moment continuity concept. (a) complete stability model,
(b) close up of equations showing how the two limit states are constructed

A summary of the failure types and the evaluations as per in Takeuchi's method are presented in Table 5-5 and Table 5-6, where N_{cr}^{B} = the critical buckling load of the BRB system with connections, N_{cr}^{r} = the inelastic compressive capacity of the BRB end connection using an equivalent slenderness ratio in an appropriate column buckling curve, M_{p}^{r} = the plastic moment capacity of either the restrainer or cruciform, N_{lim}= the least of the two forces from the load limit paths that intersect the elastic path (Takeuchi et al. 2013).

Table 5-5. Summary of failure loads predicted by FEA and stability limits calculated using Takeuchi's method for gusset plates designed with NZS3404 (in plane loading)

Model ID	N_{cr}^{B} [kN]	N_{cr}^{r} [kN]	M_{p}^{r} [kNm]	N_{lim} [kN]	Maximum compressive displacement	Maximum compressive force
D6.5b_0.5 GP1	1185	NA	0	324	$2.0\Delta_{bm}$	1850
D6.5b_0.5 GP2	740	NA	0	116	$1.0\Delta_{bm}$	1850
D6.5b_1.5 GP1	1609	1573	102.2	1000	$3.25\Delta_{bm}$	(1850)
D6.5b_1.5 GP2	1155	1430	102.2	750	$1.0\Delta_{bm}$	1850
D6.5b_2.5 GP1	3003	1338	156.7	1800	$3.5\Delta_{bm}$	(1850)
D6.5b_2.5 GP2	2527	830	156.7	1500	$1.0\Delta_{bm}$	1800
D6.5b_4.0 GP1	6933	905	156.7	3200	$3.0\Delta_{bm}$	(1850)
D6.5b_4.0 GP2	6397	500	156.7	3000	$1.0\Delta_{bm}$	1800

( ): means instability was not predicted by Takeuchi's method or the models were able to achieve $\pm 3.0\Delta_{bm}$ without any instability.

Table 5-6. Summary of failure loads predicted by FEA and stability limits calculated using Takeuchi's method for gusset plates design with Thornton's method for gusset plates (in plane loading)

Model ID	N_{cr}^{B}	N_{cr}^{r}	M_{p}^{r}	N_{lim}	Maximum compressive displacement	Maximum compressive force
D6.5b_0.5 GP1'	5473	96	69.1	2050	$1.0\Delta_{bm}$	1850
D6.5b_0.5 GP2'	3596	354	69.1	1500	$1.0\Delta_{bm}$	1900
D6.5b_1.5 GP1'	5170	56	156.7	(2750)	$4.0\Delta_{bm}$	(1850)
D6.5b_1.5 GP2'	3633	240	156.7	(2050)	$3.0\Delta_{bm}$	(1850)
D6.5b_2.5 GP1'	4700	35	156.7	(2600)	$4.0\Delta_{bm}$	(1850)
D6.5b_2.5 GP2'	3120	170	156.7	(1800)	$2.8\Delta_{bm}$	(1700)
D6.5b_4.0 GP1'	5040	19	156.7	(2250)	$3.0\Delta_{bm}$	(1850)
D6.5b_4.0 GP2'	3278	100	156.7	(1800)	$2.0\Delta_{bm}$	(1900)

( ): means instability was not predicted by Takeuchi's method or the models were able to achieve $\pm 3.0\Delta_{bm}$ without any instability.

All FEA models (except for D6.5b 4.0 GP2) that indicate loss of stability before reaching $\pm 3\Delta_{bm}$ were predicted by Takeuchi's method. However, for D6.5b 1.5 GP1 failure was predicted by Takeuchi's method when no stability issues were predicted in FEA. Important to note: Takeuchi's method requires the initial geometric imperfection to be estimated. When using the conservative approximation of the geometric imperfections as proposed by Takeuchi et al. (2013) to calculate initial geometric imperfection, it was found that the displacements reached up to 100 mm at the restrainer end ($\approx 2\Delta_{bm}$). These estimates would lead to very low and unrealistic stability limits. As an alternative, the initial imperfection at this location was set to ~15 mm. This corresponds to the distribution of displacements, according to the first mode of buckling with a peak displacement equal to ~0.5% of the total brace length (L_0).

For the two D6.5b_0.5 models, the assumption made by the Takeuchi method is that when $L_{in}/B_w < 1$ the cruciform restrainer interface acts as pin connection once the core yields. This requires the Cantilever Connection Concept to be applied. As the gusset plates in this study are unstiffened, Takeuchi's method predicts elastic buckling of the BRB end connection when calculating the critical buckling load of the BRBs end connection (Takeuchi et al. 2017). However, FEA did not demonstrate pin-like behaviour. Rather, sufficient rotational stiffness was provided by the restrainer and casing such that displacements of $\pm 2\Delta_{bm}$ could be achieved for GP1 designs and $\pm 1\Delta_{bm}$ for GP2 designs.

For the two D6.5b_1.5 models, the assumption made by the Takeuchi method is that when $1< L_{in}/B_w < 2$, local yielding of the steel casing restrainer wall limits the moment carrying capacity of the plastic hinge zone at the restrainer end. However, FEA results show that the cement based grout maintains its strength and therefore provides increased moment capacity of this zone. For designs with compact gusset plates (GP1), Takeuchi's method predicts early instability (< core yielding) whereas FEA results show displacements of $\pm 3\Delta_{bm}$ were achieved. For designs with semi-slender gusset plates (GP2) designs, Takeuchi's method predicts instability to occur before the yield strength of the core is reached, whereas FEA results showed instability to occur much later, when displacement approached $-2\Delta_{bm}$.

When $L_{in}/B_w > 2$, the Takeuchi method assumes that under compressive loading, the restrainer is able to transfer a bending moment to the cruciform. This means that the plastic bending strength of the cruciform section governs the moment capacity of the hinge at the restrainer end. The FEA results also show this to occur. For designs with compact gusset plates (GP1), Takeuchi's method predicts instability to occur when the BRB core reaches ultimate strength. FEA results predict displacements of $\pm 3\Delta_{bm}$ can be achieved. For designs with semi-slender gusset plates (GP2), Takeuchi's method predicts early instability whereas FEA results predict instability to occur in the lower gusset when approaching $-2\Delta_{bm}$.

Again for both the D6.5b_4.0 BRBs, L_{in}/B_w is greater than 2. For this case, the Takeuchi method assumes that under compressive loading, the restrainer is able to transfer moment to the cruciform. The FEA results agree with this assumption.

The maximum elastic buckling load is a key feature in Takeuchi's method. However, eigenvalue analysis from the FEA models was found to be different when compared to values calculated by equations developed by Matsui et al. (2010) (derived from the differential equations proposed by Timoshenko et al. (1965)) and employed by Takeuchi (Takeuchi et al. 2013). Table 5-7 compares elastic buckling loads between the equations in Matsui et al. (2010) and the FE eigenvalue analysis.

Table 5-7. Estimates of maximum elastic buckling load of BRB and connections (using NZS3404 gusset plate design)

L_{in}/ B_{cruc}	4.0	4.0	2.5	2.5	1.5	1.5	0.5	0.5
Gusset type	GP1	GP2	GP1	GP2	GP1	GP2	GP1	GP2
Eigenvalue (FEA) [kN]	3971	2837	4378	2822	4829	3032	4938	2837
Matsui et al. (2010) [kN]	6933	6397	3003	2822	1609	1155	1185	740
% difference	+75%	+125%	-31%	-10%	-67%	-62%	-76%	-74%

The main cause for the variation shown in Table 5-7 stems from how the equations in Matsui et al. (2010) define the relationship between L_{in}, and the rotational stiffness of the restrainer. This study found that using the critical elastic buckling load from FEA in the Takeuchi method improved comparisons between Takeuchi's method for predicting out-of-plane stability and FEA results. Figure 5-28 and Figure 5-29 show the load paths and out-of-plane evaluation as per Takeuchi's method.

The traditional equations used to construct each load path (in terms of out-of-plane displacement at the restrainer) as described in Takeuchi et al. (2013) are plotted using dashed lines. The adjusted load paths, calculated using the critical buckling load from each FEA models, are plotted in continuous lines. The FEA results are shown using solid yellow lines. These results suggest the assumptions made by the equations described by Matsui et al. (2010) to calculate the elastic buckling load of the BRB system should to be reviewed to improve predictions made by Takeuchi's method.

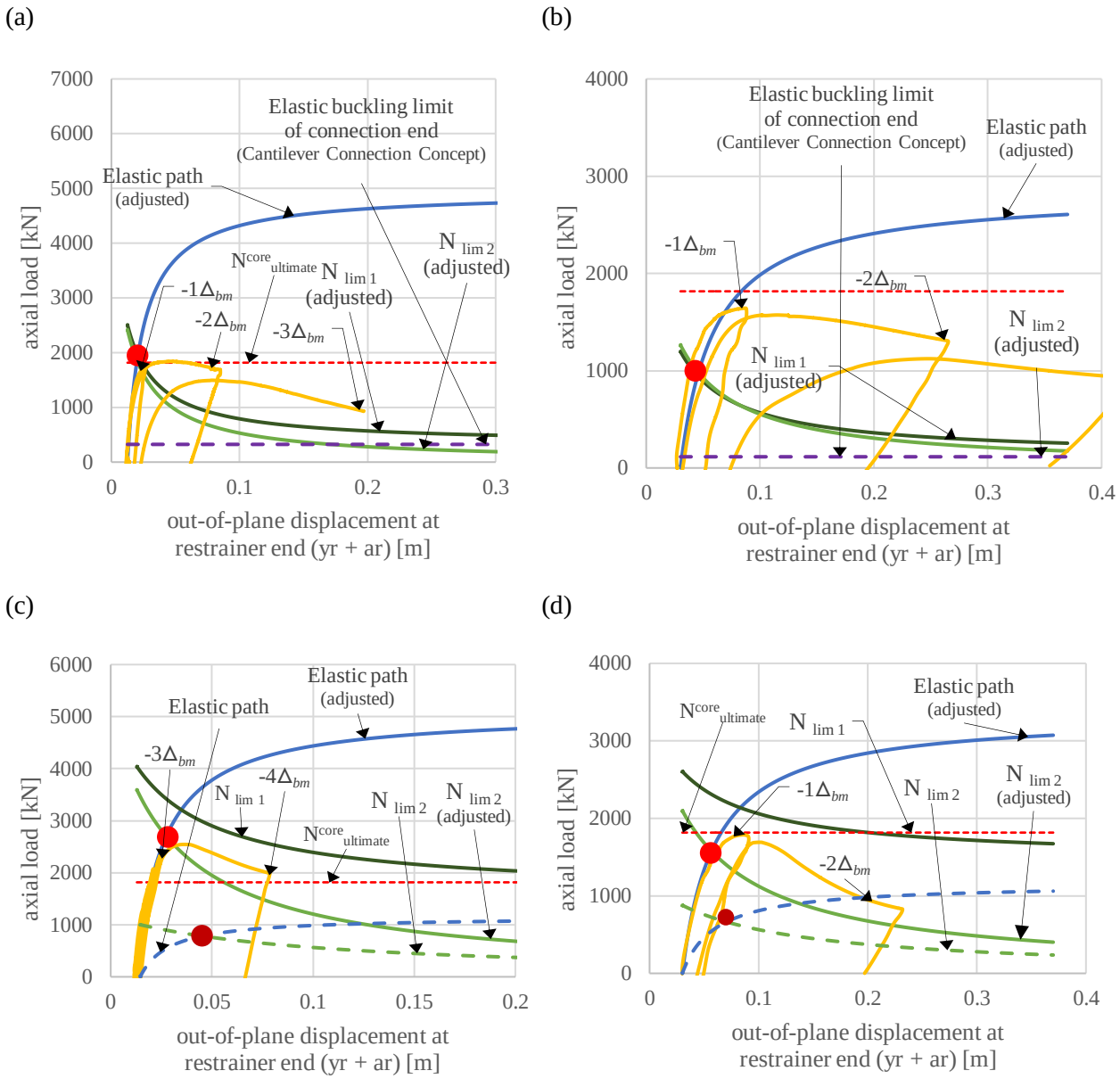

Figure 5-28. Out-of-plane stability
(a) D6.5b_0.5 GP1 (L_{in}/B_w=0.5), (b) D6.5b_0.5 GP2 (L_{in}/B_w=0.5),
(c) D6.5b_1.5 GP1 (L_{in}/B_w=1.5), (d) D6.5b_1.5 GP2 (L_{in}/B_w=1.5)

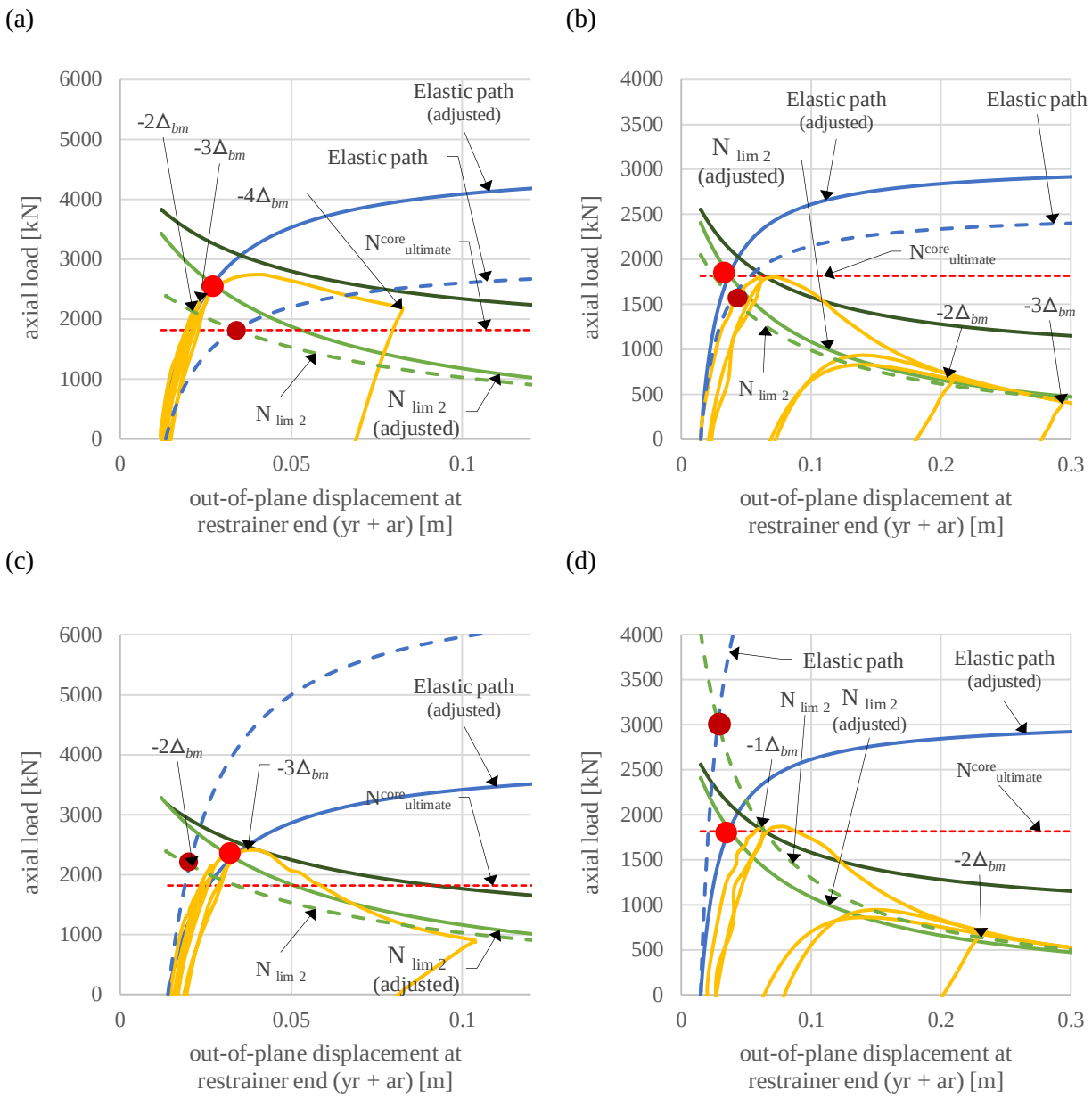

Figure 5-29. Out-of-plane stability
(a) D6.5b_2.5 GP1 (L_{in}/B_w=2.5), (b) D6.5b_2.5 GP2 (L_{in}/B_w=2.5),
(c) D6.5b_4.0 GP1 (L_{in}/B_w=4.0), (d) D6.5b_1.5 GP2 L_{in}/B_w=4.0)

Table 5-8 shows the variation in maximum elastic buckling loads between the equations in Matsui et al. (2010) and the eigenvalue analysis of each of the BRBF models vary between 23% - 165%.

Table 5-8. Estimates of maximum elastic buckling load of BRB and connections (using NZS3404 gusset plate design)

L_{in}/ B_{cruc}	4.0	4.0	2.5	2.5	1.5	1.5	0.5	0.5
Gusset type	GP1'	GP2'	GP1'	GP2'	GP1'	GP2'	GP1'	GP2'
Eigenvalue (FEA) [kN]	4297	3354	4767	3431	5334	3964	5573	3697
Matsui et al. (2010) [kN]	6933	6308	3062	2523	1702	1170	1293	774
% difference	+61%	+91%	-37%	-26%	-70%	-71%	-79%	-77%

Figure 5-30 and Figure 5-31 show the FEA results and out-of-plane stability predictions for the designs with increased gusset plate thickness. Improved performance was observed in all BRBFs (except when L_{in}/B_w=0.5).

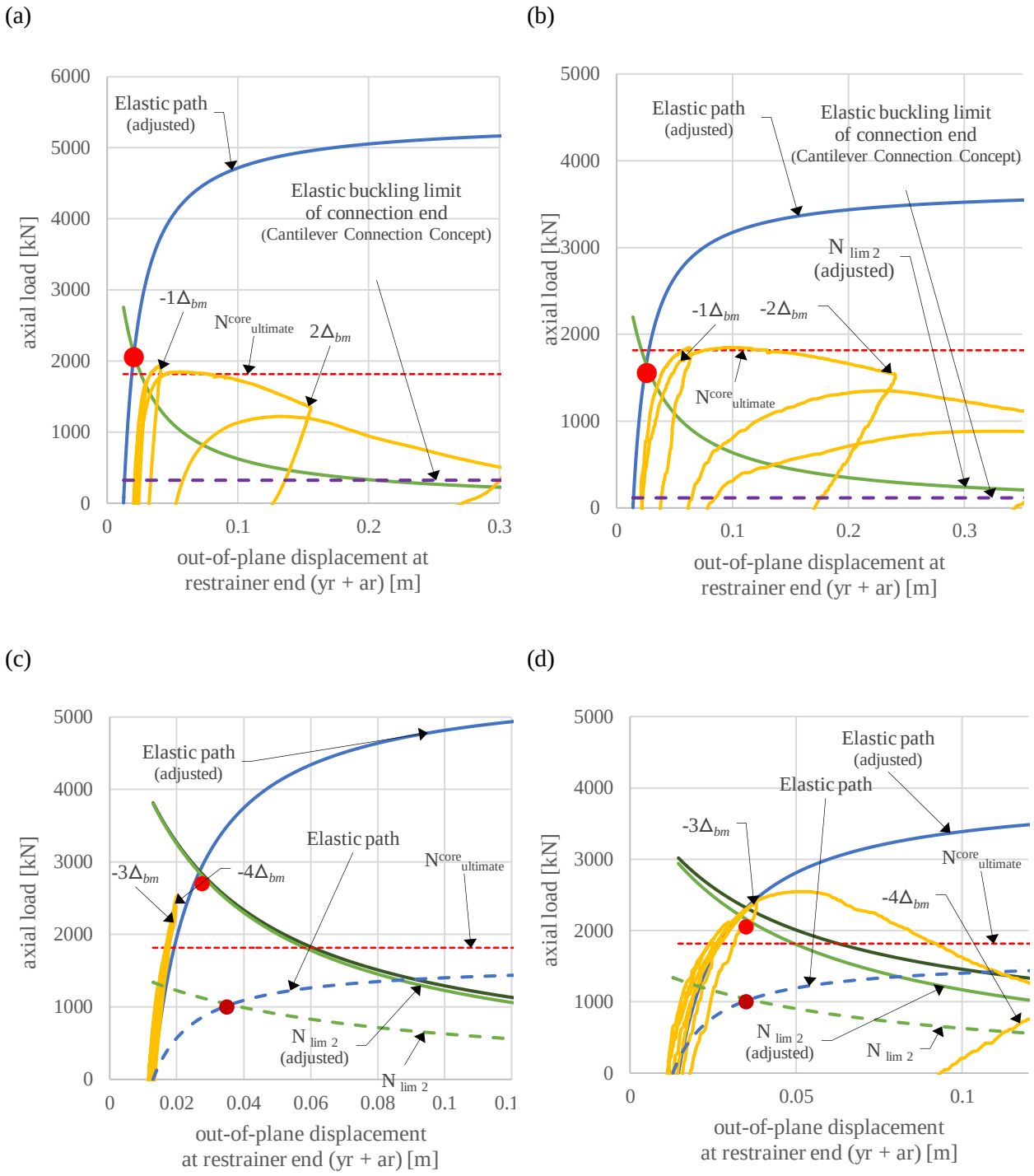

Figure 5-30. Out-of-plane stability (with gusset plate modification)
(a) D6.5b_0.5 GP1 (L_{in}/B_w=0.5), (b) D6.5b_0.5 GP1 (L_{in}/B_w=0.5)
(c) D6.5b_1.5 GP1 (L_{in}/B_w=1.5), (d) D6.5b_1.5 GP2 (L_{in}/B_w=1.5)

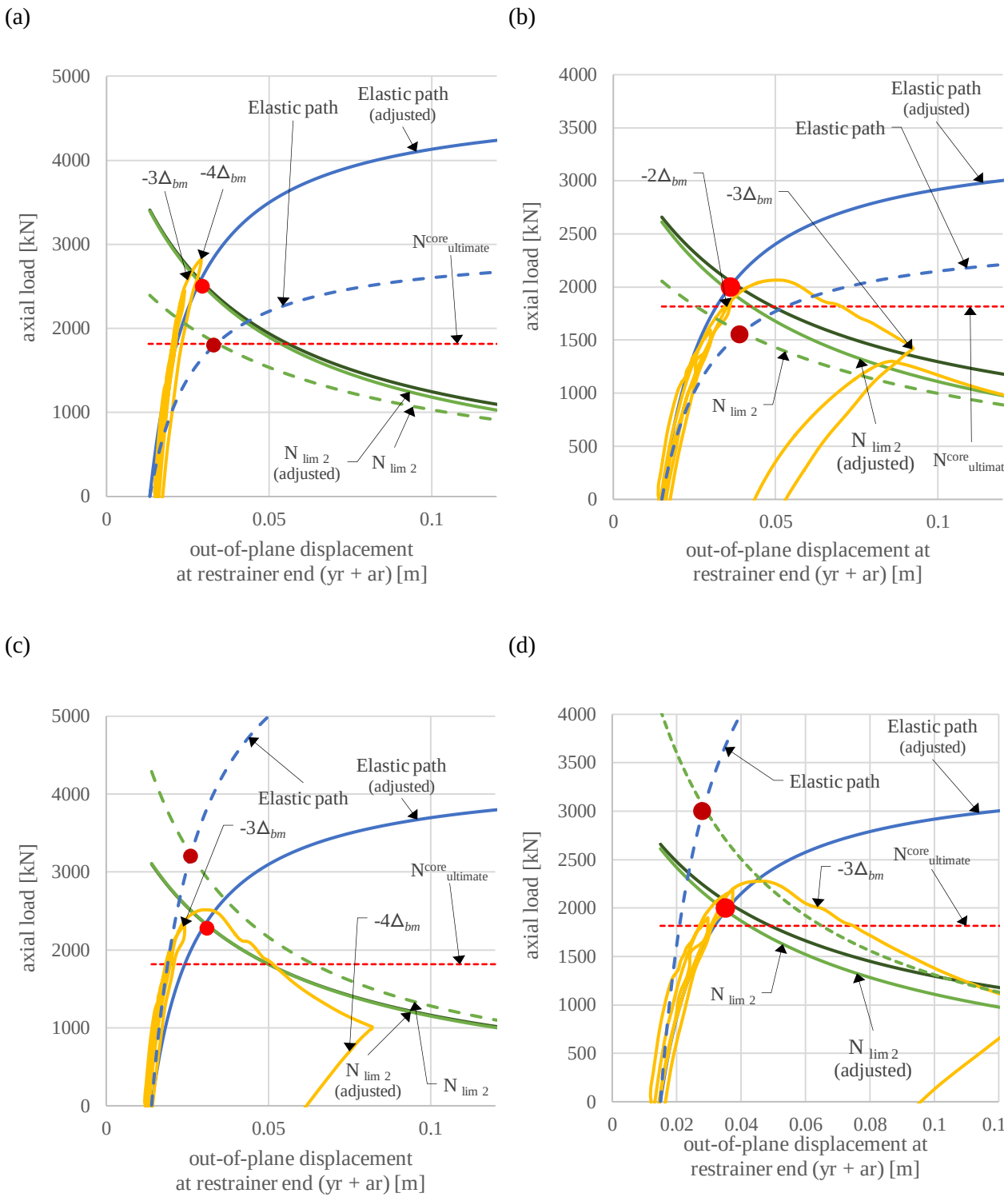

Figure 5-31. Out-of-plane stability (with gusset plate modification)
(a) D6.5b_2.5 GP1 (L_{in}/B_w=2.5), (b) D6.5b_2.5 GP2 (L_{in}/B_w=2.5)
(c) D6.5b_4.0 GP1 (L_{in}/B_w=4.0), (d) D6.5b_4.0 GP2 (L_{in}/B_w=4.0)

5.7 **Observations and discussion**

Following the simulations of each model presented in this chapter, it is of interest to make observations of each model and compare results against Takeuchi's method. A BRBF that maintains stability at interstorey drifts up to $\pm 3\Delta_{bm}$ should be deemed as desirable.

For all models, when comparing results of in-plane loading to bi-directional loading for the same magnitude, observations in Figure 5-21 through to Figure 5-24 showed bi-directional loading achieved the same or even higher relative displacements. However, when comparing only the in-plane component, it is noted that combined loading did not perform as well. This suggests that regardless of the direction of the earthquake, in-plane loading may be sufficient for BRBF test conditions but that eccentricity due to residual loading cannot be ignored.

A comparison of measured FEA results to the prediction made by Takeuchi's method are shown in Figure 5-28 through to**Error! Reference source not found.** A summary of the evaluations used in Takeuchi's method are presented in Table 5-5 and Table 5-6. It was found that Takeuchi's method for predicting out-of-plane stability was generally conservative. All FEA models (except for D6.5b 4.0 GP2) that exhibited loss of stability before reaching $\pm 3\Delta_{bm}$ were predicted by Takeuchi's method. However, for D6.5b 1.5 GP1 failure was predicted by Takeuchi's method when no stability issues were predicted in FEA.

Important to note: Takeuchi's method requires the initial geometric imperfection to be estimated. When using Equation 5.1 to calculate initial geometric imperfection, it was found that the displacements were unrealistic and required adjustment. Using Equation 5.1 meant initial imperfections reached up to 100 mm at the restrainer end ($\approx 2\Delta_{bm}$). These estimates would lead to very low and unrealistic stability limits. As an alternative, the initial imperfection at this location was set to ~15 mm. This corresponds to the distribution of displacements, according to the first mode of buckling with a peak displacement equal to ~0.5% of the brace length, as per Figure 5-20.

For the two D6.5b_0.5 models, the assumption made by the Takeuchi method is that when $L_{in}/B_w < 1$ the cruciform restrainer interface acts as pin connection once the core yields. This requires the Cantilever Connection Concept to be applied. As the gusset plates are unstiffened, Takeuchi's method predicts elastic buckling of the BRB end connection when calculating the critical buckling load of the BRBs end connection. However, FEA did not demonstrate pin-like behaviour, rather sufficient rotational stiffness was provided by the restrainer and casing such that displacements of $\pm 2\Delta_{bm}$ could be achieved for GP1 and $\pm 1\Delta_{bm}$ for GP2.

For the two D6.5b_1.5 models, the assumption made by the Takeuchi method is that when $1 < L_{in}/B_w < 2$, local yielding of the steel casing restrainer wall limits the moment carrying capacity of the plastic hinge zone at the restrainer end. However, FEA results show that the cement based grout maintains its strength and therefore provides increased moment capacity of this zone. For GP1, Takeuchi's method predicts early instability (< core yielding) whereas FEA results show displacements of $\pm 3\Delta_{bm}$ were achieved. For GP2, Takeuchi's method predicts early instability (< core yielding) whereas FEA results showed instability to occur in the lower gusset when approaching $-2\Delta_{bm}$.

When $L_{in}/B_w > 2$, the Takeuchi method assumes that under compressive loading, the restrainer is able to transfer moment to the cruciform. This means that the plastic bending strength of the cruciform section governs the moment capacity of the hinge at the restrainer end. The FEA results also show this to occur. For GP1, Takeuchi's method predicts instability to occur when the BRB core reaches ultimate strength. FEA results show displacements of $\pm 3\Delta_{bm}$ were achieved. For GP2, Takeuchi's method predicts early instability whereas FEA results showed instability to occur in the lower gusset when approaching $-2\Delta_{bm}$.

Again, for both the D6.5b_4.0 models, L_{in}/B_w is greater than 2. The Takeuchi method assumes that under compressive loading, the restrainer is able to transfer moment to the cruciform. The FEA results agrees with this assumption.

5.7.1 **Shortcomings and limitations of FEA predictions and Takeuchi's method**

The models and equations in this study are not without limitations for predicting BRB behaviour:

In addition to the limitations of the Chaboche plasticity model discussed in Section 2.2.1, rupture of the core, low cycle fatigue failure has not been validated. To capture the behaviour of grout used to form the restrainer, the concrete plasticity model described in Section 3.2.4 (Chapter 3) was used. This material model does not incorporate fully brittle material law for the constitutive description of concrete behaviour and could be a limitation in the FEA models. In the FEA modelling, when the concrete restrainer begins to yield, the gradient of force-displacement flattens out (Figure 5-33). However, realistic post-yielding behaviour of concrete would cause the cruciform to bend at a faster rate, which would lead to a greater reduction in the stiffness.

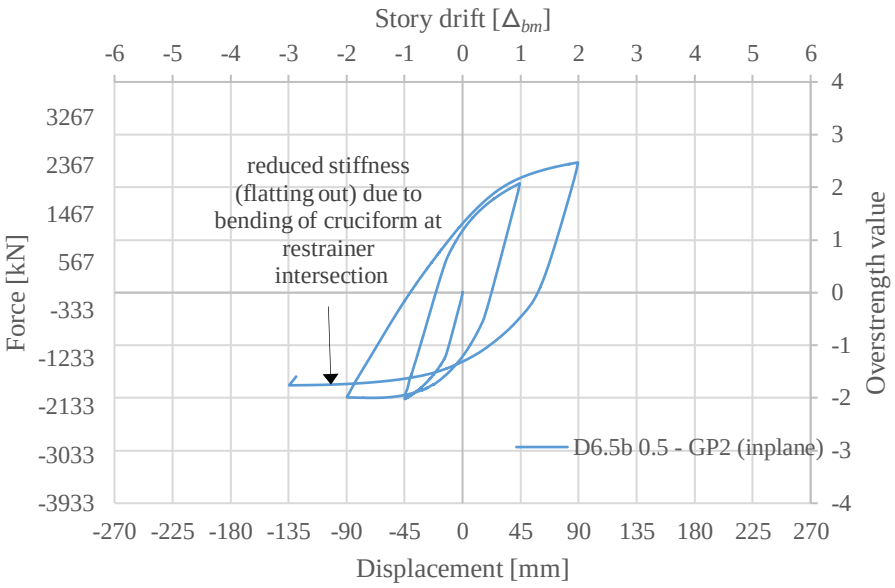

Figure 5-32. Example of how concrete material model effects results. D6.5b_0.5 GP2

It is also of interest to study the initiation of the different failure mechanisms. This would improve upon the assumptions made by Takeuchi's method. Additional sensitivity/parametric studies could improve our understanding of when and under what conditions particular failure mechanisms govern. This could be achieved through physical testing and modelling of more BRB designs and variants, increasing the length of the insert zone more gradually, and for different BRB designs.

One aspect not captured by the Takeuchi's method is how the length of the BRB changes as compressive loading increases. As a BRB undergoes compressive loading, the cruciform section pushes into the restrainer, effectively shortening the BRB. For the BRB models in this study, the change in length could be as much as 133 mm (half the displacement equivalent to $4\Delta_{bm}$). This could change the predicted failure mechanism as set by the L_{in}/ B_{cruc} ratio. According to Matsui et al. (2010), as the L_{in}/ B_{cruc} ratio increases, the ability for the cruciform to transfer a moment to the restrainer increases therefore increasing the stability limit. The elastic buckling capacity of the system is also increased by having a greater L_{in}/ B_{cruc} ratio and a shorter BRB. This change in length effects all BRBs but particularly those with a low initial L_{in}/ B_{cruc} ratio.

The effect repeated cycles have on stability is another feature not well captured by Takeuchi's method. Over repeated and increased cycles of loading, if the stability limit is above $N^{core}{}_{ultimate}$, Takeuchi's method assumes the BRB system will remain on the elastic path. However, according to the FEA modelling results, the load path can accumulate residual displacement upon each cycle, effectively creeping along the $N^{core}{}_{ultimate}$ limit. This can lead to instability even if the intersection of the elastic path and load limit path is above $N^{core}{}_{ultimate}$. Figure 5-33 shows how instability can occur after the first cycle, even though the stable limit is above $N^{core}{}_{ultimate.}$ To reduce the chance of instability in later cycles, it is recommended that the stability limit is adjusted such that the lowest load limit path does not drop below the ultimate compressive load of the BRB core until out-of-displacements of $2.0\Delta_{bm}$ are achieved at the restrainer end, as demonstrated in Figure 5-34.

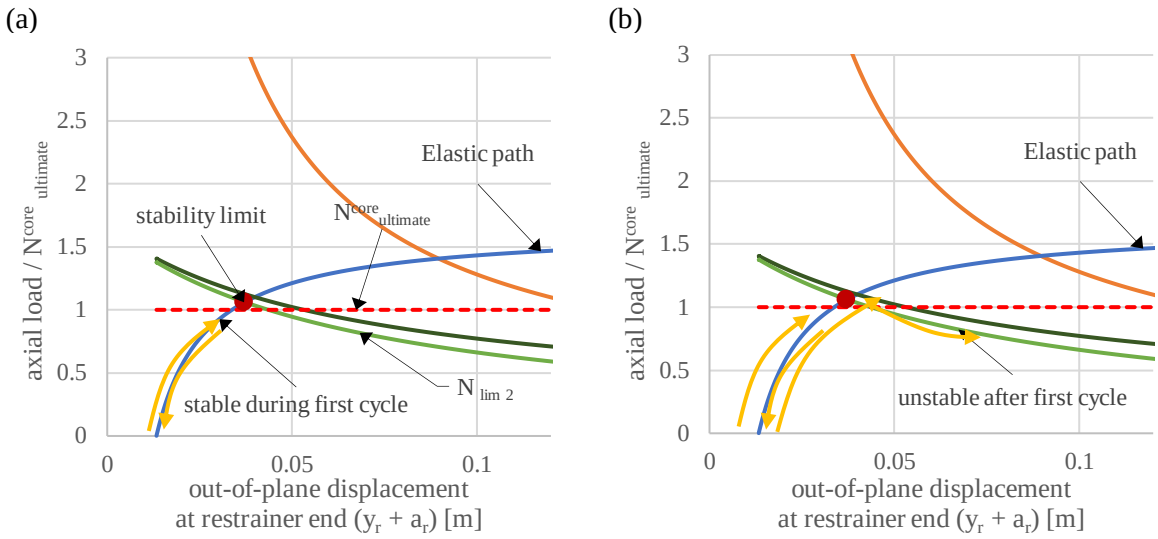

Figure 5-33. BRBF stability limit concept (Takeuchi et al. 2017)
(a) Stable during first cycle (N_{cu} < stability limit), (b) Unstable after first cycle (N_{cu} < stability limit)

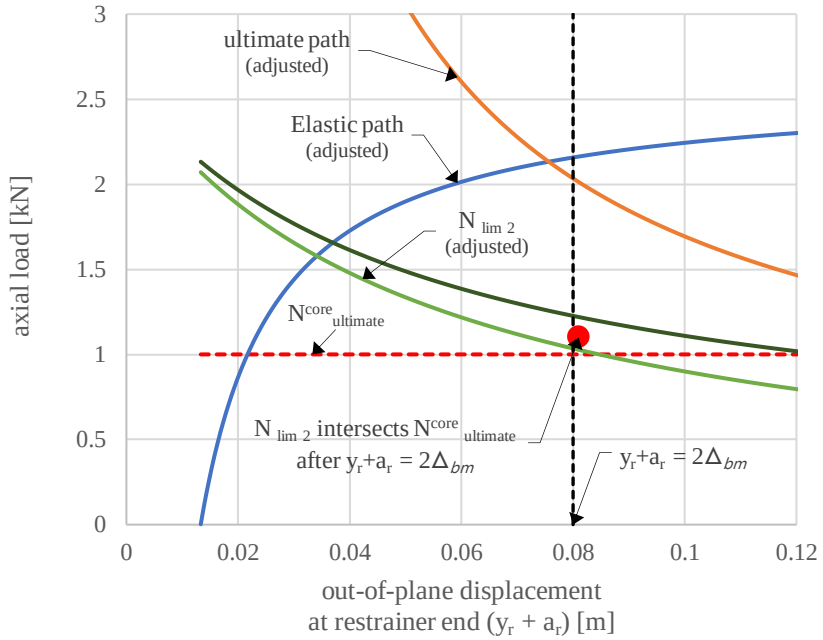

Figure 5-34. Takeuchi's BRB stability model with proposed new stability limit rule

As stated, an analytical method that can be used in combination with prequalification testing is an attractive alternative to full-scale testing. Takeuchi's method has been shown to generally provide conservative results. Although, this study is not a sensitivity study it recommends the following in order to improve upon the Takeuchi method for assessing out-of-plane stability of BRBFs.

- Develop more detailed FEA models to pin-point when particular failure mechanisms govern and under what design criteria this occurs.

- Modify the equations in Matsui et al. (2010) to better predict the maximum elastic buckling limit for BRBF designs.

- Increase the stability limit to reduce the change of instability at large displacements. To achieve this, the lowest limit load path should not drop below the ultimate compressive load of the BRB core until out-of-displacements of $2.0\Delta_{bm}$ are achieved at the restrainer end.

5.8 **Conclusion**

A previously developed FE model was used to demonstrate the capability of detailed FE modelling to study the cyclic performance of a subassemblage test representing a diagonal BRBF with bolted connections. One BRB design with four variants were modelled. Each BRB varied the length that the cruciform section inserts into the restrainer, all other variables remained the same. In addition, the suitability of using NZS 3404 to design compact or semi-slender gusset plates for each BRB was investigated. The effect of bi-directional loading was also evaluated. Results were compared against Takeuchi's method for assessing the out-of-plane stability of BRBFs. Based on the FEA results from this study, the following observations and recommendations were made.

1 When compact gusset plates were designed according to NZS 3404, all designs achieved $\pm 3.0\Delta_{bm}$ expect when $L_{in}/ B_{cruc} = 0.5$ where the bending of compact gusset at $1.5\Delta_{bm}$ limited performance. For the semi-slender gusset plates designed according to NZS 3404, sway buckling limited BRBF performance to $\pm 1.0\Delta_{bm}$ according to predictions of the FEA models.

2 It was found that increasing the thickness of the gusset plates according to Thornton's method for gusset plate design (Court-Patience 2020) improved overall performance for all variants. All models were able to achieve $\pm 3.0\Delta_{bm}$ expect for models when $L_{in}/ B_{cruc} = 0.5$. This suggests that out-of-plane stiffeners may not be required for all BRBFs designs.

3 The effect of bi-directional loading was not found to significantly affect out-of-plane stability for models in this study.

4 For the cases considered, Takeuchi's method was found to be conservative in predicting out-of-plane stability of each BRBF model (except for D6.5b 4.0 GP2). However, for D6.5b 1.5 GP1, failure was predicted when no stability issues were present.

5 The accuracy of Takeuchi's method was also improved when the critical elastic buckling load from the FEA models was used to estimate the critical bucking load, instead of the equations based on the differential equation method that are traditionally used in Takeuchi's method.

6 To further broaden the applicability of Takeuchi's method, more models and more details are required to better understand when particular failure mechanisms govern and under what design criteria these occur.

7 To reduce the chance of instability occurring at large displacements, instead of assuming stability is maintained when the intersection of the elastic path and lowest limit load path is above the ultimate compressive load, it is recommended the lowest limit state should not drop below the ultimate compressive load of the core until out-of-plane displacements of $2.0\Delta_{bm}$ at the restrainer end are achieved.

5.9 **References**

ANSI/AISC (2010). Seismic provisions for structural steel buildings - ANSI/AISC. One East Wacker Drive, Suite 700, Chicago, Illinois 60601-1802, American Institute of Steel Construction

Architectural Institute of Japan (AIJ) (2009). Recommendations for stability design of steel structures. Japan, AIJ 74-79. (in Japanese)

Architectural Institute of Japan (AIJ) (2013). Stability problems of steel structures. Japan, AIJ 74-79. (in Japanese)

Architectural Institute of Japan (AIJ) (2014). Recommended provisions for seismic damping systems applied to steel structures. Japan, AIJ 24-59. (in Japanese)

Chou, C.-C. and J.-H. Liu (2012). Frame and brace action forces on steel corner gusset plate connections in buckling-restrained braced frames. Earthquake Spectra **28**(2): 531-551

Dassault Systems (2014). ABAQUS 6.14 Analysis User's Guide, Volume IV: Elements

Field, C. (2003). Simulation of full-scale siesmic-resistanct structural frame tests using LS-DYNA 960 Implicit solver. LS-DYNA European Conference

Hikino, T., T. Okazaki, L. Kajiwara and M. Nakashima (2013). Out-of-plane stability of buckling-restrained braces placed in chevron arrangement. Journal of Structural Engineering **November**(139): 1812-1822

Ida, M., T. Takeuchi, R. Matsui and Y. Konishi (2013). Stability assessment of buckling-restrained braces taking connection in account (Part. 2 Evaluation of rotational stiffness of brace connections). Summaries of technical papers of Annual Meeting Architectural Institute of Japan.(in Japanese)

Kinoshita, T., Y. Koetaka and I. L. Inoue, K. (2008). Out-of-plane stiffness and yield strength of cruciform connections for buckling-restrained braces. AIJ Journal of Structural and Construction Engineering **73**: 1865-1873.(in Japanese)

Koetaka, Y. K., T. and K. L. Inoue, K. (2008). Critera of buckling-restrained braces to prevent out-of-plane buckling. 14th World Conference on Earthquake Engineering

Mahin, S., P. Uriz, I. Aiken, C. Field and E. Ko (2004). Seismic performance of buckling-restrained braced frame systems. 13th World Conference on Earthquake Engineering. Vancouver, B.C., Canada

Matsui, R., T. Takeuchi, L. Nishimoto, S. Talahashi and T. Ohyama (2010). Effective buckling length of buckling-restrained braces considering rotational stiffness at restrainer ends. 5th International Conference on Earthquake Engineering (5ICEE). Tokyo Institute of Technology, Tokyo, Japan

Pettinga, D. S., M. and K. J. Elwood (2019). The serviceability of reesilient seismic design in New Zealand. 2019 Pacific Conference on Earthquake Engineering. Auckland, New Zealand

Saeki, E., Y. Maeda, H. Nakamura, M. Midorikawa and A. Wada (1995). Experimental study on practical-scale unbonded braces. AIJ Journal of Structural and Construction Engineering **60**: 149-158.(in Japanese)

Takeuchi, T., H. Ozaki, R. Matsui and F. Sutcu (2013). Out-of-plane stability of buckling-restrained braces including moment transfer capacity. Earthquake Engineering & Structural Dynamics **43**: 851–869

Takeuchi, T. and A. Wada (2017). Buckling-restrained braces and applications. Tokyo, Japan, The Japan Society of Seismic Isolation.

Timoshenko and Gere (1965). Theory of elastic stability, McGraw Hill.

Tsai, C.-Y., K.-C. Lin, K. C. Tsai, L.-W. Chen and A.-C. Wu (2018). Seismic performance analysis of BRBs and gussets in a full-scale 2-story BRB-RCF specimen. Earthquake Engineering & Structural Dynamics: 1-24

Tsai, K. C. and P.-O. Hsiao (2008). Pseudo-dynamic test of a full-scale CFT/BRB frame—Part II: Seismic performance of buckling-restrained braces and connections. Earthquake Engineering & Structural Dynamics **37**: 1099-1115

Tsai, K. C., Y. C. W. Huang, C.S., T. Shurau and H. Nakamura (2002). Experimental tests of large scale buckling-restrained braces and frames. 2nd Passive Control Symposium, Tokyo Institute of Technology

Westeneng, B. (2016). Buckling behaviour of gusset plates in buckling-restrained braced frames. Masters of Engineering, University of Canterbury.

6 SUMMARY OF THESIS

The research presented is this thesis initially reviewed the application of buckling-restrained braces (BRBs) in New Zealand. Although BRBs have shown to perform well in uniaxial testing providing stable hysteretic performance (Black et al. 2002, Dunai et al. 2011), there is not yet any documented guidance or specific instructions in regulatory standards for the design of buckling-restrained braced frames (BRBFs). This makes it difficult for engineers to anticipate all the possible stability and strength issues within a system and actively mitigate them in each design. To help ensure BRBF designs perform as intended, a peer review and physical testing are currently required to gain building compliance in New Zealand. As such, prequalification testing of five commercially available BRB designs that have now been installed in medium to high-rise buildings throughout New Zealand is presented (Chapter 2). This type of testing isolates the brace, checking the design, manufacture and materials under ideal conditions.

Once a BRB design is proven, it is important to assess both local and combined global stability of the BRB and its frame elements. Checking stability conditions prior to installation is particularly important as there is limited data of BRBF performance in actual earthquake events. Subassemblage testing is one way to access this performance. Again, previous test results have shown BRBs can perform well in full-frame systems provided the gusseted connection zones are adequately designed (Watanabe et al. 1988, Wada et al. 1989, Watanabe 1992, Konami et al. 1999, Hasegawa et al. 2000, Iwata et al. 2000, Tremblay et al. 2006, Palmer et al. 2014). However, each subassemblage test investigates only one specific set of design features.

As it is cost prohibitive to test every BRBF variation, alternative methods to check global and local stability of a BRBF are required. Japan and Taiwan have developed methods aimed to ensure safe BRBF design (Takeuchi et al. 2013, NCREE 2014). Although these methods have only been validated over a selection few designs, they provide a basis for other methods to be developed. To further develop these method to cater for all the design options used worldwide we must first study each component in a BRBF and how they interact together under cyclic loading. Continuum modelling offers a way to study the local deformation and stress-strain behaviour of BRBs. However, there are significant challenges in developing computer models that capture realistic BRB behaviour. Specifically, the interaction of the core and the restrainer is a complex nonlinear phenomenon that has limited the development of such detailed BRB computer models. As such, a novel strategy for modelling generic BRBs is presented (Chapter 3). Models using this strategy capture the combination of instability, nonlinear constitutive laws and frictional contact. The development of nonlinear material and contact models were found to be important aspects that affect accuracy and convergence in each model. The Chaboche method, using six backstress curves is used to characterize the combined kinematic and isotropic hardening exhibited in a BRBs steel core. A simplified approach was developed to model the

contact interaction between the restrainer and the core. The methodology sought to minimize computational expense for this highly nonlinear system. The strategy was validated by simulating the prequalification testing presented in Chapter 2.

Next, in Chapter 4, options and design tools used to size gusset plates are explored. Finite element modelling was used to study the development of yielding, buckling and plastic collapse behaviour of a brace end bolted to a series of corner gusset plates. In total 184 variations of gusset plate geometries were modelled using Abaqus®. It was found that some of the underlaying assumptions used in the design of gusset plates do not accurately represent the behaviour of all gusset plate geometries. Upon comparing FEA modelling results to current design methods, it was found that the Whitmore width is generally un-conservative in predicting initial yielding of gusset plates. FEA observations of gusset plate behaviour were used to propose modifications to current methods used to calculate the yield area and compressive strength of gusset plates.

Lastly, Chapter 5 demonstrates the capability of FEA to study to the performance of a subassemblage test under cyclic loading – resembling that of a ground storey frame with a diagonal BRB with bolted connections. A series of detailed models using the strategy presented in Chapter 3 were developed. Detailed modeling of this nature is a first with only simplier approaches used by other researchers. Initially, a total of eight BRBF variants were modelled in Abaqus®. To capture the different failure mechanisms identified in Takeuchi et al. (2017), models varied the length that the cruciform (non-yielding) section inserts into the restrainer. Results indicate that when gusset plates are designed according to NZS 3404, the cyclic performance of each BRBF was limited. Increasing the thickness of the gusset plates according to modifications discussed in Chapter 4, improved the overall performance for all variants (except when $L_{in}/B_{cruc} = 0.5$). The effect of bi-directional loading was not found to significantly affect out-of-plane stability. Takeuchi's method was found to be generally conservative in predicting out-of-plane stability of each BRBF model. Recommendations to improve the accuracy of Takeuchi's method are also provided.

The outcomes from this thesis should be helpful for BRB manufacturers, researchers, and in the development of further design guidance of BRBFs. This project partnered with the Building Research Association of New Zealand (BRANZ) and was supported by Callaghan Innovation to ensure outcomes were related to industry requirements.

7 SUGGESTIONS FOR FUTURE RESEARCH

The outcomes and methods discussed in this research can be used as a foundation for future research. Presented in the following subsections are some ideas for ongoing research in this field.

7.1 **Characterising rotational stiffness of gussetted connection zones**

Discussed in Chapter 2 is how researchers in Japan have developed an alternative approach to assess the stability of a BRBF system (Takeuchi et al. 2017). The approach uses analytical methods to assess stability under different collapse mechanisms by focusing on moment transfer. The methods are based on two stability design concepts proposed by Architectural Institute of Japan (AIJ) (2009) as shown in Figure 1-17.These methods make assumptions about the BRB and rigidity of the gusseted connection zone. The suitability of a gusseted connection zone (specifically its rigidity) depends on the ability of the BRB to transfer moment to the end connections. To solve the set of equations describing each of the concepts depicted in Figure 6.1, designers need the rotational stiffness of both the adjacent frame elements and gusset plate. This is far from straight forward, requiring testing or finite element modeling. Published research only contains the required stiffness properties for a select few tested designs, all of which have some form of stiffeners (Matsui et al. 2010, Takeuchi et al. 2017). As the flexibility and geometries of gusseted connections varies greatly internationally, more research and analysis is required before these methods can be adopted outside of Japan. The FEA study in Chapter 4 could be expanded to obtain rotational stiffness properties among different gusset plate types.

7.2 **Yeilding and buckling analysis of pinned gusset plate types**

For gusset plates that have a BRB connected via a pinned connection there are no instructions in NZS3404 for dealing with buckling (Standards New Zealand 1997). Currently, bearing and pin pullout failure are the only considerations. This is likely because until recently bracing that used pinned joints were often governed by tension loading. The implementation of BRBs means design codes need to consider load actions for all gusset connection types. The FEA study in Chapter 4 could be expanded to include pinned type gusset plates.

7.3 **Investigating the replaceability of BRBs**

BRBs are marketed as a low damage system that can be easily replaced following a moderate/severe earthquake event. However, the exact process and cost of replacing these devices is unclear. As BRBs are relatively new and because large earthquakes are infrequent there are not yet any cases of earthquake damaged building with BRBs outside of Japan.

Although the steel core of a BRB is designed to be the yielding section, the rotation demands expected in realistic earthquakes loadings can cause residual eccentricity and plastic damage to other sections within the frame (aside from the brace). This damage makes replacing the BRB with an off the shelf BRB challenging. When designing BRBFs, ideally, gusseted connections are stiffened to reduce rotation. However, this can be uneconomical and have less ascetic appeal. This means not only the BRB but the gusseted zone may need to be replaced. If this were the case then repair costs and down time would significantly increase and be similar to fixing traditional forms of braced frames systems. Physical testing and modelling effort could help evaluate methods for replacing BRBs while minimising damage to other structural components. Do we want the gusset plate to be the sacrificial piece or do we want really stiff (more expensive) gusset plates and let bending only occur at the restrainer interface of the BRB? It would also be of interest to investigate the residual ductility of a BRB following a moderate to severe earthquake event. This would help engineers decide if replacing certain BRBs is necessary.

7.4 Estimating the onset of higher mode buckling

The difficulty to capture stress-strain data inside the restrainer during physical testing means there is a lack of understanding of how strain develops along the core of a BRB. The restrainer is designed to confine transverse displacements of the core and prevent global buckling of the BRB core. However, the slender nature of the core causing transverse displacements that can lead to constrained buckling at very low axial compressive loads and can progress through several buckling modes. The greater the curvature associated with the constrained buckling, the higher the local strains are, which could lead to tensile failure. Figure 3-27 is presented here again in Figure 3-28a. This figure shows snapshots of the strain profile at the outer edge along the length of the core for a series of cycles at peak tensile and compressive displacement loads. Figure 3-28a indicates high levels of strain (up to 25%) for BRB 2A that occur closer to the ends as a result of constrained buckling. However, Figure 3-28b shows the strain profile for BRB 6.5a and even through constrained buckling occurs the maximum strain is only 8%, suggesting this BRB is less likely to failure in tension.

It is off interest to estimate where and how high localization of strain occur. Predicting the onset and degree of higher mode buckling could help BRB designers select geometries that minimize high localized strain and therefore reduce the chance of failure associated with this behaviour. The ratio of the thickness of the debonding material and the thickness of the BRB core is thought to be a key factor.

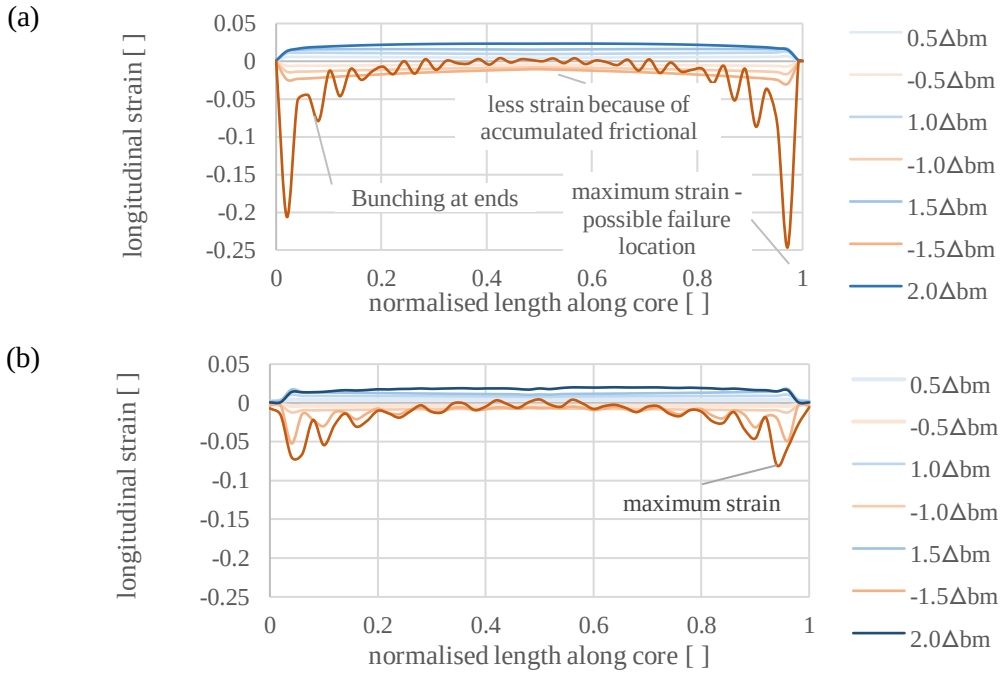

Figure 7-1. Strain profile along core at first cycle of each target displacement (a) BRB 2A, (b) BRB 6.5a

7.5 **References**

Architectural Institute of Japan (AIJ) (2009). Recommendations for stability design of steel structures. Japan, AIJ 74-79. (in Japanese)

Black, C., N. Makris and I. Aiken (2002). Component testing, stability analysis and characterization of buckling-restrained unbonded braces, Pacific Earthquake Engineering Research Center

Dunai, L., L. Kaltenbach, M. Kallo, M. Kachichian and A. Halasz (2011). Type testing of buckling-restrained braces according to EN 15129, Budapest University of Technology and Economics

Hasegawa, H., T. Takeuchi, Y. Nakata, M. Iwata, S. Yamada and H. Akiyama (2000). Experimental study on dynamic behavior of unbonded braces. AIJ Journal of Technology and Design - in Japanese: 103-106

Iwata, M. and T. W. Kato, A. (2000). Buckling-restrained braces as hysteretic dampers. Third International Conference on Behavior of Steel Structures in Seismic Areas (STESSA 2000). Montreal, Canada

Konami, S., H. Sugihara, M. Narikawa, Y. H. Huan, Y. Maeda and A. Wada (1999). Seismic performance of moment resisting frames with hysteretic damper. Annual Meeting of the Architectural Institute of Japan (in Japanese)

Matsui, R., T. Takeuchi, L. Nishimoto, S. Talahashi and T. Ohyama (2010). Effective buckling length of buckling-restrained braces considering rotational stiffness at restrainer ends. 5th International Conference on Earthquake Engineering (5ICEE). Tokyo Institute of Technology, Tokyo, Japan

NCREE (2014). National Center for Research on Earthquake Engineering - User Guide for BOD: Buckling-restrained brace and connection design procedure. Taiwan, National Taiwan University

Palmer, K. D., A. S. Christopulos, D. E. Lehman and C. W. Roeder (2014). Experimental evaluation of cyclically loaded, large-scale, planar and 3-d buckling-restrained braced frames. Journal of Constructional Steel Research **101**: 415-425

Standards New Zealand (1997). NZS 3404:1997 Steel Structures Standard. Wellington, New Zealand

Takeuchi, T., H. Ozaki, R. Matsui and F. Sutcu (2013). Out-of-plane stability of buckling-restrained braces including moment transfer capacity. Earthquake Engineering & Structural Dynamics **43**: 851–869

Takeuchi, T. and A. Wada (2017). Buckling-restrained braces and applications. Tokyo, Japan, The Japan Society of Seismic Isolation.

Tremblay, R., R. Bolduc, R. Neville and R. DeVall (2006). Seismic testing and performance of buckling-restrained bracing systems. Canadian Journal of Civil Engineering **33**

Wada, A., E. Seaki, T. Takeuchi and A. Watanabe (1989). Development of unbonded brace, A Nippon Steel Publication. **115:** 12

Watanabe, A., Y. Hitomi, E. Saeki, A. Wada and M. Fujimoto (1988). Properties of brace encased in buckling-restraining concrete and steel tube. Ninth World Conference on Earthquake Engineering, Tokyo-Kyoto

Watanabe, A. N., H. (1992). Study on the behavior of buildings using steel with low yield point. Proceedings of Tenth World Conference on Earthquake Engineering. Rotterdam**:** 4468-4468

8 APPENDIX A (BRB DESIGN DRAWINGS)

8.1 **Specimen – BRB 6.5**

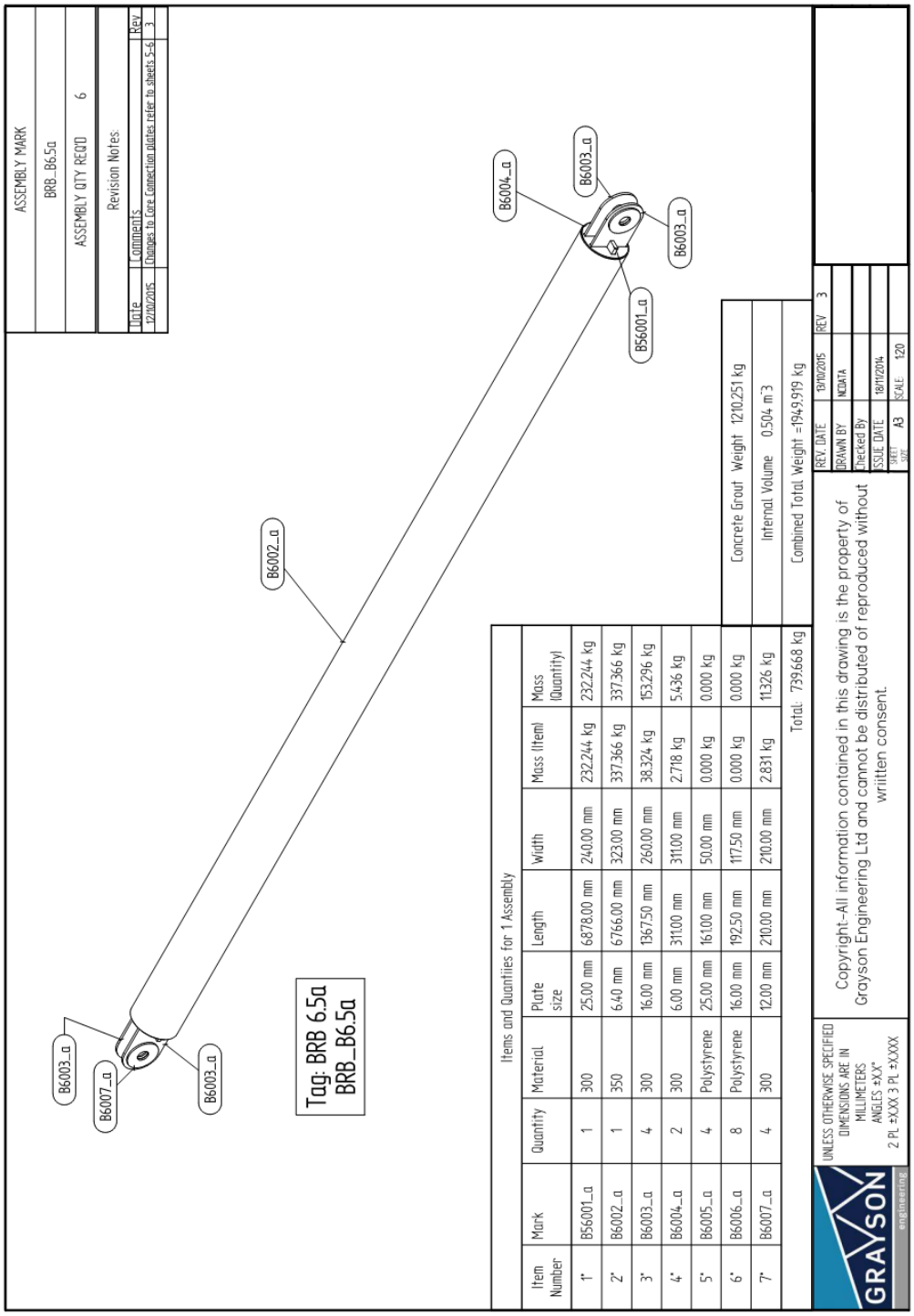

ASSEMBLY MARK
BRB_B6.5a
ASSEMBLY QTY REQ'D 6

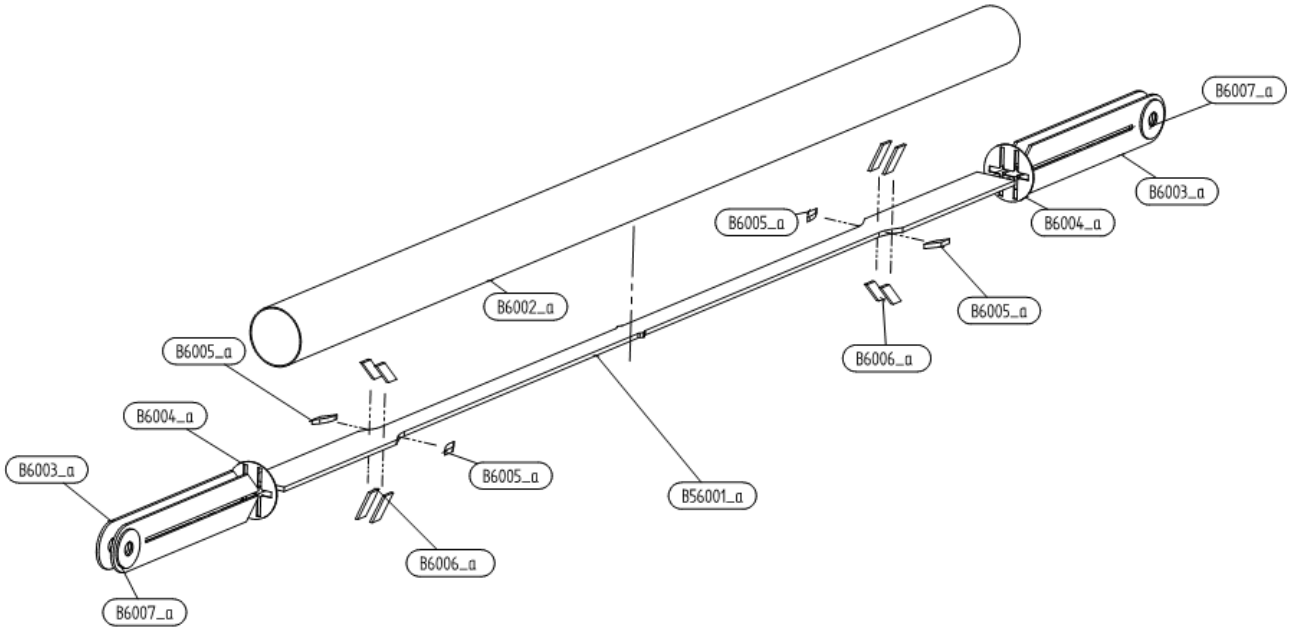

GRAYSON engineering

UNLESS OTHERWISE SPECIFIED
DIMENSIONS ARE IN
MILLIMETERS
ANGLES ±X.X°
2 PL ±X.XX 3 PL ±X.XXX

REV. DATE	13/10/2015	REV 3
DRAWN BY	NCDATA	
Checked By		
ISSUE DATE	18/11/2014	
SHEET SIZE A3	SCALE: 1:20	

ASSEMBLY MARK
BRB_B6.5a
ASSEMBLY QTY REQ'D 6

Revision Notes

Date	Comments	Rev No
5/10/2015	Change to bonding length- was 75mm each side	2

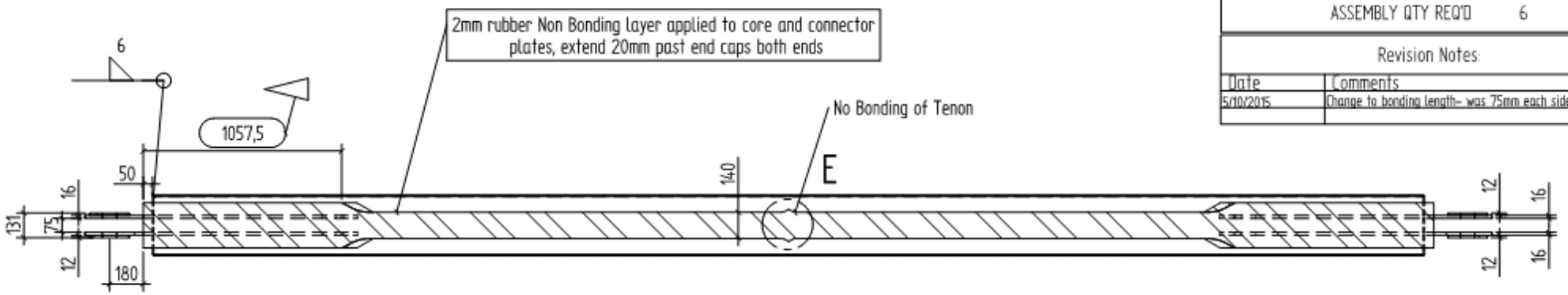

SECTION C-C

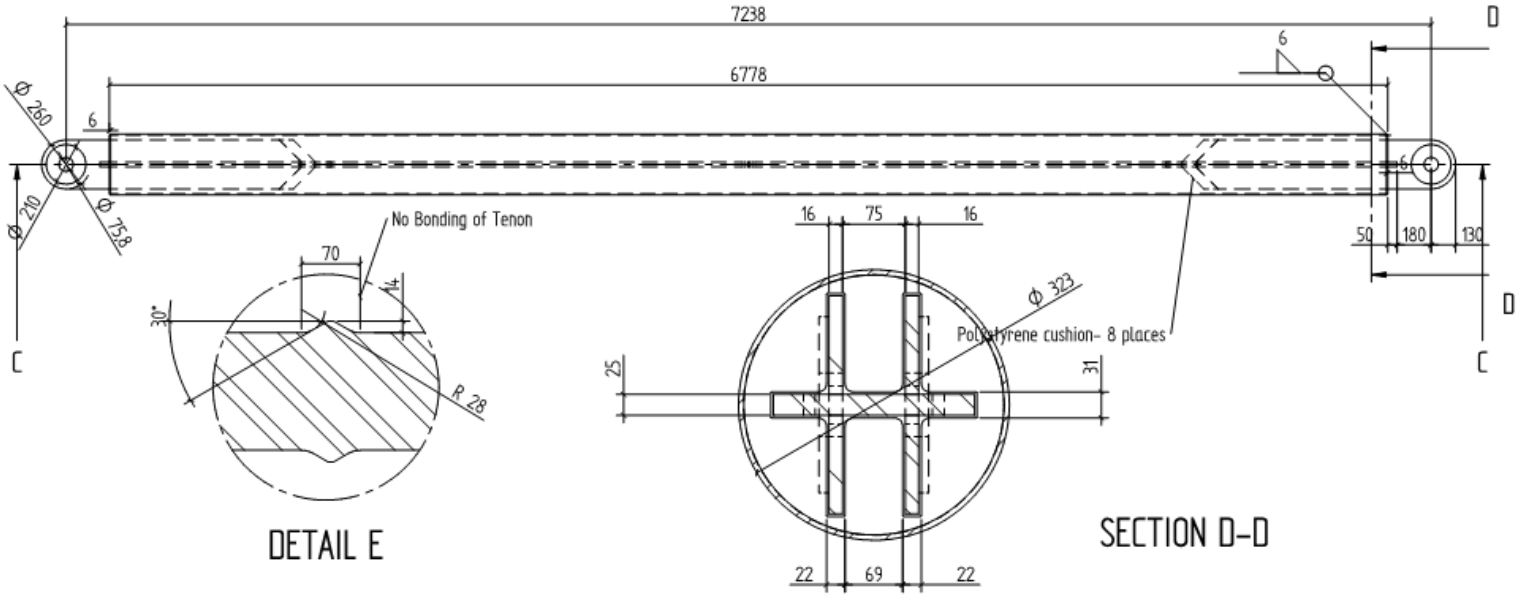

DETAIL E

SECTION D-D

REV. DATE	13/10/2015	REV	3
DRAWN BY	MCDATA		
Checked By			
ISSUE DATE	18/11/2014		
SHEET SIZE	A3	SCALE:	1:22.22

GRAYSON engineering

UNLESS OTHERWISE SPECIFIED DIMENSIONS ARE IN MILLIMETERS ANGLES ±X.X° 2 PL ±X.XX 3 PL ±X.XXX

ASSEMBLY MARK		
BRB_B6.5a		
ASSEMBLY QTY REQ'D 6		
Revision Notes:		
Date	Comments	Rev No
12/10/2015	Core plates section changed	3

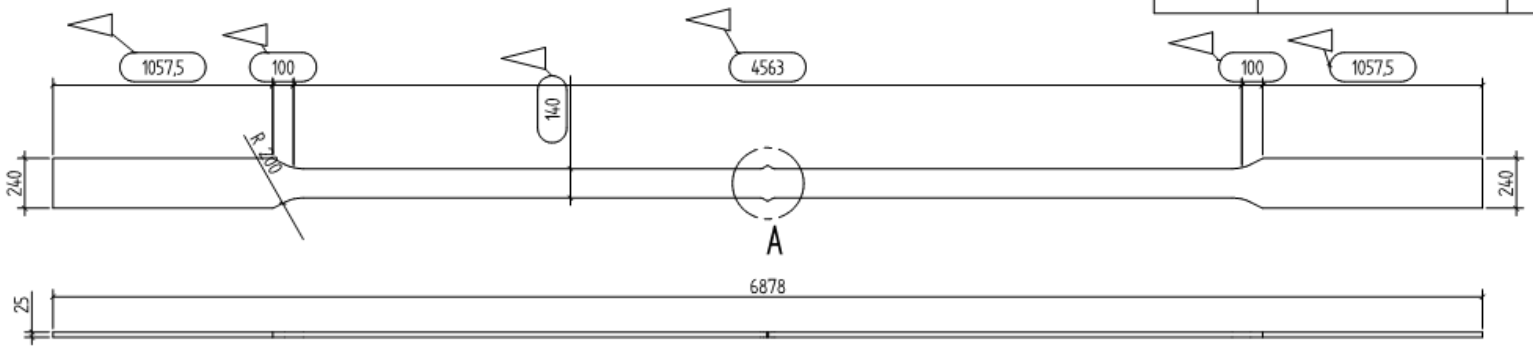

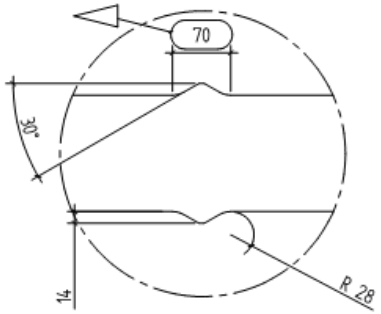

DETAIL A

Material: Grade 300
Mark: B56001_a
Qty Required 6 each

Material Heat # _____

Mark	Quanity	Grade	Plate Size	Length	Width	Mass
B56001_a	6	300	25.00 mm	6878.00 mm	240.00 mm	232.244 kg
MATERIAL LIST FOR WORKSHOP						

GRAYSON engineering

UNLESS OTHERWISE SPECIFIED DIMENSIONS ARE IN MILLIMETERS
ANGLES ±X.X°
2 PL ±X.XX 3 PL ±X.XXX

REV. DATE	13/10/2015	REV	3
DRAWN BY	NCDATA		
Checked By			
ISSUE DATE	18/11/2014		
SHEET SIZE	A3	SCALE:	1:20

ASSEMBLY MARK
BRB_B6.5a
ASSEMBLY QTY REQ'D 6

Revision Notes:

Date	Comments	Rev
12/10/2015	Length Change to match core brace	3

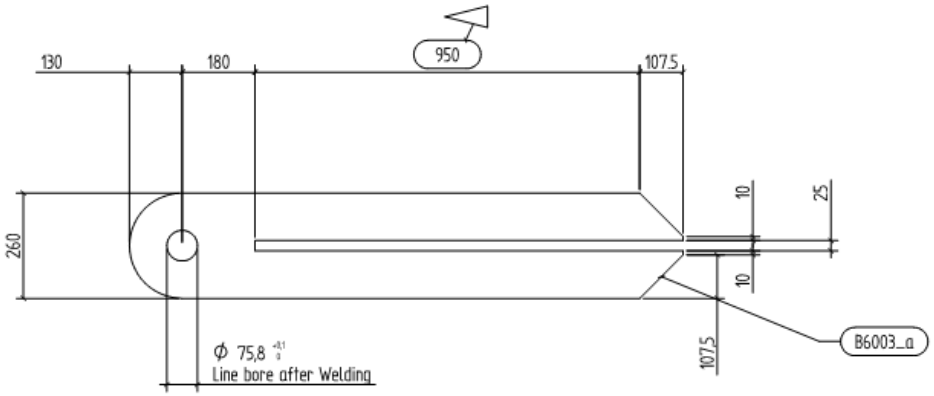

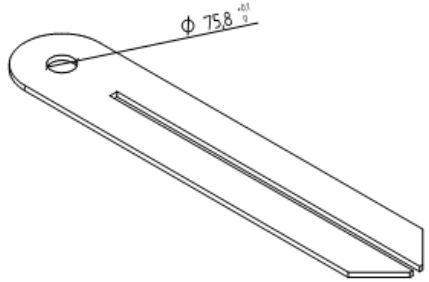

Material: Grade 300
Mark: B6003_a
Qty Required = 24

Material Heat #_____

Mark	Quanity	Grade	Plate Size	Length	Width	Mass
B6003_a	24	300	16.00 mm	1367.50 mm	260.00 mm	38.324 kg

MATERIAL LIST FOR WORKSHOP

GRAYSON engineering

UNLESS OTHERWISE SPECIFIED
DIMENSIONS ARE IN
MILLIMETERS
ANGLES ±X.X°
2 PL ±X.XX 3 PL ±X.XXX

REV. DATE	13/10/2015	REV 3
DRAWN BY	NCDATA	
Checked By		
ISSUE DATE	18/11/2014	
SHEET SIZE A3	SCALE: 1:10	

8.2 **Specimen – BRB S3**

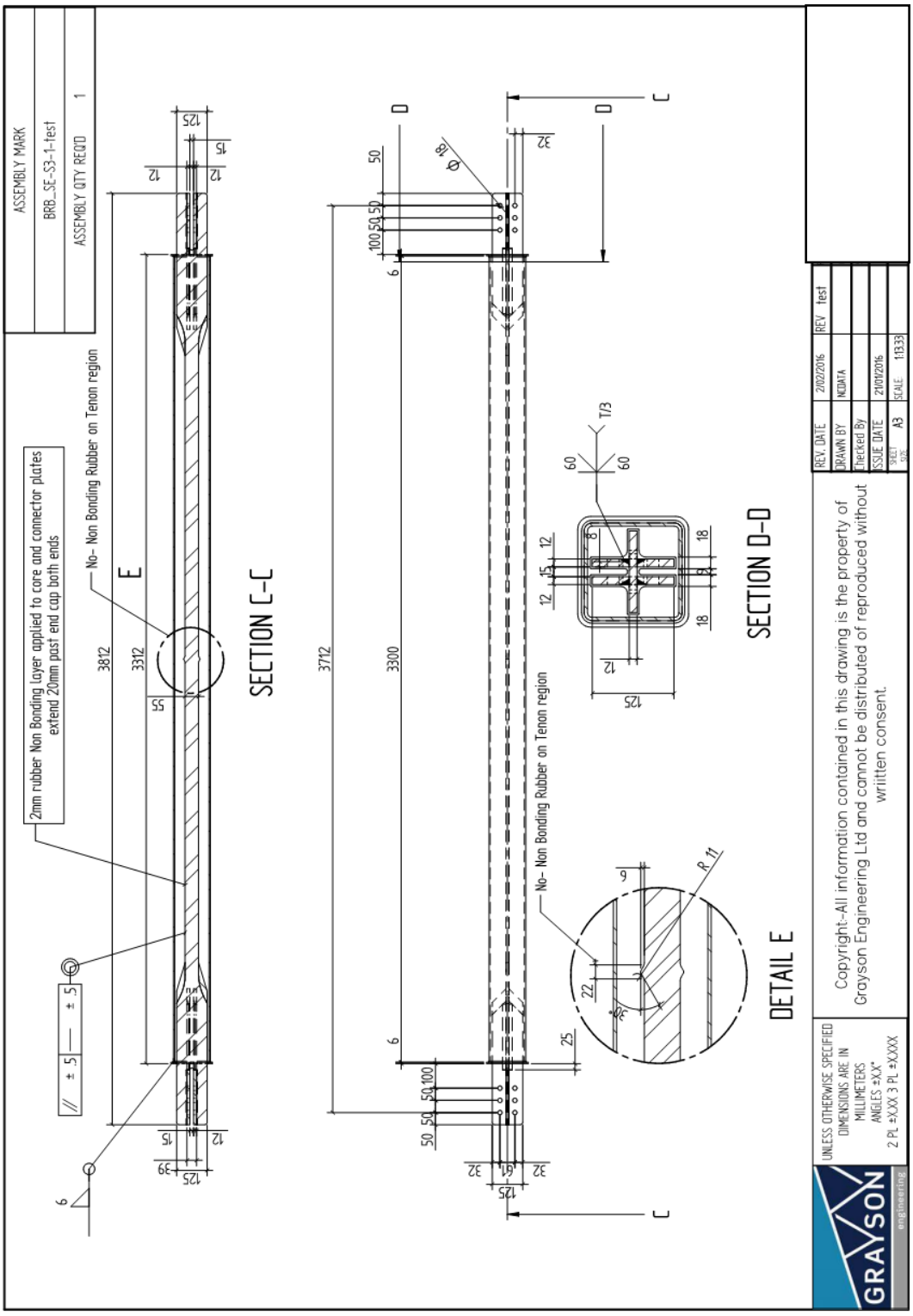

ASSEMBLY MARK
BRB_SE-S3-1-test
ASSEMBLY QTY REQ'D 1

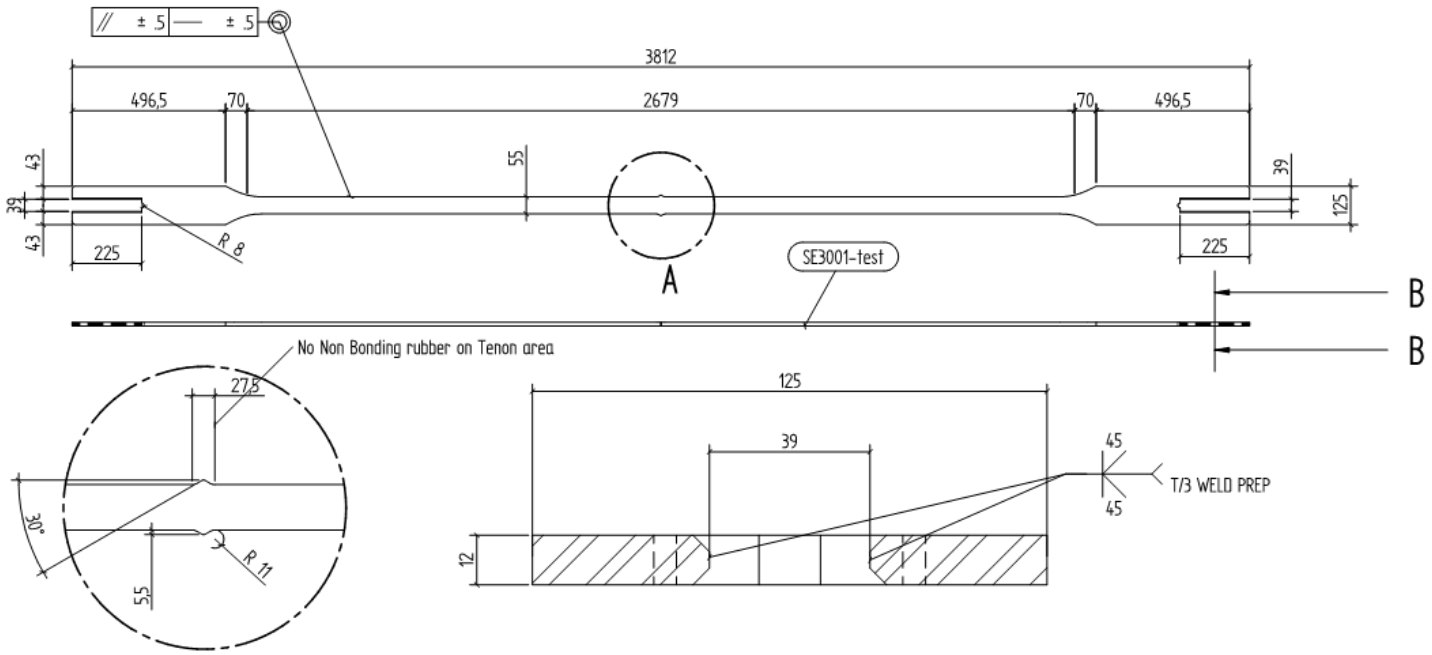

DETAIL A

SECTION B-B

Material: Grade 300
Mark: SE3001-test
Qty Required :1

Material Heat #_____

Mark	Quanity	Grade	Plate Size	Length	Width	Mass
SE3001-test	1	300	12.00 mm	3812.00 mm	125.00 mm	24.991 kg
MATERIAL LIST FOR WORKSHOP						

GRAYSON engineering

UNLESS OTHERWISE SPECIFIED
DIMENSIONS ARE IN
MILLIMETERS
ANGLES ±X.X°
2 PL ±X.XX 3 PL ±X.XXX

REV. DATE	2/02/2016	REV test
DRAWN BY	NCDATA	
Checked By		
ISSUE DATE	21/01/2016	
SHEET SIZE A3	SCALE: 1:13.33	

ASSEMBLY MARK
BRB_SE-S3-1-test
ASSEMBLY QTY REQ'D 1

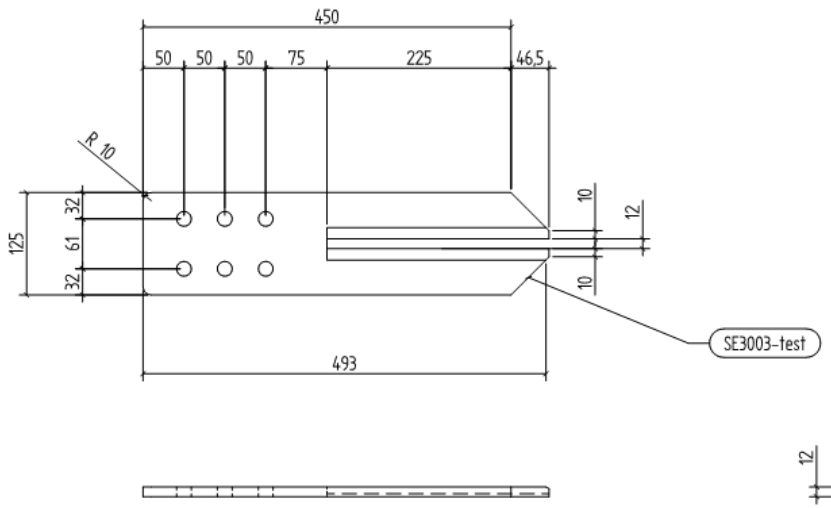

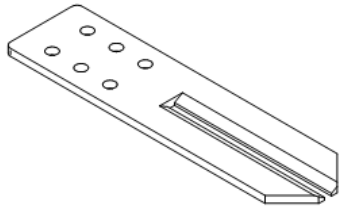

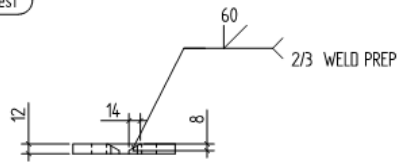

Material: Grade 300
Mark: SE3003-test
Qty Required : 4

Material Heat #_____

Mark	Quanity	Grade	Plate Size	Length	Width	Mass
SE3003-test	4	300	12.00 mm	496.50 mm	125.00 mm	4.941 kg
MATERIAL LIST FOR WORKSHOP						

GRAYSON engineering

UNLESS OTHERWISE SPECIFIED
DIMENSIONS ARE IN
MILLIMETERS
ANGLES ±X.X°
2 PL ±X.XX 3 PL ±X.XXX

REV. DATE	2/02/2016	REV test
DRAWN BY	NCDATA	
Checked By		
ISSUE DATE	21/01/2016	
SHEET SIZE A3	SCALE: 1:5	

8.3 **Specimen – BRB C6**

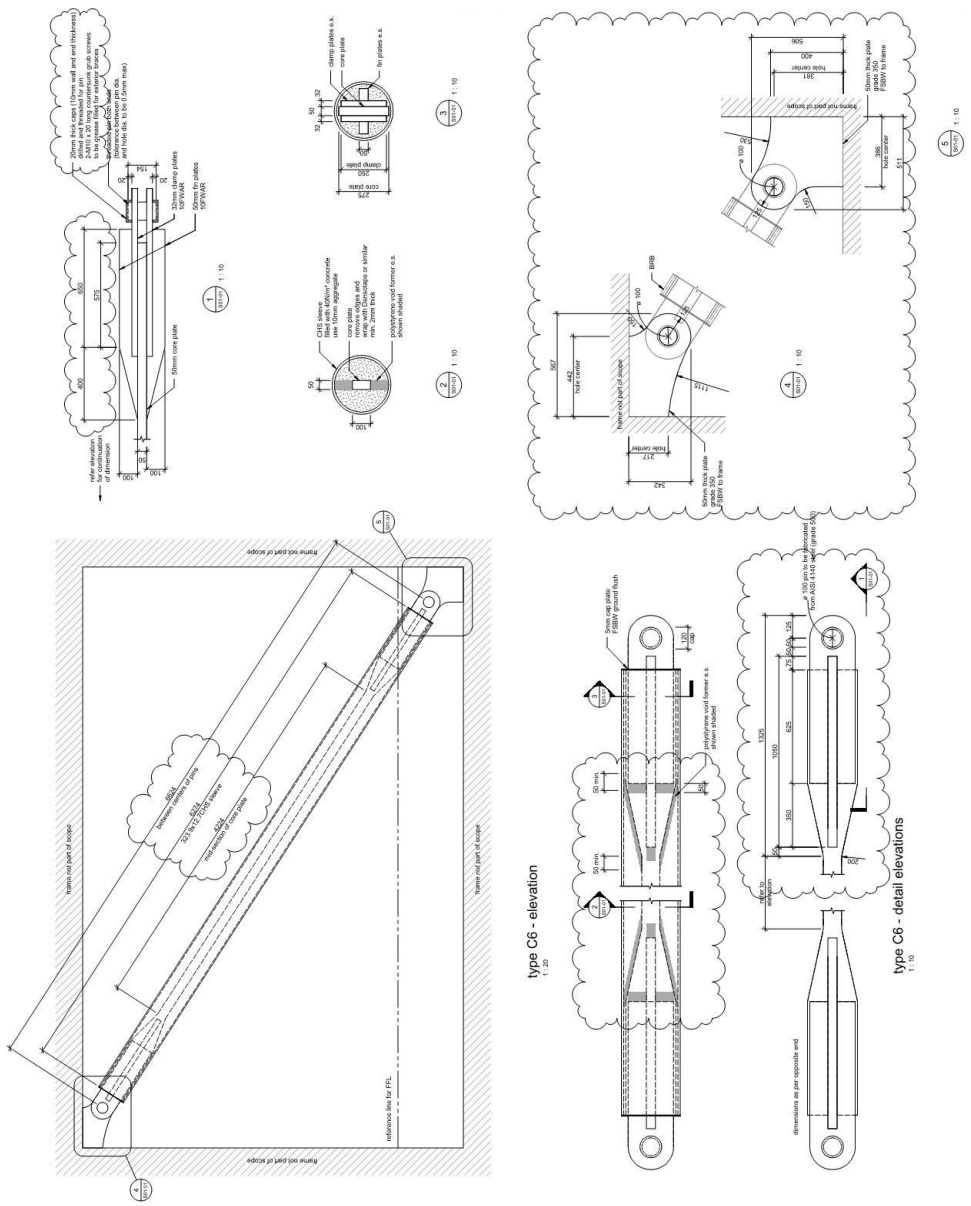

8.4 **Specimen – BRB 9.5**

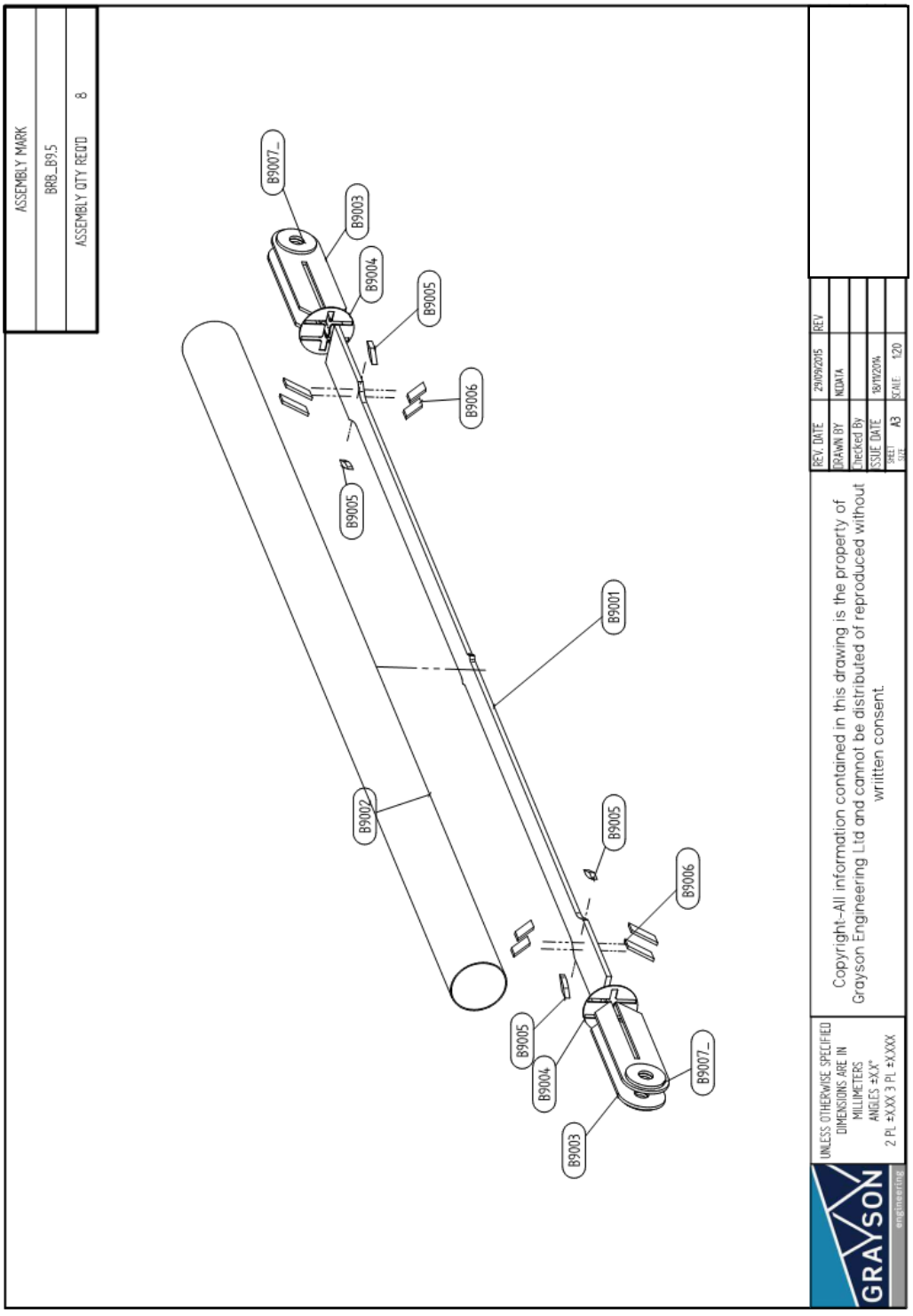

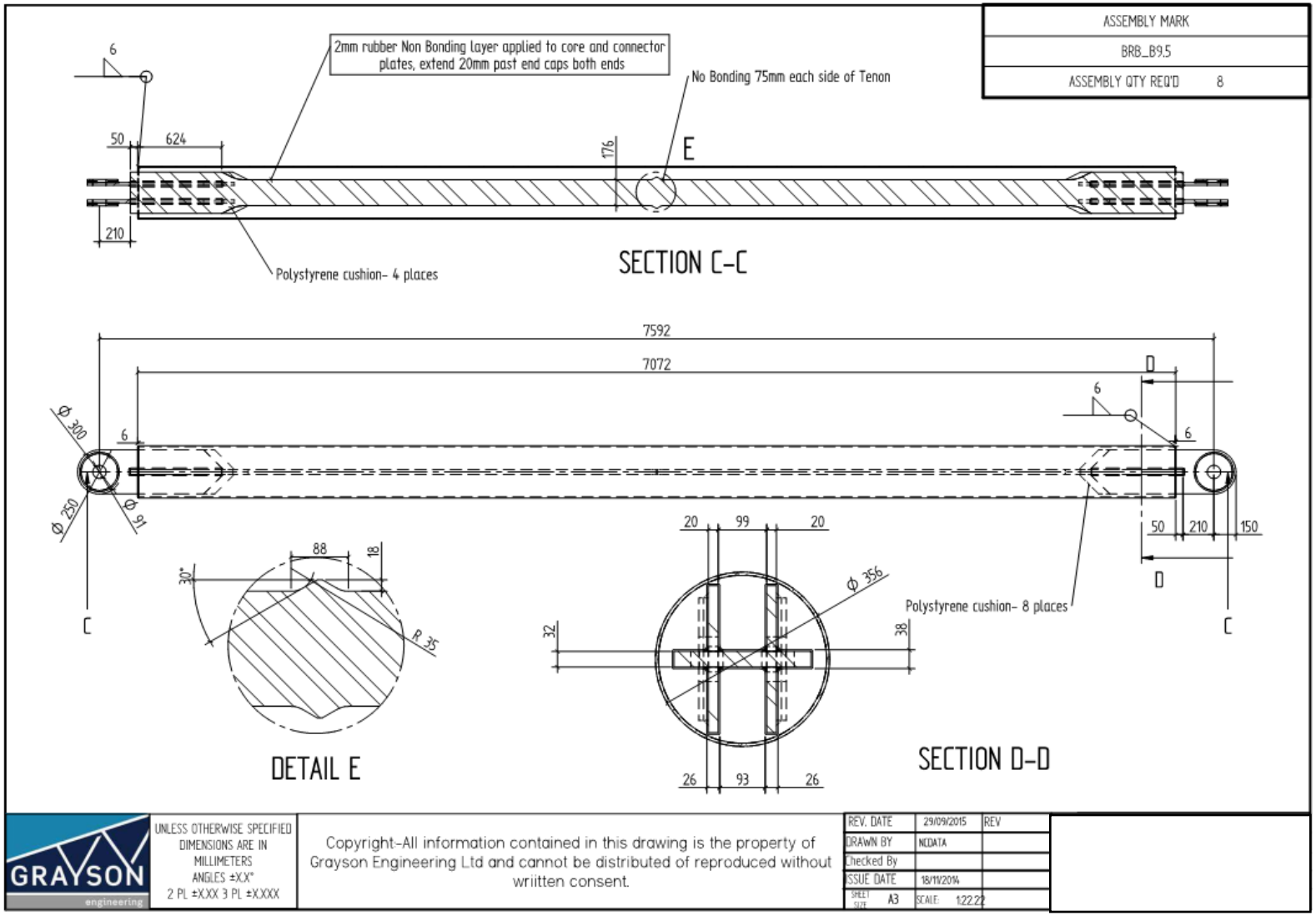
ASSEMBLY MARK
BRB_B9.5
ASSEMBLY QTY REQ'D 8
2mm rubber Non Bonding Layer applied to core and connector plates, extend 20mm past end caps both ends
No Bonding 75mm each side of Tenon
Polystyrene cushion- 4 places
SECTION C-C
Polystyrene cushion- 8 places
DETAIL E
SECTION D-D
GRAYSON engineering
UNLESS OTHERWISE SPECIFIED DIMENSIONS ARE IN MILLIMETERS ANGLES ±X.X° 2 PL ±X.XX 3 PL ±X.XXX
Copyright-All information contained in this drawing is the property of Grayson Engineering Ltd and cannot be distributed of reproduced without written consent.
REV. DATE 29/09/2015 REV
DRAWN BY NEDATA
Checked By
ISSUE DATE 18/11/2014
SHEET SIZE A3 SCALE: 1:22.22

ASSEMBLY MARK		
BRB_B9.5		
ASSEMBLY QTY REQ'D 8		
Revision Notes:		
Date	Comments	Rev

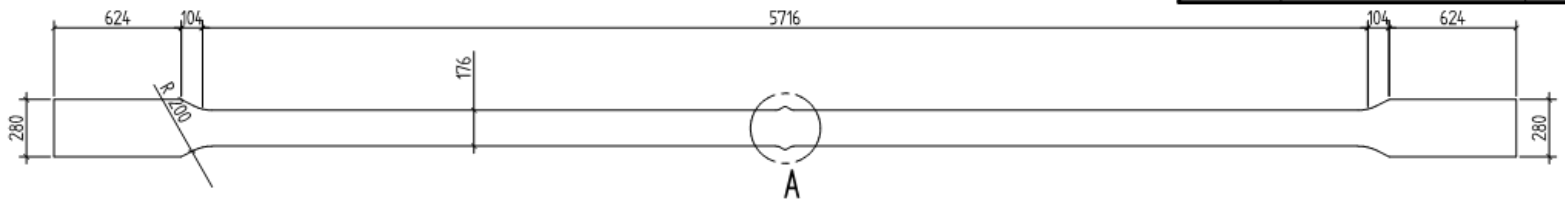

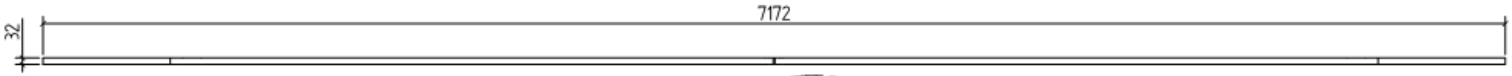

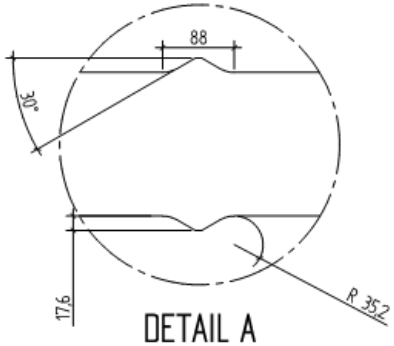

DETAIL A

Material: Grade 300
Mark: B9001
Qty Required 8 each

Mark	Quanity	Grade	Plate Size	Length	Width	Mass
B9001	8	300	32.00 mm	7172.00 mm	280.00 mm	352.159 kg
MATERIAL LIST FOR WORKSHOP						

Material Heat # _____

GRAYSON engineering

UNLESS OTHERWISE SPECIFIED
DIMENSIONS ARE IN
MILLIMETERS
ANGLES ±X.X°
2 PL ±X.XX 3 PL ±X.XXX

REV. DATE	29/09/2015	REV
DRAWN BY	NCDATA	
Checked By		
ISSUE DATE	18/11/2014	
SHEET SIZE A3	SCALE: 1:20	

ASSEMBLY MARK
BRB_B9.5
ASSEMBLY QTY REQ'D 8

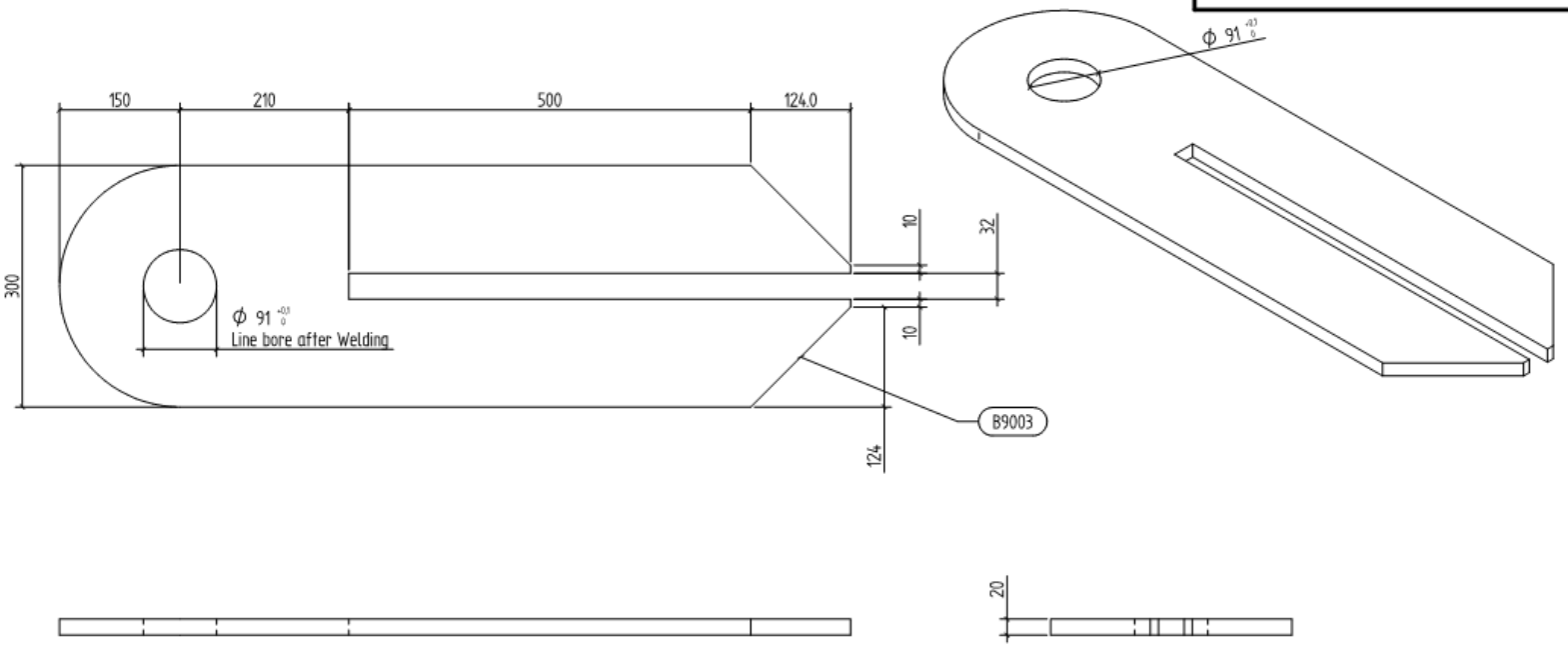

Material: Grade 300
Mark: B9003
Qty Required = 32

Material Heat #_____

Mark	Quanity	Grade	Plate Size	Length	Width	Mass
B9003	32	300	20.00 mm	984.00 mm	300.00 mm	38.177 kg
MATERIAL LIST FOR WORKSHOP						

GRAYSON engineering

UNLESS OTHERWISE SPECIFIED DIMENSIONS ARE IN MILLIMETERS
ANGLES ±X.X°
2 PL ±X.XX 3 PL ±X.XXX

REV. DATE	29/09/2015	REV
DRAWN BY	NEDATA	
Checked By		
ISSUE DATE	18/11/2014	
SHEET SIZE A3	SCALE: 1:5	

8.5 **Specimen – BRB 2A**

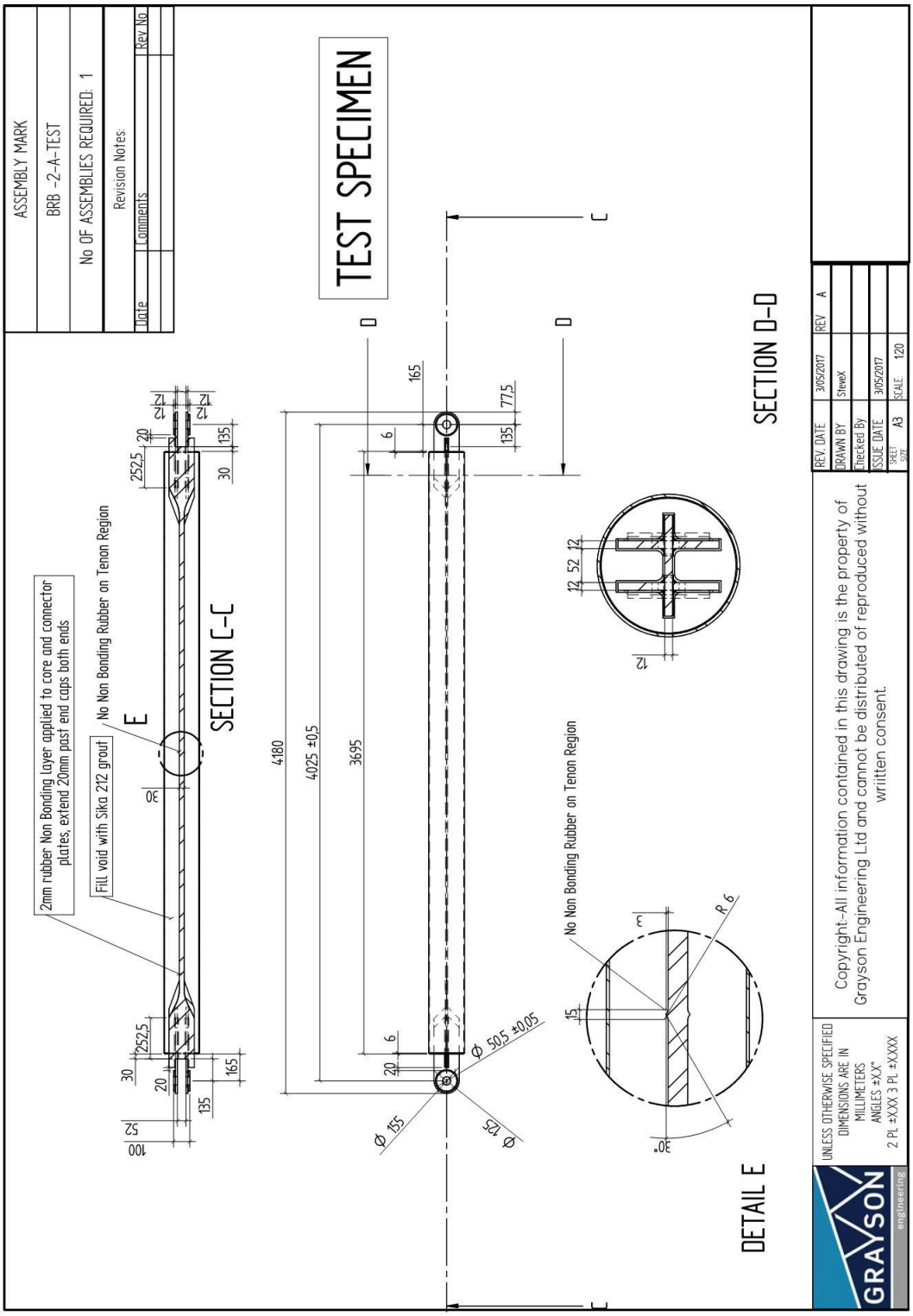

ASSEMBLY MARK
BRB -2-A-TEST
No OF ASSEMBLIES REQUIRED: 1

Revision Notes:

Date	Comments	Rev No

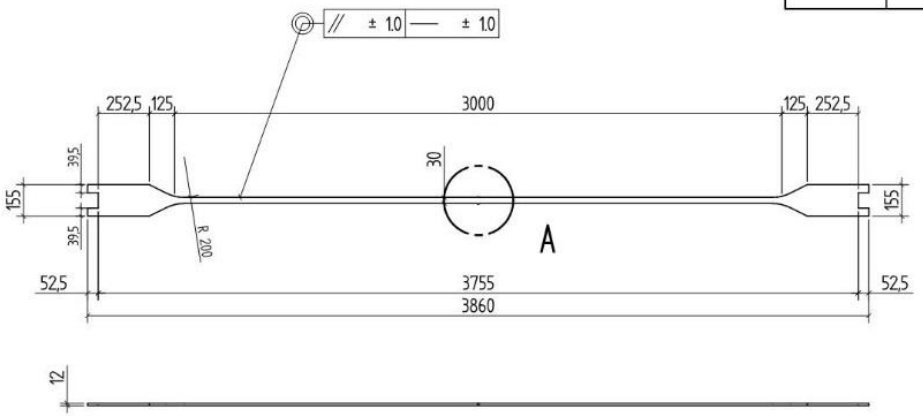

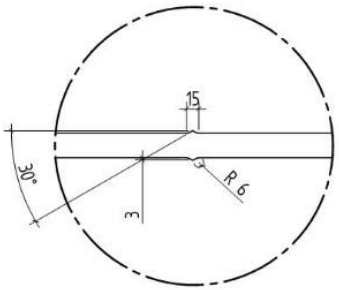

DETAIL A

TEST SPECIMEN

Material: Grade 300
Mark: B2001-A
Qty Required 1

Material Heat # ___6433349_____

Mark	Quanity	Grade	Plate Size	Length	Width	Mass
B2001-A	1	300	12.00 mm	3755.00 mm	155.00 mm	18.838 kg

MATERIAL LIST FOR WORKSHOP

GRAYSON engineering

UNLESS OTHERWISE SPECIFIED
DIMENSIONS ARE IN
MILLIMETERS
ANGLES ±X.X°
2 PL ±X.XX 3 PL ±X.XXX

REV. DATE	3/05/2017	REV	A
DRAWN BY	SteveX		
Checked By			
ISSUE DATE	3/05/2017		
SHEET SIZE	A3	SCALE:	120

ASSEMBLY MARK
BRB -2-A-TEST
No OF ASSEMBLIES REQUIRED: 1

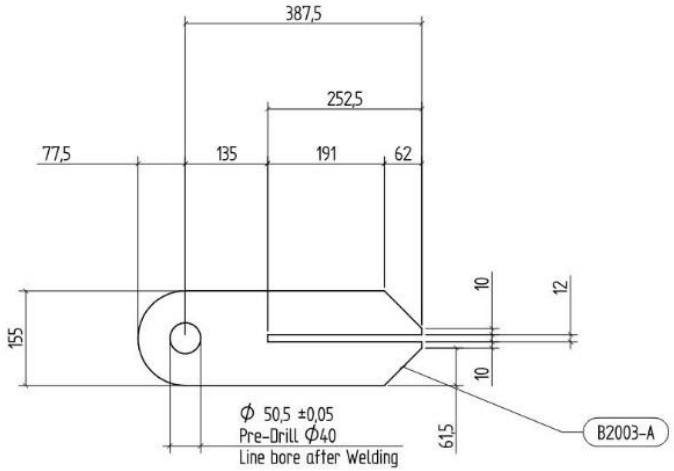

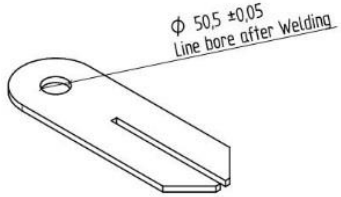

TEST SPECIMEN

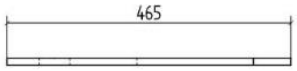

Material: Grade 300
Mark: B2003-A
Qty Required = 4

Material Heat #_____

Mark	Quanity	Grade	Plate Size	Length	Width	Mass
B2003-A	4	300	12.00 mm	465.00 mm	155.00 mm	5.704 kg

MATERIAL LIST FOR WORKSHOP

GRAYSON engineering

UNLESS OTHERWISE SPECIFIED
DIMENSIONS ARE IN
MILLIMETERS
ANGLES ±X.X°
2 PL ±X.XX 3 PL ±X.XXX

REV. DATE	3/05/2017	REV	A
DRAWN BY	SteveX		
Checked By			
ISSUE DATE	3/05/2017		
SHEET SIZE	A3	SCALE:	16.67

9 APPENDIX B (STEEL COUPON TENSILE TEST RESULTS)

MATERIALS & TESTING LABS
TENSILE

Report no : 43901
Date : 2015/10/06
Temperature : 21

Client : Grayson Engineering
Operator : TM
V1 : 10 mm/min

Shape: Plate

	Thickness	Width	Gauge Length	Break position
Units	mm	mm	mm	
25mm F0 05436.41	24.9000	20.4600	120.0000	0.0000

Name	Max_Force	UTS	YP_Force	YP_Stress	Area
Parameter			0.1 %/FS	0.1 %/FS	
Units	kN	MPa	kN	MPa	
25mm F0 05436.41	258.0	506.425	178.0	349.363	509.454

Name	elongation	fitted back
Units	%	
25mm F0 05436.41	30.0000	156.000

Comment

MATERIALS & TESTING LABS

TENSILE

Report no :	44561.1	**Client :**	Grayson Engineering
Date :	2016/01/18	**Operator :**	JS
Temperature :	22.6	**V1 :**	10 mm/min

Shape: Plate

	Thickness	Width	Gauge Length	Break position
Units	mm	mm	mm	
FD09105-20509	11.9300	20.2000	90.0000	0.0000

Name	Max_Force	UTS	YP_Force	YP_Stress	Area
Parameter			0.1 %/FS	0.1 %/FS	
Units	kN	MPa	kN	MPa	
FD09105-20509	106.7	442.745	75.0	311.299	240.986

Name	elongation	fitted back
Units	%	
FD09105-20509	34.4444	121.000

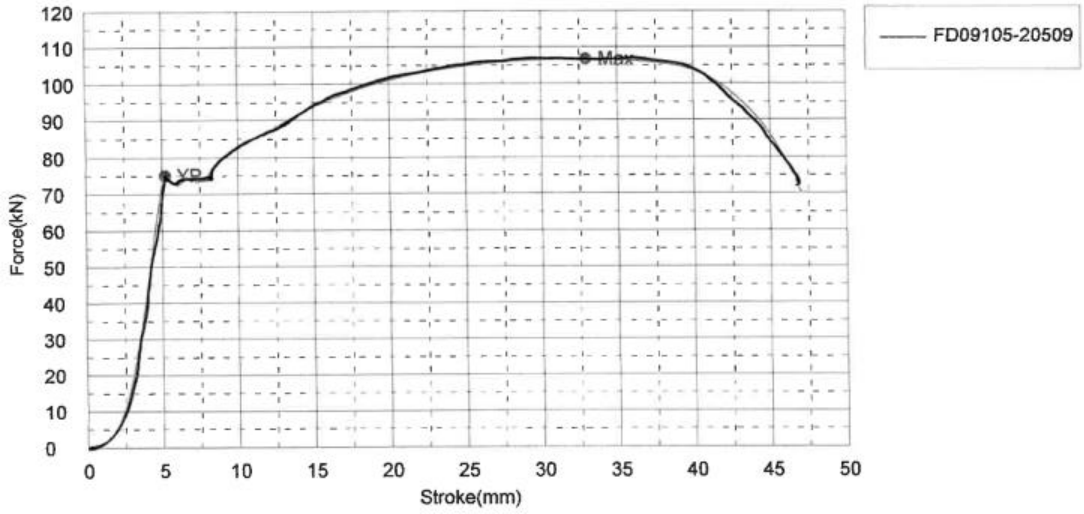

MATERIALS & TESTING LABS

TENSILE

Report no :	43901	**Client :**	Grayson Engineering
Date :	2015/10/06	**Operator :**	TM
Temperature :	21	**V1 :**	10 mm/min

Shape: Plate

	Thickness	Width	Gauge Length	Break position
Units	mm	mm	mm	
32mm F0 5380.41	31.6500	19.9600	140.0000	0.0000

Name	Max_Force	UTS	YP_Force	YP_Stress	Area
Parameter			0.1 %/FS	0.1 %/FS	
Units	kN	MPa	kN	MPa	
32mm F0 5380.41	314.1	497.168	206.5	326.890	631.734

Name	elongation	fitted back
Units	%	
32mm F0 5380.41	29.2857	181.000

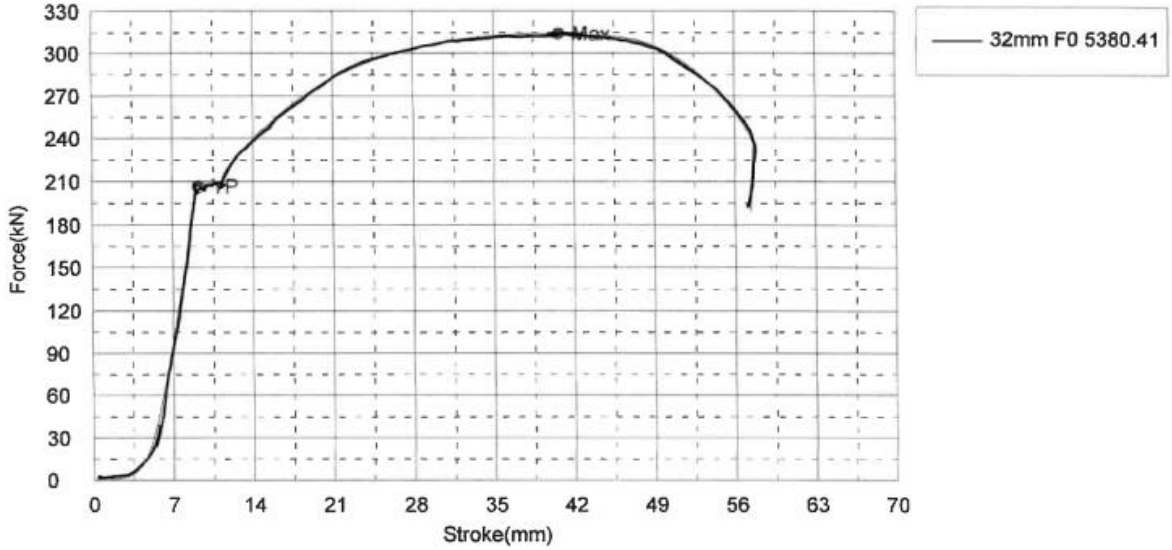

Comment

MATERIALS & TESTING LABS

TENSILE

Report no :	47351.1	**Client :**	Grayson Engineering
Date :	2017/03/01	**Operator :**	JS
Temperature :	21.4	**V1 :**	5 mm/min

Shape: Plate

	Thickness	Width	Gauge Length	Break position
Units	mm	mm	mm	
12mm plate H#6433349	11.7900	19.2100	85.0000	0.0000

Name	Max_Force	UTS	YP_Force	YP_Stress	Area
Parameter			0.1 %/FS	0.1 %/FS	
Units	kN	MPa	kN	MPa	
12mm plate H#6433349	98.4	434.319	74.5	328.980	226.486

Name	elongation	fitted back
Units	%	
12mm plate H#6433349	34.1176	114.000

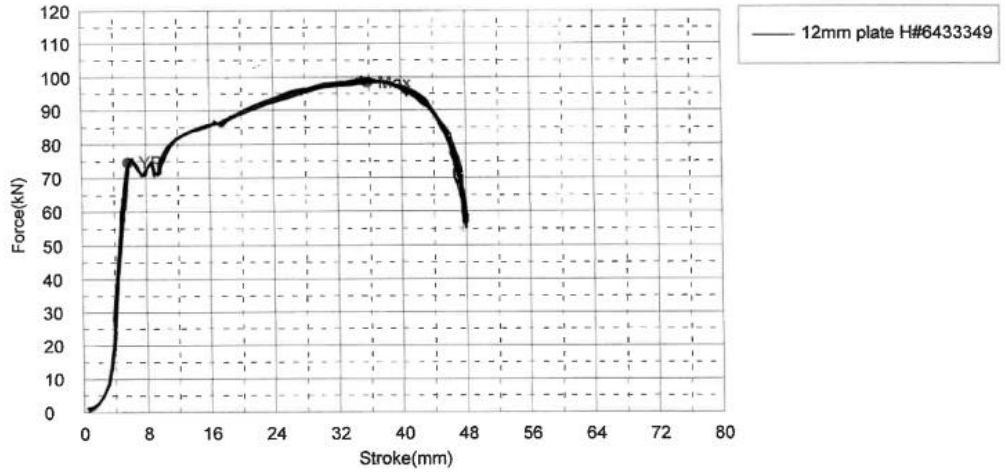

Comment

10 APPENDIX C (ELASTIC BUCKLING CAPACITY)

The elastic buckling capacity of a BRB and its end connections can be derived using several methods. In the analysis conducted by Takeuchi's method (Chapter 5), the differential equation method presented in (Matsui et al. 2010) is used and is expanded upon here. This method uses the general displacement function of the simplified prismatic BRB system (Figure 5-4) given by equation (AD.1). The boundary conditions set by either symmetric or asymmetric mode shapes enable a set of simultaneous equations to be developed. These equations can be assembled into a matrix. Through static condensation these equations can be solve analytically. Instead of solving the unknowns (${}_iC_j$), the non-trivial solution requires the determinate to be equal to zero. The lowest value of α can then be found incrementally and substituted in equation (AD.2) to solve for the maximum elastic buckling capacity. Equation (AD.3) describes the static condensation of these equations for a single diagonal symmetric mode and Equation (AD.4) describes the static condensation of for the single diagonal anti symmetric mode.

$$Y_i = {}_iC_1 \sin \alpha x = {}_iC_2 \cos \alpha x + {}_iC_3\, x + {}_iC_4 \tag{AD.1}$$

$$\alpha = \sqrt{\frac{N_{cr}^B}{EI_B}} \tag{AD.2}$$

$$\alpha^2 (EI_B)^2 S_1 C_4 + \alpha EI_B \left(K_{Rr} S_1 S_4 - \frac{K_{Rg}+K_{Rr}}{\sqrt{\Upsilon_J}} C_1 C_4 \right) - K_{Rg} K_{Rr} \left(\frac{1}{\Upsilon_J} S_1 C_4 + \frac{1}{\sqrt{\Upsilon_J}} C_1 S_4 \right) = 0 \tag{AD.3}$$

$$\alpha^3 (EI_B)^2 L_0 S_1 S_4 - \alpha^2 (EI_B) L_0 \left(K_{Rr} S_1 C_4 + \frac{K_{Rg} + K_{Rr}}{\sqrt{\Upsilon_J}} C_1 S_4 \right) + 2\alpha EI_B K_{Rg} S_1 S_4 + \alpha\, K_{Rg} K_{Rr} L_0 \left(\frac{1}{\sqrt{\Upsilon_J}} C_1 C_4 - \frac{1}{\Upsilon_J} S_1 S_4 \right) - 2K_{Rg} K_{Rr} \left(S_1 C_4 + \frac{1}{\sqrt{\Upsilon_J}} C_1 S_4 \right) = 0 \tag{AD.4}$$

Where,

$S_1 = \sin \frac{\alpha}{\sqrt{\Upsilon}} \xi L_0$, $C_1 = \cos \frac{\alpha}{\sqrt{\Upsilon}} \xi L_0$

$S_2 = \sin \alpha \xi L_0$, $C_2 = \cos \alpha \xi L_0$

$S_3 = \sin \alpha \frac{L_0}{2}$, $C_3 = \cos \alpha \frac{L_0}{2}$

$S_4 = \sin \alpha L_0 \left(\frac{1}{2} - \xi \right)$, $C_4 = \cos \alpha L_0 \left(\frac{1}{2} - \xi \right)$